# Performance Assessment of Seismic Resistant Steel Structures

Jordan Alesa Jarrett

Dissertation submitted to the faculty of the Virginia Polytechnic Institute and State University in partial fulfillment of the requirements for the degree of

Doctor of Philosophy
In
Civil Engineering

Finley A. Charney, Chair
Matthew R. Eatherton
Cristopher D. Moen
Adrian Rodriguez-Marek

December 2, 2013
Blacksburg, VA

Keywords: Nonlinear Response History Analysis, FEMA P-58, FEMA P-695, ASCE 7, Innovative Systems

# Performance Assessment of Seismic Resistant Steel Structures

Jordan Alesa Jarrett

## Abstract

This work stems from two different studies related to this performance assessment of seismic resistant systems. The first study compares the performance of newly developed and traditional seismic resisting systems, and the second study investigates many of the assumptions made within provisions for nonlinear response history analyses.

In the first study, two innovative systems, which are hybrid buckling restrained braces and collapse prevention systems, are compared to their traditional counterparts using a combination of the FEMA P-695 and FEMA P-58 methodologies. Additionally, an innovative modeling assumption is investigated, where moment frames are evaluated with and without the lateral influence of the gravity system. Each system has a unique purpose from the perspective of performance-based earthquake engineering, and analyses focus on the all intensity levels of interest. The comparisons are presented in terms consequences, including repair costs, repair duration, number of casualties, and probability of receiving an unsafe placard, which are more meaningful to owners and other decision makers than traditional structural response parameters. The results show that these systems can significantly reduce the consequences, particularly the average repair costs, at the important intensity levels.

The second study focuses on the assumptions made during proposed updates to provisions for nonlinear response history analyses. The first assumption investigated is the modeling of the gravity system's lateral influence, which can have significant effect on the system behavior and should be modeled if a more accurate representation of the behavior is needed. The influence of residual drifts on the proximity to collapse is determined, and this work concludes that a residual drift check is unnecessary if the only limit state of interest is collapse prevention. This study also finds that spectrally matched ground motions should cautiously be used for near-field structures. The effects of nonlinear accidental torsion are also examined in detail and are determined to have a significant effect on the inelastic behavior of the analyzed structure. The final investigation in this study shows that even if a structure is designed per ASCE 7, it may not have the assumed probability of collapse under the maximum considered earthquake when analyzed using FEMA P-695.

# Acknowledgements

I would especially like to thank my advisor Dr. Finley Charney for the opportunity to work on these interesting and challenging projects. I am eternally grateful for all his guidance, expertise, and encouragement. I would also like to thank my Masters advisor, Dr. Paul Heyliger, for inspiring me to get my Ph.D. in the first place. I am also indebted to my committee, Dr. Matthew Eatherton, Dr. Cris Moen, and Dr. Rodriguez-Marek for their comments and suggestions throughout this process.

I am also appreciative of my colleagues Francisco Flores, Andy Hardyneic, Johnn Judd, Ozgur Atlayan and Reid Zimmerman for their contribution and collaboration. I would also like to acknowledge the help provided by Clint Rex, Jim Sexton, Vickie Mouras, Jack Baker, and Curt Haselton during the process of this research. I would furthermore like to thank the Charles E. Via Fellowship Program, the Department of Civil and Environmental Engineering, and NIST grant 60ANB10D107 for funding my education.

This would not be possible without the support of my family, for which I am forever appreciative. And finally, I want to thank all my friends from Colorado State University and Virginia Tech for making the past ten and a half years an amazing experience. Go Rams and Hokies!

# Table of Contents

# List of Figures

# List of Tables

# Chapter 1: Introduction

## 1.1. Overview and Purpose of Work

There are numerous methodologies available to assess the nonlinear performance of seismic resisting systems, and this research investigates the applicability and uses of many of these procedures. The preliminary goal of this work is to determine which methodology or combination of methodologies provides the most comprehensive analysis, particularly from the perspective of performance based earthquake engineering. Understanding the benefits and limitations of the various methodologies is crucial to determining the most accurate representation of structural behavior.

When investigating these methodologies, it is necessary to study every facet of the procedure. How detailed and accurate is the mathematical model? Which performance objectives are evaluated? Are risk and/or hazard determined and used in the analysis? What is the level of computational demand of each the analyses? What level(s) of ground motion intensity are investigated? What are the target spectra used? What types of assessments are used? How many ground motion records are applied to the structure? How are the results presented? How useful are those outputs are to decision makers? Does the provision include prescriptive acceptance criteria? How accurate are the results? All of these factors play a crucial role in how advantageous a methodology is to the nonlinear dynamic analysis of structures. While this list of factors is not yet exhaustive, these are the some of the aspects that will be investigated in order to determine a recommended methodology.

While the preliminary work is to compare these different methodologies, the majority of the research presented in this dissertation stems from two other studies. The first study compared the performance of newly developed and traditional seismic resisting systems, and the second study investigated many of the assumptions made within provisions for nonlinear response history analyses.

The first study comes from a larger project funded by NIST entitled the "Development and Evaluation of Performance-Based-Earthquake-Engineering Compliant Structural Systems." This broad study, referred herein as the NIST study, was broken into three parts: design of innovative systems, system modeling, and performance assessment. The performance assessment portion of the project is presented in this dissertation and consists of the comparison of traditional seismic resisting systems to new systems that were developed by other members of the research team. These innovative structures and modeling techniques include hybrid buckling restrained braces, collapse prevention systems, and the modeling of the lateral strength and stiffness of the gravity system. The preliminary study of assessing the various methodologies was mainly utilized within this study. Based on the comparison of the methodologies, a combination of the FEMA P-58

(FEMA 2012) and FEMA P-695 (FEMA 2009) methodologies is determined to be the most comprehensive and advantageous procedure, and using these recommended provisions, the performance of the new and traditional systems can be contrasted. The FEMA P-695 analyses were performed in the design work, and those results are expanded in this work using FEMA P-58.

These innovative systems were developed to provide alternative methods of seismic resistance, with an emphasis on the principles of Performance Based Earthquake Engineering (PBEE). The general concept of PBEE is to allow stakeholders and decision-makers to determine specific acceptable levels of performance on a structure-by-structure basis. By shifting the focus from generic, prescriptive methodologies, the needs of each individual system can be determined and evaluated. Additionally, the application of PBEE will promote buildings that are safer and better suited for specific challenges. As Krawinkler stated (2000):

> *"The final challenge for PBEE researchers is not in predicting performance or in estimating losses, but in contributing effectively to the reduction of losses and the improvement of safety. We must never forget this. It is easy to get infatuated with the numbers and analytical procedures, but neither is useful unless it contributes to this final challenge".*

The innovative systems aim to satisfy these ideals. Primarily, they are developed for areas of different hazard and can be suited to a wide variety of needs. The hybrid buckling restrained braces (BRBs), for example, utilize the behavior of numerous steel materials to control the sequence of yielding. This minor adjustment to the design philosophy of buckling restrained brace frames can provide improved behavior under numerous levels of ground motion intensity. These systems would be ideally suited for locations where a wide variety of hazard is of interest, like California. Large ground motions are certainly a concern for areas located along active faults like those found in California; additionally, the more frequent ground motions are still sufficiently large to cause damage to structures. By developing a system like the hybrid buckling restrained braces, all these potential hazards can be incorporated in design.

On the other hand, there are locations around the world that do not experience a wide variety of potential hazards. In the Central and Eastern United States, for example, catastrophic earthquakes are often a concern, as in Charleston, SC or the New Madrid seismic zone. However, the frequent earthquakes tend to be so small that the wind hazards would likely control the design over lower intensity seismic hazards. The Collapse Prevention Systems are developed to accommodate such a design. The structural systems are designed with little or no seismic detailing, and the inherent lateral resistance in the gravity framing system along with a collapse prevention device would provide resistance to large, rare earthquake events. The design becomes

significantly more economical, while still providing sufficient resistance to the pertinent seismic hazard levels. By rejecting a "one-size-fits-all" seismic resisting system, the design can become focused on the needs of the site, and the principles of PBEE can be applied. The third system evaluated is not a traditional system, but a modeling assumption. This investigation into the influence of the lateral resistance of the gravity system is crucial to understanding the behavior of these collapse prevention systems. Since the collapse prevention systems rely on the inherent lateral strength and stiffness of the gravity framing, it is necessary to also incorporate a study of this modeling assumption into the research.

The assessment portion of this broad project (which again is the portion of the project presented in this dissertation) aims to determine if these new systems are in fact providing an improvement in behavior under the hazards of interest. The performance assessment will determine if these new systems are effective in reducing losses and improving safety, just as Krawinkler stated. Structures that can effectively do so would be a valuable asset to the earthquake engineering community, and this work aims to prove that two such structures have been developed.

The second study, referred herein as the assumptions study, stems from work with the Building Seismic Safety Council Response History Analysis Issue Team. The committee is tasked with suggesting changes to Chapter 16 of ASCE 7 (ASCE 2010) for the 2016 update, which discusses provisions for nonlinear response history analysis. Numerous assumptions were made during the development of these proposed updates, and this research focuses on the investigation of the validity of these assumptions. The aspects of the proposed updated that are researched include: (1) the influence of the inclusion of the lateral strength and stiffness of the gravity system, (2) the practicality of a residual drift check, (3) the applicability of spectral matched ground motions, (4) the necessity of an accidental torsion check, and (5) the accuracy of the assumed implicit satisfaction of a specified percent probability of collapse under the $MCE_R$ level ground motion.

As mentioned previously, understanding the benefits and limitations of a methodology developed for the performance assessment of structures is crucial to determining the most accurate representation of structural behavior. This research provides an opportunity to investigate these potential advantages and disadvantages at the very foundation and creation of a proposed methodology. Again, there are an abundance of methodologies available for this assessment, but there is little agreement on the best methods of assessment. The differences between all the methodologies prove that there is not sufficient research on all the aspects that make up these provisions, and this work aims to provide a contribution to this necessary research.

In doing so, this research also provides a starting point for a discussion about the ideal aspects of a comprehensive assessment strategy. While these assumptions are investigated under the framework of proposed updates to ASCE 7 Chapter 16, the results and conclusions could be

expanded to any provision that provides recommendations regarding nonlinear response history analysis. A discussion of this nature would be highly beneficial to the earthquake engineering community, and ideally, and single assessment methodology could emerge.

While the subject of performance assessment of seismic resistant systems encompasses a significant amount of different topics, this dissertation provides interesting research regarding some of these topics. Primarily, a comparative study into the variety of methodologies available for the performance assessment of these systems investigates the current state of practice and allows for a recommendation on the most comprehensive method. Using the recommended methodology, the performance of innovative systems is compared to the performance of their traditional counterparts. Not only does this comparative assessment provide an example of the recommended methodology, but it shows the benefit of these newly developed systems. Finally, this work investigates numerous assumptions that go into the development of these performance assessment provisions. This portion of the study helps determine the advantages and disadvantages of a newly proposed provision, while providing a framework for the discussion of the ideal components of future provisions.

### 1.2. Dissertation Organization

This dissertation is organized using the manuscript format, where the traditional chapters in a dissertation are replaced by manuscripts that have been submitted to peer-reviewed journals and conferences. For this dissertation, two journal papers and one conference paper are presented.

The dissertation begins with a literature review in Chapter 2 to provide additional background on numerous topics of interest, including: (1) Performance Based Earthquake Engineering Principles, (2) Incremental Dynamic Analyses, (3) Fragility Curves, (4) ASCE 7 Nonlinear Dynamic Analysis Procedure, (5) the FEMA P-695 Procedure, (6) the FEMA P-58 Procedure, and (7) Accidental Torsion in Dynamic Analyses.

Chapter 3 is a manuscript that focuses on the results of the NIST study and is entitled "Comparative Evaluation of Innovative and Traditional Steel Seismic Resisting Systems Using the FEMA P-58 Procedure," which will be submitted to the *Journal of Constructional Steel Research*. Chapter 4 is a manuscript entitled "Response-History Analysis for the Design of New Buildings: A Study of Assumptions," which will be submitted to *Earthquake Spectra*. This paper is part of a multiple-part series discussing the proposed update to ASCE 7 Chapter 16. The other parts are written by other members on the BSSC committee and discuss the development of the proposed updates and examples of the new procedure. Chapter 5 is a manuscript entitled "Accidental Torsion in Nonlinear Response History Analysis," which has been submitted to the *10$^{th}$ U.S. National Conference on Earthquake Engineering*. Both Chapters 4 and 5 present results from the assumptions study. It should be noted that there may be some minor variation between these chapters and the published papers after the peer review process.

Chapter 6 summarizes the results, gives overall conclusions, and provides recommendations for future work. The references for all chapters are then provided at the end of the dissertation. Finally, three appendices are provided. Appendix A discusses additional information about the buildings and models used in all three the manuscript. Appendix B provides additional data and results that could not be included in the manuscript "Comparative Evaluation of Innovative and Traditional Steel Seismic Resisting Systems Using the FEMA P-58 Procedure" due to page limitations. Finally, Appendix C further discusses the ground motions used during the research presented in the manuscripts "Response-History Analysis for the Design of New Buildings: A Study of Assumptions" and "Accidental Torsion in Nonlinear Response History Analysis."

### 1.3. Attribution

Several colleagues have contributed to the work presented in the manuscripts, and their contributions are included here.

Primarily, due to the magnitude of the NIST study, numerous other Virginia Tech Ph. D. students contributed to the work, and a great deal of collaboration occurred. The study was broken into three parts: modeling assumptions, design, and assessment. Andy Hardyneic developed a tool to perform P-695 analyses (NIST 2012), and Flores and Charney (2013) focused on the modeling of the lateral resistance of the gravity system. Atlayan and Charney (2013) and Judd and Charney (2013b) designed and modeled the innovative systems of buckling restrained braces and collapse prevention systems, respectively. This work focuses on the assessment portion of the project and utilizes the preliminary modeling and P-695 analyses to expand the results to the P-58 procedure and provide the comparative assessment.

In addition to the collaboration within the project, the contributions of the co-authors of the manuscripts are discussed here. Dr. Finley Charney is a co-author on all the manuscripts, as he is the main advisor of the research and provided valuable leadership, expertise and reviews. For the manuscript entitled "Comparative Evaluation of Innovative and Traditional Steel Seismic Resisting Systems Using the FEMA P-58 Procedure," Johnn Judd is a co-author, as he provided additional analyses for the P-58 process of the collapse prevention systems and wrote the section regarding modeling of these systems. For the manuscript entitled "Response-History Analysis for the Design of New Buildings: A Study of Assumptions," two additional co-authors are provided, both of whom are engineers for Rutherford + Chekene working with the BSSC committee. Reid Zimmerman was the primary modeler of the Perform-3D model and provided continuous feedback and edits during the process. Additionally, Afshar Jalalian provided expertise and guidance for the development of the model. The manuscript entitled "Accidental Torsion in Nonlinear Response History Analysis" presents work from the same study as the previous manuscript, and Reid Zimmerman is once again a co-author.

# Chapter 2: Literature Review

## 2.1. Summary of Performance Based Earthquake Engineering Principles

Performance Based Earthquake Engineering (PBEE) is a design philosophy that allows for stakeholders to determine the ideal performance of a structure. As with traditional seismic resistant design, Performance Based Earthquake Engineering (PBEE) typically recommends that the building satisfy life safety limit states (e.g., low probability of collapse) when subjected to the rare design level earthquake. However, unlike traditional design, PBEE also often attempts to ensure that the building will not have extensive damage or excessive economic losses when subjected to more frequent, lower intensity ground motions. When necessary, PBEE also takes into account many factors, including damage to structural and non-structural components, loss of use of the structure, repair costs, and loss of life (Vamvatsikos and Cornell 2002).

While a structural design should accommodate heavy damage during the maximum considered earthquake (MCE), the design should also account for less damage as the magnitude of the earthquake decreases, as deemed necessary by the decision makers and stakeholders. As can be seen in Figure 2-1, it is possible for several designs of the same building to satisfy the life safety requirement but have differing performance under lower intensity earthquakes. At the MCE, all three structural designs shown exhibited extreme damage, but under all other levels of earthquake occurrence, none of the designs had the same level of damage.

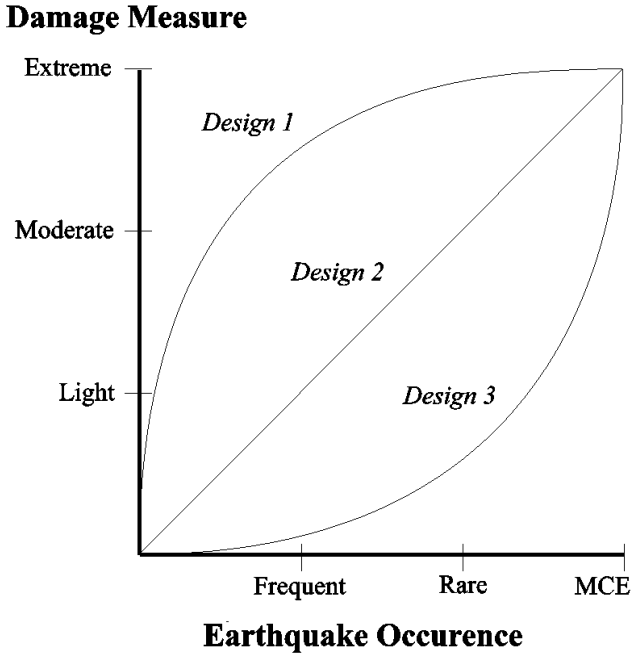


**Figure 2-1.** Potential behavior of structural designs when subjected to various earthquakes

Design 1 behaves poorly under small ground motions, as the damage is high even under frequent earthquakes. On the other end of the spectrum, Design 3 has very little damage to the structure for all earthquakes other than the MCE, which could potentially be a costly overdesign. Design 2 may represent an economic design, as it meets life safety requirements for extreme earthquakes, has moderate damage during rare earthquakes, and minimal damage under frequent earthquakes. The goal of PBEE is to provide a framework for stakeholders to determine to acceptable levels of damage and safety for each individual project (FEMA 2006). Both Incremental Dynamic Analysis and fragility curves are useful tools in the application of Performance Based Earthquake Engineering. These two related topics will be reviewed in detail within this Literature Review.

## 2.2. Incremental Dynamic Analysis

### *2.2.1. Background*

Incremental Dynamic Analysis (IDA) is a method of structural analysis that is used to predict the behavior of structures under varying levels of dynamic loads. IDA provides a way to determine the behavior of a structure at multiple limit states to make sure that an economical design is being provided for a wide range of potential hazard levels, not just the maximum considered earthquake. IDA is generally performed by incrementally scaling a suite of ground motions to increasingly higher levels and determining the structural response at each one of these intensity levels. In IDA, intensity measures (IM) are generally the scale factors applied to the suite of motions, and damage measures (DM) are the specific responses of the system that is measured with respect to the different intensity measures. Possibilities for these damage measures include peak floor accelerations, interstory drifts, and plastic hinge rotations (Vamvatsikos 2002). The levels of damage are typically shown with the use of an IDA curve, which plots the damage measure with respect to the intensity measure.

### *2.2.2 General Procedure of Incremental Dynamic Analysis*

IDA relies on scaled ground motions to determine the behavior of the structure at various limit states. The ground motions used must first be scaled to a common value of spectral acceleration to remove variability between records. Shome and Cornell (1998) found that scaling to the design spectral acceleration (using between 5 and 20 percent damping) of the structure's first mode period of vibration (or the highest period of vibration) is the best alternative for scaling. These ground motions are then incrementally scaled to a variety of intensities to relate behavior and damage to the intensity of the earthquake.

Figure 2-2 shows an example of an IDA plot and the different behaviors that can be typically on such a plot. In this example, each line on a plot represents the behavior as subjected to one earthquake record, and 44 different records were used in analysis. Each ground motion record was systematically scaled up until collapse occurs. At each intensity, the maximum damage

measure (which in this case is the drift ratio) is recorded and plotted against the corresponding scale factor. There are three possible trends that can be seen in the IDA curves. One earthquake could produce a softening curve (where the slope of the curve decreases between scale factors), which indicates more damage for increasing increments of intensity, or behavior tending toward collapse. A different record could result in a hardening curve (where the slope increased between scale factors), which indicated less damage for increments of intensity. The third trend is a weaving curve, where the slope increases between some scale factors but decreases between others.

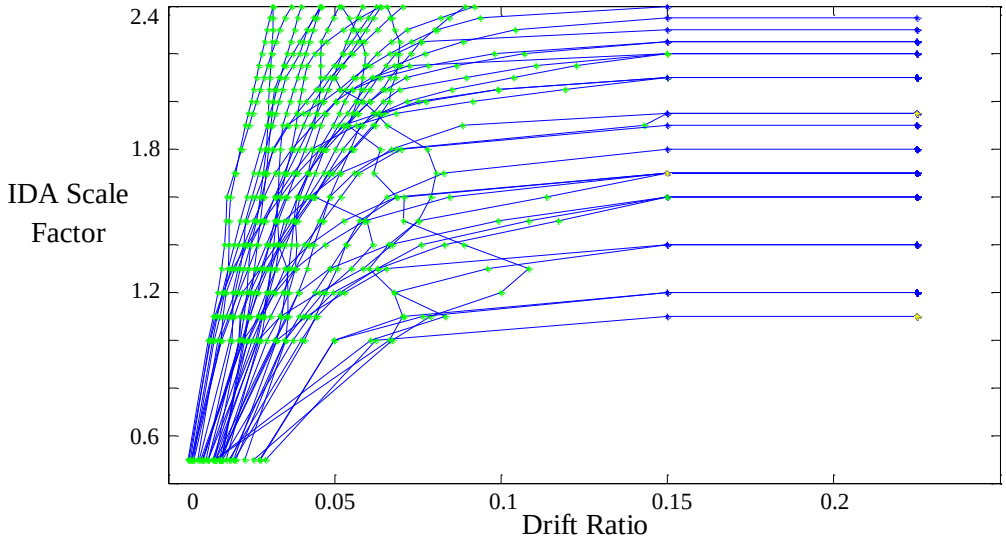


**Figure 2-2.** Example IDA curve

IDA curves can be used to predict behavior under a wide range of earthquake intensities, and therefore, can be used to design and evaluate structures for varying limit states, which is the principle behind PBEE. For use in PBEE, these physical damages measures are converted into consequences, which describe the damage in a fiscally quantifiable way. These consequences (also known as damage variables) could include loss of use, repair costs, potential loss of life, etc. They can be expressed either as annual probability of occurrence or life cycle probabilities, depending on the desire of the shareholders (Deierlein et al. 2003).

The process of performing an IDA analysis is focused on determining the behavior of a structure from its elastic behavior all the way up to failure. The first step in performing the analysis is to select a suite of ground motion records that could adequately represent the potential hazard of the site. These ground motions should be sufficient in number to include a wide variety of possible earthquakes that could occur near the structure and should be carefully determined based on the soil and fault types that are typical in the vicinity of the structure (Dhakal et al. 2006).

While the example in Figure 2-2 shows the results of Incremental Dynamic Analyses from multiple ground motions applied to one structure, IDA curves can also be developed for one ground motion applied to multiple variations of a structure. These "variation of parameter" IDAs can be useful to determine the potential influence that modeling assumptions or various designs can have on the behavior of a structure. In this case, the ground motion record used is the constant, and the mathematic model is the variable that is being altered.

For IDAs to provide the most helpful results, care should be taken to decide which damage measures and intensity measures would be the most appropriate. For example, for the intensity measure, the spectral acceleration of the dominant mode would be a good measure, which for low rise buildings would be the first mode. However, this would not be an accurate assumption for high rise buildings, as dominant modes could include the higher ones. Each individual structure will react differently to an earthquake, and selecting a representative intensity measure is crucial for predicting accurate behavior. Similarly, the damage measure will vary based on what part of the structure is being analyzed. Peak floor accelerations would be most applicable to measure the damage to equipment and some non-structural components, while interstory drift ratios may be the best choice to measure the damage and potential for instability of structural components (Vamvatsikos and Cornell 2002). The IDA curves are then produced by interpolating between the measured values of intensity versus damage, and then PBEE can be applied by defining the desired limit states at specified ground motion intensities and using the curves to determine how often the chosen limit state is exceeded.

The major limitation of IDA is the heavy computational demand of the analysis. Due to the high number of analyses that need to be run to produce the IDA curves, this method may not be reasonable for some applications that require a method with minimal computational requirement. There is also a significant amount of subjectivity when it comes to determining the appropriate ground motions, intensity measures and damage measures. Choosing different ground motions can have significant effects on the results (showing high variability on the response), and choosing incorrect measures may provide results that do not clearly describe the most critical behavior of the system (Villaverde 2007).

### *2.2.3 Applications of Incremental Dynamic Analysis*

Despite potential limitations, numerous successful applications of traditional IDA have been studied and presented. Many examples of these applications came from research performed at Virginia Polytechnic Institute and State University. Early research was performed on steel moment frames with viscous fluid dampers that used IDA to investigate the effect of different types of dampers in the system (Oesterle 2003). This study used 12 earthquakes, half of which were near fault earthquakes and half of which were far-field earthquakes measured in Los Angeles, scaled to twenty different intensities. The damage measures included interstory drift

ratios, base shears and residual deformations, and the IDA curves were used to determine behavior changes of different damper types.

The following year, IDA was used at Virginia Tech to investigate the behavior of structures with hyperelastic braces (Saunders 2004) and to investigate behavior of low-rise buildings in the Western United States versus the Central and Eastern United States (Spears 2004). The study by Saunders explored the behavior of hyperelastic elements, which were defined as nonlinear elastic members that gain stiffness as they are deformed and are beneficial to the structure primarily near instability. IDA curves were developed using two different scaled earthquakes and two different P-delta scenarios, using interstory drift and base shear as damage measures. The study by Spears (2004) investigated whether buildings in Central and Eastern United States were more susceptible to collapse as associated with vertical accelerations than the structures in the Western United States. The study used five different locations for each with varying periods and used IDA to determine the post yield stiffness ratio of each scenario. This research found that structures in the Central and Eastern United States designed to code were more prone to sudden collapse that structures designed to code in the Western United States.

Another thesis from Virginia Tech studied the behavior of hybrid steel moment frames, which considered combinations of ordinary, intermediate and special moment frame connection in the same structure (Atlayan 2008). For this work, the base intensity measure used was the 5 percent damped ASCE 7 design spectral acceleration for the period at the first mode of vibration. Ten sets of ground motion data were used in this research, each of which was scaled to match the ASCE 7 design spectrum. They were each then scaled 10 more times with scale factors ranging from 0.2 to 2.0, which means that the structure was analyzed up to two times the ASCE design strength. For the damage measures, interstory drift, base shear, and maximum and residual roof displacement were investigated. The focus of the results was determining the potential that the structure would exceed ASCE 7 drift limits and what the probability of collapse was of the system under the varying loads. For the hybrid steel systems, the damages measures were maximum and residual roof displacements, peak base shear, and ductility demand, and the focus of the analysis was to determine improvements that were given by using a hybrid moment frame over a traditional one.

An additional hybrid moment frame was investigated at Virginia Tech using IDA, but with this one focusing on the addition of hybrid passive control devices (Marshall 2008). These hybrid passive control devices combined two different passive control devices: one that helps dissipate energy at all deformations (a viscoelastic damper) and one that only engages to dissipate energy under heavy loading (a buckling restrained brace). To perform IDA on these systems, multiple earthquakes were scaled 8 times, including a scale factor of 1.0 to represent the design basis earthquake and another scale factor of 1.5 to represent the maximum considered earthquake.

Multiple damage measures were used to determine overall behavior of the systems, including the maximum roof drifts, base shears and roof accelerations.

Another group of researchers used IDA to investigate the behavior of wood-framed buildings under seismic loads (Christovasilis et al. 2009). The motivation for this research came from the significant property loss and loss of life from damage to wood-framed structures in both the 1994 Northridge earthquake and the 1995 Kobe earthquake. Due to the short height of the structures investigated in this study, the intensity measure used was based on a set of ground motions scaled to the median spectral acceleration analyzed at a period equal to 0.2 seconds. The set of ground motions consisted of the 22 bi-directional records used in the FEMA P-695 project (FEMA 2009a). The prominent mode of failure investigated in this research was global side sway, which was quantified using a damage measure of peak interstory drift along any wall line. The probability of collapse was determined by how many ground motions caused the structure to exceed the predetermined drift limit with respect to how many ground motions were analyzed, and fragility curves were produced to show the relationship between intensity and probability of failure.

Further research has also been performed on steel moment frames using IDA to determine the differences between ordinary, intermediate and special moment frames (Asgarian et al. 2010). In light of the failure of welded moment frames in the 1994 Northridge earthquake, part of this research focused on the modeling of the beam column connections, which are especially crucial during inelastic behavior. OpenSEES (McKenna 2011) was the program used to analyze the system, including these carefully modeled connections. Three five-story and two ten-story buildings were used in the analysis, and 15 ground motion records were used for the analysis. Similar to the works performed by Vamvatsikos (2002) and Atlayan (2008), the damage measure was chosen to be the maximum interstory drift ratio, and the intensity measure was the 5 percent damped spectral acceleration associated with the first mode. Once again, IDA proved to be a beneficial tool for analysis and comparison of systems for more than just life safety limit states.

A similar study (Medina and Krawinkler 2005) investigated the behavior of non-deteriorating seismic-resisting frames under seismic loads including the influence from P-delta effects. The height of the buildings varied from three to eighteen stories, and each height was analyzed at two different periods: 0.1N and 0.2N, where N equals the number of stories. Forty ground motion records were used, and they all were California earthquakes that were not measured at near fault locations. Again, drift values, both peak roof and interstory, were the chosen damage measure, and IDA curves were created for these parameters.

An example of the “variation of parameter” IDA can be found in a study by Dolsek (2009). A four-story reinforced concrete building was used to examine the effect of these variations

including mass between stories, strength of the materials, damping and modeling of the plastic hinge regions. Fourteen sets of ground motions were used, and multiple models were analyzed to investigate the effects of these modeling variations, as well as the effects of sample size. The study determined that a sample size of twenty structures was adequate for this analysis, and that increasing the sample size beyond that does not significantly change the results. The intensity measure used was the peak ground acceleration, and the damage measure of maximum drift was used to quantify the influence of the modeling uncertainties listed previously. The study found that the extended IDA did not differ much from the traditional IDA in the stages far from collapse; however, there was a noticeable reduction in collapse capacity for some of the modeling uncertainties. The uncertainties that had the greatest effect were the ones that contributed to the failure mechanism, including initial stiffness and rotation in plastic hinge regions. While this additional aspect of IDA may produce more conservative results for life safety limit states, the additional computational time and computing power necessary to run such analysis should be taken into consideration.

IDA has also been used to evaluate the effectiveness of current and past codes to design seismic resisting systems. There have been numerous studies where both new and existing structures were investigated in high and low seismic area in the United States. In one example, several reinforced concrete structures conforming to different code editions with varying seismic-resisting systems were analyzed using IDA (Liel et al. 2006). Using 22 sets of ground motion with two components each, curves were plotted to predict the probability of collapse with respect to the ground motion acceleration. While the research showed that current codes provide better resistance to seismic loads than previous codes, it found that there was still work to be done to account for variability in the design and loading of seismic-resistant systems.

Similar analyses have been performed for steel moment frames with a focus on the differences in code provisions before and after the 1994 Northridge earthquake (Yun et al. 2002). As a result of this earthquake, there were noticeable problems with the design of moment frames, which spurred a revamping of the code requirements of these systems. IDA using 20 ground motions and a damage measure of interstory drifts found nearly identical results to the study on reinforced concrete resisting systems by Liel et al. (2006). Both studies determined that systems designed to newer codes have a much lower probability of collapse, but that variability in loading and behavior provide a difficulty in dynamic analysis.

Another interesting example of the use of IDA has been to use the procedure to quantify the residual capacity in a structure after the earthquake and determine the probability of collapse due to an aftershock (Luco et al. 2004). While all the other examples have investigated the behavior of initially undamaged structures that are subjected to earthquakes for the first time, this study takes it one step further to determine the likely behavior of buildings that were damaged during a

previous earthquake, and then subjected to an aftershock. After an earthquake occurs, many standing structures will not be safe to occupy and will need to be kept vacant. To realistically determine if this is a necessity, nonlinear dynamic analysis should be performed, but in the critical time after an earthquake, this would often not be a possibility. This study presents a case study that analyzes the structure both during the earthquake and during an aftershock to determine the residual capacity the building could have using IDA. Performing an analysis of this nature before an earthquake even occurs could provide valuable information about the probable condition of the building, which would then be available immediately after the earthquake. Accuracy in determining residual capacity is critical to understanding both potential life safety and down-time losses of the structure after the event. In the case study, IDA curves were provided for the peak displacement for sequences of accelerations from main shocks followed by aftershocks.

While the vast majority of examples of IDA have been performed in two dimensions (2D), the process can be expanded to three dimensions (3D). Analyzing a structure in 3D is necessary for structures that are not symmetric and require the scaling of two components of ground motion. Analysis using two ground motions together to determine response is the major difference in 3D analysis, an example of which was investigated for a 20-story steel space frame (Vamvatsikos 2006). Another example of this application of 3D IDA analysis was a circular prestressed bridge (Vamvatsikos and Sigalas 2005). Special care was taken when selecting the intensity measures and damage measures to ensure that the analysis would accurately represent the structural response in both directions, as different parameters would control the maximum response in each direction and the governing case needs to be predicted. Twenty-two ground motions were used, and they were applied to system using the two orthogonal ground components applied simultaneously.

Incremental Dynamic Analysis has become increasingly popular due to its use in the FEMA P-695 Methodology (FEMA 2009a). This methodology was been developed to "provide a rational basis for establishing global seismic performance factors, including the response modification coefficient ($R$), the system over-strength factor ($\Omega_0$), and the deflection amplification factor ($C_d$) of new seismic-force-resisting systems proposed for inclusion in model building codes" (FEMA 2009a). In this procedure, Incremental Dynamic Analysis is performed using a suite of 44 or 56 ground motions components that are incrementally scaled until structural collapse occurs. This methodology has become widely used in the earthquake engineering research community, and numerous examples of this procedure can be found, many of which are compiled in the ATC-76 report (NIST 2010a). As an example, Figure 2-2 shows the IDA results of the FEMA P-695 procedure applied to a seven-story steel moment frame that included the modeling of the lateral resistance of the gravity system (Flores et al. 2012).

### *2.2.4. Alternative Methods to Incremental Dynamic Analyses*

#### *2.2.4.1. Comparison to Nonlinear Static Pushover Analysis*

Simplified methods, including nonlinear pushover analysis, have been used as an alternative to Incremental Dynamic Analysis, as they provide a method that is considerably less computationally demanding. However, IDA provides significantly more insight into the inelastic behavior of a structure, particularly its behavior near collapse. The major limitation of this simplified method is that static pushover analyses do not usually take into account the change in modal properties that occurs when a structure is deformed inelastically under seismic loads. When comparing the results of IDA and pushover analysis, it has been shown that they correspond well in the linear range of the structural behavior, although, after yield, the two methodologies produce different results. While static pushover analysis can provide accurate results for the sequencing of yielding or failure in more ductile systems, this method does not include higher modes and can easily become inaccurate during inelastic behavior (Antoniou and Pinho 2004). The static pushover method determines the "capacity" of a given structure, but does not inherently consider the "demand" of a potential seismic event. Because both are needed to accurately design a structure, dynamic analysis does seem to be a necessary computational tool (Elnashai 2002).

IDA provides an alternative method to the traditional static pushover analysis that does not have the same shortcomings regarding the inelastic range and higher modes. The results from the IDA will generally follow an extrapolation of the static pushover results using the equal displacement concept up until hardening occurs. Work has been done (Vamvatsikos 2002) to produce IDA type curves using static pushover analysis, which simplifies the analysis. While the concept of IDA provides more accurate, in-depth results, it was shown that the static pushover test can create approximate curves with significantly less computational need.

This idea that pushover tests can be sufficient in analysis of structures under seismic events was further investigated (Han and Chopra 2006). The study by Vamvatsikos (2002) only investigated a nine-story steel moment frame system, but this newer research used three buildings varying in height that included a three-story, nine-story and twenty-story building. Results were similar to that of the Vamvatsikos study and stated that a modal pushover analysis (MPA) could be an appropriate simplified method of analysis to create fragility curves without the use of response history analysis. According to the results of this study, the accuracy did not vary between the buildings of varying height, although the dynamic analysis became more involved, and the pushover method of analysis produced accurate behavior even up through instability and collapse as long as a proper hysteretic model was chosen to represent the modal behavior.

Another study comparing IDA to pushover analysis investigated reinforced concrete structures (Mwafy and Elnashai 2001). Twelve reinforced concrete frames of varying height and structural

system were used in the analysis. This research found that the two methods have similar results in the elastic regions, and although they often vary after yield, the pushover method provides a conservative analysis, when compare to the Incremental Dynamic Analyses. This study also concludes that pushover analysis appears to be a good approximation for IDA results, particularly in the elastic region (even though the elastic range rarely provides the information desired from an IDA), and could be an applicable alternative, especially in a real-world design scenario where simplicity in analysis is highly preferred.

However, research has been performed that disagrees with this conclusion. In a literature review (Villaverde 2007) discussing multiple methods to analyze collapse of buildings, numerous studies were found that analyzed the steel moment frames designed prior to the 1994 Northridge earthquake with both static pushover and non-linear dynamic analyses, like IDA. In these studies, the results of the methods differed greatly, and they found that the pushover tests actually calculated drifts that were un-conservative and predicted the incorrect locations of yielding regions. This same literature review states that these problems can arise in a pushover test because "it neglects duration and cyclic effects, the progressive changes in the dynamic properties that take place in a structure as it experiences yielding and unloading during an earthquake, the fact that nonlinear structural behavior is load-path dependent, and the fact that the deformation demands depend on ground motion characteristics."

*2.2.4.2. Additional Alternative Methods of Incremental Dynamic Analysis*

Other methods have been introduced that provide alternatives to IDA. One such method that has been presented is the Endurance Time Method (Estekanchi et al. 2004). The basis of this method is determining how long a structure can remain stable under certain dynamic loading; in other word, what is the structure's endurance? Accelerations are applied to the structure in a ramp type loading, so the method determines how long the structure will be able to withstand this increasing loading. The longer the structure stays standing, the better the performance. Endurance limit points are specified to desired levels of performance, and the endurance time is the length of time it takes to reach the specified limit points. Similar to IDA, these limit points will be based on physical behavior like drift and accelerations in the structure and need to be chosen based on relevance to the structure that is being investigated. Like any method of dynamic analysis, determining appropriate dynamic simulation and performance of the collapse analysis can prove to be a hindrance in this type of method.

Another method that has been presented as an alternative to IDA is probabilistic seismic demand analysis (Mackie and Stojadinovic 2002). As opposed to IDA, which selects a set of earthquakes and scales them to different intensities, the probabilistic seismic demand analysis (PSDA) uses a large set of earthquake data that inherently incorporates a range of intensities. The main difference in the two methods is that PSDA uses the "bin strategy," which uses a large number of

earthquake records in analysis and subdivides them according to magnitude, distance and soil type. IDA, on the other hand, relies on a small number of records that are scaled multiple times to imitate other potential earthquake records. In the Mackie and Stojadinovic study, both the IDA and the PSDA are run 80 times; the PSDA did so using four bins of 20 earthquakes, while the IDA used four ground motions scaled 20 times. If behavior with respect to intensity is not the only concern, PSDA can be a more informative method, as it also provides information response at different distances and on different soil types. However, this study shows that with careful selection of the earthquake records for IDA, the two methods can be used interchangeably. The same information can be determined in IDA, but the smaller batch of earthquakes chosen must have necessary variation.

One last method that will be discussed in this paper is a method that combines pushover analysis with aspects of Incremental Dynamic Analysis to provide a more computationally efficient method (Liel and Tuwair 2010). In this method, an initial nonlinear static pushover test is performed to find an initial estimation of median spectral acceleration of the collapse resistance of the structure, and numerous methods are proposed to estimate this parameter from a pushover analysis. The suite of ground motions selected to analyze the building are then scaled to this acceleration, and analysis is run. If this spectral acceleration does not equal the median acceleration (half of the analyses result in collapse), the acceleration is iterated and the analysis repeated until it does reach the median acceleration.

An advantage of the Leil and Tuwair method is the reduction in the number of ground motions required for subsequent analysis. Once a ground motion is known to cause a collapse at a certain intensity, it is assumed that it would cause collapse under stronger ground motions and can be eliminated in iterations if the initial median acceleration value was found to be too small. The opposite holds true if the initial value should be decreased; ground motions that did not cause collapse can be ignored for weaker ground motions. The computation saved by having an initial estimate from pushover analysis and reducing ground motions used in subsequent runs decreases run times by approximately 90 percent and provides answers within 8 percent of the answers from Incremental Dynamic Analysis of the same structures.

## 2.3. Fragility Curves

### *2.3.1. Introduction to Fragility Curves*

Fragility curves provide a method to summarize the results of numerous dynamic analyses (like IDA) from a probabilistic perspective. A fragility curve, in the most simple terms, is a statistical distribution that can describe the probability of any occurrence, whether that occurrence is collapse or minor structural damage or something in between. Fragility curves are developed by defining an engineering demand parameter (EDP) and a damage measure (DM), which are recorded during numerous dynamic analyses. The fragility curve provides the probability of

exceeding a certain damage limit state, given as a value of the DM, with respect to the EDP (Porter et al. 2007).

### *2.3.2. Relationship between IDA and Fragility Curves*

Incremental Dynamic Analysis is a popular tool used for dynamic assessment of structures and the application of Performance Based Earthquake Engineering, and it is more prevalently used than any of the alternative methods. However, IDA provides an extensive set of structural response results, which needs to be summarized to be practical for engineers and researchers. Fragility curves provide a method to summarize these results from a probabilistic perspective. As mentioned previously, fragility curves show the probability of exceeding any limit state, which is typically defined by a damage measure or intensity measure recorded during the Incremental Dynamic Analyses. The development and application of fragility curves is discussed in the remainder of this section, including the procedure to develop fragility curves from IDA results. In order to begin the discussion on fragility curves, however, review of basic statistics is needed, which is provided in the next section.

### *2.3.3. Background on Necessary Statistics*

To develop the necessary statistical tools, two textbooks were consulted (Ang and Tang 2007, Ott and Longnecker 2010), and all the equations and discussion for the remainder of this section were from these sources.

#### *2.3.3.1. Mean and Standard Deviation*

The first step in statistics that is necessary to develop fragility curves is to define the mean and standard deviation of a set of data with *n* number of data points, with the data points represented as $x_n$. This data set could be anything of interest to the user. For example, the data set could define the lateral deformations in racking tests of drywall that correlate with the first observations of cracking, or it could contain the acceleration values where each individual ground motion caused collapse of a structure during a P-695 analysis. Any set of results can be summarized in a fragility curve by finding some key statistical properties, including the mean and standard deviation. The mean, $\mu$, is the average of the data, and the standard deviation of the population, σ, is a measure of the variability or spread of the entire data set. The equations for these two variables are shown below in Equation 2-1 and Equation 2-2, respectively.

$$\mu = \frac{1}{n}\sum x_n \tag{2-1}$$

$$\sigma^2 = \frac{1}{n}\sum (x_n - \mu)^2 \tag{2-2}$$

These two parameters become the basis for developing the distributions that will be discussed later in this section.

*2.3.3.2. Probability Density Functions and Cumulative Distribution Functions*

A probability density function (PDF) represents the frequency of occurrence of a value in a set of random variables. The total area under a PDF is always equal to 1.0, and the probability that a random variable is between two values is the integral under the PDF between those two values, as shown in Equation 2-3. By integrating under the entire area of a PDF, a cumulative distribution function (CDF) is developed, which shows the probability of occurrence of a random variable. These curves approach zero for -∞ and 1 for +∞, and the probability of occurrence that a random variable is less than or equal to a value of interest is shown below in Equation 2-4.

$$P(a \leq X \leq b) = \int_a^b f_x(x)dx \tag{2-3}$$

$$P(X \leq x) = F_x(x) = \int_{-\infty}^{x} f_x(x)dx \tag{2-4}$$

where:

| | | |
|---|---|---|
| | $f_x(x)$ | is the equation of the PDF |
| | $F_x(x)$ | is the value of the CDF |
| | $X$ | is the random variable |
| | $x$ | is the value of interest |

Figure 2-3 shows an example of a PDF (left) and its corresponding CDF (right) for a set of normally distributed randomly generated variables between 1 and 100.

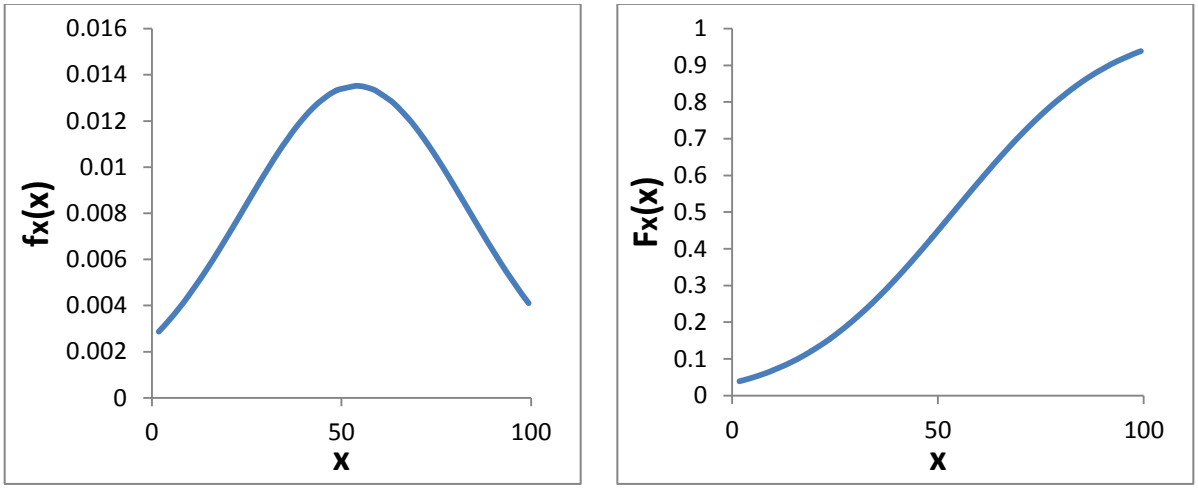


**Figure 2-3.** A probability density function (left) and its corresponding cumulative distribution function (right) of a set of randomly generated numbers

The CDF shows the typical shape of a fragility curve, where for any value of x, the probability of occurrence, $F_x(x)$, can be determined. Traditionally in fragility curves, x will represent the range of the engineering demand parameter, and the CDF will give the probability of occurrence for a value of a limiting damage measure. In order to solve for the CDF, a PDF needs be defined. To do so, one of the numerous statistical distributions can be fit to the set of data. Two of the more popular distributions, normal and lognormal, are discussed next.

*2.3.3.3. Normal distributions*

One potential distribution that can be applied to data is the normal distribution. This distribution assumes x values can be between -∞ and +∞, and the PDF is defined next in Equation 2-5.

$$f_x(x) = N(\mu, \sigma) = \frac{1}{\sigma\sqrt{2\pi}} e^{\left[-\frac{1}{2}\left(\frac{x-\mu}{\sigma}\right)^2\right]} \tag{2-5}$$

where: $N(\mu, \sigma)$ is the normal distribution

*2.3.3.4. Lognormal distributions*

Another potential distribution is the log-normal distribution. This distribution differs from the normal distribution in that it assumes that *x* values can be between 0 and +∞, which makes it a good distribution for data sets consisting only of positive numbers. The PDF for this distribution is defined in Equation 2-6.

$$f_x(x) = N(\lambda, \varsigma) = \frac{1}{\varsigma\sqrt{2\pi}} e^{\left[-\frac{1}{2}\left(\frac{\ln(x)-\lambda}{\varsigma}\right)^2\right]} \tag{2-6}$$

where: $N(\lambda,\zeta)$ is the lognormal distribution
$\lambda$ is the mean of ln(x), the natural log of the data set
$\zeta$ is the standard deviation of ln(x)

*2.3.3.5. Defining distributions in software*

PDFs and CDFs for distributions are easy to build in software programs given a set a data values, and this section is included to give the Microsoft Excel (Microsoft 2010), Mathcad (PTC 2012) and Matlab (Mathworks 2011) commands used to build these functions. This section will focus on the commands to build normal and lognormal distributions, but it is important to note that many other distributions are available in these programs, even though they are not discussed here. The data points should be sorted from smallest to largest value, and then the mean and standard deviation need to be determined for the set of data. The command to find the mean, standard deviation, PDF and CDF for each program is shown in Table 2-1.

**Table 2-1.** Statistical commands in common software programs

| | Excel | Mathcad | Matlab |
|---|---|---|---|
| Mean, $\mu$ | = average(X) | = mean(X) | = mean(X) |
| Std. deviation, $\sigma$ | = stdev(X) | = stdev(X) | = std(X) |
| Normal PDF | = NORM.DIST($x,\mu,\sigma$,false) | = dnorm($x,\mu,\sigma$) | = normpdf($x,\mu,\sigma$) |
| Normal CDF | = NORM.DIST($x,\mu,\sigma$,true) | = pnorm($x,\mu,\sigma$) | = normcdf($x,\mu,\sigma$) |
| Lognormal PDF | N/A | = dlnorm($x,\mu,\sigma$) | = lognpdf($x,\mu,\sigma$) |
| Lognormal CDF | = LOGNORM.DIST($x,\mu,\sigma$) | = plnorm($x,\mu,\sigma$) | = logncdf($x,\mu,\sigma$) |

where: X is the full set of data points in vector form
$x$ is each individual data point

In Excel, the commands are simply typed in the cells, while in Matlab and Mathcad, the commands must be assigned to a variable.

### *2.3.4. Building Fragility Curves*

When a large set of results has been collected, it is important to summarize the results, which can be done using fragility curves. From the perspective of earthquake engineering, these results can come from Incremental Dynamic Analyses, lab tests, or any other method of producing a set of data that describes behavior under dynamic loading. Initially, a measure of the limit state will need to be determined to begin the process of developing a fragility curve. Again, this limit state could be the first observations of cracking in drywall defined by the lateral displacement, or structural collapse defined by the acceleration level, or any other behavior of interest. Once the measure is chosen, it is crucial to note whether it is a numerical measure or an event, because this will determine how the curve is constructed.

If the damage measure is a numerical value, like interstory drift, the fragility curve can be developed using a statistical distribution. For structural response, a lognormal distribution is typically used because the peak absolute value of drift is always positive. For the chosen probability distribution (normal or lognormal), the appropriate mean and standard deviation of the data should be found and used to build the CDF of that distribution. This CDF is the fragility curve that will provide the probability of occurrence of a damage state (e.g. first cracking of drywall) for the range of the numerical damage measure (e.g. interstory drift).

If the damage measure is an event, for example collapse, a different approach is needed to develop the distribution. Instead of using a distribution function, a count will be necessary to build the fragility curve. At each ground motion intensity the number of earthquakes that cause the collapse event to occur will need to be counted. The probability of this event for one intensity of motion will equal the number of occurrences at that intensity divided by the total number of

earthquakes analyzed. This process will be repeated for each intensity, and the fragility curve will plot the probabilities of occurrence with respect to the intensity used in analysis.

### *2.3.5. Application to FEMA P-695*

For this methodology, a collapse fragility curve is built as a cumulative distribution function of a lognormal distribution using the median collapse intensity ($\hat{S}_{CT}$) and a standard deviation value called the record-to-record dispersion ($\beta_{RTR}$). The median collapse spectral acceleration is found during the Incremental Dynamic Analyses as the intensity at which 50 percent of the analyses have caused structural collapsed. Typically, $\beta_{RTR}$ is equal to 0.4, but can be as low as 0.2 for systems with low ductility. The calculation of this value is shown in Equation 7.2 of FEMA P-695 (FEMA 2009a). It is important to note that this differs from traditional lognormal distributions where the mean of the natural log of the data is usually used instead of the natural log of a median value.

The procedure for developing a collapse fragility from a set of P-695 Incremental Dynamic Analyses will be shown for the same example presented in Figure 2-2. Again, these results are for a seven-story steel moment frame that included the modeling of the lateral resistance of the gravity system (Flores et al. 2012). The IDA results are shown again in Figure 2-4, but with additional information. In the FEMA P-695 procedure, the collapse margin ratio (CMR) is defined as the scale factor on the spectral acceleration of the maximum considered earthquake (MCE) at the fundamental period of the structure where half of the ground motions have caused the structure to collapse. In other words, the CMR is the ratio of median collapse intensity ($\hat{S}_{CT}$) to the MCE intensity ($S_{MT}$).

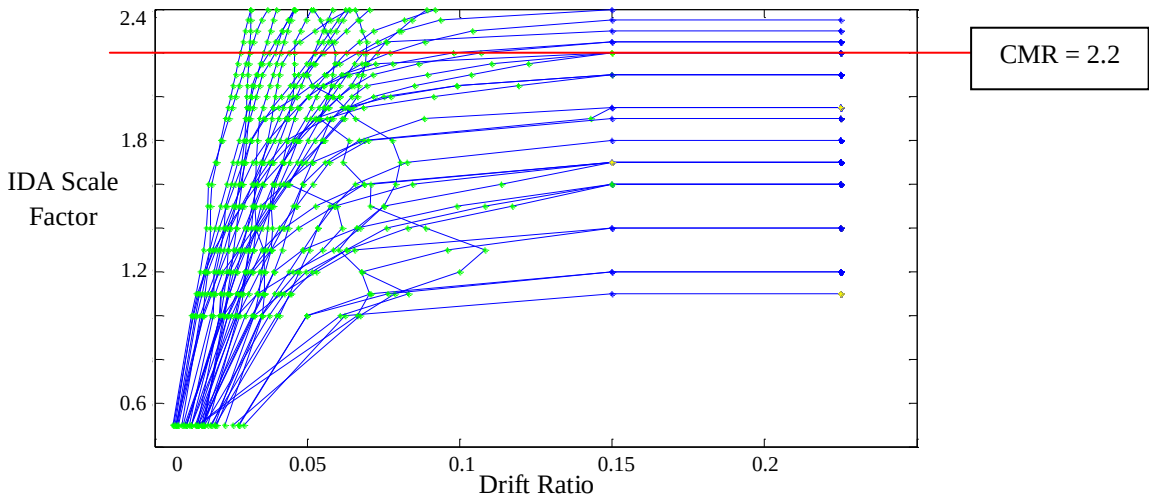


**Figure 2-4.** Example IDA curve with Collapse Margin Ratio shown

For this example, half of the ground motions had caused the structure to collapse by a scale factor of 2.2, which defines the CMR for this structure. This structure had a MCE intensity of 0.5625g, and therefore, the median collapse intensity is 1.2375g. The collapse fragility, shown in Figure 2-5, is then developed using a lognormal distribution defined by the natural log of the median collapse intensity and a record-to-record dispersion of 0.4.

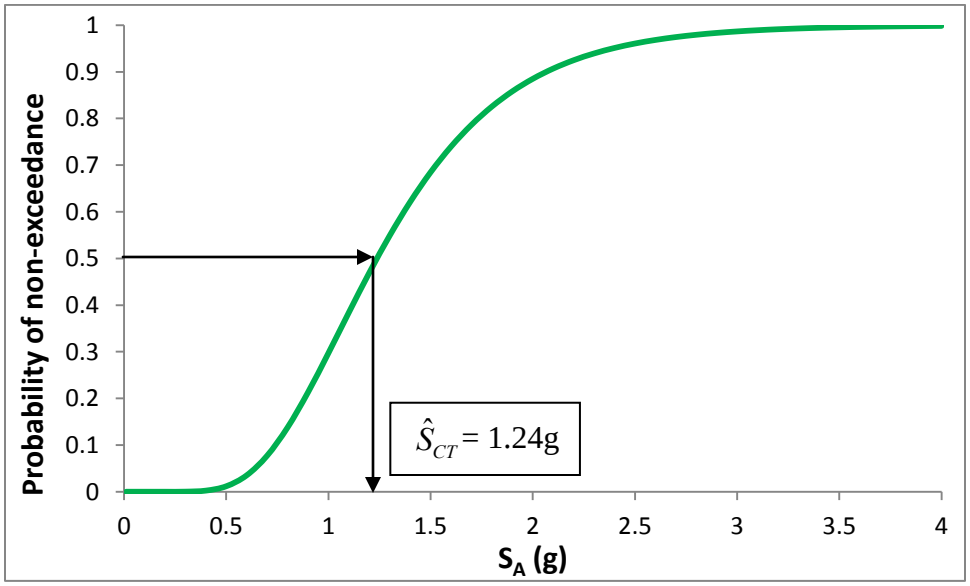


**Figure 2-5.** Example collapse fragility curve

### *2.3.6. Other Examples of Previous Fragility Analysis*

FEMA P-695 type applications are not the sole use for fragility curves in structural engineering. Numerous other research projects have discussed the use and development of fragility curves, many of which will be discussed in this section.

One study investigated the influence of the number of stories on the behavior of an ordinary concrete building (Akkar et al. 2005). This paper found the capacity of typical concrete buildings in Turkey using real data from 32 buildings and subjected them to a suite of 82 ground motions. Peak ground velocity was chosen as the engineering demand parameter, as it was believed to be a better representation of the inelastic behavior, and a displacement-based limit state of global drift was chosen as the damage measure. Fragility curves were made for each building height to plot the probability of exceeding a limit for the chosen limit values of light, moderate and severe drift with respect to the peak ground velocity.

Another study on concrete behavior investigated slab column connections of 82 specimens and used interstory drift and vertical shear ratio limits to define four limit states: light cracking, heavy cracking, punching shear failure, and loss of vertical carrying capacity (Aslani and Miranda 2005). In that study, the fragility functions were developed using a log-normal

distribution of probability of exceedance versus the interstory drift or vertical shear ratio. Concrete moment frames have also been investigated using fragility analysis (Lowes and Li 2010). Seven different moment frames were investigated, and damage levels for three damage states (cracking, spalling and crushing) were correlated to story drift via fragility curves.

These previous three papers showed examples of how fragility curves can be developed when the damage measure was a numerical value. An example of developing fragility curves for an event can be seen in a study on the collapse of structures using varying hysteretic models (Ayoub et al. 2004). Three degradation models were investigated: a bilinear model, a modified Clough model, and a pinching model. The number of analyses that produced a collapse was divided by the total number of analyses to determine the probability of occurrence.

Another system that has been studied was a frame with passive controllers (Cundumi and Laboy 2010). This research investigated 30 concrete frames, some high rise and some low rise buildings that had been augmented with varying additional dampers placed in a variety of configurations, including a diagonal, chevron, lower toggle or upper toggle. This was also an example where the occurrence of an event was used to calculate the fragility. If the structure passed a limit state, a 1 was assigned, otherwise a 0 was assigned to indicate that it had not reached the limit state. The fragility curves for slight, moderate, extensive and complete damage were plotted against the peak ground acceleration by dividing the sum of the assigned numbers by the total analyses.

While Incremental Dynamic Analysis using multiple response history analyses (RHA) is typically used in FEMA P-695 type projects to build fragility curves, alternative methods have been presented. One method used a modal pushover analysis (MPA) that analyzed the structure only once (Han et al. 2010). Two steel moment frames were analyzed using both RHA and MPA to compare the differences in collapse fragilities of structures. This study found that MPA combined with an empirical relationship of collapse strength ratios provided good approximate results.

While FEMA P-695 provides a suite of ground motions for analysis, alternatives can be used to develop the suite of ground motions. One popular alternative is Monte Carlo simulation, which predicts the behavior through random number generation applied to a given probability density function. One such example was applied to a four-story ordinary reinforced concrete moment frame (Korkmaz 2008), which compared the results with a more traditional nonlinear dynamic analysis. This study found comparable results between the Monte Carlo simulation and the traditional response history analysis, although it recommended that more structures and ground motions would be necessary to make a valid comparison between the two.

A relatively new methodology, FEMA P-58 (FEMA 2012), utilizes fragility curves extensively. This procedure uses collapse fragilities, like those developed for FEMA P-695, as well as component fragilities. One of the major goals of this method is to provide results that are meaningful to owners and decision makers (consequences like costs, repairs and casualties). In order to convert structural response to these consequences, the component fragilities are used to show the probability of exceeding discrete damage states with respect to structural response parameters, like drift or acceleration. These discrete limit states have an associated set of consequences, and through the use of a few nonlinear response history analyses and Monte Carlo simulation, the P-58 procedure provides a potential distribution of consequences for any given ground motion or hazard. The fragility curves play a crucial part in connecting structural response to the more meaningful consequences.

Further works have used fragility curves to analyze suspended ceilings (Badillo-Almaraz et al. 2007), light frame wood construction (Ellingwood et al. 2004), wood shearwalls (Kim and Rosowsky 2005), rocking connections (Cimellaro and Roh 2010), and concrete bridges (Karim and Yamazaki 2003, MacKie and Stojadinovic 2007, Moschonas et al. 2009, Saxena et al. 2000). Fragility curves have also been developed to investigate the effects of ground motion duration (Iervolino et al. 2006) and soil-structure interaction due to liquefaction (Koutsourelakis et al. 2002). These studies are mentioned to provide additional resources regarding the uses of fragility curves, but will not be discussed in more detail, because they are of less relevance to this research than previously discussed examples and do not provide any additional, unique information regarding the development and use of these curves.

With any fragility curve, there is uncertainty that can be accounted for. Initially, there are uncertainties involved with the chosen distribution, and a measure of the goodness of fit should be performed. Examples and applications of this have been discussed, including in studies on slab column connections and on bridge damage from the 1995 Kobe earthquake (Aslani and Miranda 2005, Shinozuka et al. 2000). There is also uncertainty involved in the behavior of the structure in analysis. Two types of these uncertainties are discussed in Zareian and Krawinkler (2007). Aleatory uncertainties come from natural randomness, which in this study was from record-to-record variation of the ground motion. Epistemic uncertainty, on the other hand, comes from inaccurate representation of the structure and the idealization of the model. Both can cause large variations in results, and the Zareian and Krawinkler study provides a method to find the effects of these uncertainties by determining the confidence of the fragility curve and adjusting the curves to account for highly spread confidences.

Studies have also been performed to identify which damage measures and engineering demand parameters are best to use to determine the inelastic behavior of structures. One such study investigated structures with energy-dissipating devices and found the behavior with damage

measures of story drifts, maximum column moments and axial force in bracings analyzed with respect to engineering demand parameters of peak ground acceleration, peak ground velocity, spectral pseudo velocity and spectral pseudo acceleration (Dimova and Elenas 2002). This paper provided a general procedure to determine which parameters provide the most accurate and insightful results, and examples of this procedure were given for four structural systems analyzed with combinations of the damages measures and demand parameters listed above.

### *2.3.7. Goodness of Fit Tests*

If a statistical distribution is fit to the data, a goodness of fit test is needed to determine how accurate the assumed distribution fits that data. There are numerous goodness of fit tests available, three of which will be discussed in this section.

#### *2.3.7.1. Chi Square Test*

The Chi Squared test is a goodness of fit test for a PDF where the observed frequency, $n_i$, for a given interval is compared against the theoretical frequency, $e_i$, where $i$ ranges from 1 to the number of intervals, $k$ (Ang and Tang 2007). The assumed distribution is acceptable at the analyzed significance level if:

$$\sum_{i=1}^{k} \frac{(n_i - e_i)^2}{e_i} < c_{1-\alpha,f} \tag{2-7}$$

where: $c_{1-\alpha,f}$ is the value of the $\chi^2$ distribution
$\alpha$ is the significance level
$f$ is the degree of freedom = k-1

The assumptions for this test are that $k$ must be greater than or equal to 5, and the values of $e_i$ must also be greater than 5. Since the method is used for PDFs, this one is not applicable to typical fragility curves, which are CDFs.

#### *2.3.7.2. Kolmogorov-Smirov (K-S) Test*

The K-S test is a goodness of fit test to compare test data with the CDF of the desired distribution. To test the fit, a stepwise distribution, $S_n(x)$, is developed as follows:

$$\begin{aligned} S_n(x) &= 0 && x \le x_1 \\ &= \frac{k}{n} && x_k \le x \le x_{k+1} \\ &= 1 && x \ge x_n \end{aligned} \tag{2-8}$$

where: $x_k$ are the values of the data set listed from low to high
$n$ is the sample size

The maximum difference between this function and the CDF of the assumed distribution, $F_x(x)$, is determined using Equation 2-9. The upper limit is calculated as $D_n{}^{\alpha}$, which is tabulated in Table A.5 of Ang and Tang (2007) and is dependent on $\alpha$.

$$D_n = max|F_x(x) - S_n(x)| \tag{2-9}$$

The assumed distribution is acceptable at the analyzed significance level if:

$$D_n < D_n{}^{\alpha} \tag{2-10}$$

*2.3.7.3. The Anderson-Darling (A-D) Test*

As opposed to the K-S test, the A-D test puts more weight on the tails of the distribution, which can be helpful to determine the influence of outliers. The data is listed from low to high, where *i* ranges from 1 to *n*, with n being the sample size. The CDF is then evaluated at each data point using the desired distribution, $F_x(x_i)$. The A-D statistic, $A^2$, is determined as shown in Equation 2-11, and the adjusted A-D, $A^*$, statistics is calculated as shown in Equation 2-12.

$$A^2 = -\sum_{i=1}^{n}\left[\frac{(2i-1)\{ln[F_x(x_i)]+\ln[1-F_x(x_{n+1-i})]\}}{n}\right] - n \tag{2-11}$$

$$A^* = A^n\left(1.0 + \frac{0.75}{n} + \frac{2.25}{n^2}\right) \tag{2-12}$$

The next step is to calculate the critical value, $c_\alpha$, which depends on the desired distribution. For the normal and lognormal distributions, $c_\alpha$ is determined as:

$$c_\alpha = a_\alpha\left(1.0 + \frac{b_0}{n} + \frac{b_1}{n^2}\right) \tag{2-13}$$

where: $a_\alpha$, $b_0$, $b_1$ are tabulated values (Ang and Tang 2007)

The assumed distribution is acceptable at the analyzed significance level if:

$$A^* < c_\alpha \tag{2-14}$$

The assumption for this test is that the sample size, *n*, is larger than 7. Like the other two tests, the result also depends on the significance level, making all three tests subjective.

*2.3.7.4. An example of the K-S and A-D test*

Since these two tests check the validity of the CDFs of a chosen distribution, they will both be used to determine the acceptability of fitting a normal distribution to the data used for the standard fragility curve in the previous section. Using a significance level of 0.05, the critical values for both tests are determined and shown in Table 2-2 for the K-S test and Table 2-3 for the A-D test. For the A-D test, $a_\alpha$, $b_0$ and $b_1$ were calculated as 0.7514, -0.795 and -0.89, respectively.

**Table 2-2.** Results for K-S Test

| x | $S_n(x)$ | $F_x(x)$ | $D_x$ |
|---|---|---|---|
| 1 | 0.000 | 0.000 | 0.000 |
| 2 | 0.143 | 0.029 | 0.114 |
| 3 | 0.214 | 0.331 | 0.117 |
| 4 | 0.286 | 0.517 | 0.231 |
| 5 | 0.357 | 0.526 | 0.169 |
| 6 | 0.429 | 0.527 | 0.098 |
| 7 | 0.500 | 0.530 | 0.030 |
| 8 | 0.571 | 0.562 | 0.009 |
| 9 | 0.643 | 0.602 | 0.041 |
| 10 | 0.714 | 0.634 | 0.080 |
| 11 | 0.786 | 0.653 | 0.133 |
| 12 | 0.857 | 0.698 | 0.160 |
| 13 | 0.929 | 0.735 | 0.194 |
| 14 | 1.000 | 0.972 | 0.028 |

| | |
|---|---|
| $D_n = \max(D_x) =$ | 0.231 |
| $D_n^{\alpha} =$ | 0.29 |

**Table 2-3.** Results from the A-D test

| i | $F_x(x)$ | $A^2_i$ |
|---|---|---|
| 1 | 0.029 | 0.546 |
| 2 | 0.331 | 0.562 |
| 3 | 0.517 | 0.714 |
| 4 | 0.526 | 0.916 |
| 5 | 0.527 | 1.141 |
| 6 | 0.530 | 1.317 |
| 7 | 0.562 | 1.402 |
| 8 | 0.602 | 1.456 |
| 9 | 0.634 | 1.573 |
| 10 | 0.653 | 1.714 |
| 11 | 0.698 | 1.758 |
| 12 | 0.735 | 1.256 |
| 13 | 0.972 | 0.112 |
| | sum = | 14.466 |

| | |
|---|---|
| $A^2 =$ | 1.466 |
| $A^* =$ | 1.570 |
| $c_\alpha =$ | 0.701 |

For the K-S test, the chosen distribution was acceptable, because $D_n < D_n^{\alpha}$. However, this distribution was not acceptable for the A-D test, since $A^* > c_{\alpha}$. Given these results, the A-D test is more conservative for tests where outliers may be an issue. It is also important to note that the results could change as $\alpha$ changes, leaving these tests subjective.

### *2.3.8. Integrating Fragility with Seismic Hazard Curves*

While fragility curves give a good estimate of the probability of occurrence of a damage state for a given structure, it does not give any information about the location and seismic hazard of the structure. In order to integrate the fragility curves and seismic hazard curves, conditional probability is used (Ellingwood and Kinali 2009). Conditional probability takes the probability of exceeding a limit state given an intensity measure, IM, and multiplies it by the probability of exceeding that intensity. The probability of exceeding a limit state given an intensity, IM, is the fragility, and the probability of exceeding that intensity for a given site is the hazard.

This integration provides information for the determination of risk, which is defined as the probability that the loss will occur to humans or structures (McGuire 2004). In order to calculate risk, which is typically quantified in terms loss, casualties or repair costs associated with the damage, the specific hazards need to be combined with the fragility information for a structure in the same area. This integration provides the probability of reaching a given damage measure or intensity for a specific location, which can then be transformed into a measure of risk. For a fragility curve developed for an engineering design parameter (EDP), the equation to integrate the fragility with the hazard is shown in Equation 2-15 (Bozorgnia and Bertero 2004).

$$\lambda_{EDP}(y) = \int P(EDP \geq y | IM = x) d\lambda_{IM}(x) \tag{2-15}$$

where:

| | |
|---|---|
| $\lambda_{EDP}(y)$ | frequency that EDP exceeds the value y in a given time |
| $P(EDP \geq y \mid IM = x)$ | probability that EDP exceeds y if IM equals x (fragility) |
| $\lambda_{IM}(x)$ | frequency of IM exceeding x in the same time (hazard) |

Seismic hazard curves can be found on the United States Geological Survey (USGS) website for a given latitude and longitude. These hazards will give the probability of exceedence for an acceleration intensity at the locations. Intensities are also given in terms of the percent chance of failure in 50 years. Given these hazard values, the fragility curves of a damage measure at a given intensity can be integrated.

## 2.4. Background on ASCE 7 Nonlinear Dynamic Analysis Procedure

### *2.4.1. Methodology*

Chapter 16 of ASCE 7-10 (ASCE 2010), which is currently the most recent version of *ASCE7 Standard Minimum Design Loads for Buildings and Other Structures*, describes the process for response history analysis. It provides an option for linear response history analysis; however, this is not of interest to this research and will not be discussed. The nonlinear response history analysis requires that a model be created to capture all nonlinear behavior of the structure. The modeling requirements state that the hysteretic behavior must account for any yielding, strength and stiffness degradation and pinching. The strength of the elements must be the expected strength and should consider over-strength, strain hardening and degradation. The model should include a fixed base or appropriate soil-structure interaction. Two-dimensional modeling is only permitted for systems with independent, orthogonal resisting systems.

This mathematical model is then analyzed with 3 to 7 ground motions scaled to the design spectrum for the design base earthquake (DBE). The design spectrum assumes an intensity-based assessment, which means the analysis is performed for one level of potential intensity, which is the DBE in this case. These ground motions should match in magnitude, fault distance and source mechanisms of the maximum considered earthquake (MCE), and simulated ground motions can be used. The building must be analyzed with these ground motions, as well as the dead load and at least 25 percent of the live load.

This scaling process requires that a SRSS spectrum is created for the 5 percent damped response spectrum of the components of the ground motion pairs. The average of all the SRSS spectra must not be less than the design response spectrum between 0.2*T and 1.5*T, where T is the fundamental period of the structure. If the site is within three miles of an active fault, the average of the fault normal component spectra should not be less than the design spectrum for the same range.

If at least seven ground motions are used in the analysis, the design values for the member forces, inelastic deformations and story drifts can be taken as the average of the results from the ground motions. If less than seven ground motions are used, the design values must be taken as the maximum values from the analyses. The member deformations must be less than two-thirds of the value that causes loss of load carrying capability, and story drift must be less than 125 percent of the story drift limit, which are defined in section 12.12.1 of ASCE 7-10.

### *2.4.2. Current Implementation*

ASCE7-10 has been adopted as the document used in the 2012 International Building Code (IBC) and the 2012 International Residential Code (IRC) for their structural provisions. A

change in philosophy has occurred since the release of this methodology, which has prompted the proposed changes to the ASCE 7, which are discussed in the next section.

### *2.4.3. BSSC Proposed Updates*

The Building Seismic Safety Council Response History Analysis Issue Team (BSSC RHA IT) has proposed changes for the next update of ASCE 7 (Haselton et al. anticipated). These proposed changes will be the focus of the ASCE 7 section of this research. Initially, the ground motion level has been proposed to be the maximum considered earthquake, instead of the design-based earthquake. Two options will be proposed for the design spectrum: the traditional code-based spectrum or one or more scenario-based spectrum.

A suite of eleven ground motions is proposed for the minimum number of records, and vertical components would now be allowed for analysis. The chosen ground motions should have a spectrum that closely matches the design spectrum, and simulated ground motions would be acceptable to fill any gaps in ground motion data. Spectral matched ground motions would be accepted with an implicit penalty from the scaling procedure. The BSSC also proposes the requirements that ground motions for near fault sites should include near site effects, including fault rupture directionality and velocity pulses, when necessary.

For the scaling of the three-dimensional ground motions, the task force proposes that the maximum direction component of the ground motion records be used, instead of the square root of the sum of the squares (SRSS). The average of these maximum direction spectra must match the design spectra as closely as possible and can never be less than 90 percent of the design spectrum between the period range of interest. For spectrum matched ground motions, single components would be used, and the average spectra of these components must never be less than the design spectrum between the period range of interest.

Modeling requirements stay similar, although a few additions are proposed. Elements that are shown to stay linear can be modeled as linear elements (force controlled elements), effective additional model damping or viscous damping must not exceed 3 percent, and buildings with foundations should have structural models that extend to the foundation level, which is where the ground motions should be applied. Additionally, two-dimensional modeling will not be allowed. Accidental torsion is ignored.

The suggested acceptance criteria have also been changed for the update. The number of dynamic instabilities or severe convergence issues is limited based on rick category. The mean story drift ratio should not exceed two times the drift limits in Table 12.12-1. Local acceptance criteria will also be provided, depending on whether the element in force-controlled or deformation-controlled.

Additionally, the design of the structure should meet the strength requirements in Chapter 12, but a few exceptions are allowed. Primarily, for Risk Category I, II, and III structures, the drift limits of Section 12.12.1 do not apply. For Risk Category IV structures, the drift limits are taken as 125 percent of those drift limits. Also, the overstrength factor, $\Omega_0$, can equal 1.0 for the seismic load effects of Section 12.4.3, and the redundancy factor, $\rho$, can also equal 1.0.

This methodology attempts to implicitly satisfy a 10 percent probability of collapse for Risk Category I or II structures under the $MCE_R$. For Risk Category III and IV structures, that maximum probability of collapse drops to 6 percent and 3 percent, respectively. The idea is that if all the criteria are barely satisfied, the building will not exceed the specified percent probability of collapse under the $MCE_R$ level ground motion. The building does not directly determine the probability of collapse, but assumes that this limit will be satisfied if all the other criteria are satisfied. The P-695 methodology, on the other hand, explicitly investigates the probability of collapse. This methodology is discussed in the next section, but performing both methodologies on the same structure will help investigate the accuracy of this implicit assumption of the proposed ASCE7 updates.

## 2.5. Background on FEMA P-695 Procedure

### *2.5.1. Full P-695 Methodology*

FEMA P-695 provides a methodology for determining probabilities of collapse of structures, as well as their seismic performance factors used in design, including the response modification coefficient, $R$, the overstrength factor, $\Omega_0$, and the deflection amplification factor, $C_d$ (FEMA 2009a). For this research, the application of this methodology will focus on the determination of the median collapse intensity. There are two variations of the methodology: a standard methodology (that is typically performed on a suite of archetypes) and an Appendix F methodology (that was developed for the evaluation of an individual structure). For this work, the focus will the on the standard methodology, and the *FEMA P-695 Toolkit* (NIST 2012) will be used to aid in the process.

The first step in the P-695 analysis is to determine a seismic design category. The P-695 process has included four "location neutral" spectra that can be used to design and analyze the structure, which are $D_{max}$, $D_{min}/C_{max}$, $C_{min}/B_{max}$, and $B_{min}$. The ASCE 7 (ASCE 2005) parameters for the spectra are shown in Table 2-4.

**Table 2-4.** ASCE 7 parameters for the P-695 spectra

| | $D_{max}$ | $D_{min}$/ $C_{max}$ | $C_{min}$/ $B_{max}$ | $B_{min}$ |
|---|---|---|---|---|
| $S_S$ (g) | 1.50 | 0.55 | 0.33 | 0.156 |
| $F_a$ | 1.00 | 1.36 | 1.53 | 1.60 |
| $S_{MS}$ (g) | 1.5 | 0.75 | 0.50 | 0.25 |
| $S_{DS}$ (g) | 1.0 | 0.50 | 0.33 | 0.167 |
| $S_1$ (g) | 0.6 | 0.132 | 0.083 | 0.042 |
| $F_v$ | 1.5 | 2.28 | 2.4 | 2.4 |
| $S_{M1}$ (g) | 0.9 | 0.3 | 0.2 | 0.1 |
| $S_{D1}$ (g) | 0.6 | 0.2 | 0.133 | 0.067 |

Once designed, the structure can be mathematically modeled, and in order to accurately determine the collapse parameters, a detailed model of the structure needs to be constructed. Two-dimensional models are generally considered sufficient, unless the building is expected to experience strong effects from three-dimensional behavior. To simulate collapse, the model should capture all significant nonlinear effects and must capture strength and stiffness degradations under large deformations. Non-simulated collapses can be indirectly evaluated using alternative limit state checks for cases where it is not possible or not practical to directly simulate all significant deterioration modes contributing to collapse behavior. Non-simulated limit state checks will generally result in lower estimates of median collapse intensity and are usually associated with component failure modes.

Once the model is complete, the next step is to select and scale ground motions. The P-695 methodology provides two suites of ground motions: 22 pairs of ground motion for far field motions and 28 pairs of ground motions for near field motions. These are normalized and then scaled so that the median spectral acceleration of the record suite matches the spectral acceleration at the fundamental period, *T*, of the index archetype that is being analyzed in the direction being analyzed. This fundamental matching period is defined as $C_u T_a$ per ASCE 7-10 (ASCE 2010).

Additionally, a nonlinear static pushover analysis is performed. Numerous results are available from this analysis, including the maximum base shear capacity, $V_{max}$, and the period based ductility, $\mu_T$. The ultimate displacement, $\delta_u$, is taken as the roof displacement at the point of 20 percent strength loss ($0.8*V_{max}$), and the period-based ductility is defined as the ratio of ultimate roof drift displacement to the effective yield roof drift displacement, $\delta_{y,eff}$.

For the full methodology, incremental dynamic analysis is then performed by systematically scaling the ground motion intensity to higher levels until the structure reaches a collapse point. This analysis is used to find the median collapse capacity, $\hat{S}_{CT}$, which is defined as the spectral

intensity at which half of the ground motions have caused the structure to collapse or exceed the non-simulated collapse parameter. The collapse margin ratio (CMR) is calculated as the median collapse spectral acceleration, $\hat{S}_{CT}$, divided by the spectral acceleration at the maximum considered earthquake, $S_{MT}$. Once the CMR has been calculated, it can be converted to the adjusted collapse margin ratio (ACMR), which is equal to the CMR multiplied by the spectral shape factor, SSF. The SSF accounts for the variability in the site specific spectral shape, is tabulated in the methodology, and depends on the fundamental period of the structure and the period based ductility found during the pushover analysis. This will be used along with the total dispersion, $\beta_{TOT}$, to determine the probability of collapse. The calculation for $\beta_{TOT}$ is shown in Equation 2-16. The record to record dispersion is based on the ductility of the structure, and all the other dispersion values are based on the confidence in the model and design. The design requirements, the test data, and the modeling are given quality ratings of superior, good, fair or poor, which correspond to dispersion values of 0.1, 0.2, 0.35, and 0.5, respectively.

$$\beta_{TOT} = \sqrt{\beta_{RTR}^2 + \beta_{DR}^2 + \beta_{TD}^2 + \beta_{MDL}^2} \leq 0.5 \tag{2-16}$$

where:
- $\beta_{RTR}$ is the record to record dispersion
- $\beta_{DR}$ is the design requirement dispersion
- $\beta_{TD}$ is the test data dispersion
- $\beta_{MDL}$ is the modeling dispersion

The probability of collapse, $P_c$, of a structure can be calculated as shown in Equation 2-17. The probability of collapse is not a required calculation in the P-695 methodology, but it can provide insight into the behavior of the structure.

$$P_c = 1 - \int_0^{ACMR} \frac{1}{\beta_{TOT}\sqrt{2\pi}} e^{\left[-\frac{1}{2}\left(\frac{\ln(ACMR)}{\beta_{TOT}}\right)^2\right]} \tag{2-17}$$

While FEMA P-695 goes well beyond determining a probability of collapse for an archetype or a performance group, only the calculation of the median collapse capacity will be utilized in P-58 evaluations performed for this research.

### *2.5.2. Appendix F Methodology for Individual Structures*

While the full P-695 process is intended for the analysis of large performance groups of generic systems to determine acceptable seismic performance factors, Appendix F of the P-695 documentation provides a methodology for analyzing individual structures. The main idea behind this portion of the methodology is to provide one scale factor used for analysis that represents an acceptable collapse factor assuming an acceptable probability of collapse, typically

10 percent. The 44 ground motions are run with this one scale factor, and if less than half of the buildings collapse, the structure is deemed acceptable.

For modeling requirements, they are very similar to the full portion of the methodology. Two-dimensional analysis can be used assuming that no important three-dimensional behavior would be neglected, and all the elements should capture the hysteretic behavior of all elements that could become nonlinear for collapse. The biggest modeling difference is that the inclusion of the gravity system resistance and its associated failure modes should be included. This differs from the full approach, because the full approach is assuming generic structures with unknown gravity systems; for individual buildings, it is assumed that the gravity system is known.

Like the full process, a nonlinear static pushover analysis is required, and the structure period based ductility and spectral shape factor, SSF, need to be determined. The total dispersion, $\beta_{TOT}$, and acceptable collapse margin ratio also need to be determined, based on the predetermined acceptable probability of collapse, which for this research will be the $ACMR_{10\%}$.

If the structure is within 6.4 miles of an active structure, the near field ground motion set should be used. Otherwise, the far field set will be used, like the full analysis. The **normalized** ground motions will all be scaled by the scale factor shown in Equation 2-18.

$$SF = \frac{ACMR_{10\%}}{C_{3D}*SSF}\left(\frac{S_{MT}}{S_{NRT}}\right) \quad (2\text{-}18)$$

where: $C_{3D}$ is the three-dimensional coefficient (1.0 for 2D analysis; 1.2 for 3D analysis)

$S_{NRT}$ is the median value of the normalized record set 5% damped spectral response acceleration at T (which is tabulated in the methodology)

Like stated previously, if less than half of the normalized ground motions scaled with this scale factor cause collapse, the building is deemed acceptable.

### *2.5.3. Current Implementation*

Numerous examples of the FEMA P-695 methodology can be seen in the literature. Obviously, there are examples located in the P-695 document itself (FEMA 2009a), and another major project, ATC 76, has been completed that expanded on the work done by ATC 63. The ATC 76 project, *Evaluation of the FEMA P-695 Methodology for Quantification of Building Seismic Performance Factors* (NIST 2010a), provided numerous examples of the methodology, including special and ordinary reinforced masonry shear walls, special and ordinary reinforced

concrete shear walls, special steel moment frames, special steel concentrically braced frames and special buckling restrained brace frames.

This methodology has been applied numerous other times to more of these traditional systems, including buckling restrained braces (Zsarnóczay 2012), concentrically braced frames (Chen and Mahin 2010), base isolated buildings (Nakazawa et al. 2011), concrete intermediate moment resisting frames (Richard et al. 2010) and concrete moment resisting frames with soil-structure interaction (Behnamfar and Haghollahi 2012). The methodology has also been applied to sensitivity studies on traditional systems, like a parameter selection of moment frames and shear walls (Zareian and Krawinkler 2010) or a study of short period buildings (Charney et al. 2012)

Like its original intent, the methodology has been used to analyze new innovative systems, including a 3D panel system (Mashal and Filiatrault 2011), a chevron knee brace system (Farahi and Mofid 2013), cold formed steel strap braced walls (Comeau et al. 2010), cold formed steel framed shear walls (Humar et al. 2012), steel moment frames with viscous fluid dampers (Miyamoto et al. 2010), a linked column frame system (Malakoutian et al. 2012), hybrid buckling restrained braces (Atlayan and Charney 2012) and partially restrained connections (Flores et al. 2012).

Some studies have simply used subsets of the methodology. The building sets designed for the P-695 project have been used elsewhere, like in the ATC 82 project, *Selecting and Scaling Earthquake Ground Motions for Performing Response-History Analyses* (NIST 2011). Research that has used only the ground motion set provided by the P-695 project includes an assessment of the seismic performance of a highway bridge isolated by lead rubber bearings (Bhuiyan et al. 2012), a study on the ground motion duration effects on structural collapse (Foschaar et al. 2012), research on steel braced frame behavior (Huang et al. 2012), an assessment of the seismic demands on wind turbines (Prowell et al. 2010), and the seismic design of a midrise wood structure (van de Lindt et al. 2012). Other studies have utilized the procedure for developing collapse fragilities, like the FEMA P-58 project (FEMA 2012) and a study looking at building collapse risk (Luco et al. 2011).

Uses of this methodology are worldwide and diverse. The applications of this idea do not seem to be slowing down, and numerous other examples of the full methodology could be found beyond what is listed in this section. However, no examples could be found more the Appendix F methodology. The research has been focused on the full method, and no comparison has been made between the two ideas, which this research will be able to fulfill.

### 2.6. Background on FEMA P-58 Procedure

FEMA P-58 (FEMA 2012) is a performance-based process that initiates with selection of one or more performance objectives, which are statements of the acceptable risk of incurring damage or

loss for identified earthquake hazards as decided by building developers/owners, design professionals, and building officials. This methodology uses a risk-based approach and quantifies the performance measures in terms of casualties, repair cost, repair time, and unsafe placards. This section will provide an overview of the P-58 methodology, but it is important to note that the P-58 procedure is not a prescriptive procedure and is designed to be flexible to the needs of the user.

### *2.6.1. Building Performance Modeling*

The first step in the methodology is to determine the necessary data including: structural system and components, non-structural components, occupancy information, number of stories, story heights, floor areas, total replacement cost, core and shell replacement costs, replacement time and total loss threshold. This Building Performance Model contains all the necessary information to convert structural response to consequences.

#### *2.6.1.1. Cost Estimations*

The cost estimations for total replacement cost and core and shell replacement costs will be based initially on data from the 2011 Engineering News-Record *Square Foot Costbook* (ENR 2011). The cost data in PACT are based on 2011 California averages, so this is the appropriate *Costbook* to use. Accurate, up to date (e.g. 2013) cost estimations are preferable; however, for the purpose of this research, it is more important to provide consistent cost estimations. This is because the project aims to compare the behavior of new structural systems to existing systems, wherein it is important to keep the cost estimation procedure as consistent as possible, as opposed to getting the estimation accurate to the dollar. The *Costbook* contains examples of costs for real structures, as well as the time behavior of construction costs and location multipliers. Inputs for region and date cost multipliers in PACT allow the program to be adjusted for different years and locations.

#### *2.6.1.2. Population Models*

Population models must also be defined to provide the potential number of persons in the building at the time of seismic loading. PACT includes models to define the number of people per 1000 square foot based on time of day, day of week and month of year for numerous typical occupancy types, including commercial offices, Education (K-12) buildings, general hospitals, multi-unit residential buildings, research laboratories, retail malls, and warehouses. If other population models are needed, they must be developed and added using the Building Population Modeler Utility. For more information on this procedure, reference the PACT user's manual (FEMA 2012). Within the PACT program, more than one population model can be applied (with an associated fraction of area), and population models can be defined for the whole structure or on a floor by floor basis.

*2.6.1.3. Fragility Groups and Performance Groups*

Once the initial data is determined, the components are divided into fragility groups. A fragility group is defined as a collection of components that has the same consequences of damage, construction characteristics, modes of damage, and probability of sustaining damage. All components in a fragility group must be subjected to the same demand parameter (e.g. component deformations and forces, story drift, floor acceleration, floor velocity), which should best predict the onset of damage with the least amount of uncertainty. For example, moment resisting frames might be best analyzed using drift, while hospital equipment might be better analyzed using floor acceleration. For each category (substructure, shell, interior, services, equipment and furnishings, and special construction and demolition), the necessary fragilities are selected and applied to zero (nondirectional), one or two directions. The performance groups, which are subsets of the fragility group in a particular direction at a particular level, are then determined.

Each fragility group is assigned a series of damage states to characterize discrete levels of damage that can occur. Each damage state is defined by a unique set of consequences consisting of one or more of the following: repair cost to fix or replace the component based on the level of damage, repair time, potential for "unsafe" placard assignment, potential impact on occupancy or on casualties. These damage states will be correlated to the demand parameter of the fragility group and can be described in three possible relationships: sequential, mutually exclusive and simultaneous. For sequential limit states, the damages progresses in order (e.g. 3% drift, 4% drift, 5% drift). For mutually exclusive limit states, only one limit state occurs (e.g. if one happens, the other(s) won't). Finally, for simultaneous limit states, the damage states can, but do not need to, exist together.

*2.6.1.4 Component Fragilities*

Component fragilities are developed to describe the probability of a damage state occurring given the level of the demand parameter. These are lognormal distributions defined by a median value of demand (50% chance the damage state initiates) and a dispersion value (SRSS of appropriate uncertainties). Many component fragilities are already derived, and Appendix D in the FEMA P-58 documentation provides a table of all the component fragilities currently included in PACT. This table presents the system name and description, as well as the subfragilities. The subfragilities represent all the damage states that were determined for the component, and often represent increasing levels of damage or associated loss. There are more than 600 fragilities that are currently included, many of which could be useful for analyzing existing structural systems and nonstructural components. PACT contains all the information on the developed fragilities under its fragility manager module.

An example of one of the component fragilities and its subfragilities, a post-Northridge reduced beam section is shown in Figure 2-6. There are three damage states (DS) for this fragility group: local beam flange and web buckling (DS1), DS1 plus lateral-torsional distortion of beam in hinge region (DS2), and low-cycle fatigue fracture in buckled region of RBS (DS3). Each damage state has a subfragility curve associated with it, which gives the probability of that damage state being exceeded with respect to that fragility's damage parameter, which in this case is drift ratio.

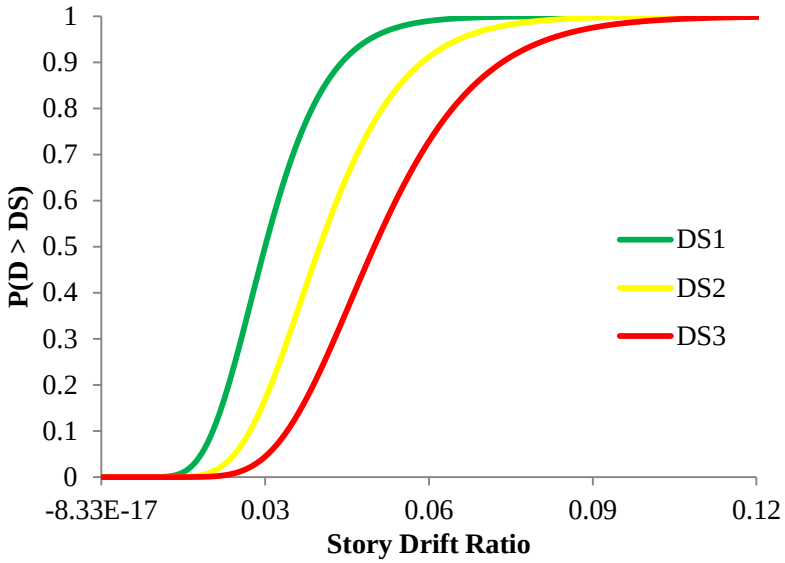


**Figure 2-6.** PACT set of fragility curves for the three damage states of a post-Northridge reduced beam section

For any component that does not have a fragility curve previously developed, one must be developed and added into PACT. Appendix H in the FEMA P-58 documentation discusses the fragility development in great detail, and for the purposes of the methodology, Section H2.4 of the FEMA P-58 documentation is the reference for developing the fragility curves analytically where needed.

*2.6.1.5 Consequence Functions*

Consequence functions are distributions of the likely consequences of a component damage state in terms of repair costs, repair time, potential for unsafe placards, and casualties. These functions are developed as companions for every subfragility. These consequence fragilities are how the physical behavior of a component is translated into the risk-based consequences.

For each damage state, there is an associated group of consequence functions that give the distribution of repair costs and time for the quantity of the component that need to be repaired. For the component fragility shown in Figure 2-6, the consequence function of the cost

distribution for DS2 is shown in Figure 2-7. Under the consequence function tab in PACT, there is also general information (which describes the typical repair), the time distribution, and other consequences (which include red flag consequences and non-collapse casualties).

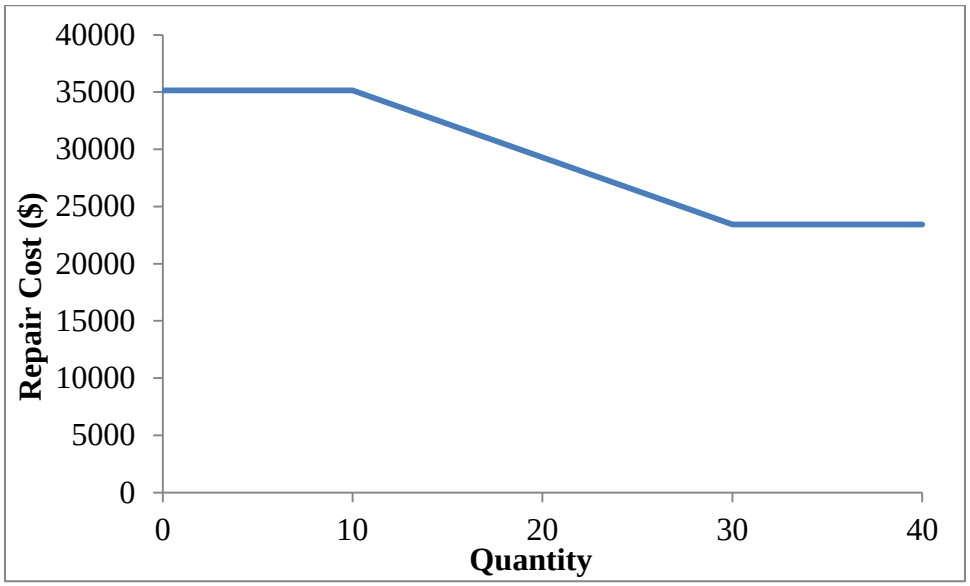


**Figure 2-7.** PACT consequence function for the second damage state of a post-Northridge reduced beam section

### *2.6.2. Assessment Types*

As discussed previously, three different types of performance assessment are available: intensity-based assessment, scenario-based assessment and time-based assessment. The intensity-based assessment evaluates the performance of the structure under a specific intensity of shaking (for example the MCE). On the other hand, the scenario-based assessment evaluates the performance for a specific magnitude distance pair. This second assessment is preferable for understanding the consequences for a known fault or seismic zones. For each assessment type, a target spectrum will be developed. For the intensity-based assessment, the spectrum can either be a Uniform Hazard Spectrum (UHS) or a Conditional Mean Spectrum (CMS). For the scenario-based assessment, the spectrum should be a Conditional Mean Spectrum (CMS).

The time-based assessment is used to evaluate performance over a time period (considering all earthquakes and their probabilities) and is the manner in which the methodology integrates fragility with hazard. This methodology runs numerous intensity-based assessments and finds a weighted average of the results based on the hazard. A hazard curve for a specific site is a plot of the probability of exceedance of the spectral response acceleration at a particular structural period as a function of intensity. The hazard curve chosen to represent the given site at the fundamental period of the structure will be sub-divided into numerous intensity intervals (at least 8). For each interval, the mean annual frequency of the interval will be calculated, and a target

spectrum will be developed for each interval frequency (either a UHS or CMS). An intensity-based analysis will then be run at each median intensity using a set of ground motions matched to the target spectrum associated with that intensity, and the final results can be summed using a weighted average based on the mean annual frequency of occurrence.

### *2.6.3. Ground Motion Selection and Scaling*

Ground motions must be selected and scaled to the target spectrum for each performance assessment. At least seven ground motion pairs should be selected and matched to each spectrum. These ground motions should be selected based on how well the geomean of the pair matches the target spectrum between $T_{min}$ and $T_{max}$. $T_{max}$ should be taken as twice the larger fundamental period in the two directions, and $T_{min}$ should be taken as 0.2 times the minimum of the two fundamental periods. These ground motions should be scaled by the ratio of the spectral acceleration of the target spectrum to the spectral acceleration of the geomen spectrum at the average of the fundamental periods.

This procedure could be modified to match the procedures in ASCE 7 Chapter 16 or FEMA P-695 as necessary. For this research, the ground motions will be selected from the P-695 far field set and scaled per the requirements of FEMA P-695. Since the P-58 methodology is not meant to be prescriptive, adjustments like this do not go against the principles of the procedure.

### *2.6.4. Analyze Building Response*

Two types of analysis are described in the FEMA P-58 methodology: collapse assessment and performance assessment. The FEMA P-695 methodology will be utilized for the collapse assessment to determine the median collapse intensities.

The performance assessment of FEMA P-58 uses the ground motion selecting and scaling procedure discussed in the previous section, and a nonlinear analysis will be run for each set of scaled ground motions. Modeling for this nonlinear analysis must include a nonlinear representation of force-deformation behavior for all modeled components, P-delta effects, gravity loads, damping, etc. The nonlinear analysis is performed for one level of intensity and is used to estimate *median* values of demand parameters (component deformations and forces, story drift, floor acceleration, and floor velocity). The median values will be used as the "seed" for Monte Carlo simulation, which is described in the next section.

Since this method records median responses, it is not practical to perform sufficient analyses to obtain valid information on the dispersion in these response parameters. Therefore, dispersions in the demand parameters are estimated through judgments about the uncertainty inherent in response calculation. The appropriate values for uncertainties due to modeling and ground motion selection are discussed in Section 5 of the FEMA P-58 documentation. For each intensity

or scenario assessment performed (multiple intensity scenarios will be run if creating a time-based scenario), the peak values of each of the demand parameters caused by each ground motion, as well as the residual drift, will be recorded for each level of the structure in each direction.

There is a simplified method described in the FEMA P-58 documentation that uses a procedure similar to the ASCE 7 (ASCE, 2005) Equivalent Lateral Force method, but this performance metric will use nonlinear dynamic analyses; therefore, the simplified method is not summarized in this documentation.

### *2.6.5. Performance Calculations*

Ideally, thousands of nonlinear dynamic analyses would be performed using a large suite of ground motions and variations of model properties. However, this is not computationally feasible, so a limited number of structural analyses are performed to predict an estimate of the median value of key building response parameters such as story drifts and floor accelerations, as described in the previous section (the performance assessment). These analyses are converted into distributions of demand based on the assessed variability of each of the random parameters using Monte Carlo simulation to assess the probable consequences of a building's response to earthquake shaking. These distributions of demand are determined using numerous, multi-step simulations called realizations, where each realization simulates a new set of consequences. The process of these realizations is shown in Figure 2-8.

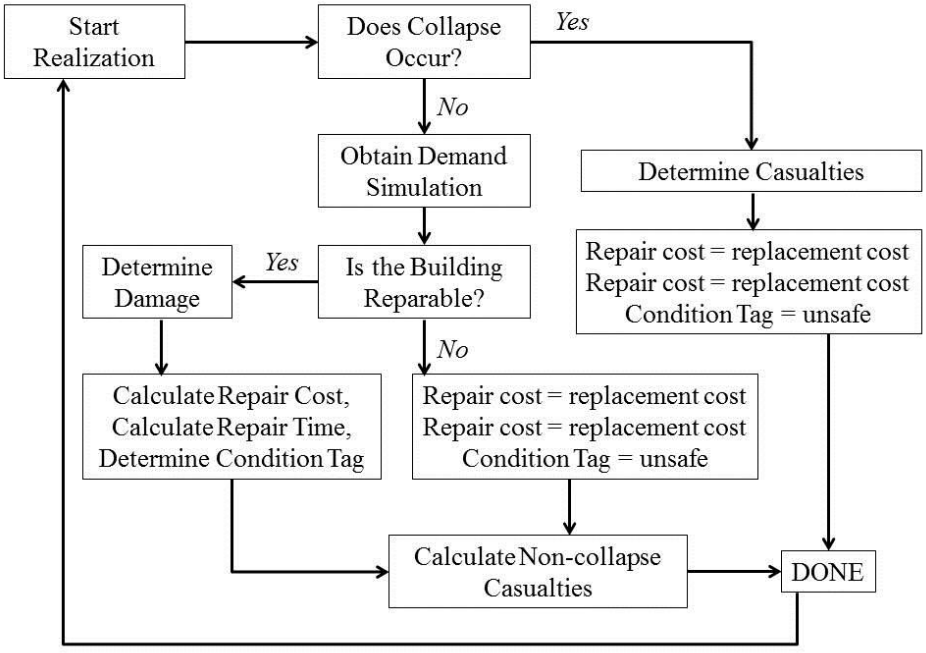


**Figure 2-8.** Process of a Monte Carlo simulation. Adapted from FEMA (2012)

The first step of the realization is to determine if collapse occurred. The probability of collapse given the intensity of the scenario can be determined from the collapse fragility. Then using a random number generator, a value between 1 and 100 is selected. If the selected number is less than or equal to the probability of collapse, the building is deemed to have collapsed and is assumed to be a total loss (the repair cost and time are taken as the building replacement values). If the structure did collapse, the number of casualties needs to be determined. The time of day and day of the week at which the realization occurred is determined using a random number generation process. Using this day and time and the population function appropriate to the building's occupancy, the number of people present in the area of collapse is determined, and the number of casualties is estimated based on the user-inputted associated fraction of floor area at each level subject to collapse together with additional casualty-specific information.

If the building did not collapse, the next step is to simulate demands. An algorithm has been implemented in PACT that uses Monte Carlo simulation to transform the small matrix of calculated median demand parameters determined by response-history analysis (the performance assessment) to a large number of simulated demand vectors used for loss calculations. More information on this algorithm can be found in Appendix G of the FEMA P-58 documentation.

Using one set of the simulated demand parameters, the damage state can be determined for each fragility. For the simulated demand vectors, the probability of reaching a damage state can be determined for each fragility group using its fragility curve. Since there generally will be multiple damage limit states for each fragility, each damage state will have an associated probability of occurrence. Once again, random number generation will be used to determine which damage state(s) have occurred. The calculation of probability and the random number simulation depend on whether the limit states are sequential, mutually exclusive or simultaneous. The process is discussed in more detail in Section 7.5 of the FEMA P-58 documentation.

In order to determine the losses of the simulation, initially it will be determined whether or not the structure is repairable using the calculated residual drift ratio and a random number generator. If the building is deemed irreparable, the repair cost and time are taken as the building replacement values, and the building is given an unsafe placard. Otherwise, the magnitude of consequences (e.g., repair cost, repair time, unsafe placards) will be determined using the simulated damage states and consequence functions. Loss distributions are created by sorting the loss calculation for each simulation and determining the probability of exceedence. To determine loss calculations for time-based scenarios, the loss distributions for each intensity are weighted by the annual frequency of occurrence of that median intensity and summed over all intervals.

All of these performance calculations are hardwired into the PACT program, so while the method is important to understand, it is not a procedure that will need to be programmed by

individuals using P-58. Once the nonlinear analysis has been performed, the results are entered into PACT, which will provide the consequence results developed for these simulations. There are two algorithms used in the PACT evaluation: a nonlinear and a simplified algorithm. The simplified algorithm analyzes median response from all the earthquakes used, while the nonlinear algorithm acknowledges that the behavior from each earthquake has a level of variability, and includes the correlation of the data within each hazard assessment. Since this metric recommends the nonlinear performance assessment, the nonlinear algorithm should be used.

### *2.6.6. Consequence Results*

The results are provided in terms of distributions of the consequences (casualties, repair cost, repair time, and unsafe placards) and can be viewed from an intensity-based assessment, a scenario-based assessment or a time-based assessment. An Office Building Example is provided with the PACT program, and results from that Example are shown as a sample of the various PACT outputs. Figure 2-9 shows an example of a PACT cost distribution from one intensity-based assessment, and Figure 2-10 shows an example of a PACT time distribution from the same intensity assessment. Each point on the plot shows the results for an individual realization, and a breakdown of the performance groups that caused the consequences is available in the PACT outputs. Figure 2-11 shows an example breakdown of the probability of receiving an unsafe placard for the highest evaluated intensity.

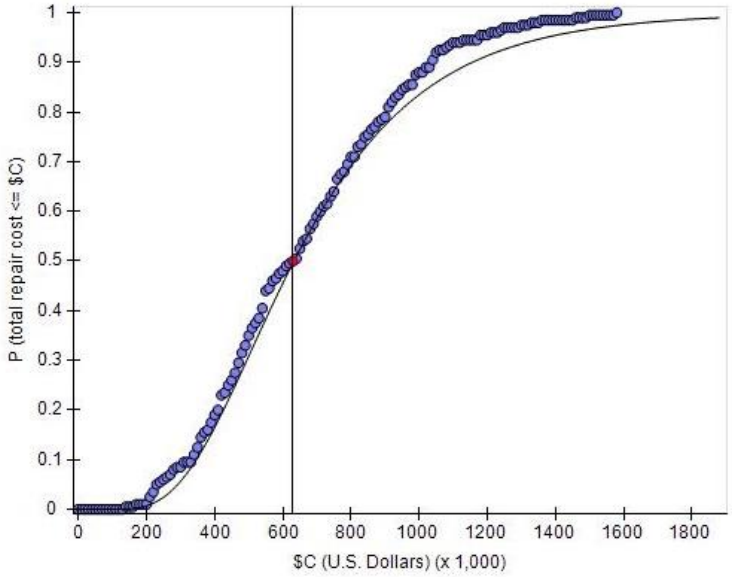


**Figure 2-9.** Example Cost Distribution for a Single Intensity Assessment

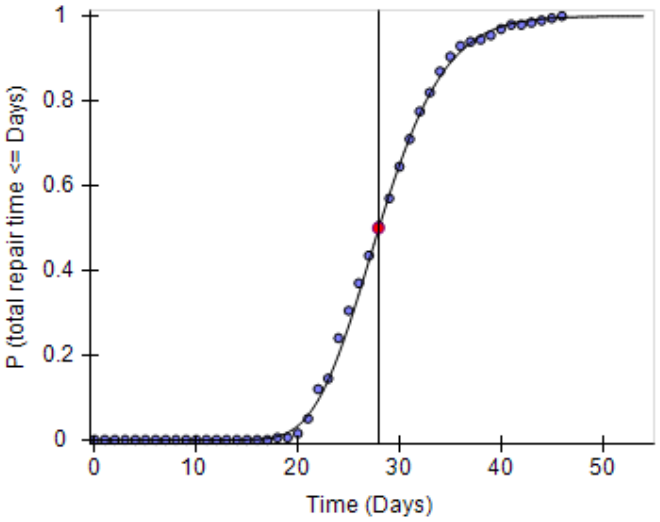


**Figure 2-10.** Example Time Distribution for a Single Intensity Assessment

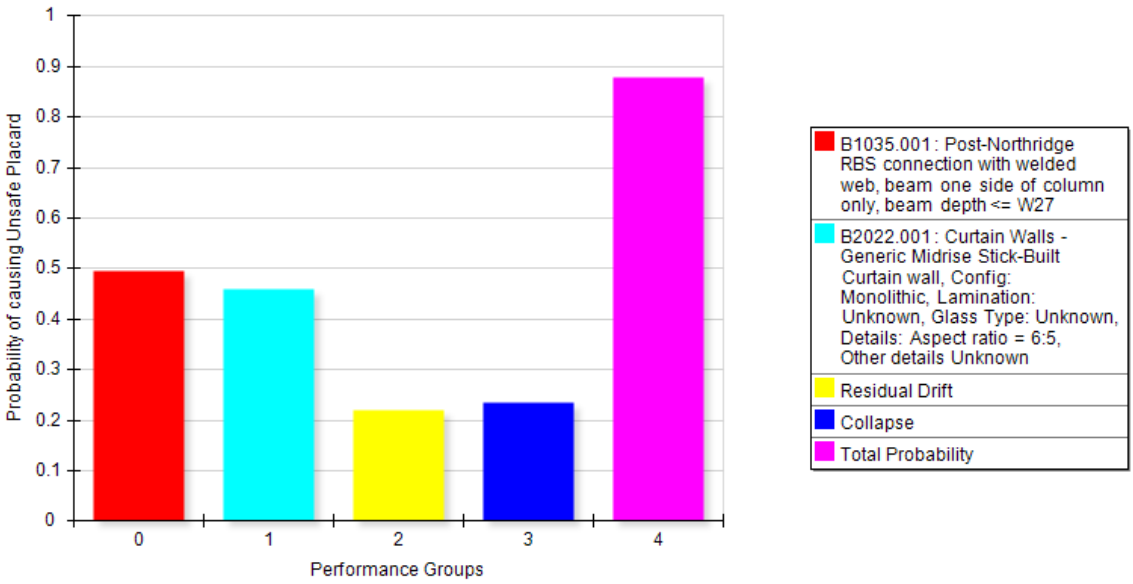


**Figure 2-11.** Example Probability of Receiving an Unsafe Placard for a Single Intensity Assessment

All these outputs are for individual intensity analyses. Figure 2-12 shows example consequence distributions from a time-based assessment (fragility integrated with hazard). The consequences are presented in terms of the annual probability of occurrence, and the distributions are broken down by the contribution (separated by color) from each analyzed intensity.

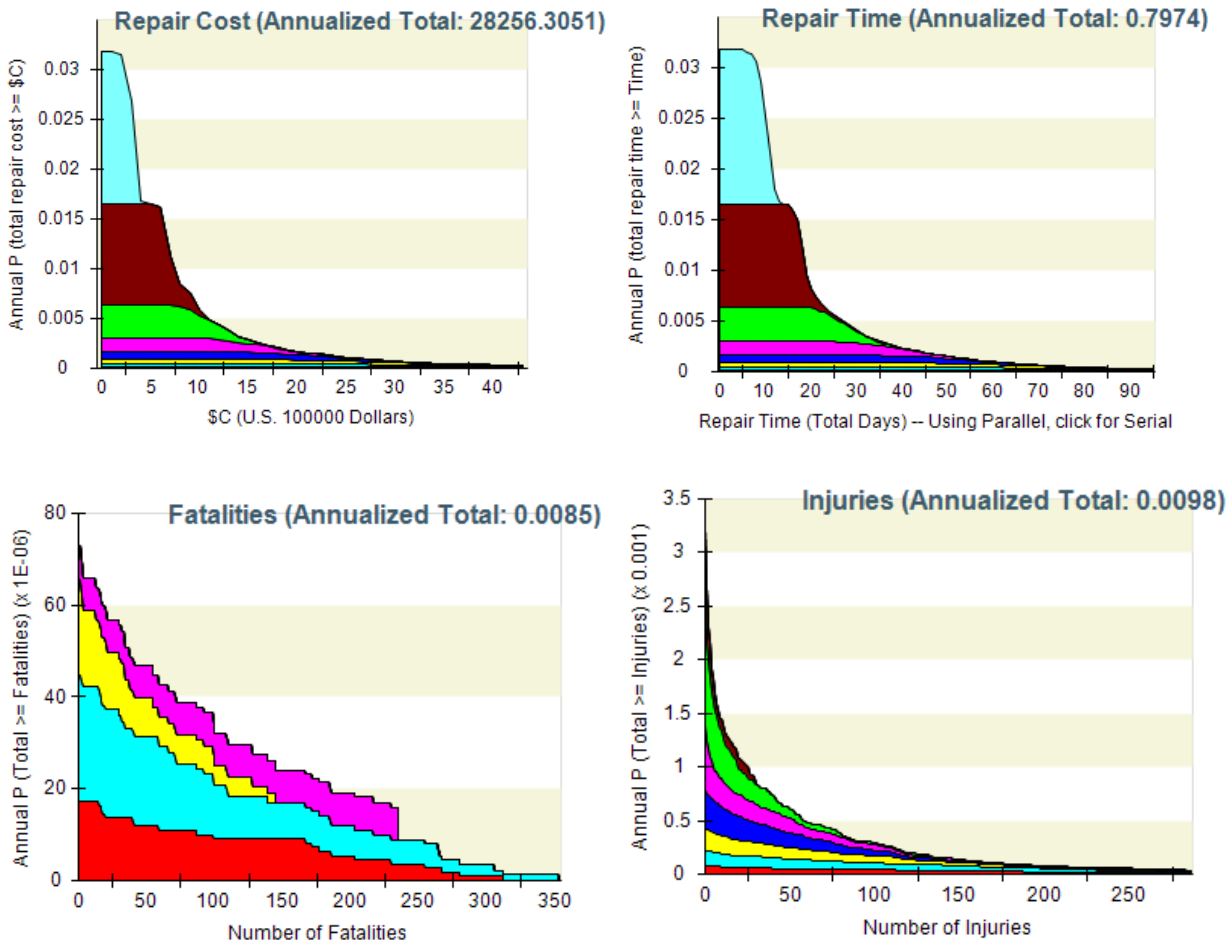


**Figure 2-12.** Consequence Distributions for a Time Based Assessment

Numerous other plot and reporting options for the consequence distributions are available under the Examine Results Module, and for more information on the PACT program, reference the user's guide (FEMA 2012).

### *2.6.7. Benefits of the FEMA P-58 Methodology from the Perspective of PBEE*

The P-58 PBEE evaluation procedure uses results from multiple nonlinear response history analyses (story drifts, acceleration, velocities, etc.) for specific levels of ground motions, the results from collapse analysis (using the P-695 methodology), as well as building cost information to provide consequence results (casualties, repair time, repair costs and potential of the issuance of unsafe placards). These results are easy to compare between systems and are meaningful to stakeholders and building officials.

Another benefit of the P-58 procedure is that it outlines three possible assessment types, each of which has its own advantage. For example, if a site were subjected to one or more specific geologic scenarios, running individual scenario assessments would be preferred. On the other

hand, the intensity assessment procedure would be beneficial to evaluate performance at specific intensities of ground motions (e.g. serviceability, DBE, MCE), which is ideal for PBEE. If integration with the seismic hazard or inclusion of all possible ground motions over a time range is most informative, the time-based assessment should be used.

While the engineer should determine what assessment type is most relevant to the system(s) being analyzed, a combination of assessments would be ideal in most circumstances. The hazard of the site should be used to select the intensities or scenarios that would best represent all the possible ground motions that the structure might be subjected to. Multiple intensity or scenario assessments can then be run, and the behavior of the structure can be analyzed and compared at all necessary performance levels (an important aspect of PBEE). If desired, these assessments can then all be combined via the time-based assessment to get the likely consequences over a period of time. The combination of flexible assessment types, numerous analyses at varying levels of seismic hazard, and results in terms of consequence make this methodology ideal for PBEE.

### 2.7. Accidental Torsion in Dynamic Analyses

Under seismic loads, structures can be subjected to effects from two types of torsional influences: inherent torsion and accidental torsion. Inherent torsion includes the effects from the offset of the center of rigidity from the center of mass, while accidental torsion includes effects from non-uniform ground motion loading or from strength and stiffness degradation during the nonlinear response of the elements that are resisting the seismic loads. Accidental torsion is generally disregarded in performance-based earthquake engineering provisions, including the Tall Building Initiative (PEER 2012), the P-695 procedure (FEMA 2009a), and the P-58 procedure (FEMA 2012). Typically, accidental torsion is only included in elastic procedures, ASCE 7 Chapter 12 (ASCE 2010) and ASCE 41 Chapter 3 (ASCE 2013), where the center of mass is shifted by 5 percent of the diaphragm dimension in each direction independently.

Numerous studies have investigated the effects of accidental torsion on structures. Early research shows these traditional methods for assessing elastic accidental torsion (where the center of mass is shifted by 5 percent of the diaphragm dimension in each direction independently) has a minimal effect on the design of structures (De la Llera and Chopra 1994a). This study found that accidental torsion is significant for structures where the torsional period of vibration exceed the lateral period of vibration (like structures with shear core wall or cruciform-shaped seismic resisting systems), for structures with one plan dimension that is significantly longer than the other, or for ground motions that create substantial rotation at the base of the structure. Only the second scenario (the long plan dimension) is captured within the linear code-based procedures.

De la Llera and Chopra also researched the different influences of elastic accidental torsion. The

uncertainty in the center of mass is normally the largest influence to accidental torsion (De la Llera and Chopra 1994b), which is likely why the 5 percent offset procedure is typically used. The second largest influence typically comes from the uncertainty in the stiffness of the lateral resisting elements (De la Llera and Chopra 1994c). These two sources typically account for around 70 percent of the accidental torsion effects (De la Llera and Chopra 1995). The effects of rotational ground motions were also investigated and were found to have more effect on torsionally flexible, short-period structures (De la Llera and Chopra 1994d). All these studies showed that the accidental torsion effects are higher for symmetric buildings than unsymmetrical buildings (De la Llera and Chopra 1994b, 1994c, 1994d).

An expansion on the previous studies by De la Llera and Chopra provided a new elastic procedure to estimate the effects of accidental torsion (De la Llera and Chopra 1995). This procedure begins by determining the ratio of the torsional fundamental period to the lateral fundamental periods. Based on this ratio, the plan dimensions and the building radius of gyration, an increase in displacements from the inclusion of accidental torsion is estimated at all crucial locations (i.e., at the building edges and at interior lateral-force resisting systems). The forces in the lateral-resisting systems are then amplified based on the increased displacements. This procedure is less cumbersome than the traditional methods of assessing accidental torsion and can include effects from all sources of accidental torsion.

While De la Llera and Chopra 1994 proposed new methods for assessing accidental torsion, the traditional method of shifting the center of mass is still the most prevalent method for including accidental torsion. The practical concern for response history analysis is that the four shifts in mass quadruples the number of analyses performed, since the structure must be analyzed with four different center of mass locations. Another concern with this method is that while the uncertainty in the center of mass tends to be the largest influence to accidental torsion, it is not the only source of accidental torsion, particularly for torsionally-regular structures, as was previously noted in the studies by De la Llera and Chopra (1994b, 1994c, 1994d). Damage during earthquakes such as experienced by the Clarendon Tower during the Canterbury Earthquake Sequence (Holmes and Zimmerman 2012) suggests that accidental torsion due to asymmetric changes in strength or stiffness can be significantly important even for structures with low elastic torsional irregularities. These effects can be especially substantial in perfectly symmetric structures, and the method of shifting the center of mass may not be sufficient to capture all the effects of accidental torsion (Dimova and Alashki 2003).

In 2002, a study was conducted on the accidental torsion effects of a single story structure (Peruš and Fajfar 2005). This study found that elastic torsional behavior is similar to inelastic torsional behavior, although the inelastic results had greater dispersion and are highly dependent on the frequency content of the ground motions. There are significant short-comings with simplistic

models (Stathopoulos and Anagnostopoulos 2005), and the studies on accidental torsion were expanded using a multi-story structure (Stathopoulos and Anagnostopoulos 2010). This was one of the first studies that used a more realistic structure to investigate torsional effects, as most previous studies use single story structures or simplified shear-beam models (De Stefano and Pintucchi 2008). This study also found that buildings designed with and without the accidental torsion provisions behaved similarly when experiencing inelasticity. Their recommendation was to remove the accidental torsion provision in its current state, except potentially for symmetric buildings. While the general conclusion of this study is that the inclusion of accidental torsion in design is unnecessary, the results could infer that linear design provisions cannot adequately capture inelastic torsional effects and that the inclusion of an accidental torsion provision should be moved to the nonlinear analysis of the structures.

Even though accidental torsion effects are typically only included in linear response history analyses, studies have shown that the inelastic response to accidental torsion can be significantly greater than the elastic response to accidental torsion (Mansuri 2009). In this study by Mansuri, the linear procedure of shifting the center of mass by 5 percent was expanded to nonlinear procedures. This procedure was also used to determine the effect of accidental torsion the on collapse capacity of structures (DeBock et al. 2013). The effects of shifting the mass in torsionally regular structures had a small effect on the collapse capacity (less than 10 percent reduction), since the collapse was controlled by lateral movements. On the other hand, shifting the mass had significant effect of the collapse capacity of torsionally irregular buildings.

As mentioned previously, the BSSC is proposing a major update to ASCE 7 Chapter 16, which encompasses the procedures for nonlinear dynamic analyses. The commentary for the proposed update to Chapter 16 states that accidental torsion in the design process (i.e., the Chapter 12 requirement) is used to determine potential torsional effects of symmetric structures and to check the torsional stability of the structure. However, it is generally considered unnecessarily conservative to also include accidental torsion in the nonlinear response history analyses, and therefore, no provisions for including this torsion are included in the proposed Chapter 16. The commentary does mentions that structures with no inherent torsion that are still sensitive to torsional effects (e.g., buildings with cruciform shaped lateral force resisting systems) should consider nonlinear torsional by artificially shifting the center of mass or unsymmetrically varying the stiffness and strength of the lateral elements, but no true provision is to be included in Chapter 16.

In the proposed updates to Chapter 16, a few exceptions are allowed, one of which is that the drift limits in Chapter 12 do not need to be applied to the design, assuming Risk Category I, II or III structure. Instead, drift limits are implemented under Chapter 16 for the nonlinear analyses (Haselton et al. 2013). With this exception, the effects of accidental torsion on the drifts of the

structure are never evaluated. Accidental torsion is included in design, where the drifts do not need to be checked. On the other hand, drifts are checked in the nonlinear analyses, but accidental torsion is not included. If the drifts in a structure are already near the nonlinear drift limits (which can be as high as 5 percent of the story height in the proposed changes to Chapter 16), the inclusion of nonlinear accidental torsion could cause dangerously high drifts.

The work presented in this dissertation will expand on the idea of expanding the linear accidental torsion procedures to inelastic analyses.

# Chapter 3: "Comparative Evaluation of Innovative and Traditional Steel Seismic Resisting Systems Using the FEMA P-58 Procedure"

Jordan A. Jarrett, Johnn P. Judd, and Finley A. Charney

[To Be Submitted to *Journal of Constructional Steel Research*]

**Abstract**

Two new innovative structural systems are investigated using the FEMA P-58 performance assessment procedure to determine the consequences (repair times, repair costs, unsafe placards and casualties) of being subjected to seismic ground shaking. These new systems were developed to display enhanced performance across multiple ground motion intensity levels. The first new system, called a Hybrid Buckling Restrained Brace System, is similar to existing BRB systems except that the core of the brace uses multiple plates, each with a different stress-strain behavior. The second new system, called a Collapse Prevention System, is designed for use in locations where the intensity of shaking under frequent earthquakes is negligible, but life-safety under rare high-intensity shaking is still a concern. These two innovative systems show how the structural system should be highly dependent on the location of the building and how Performance Based Earthquake Engineering can be applicable to multiple design philosophies. This paper also discusses the influence of including the lateral resistance of the gravity framing in the structural analysis models used to predict the seismic performance of traditional steel special moment resisting frames. This modeling assumption is investigated, as the behavior of the collapse prevention systems is dependent on the behavior of the gravity framing. In this work, these new systems and modeling philosophy are shown to reduce the consequence estimations across all pertinent limit states, particularly the average repair costs.

**Keywords:** FEMA P-58, Collapse Prevention, Buckling Restrained Braces, Gravity Systems

## 3.1. Introduction

Two new systems have been developed to satisfy the principles of Performance Based Earthquake Engineering (PBEE), and in this paper, their behavior is compared with that of traditional seismic resistant systems. Instead of designing buildings simply for the single limit state of life safety under design level ground shaking, PBEE focuses on the design of buildings that will perform efficiently under numerous earthquake intenisites. In the *Next-Generation Performance-Based Seismic Design Guidelines* (FEMA 2006), an example of potential performance objectives for systems designed to satisfy PBEE (1) should have minimal damage for small, frequent earthquakes, (2) could have up to moderate levels of damage under stronger, occasional earthquakes, and (3) must satisfy life safety and collapse prevention requirements

under large, rare earthquakes. Traditional systems are typically designed only for life safety (ASCE 2010), and this performance is generally satisfied for code-compliant designs. However, additional limit states are almost never explicitly checked in design, because this is not mandated by most current codes and standards.

PBEE takes into account many factors, including damage to structural and non-structural elements, loss of use of the structure, repair costs, and loss of life (Vamvatsikos and Cornell 2002). The assessment used to analyze structures for PBEE principles should incorporate all these factors and focus on the levels of damage that would be acceptable under varying intensities of earthquakes. In order to accomplish this, a combination of the FEMA P-58 (FEMA 2012) and FEMA P-695 (FEMA 2009a) methodologies are used for the assessments in this research. The FEMA P-58 methodology provides a framework to use structural response results from multiple nonlinear response history analyses and the results from a P-695 collapse analysis to predict potential consequences including casualties, repair time, repair costs, and probability of receiving an unsafe placard. These results are easy to compare between systems and are meaningful to stakeholders and officials. These methodologies are discussed in more detail in later sections.

Traditional seismic resisting systems that are typically designed only for the life safety limit state are compared with newly developed systems that were designed to exhibit better performance at numerous levels of ground motion intensity. The two newly developed systems analyzed in this work are Hybrid Buckling Restrained Braced Frames and Collapse Prevention Systems. Additionally, the effects of modeling the lateral resistance of gravity system connections are evaluated from the perspective of PBEE. Each of these systems has different purposes from the perspective of PBEE, which are discussed in detail later. The development and design of these systems can be found elsewhere (Atlayan and Charney 2013, Judd and Charney 2013b, Flores and Charney 2013), as this research focuses on the performance assessment of the systems. Using the FEMA P-58 and P-695 methodologies, each system is analyzed at the appropriate intensity levels, and the consequences are compared between the new and traditional systems.

## 3.2. Background on Methodologies

### *3.2.1. FEMA P-695*

FEMA P-695 (FEMA 2009a) is a methodology that was developed to determine the seismic performance factors of structural systems, including the response modification coefficient, $R$, the overstrength factor, $\Omega_0$, and the deflection amplification factor, $C_d$. However, for this research, the application of this methodology focuses on the calculation of the collapse fragility, which is one step in the process of determining the seismic performance factors. The first step in the P-695 analysis is to determine a design response spectrum. The P-695 process has included four location neutral response spectra that can be used to design and analyze the structure.

Once designed, a detailed mathematical model of the structure needs to be constructed. Two-dimensional models are generally considered sufficient, unless the building structure is expected to experience significant multi-axial load effects from three-dimensional behavior. To simulate collapse, the model should capture all nonlinear effects, including geometric nonlinearity, and must capture strength and stiffness degradation. Non-simulated collapses, which are usually associated with component failure modes, can be indirectly evaluated as an alternative limit state. Once the model is complete, the next step is to select and scale ground motions. The P-695 methodology provides two suites of ground motions: 22 pairs of pairs of orthogonal components of ground acceleration histories for far field motions and 28 pairs for near field motions. These are normalized and then scaled so that the median spectral acceleration of the record suite matches the spectral acceleration at the fundamental period, *T*, in the direction of the analysis of the index archetype. This fundamental matching period is defined as $C_u T_a$ per ASCE 7-10 (ASCE 2010).

Incremental dynamic analysis (Vamvatsikos and Cornell 2002) is then performed by scaling each ground motion until the structure reaches a collapse point. This analysis is used to find the median collapse capacity, $\hat{S}_{CT}$, which is defined as the spectral intensity at which half of the ground motions have caused the structure to collapse or exceed the non-simulated collapse parameter. A collapse fragility curve is developed using a lognormal distribution defined by this median collapse intensity and the record-to-record dispersion, $\beta_{RTR}$, which is conservatively taken as a constant 0.4. For systems with limited ductility, the record-to-record dispersion can be reduced down to 0.2. This collapse fragility is used in the FEMA P-58 process, which is discussed in the next section.

### *3.2.2. FEMA P-58*

FEMA P-58 is a process that quantifies the performance measures of a structure in terms of casualties, repair cost, repair time, and unsafe placards (FEMA 2012). These consequences can then be compared to desired performance objectives, which are defined as acceptable levels of damage or loss at a given level of earthquake intensity as determined by the decision makers. This section provides an overview of the P-58 methodology, but it is important to note that the P-58 procedure is not a prescriptive procedure and is designed to be flexible to the needs of the user. The methodology includes a companion computer program, called PACT (Performance Assessment Calculation Tool), to aid in its application.

#### *3.2.2.1. Building Performance Modeling*

The first step in the methodology is to create the Building Performance Model, which contains all the necessary information to convert the computed structural response to consequences. The information in the Building Performance Model includes: the structural system and components,

non-structural components, occupancy information, number of stories, story heights, floor areas, total replacement cost, core and shell replacement costs, replacement time, and total loss threshold.

Population models are used to define the potential number of persons in the structure at a random time of seismic loading. PACT includes numerous, generic population models to define the number of people per 1000 square feet (92.9 square meters) based on time of day, day of week and month of year for various typical occupancy types. If other, more specific population models are needed, they can be developed and added to the PACT program.

*3.2.2.2. Fragility Groups and Performance Groups*

Once the initial data is determined, the components are divided into fragility groups. A fragility group is defined as a collection of components that has the same construction characteristics, consequences of damage, and modes of damage. All components in a fragility group must be subjected to the same demand parameter (such as component deformations and forces, story drift, floor acceleration, or floor velocity), which should best predict the damage with the least amount of uncertainty. For example, the moment frames and other structural components might be best analyzed using drift, while hospital equipment and other non-structural components might be better analyzed using total floor acceleration. The performance groups, which are subsets of the fragility group in a particular direction at a particular level, are then determined.

Each fragility group is assigned a series of discrete damage states to characterize the important, distinct levels of damage that can occur. Component fragilities are developed using lognormal distributions to describe the probability of a damage state occurring given the level of the demand parameter. Hundreds of component fragilities are already derived for the PACT program, including numerous structural and non-structural components, and the methodology provides procedures to develop additional fragilities as needed. Each individual damage state is associated with a unique set of consequence functions that define the likely consequences of the component damage state in terms of repair costs, repair time, potential for unsafe placards, and casualties. These consequence fragilities translate the physical behavior of a component into the consequences.

*3.2.2.3. Assessment Types*

Three different types of performance assessment are described in the P-58 methodology: intensity-based assessment, scenario-based assessment and time-based assessment. The intensity-based and scenario-based assessments are used to evaluate the consequences for one earthquake shaking intensity or one earthquake with a specified magnitude and distance, respectively. The time-based assessment, on the other hand, combines the results of numerous intensity-based assessments to find the behavior over a given time period. For this research, only intensity-based

assessments are used. A target spectrum must be developed for each assessment, and for the intensity-based assessment, the spectrum can either be a Uniform Hazard Spectrum (UHS) or a Conditional Mean Spectrum (CMS).

*3.2.2.4. Building Response Analysis*

Two types of analyses are described in the FEMA P-58 methodology: collapse assessment and performance assessment. As mentioned before, the FEMA P-695 methodology is utilized for the collapse assessment to determine the median collapse intensities. Other simplified methods for collapse assessment are discussed in the P-58 methodology, but they are not used in this work. The performance assessment(s) of FEMA P-58 are the intensity or scenario assessments discussed previously. (Again, a time-based assessment consists of numerous intensity-based assessments). Modeling requirements are similar to those in the FEMA P-695 procedures, as they must capture all of the important nonlinear effects. Each performance assessment is run and records the maximum values of demand parameters, including component deformations and forces, story drift, floor acceleration, and floor velocity. These peak values of each of the demand parameters caused by each ground motion are recorded for each story of the structure in each direction.

It is not practical to perform sufficient analyses to obtain valid information on the dispersion in these response parameters. Therefore, dispersions in the demand parameters are defined based on the uncertainties in building definition, construction quality assurance, and quality and completeness of the analytical model. The demand parameter results of the performance assessment are used as median values that serve as the center of the response distribution for Monte Carlo simulations, which are described in the next section.

*3.2.2.5. Performance Calculations*

Ideally, thousands of nonlinear dynamic analyses would be performed using a large suite of ground motions and variations of model properties to determine all the potential behaviors. However, this is not computationally feasible, so a limited number of structural analyses are performed to predict an estimate of the median value of key building response parameters, such as story drifts and floor accelerations, as described in the previous section (the performance assessment). These analyses are converted into distributions of consequences using Monte Carlo simulations that are based on the median demand values, the dispersion of the demand values, and the component fragilities and associated consequence functions. These ranges of probable consequences are determined using numerous, multi-step simulations called realizations. The algorithm to perform these Monte Carlo simulations is programmed in the companion software, PACT, and described in detail in the FEMA P-58 methodology.

*3.2.2.6. Reason for Methodology Selection*

The P-58 evaluation procedure uses results from multiple nonlinear response history analyses for specific levels of ground motions, the results from collapse analysis (using the FEMA P-695 methodology), as well as building cost information to provide consequence results (casualties, repair time, repair costs and potential of the issuance of unsafe placards). These results are easy to compare between systems and can be used by stakeholders to develop a framework of acceptable performance measures. Another benefit of the P-58 procedure is the flexibility of possible assessment types, which allows evaluation under any intensity level(s) of interest. The lack of prescriptive acceptance criteria and hazard levels allows crucial behavior to be investigated and satisfactory performance to be developed by the building decision makers. This methodology truly envelops the principles of Performance Based Earthquake Engineering, and was therefore selected for use in this research.

## 3.3. Background on Systems Analyzed

Three different systems are analyzed using the P-58 and P-695 methodologies: (1) Hybrid Buckling Restrained Braced Frames, (2) Collapse Prevention Systems, and (3) steel Special Moment Resisting Frames systems modeled with and without the influence of gravity connections. The first two systems are innovative systems that have been recently developed using the principles of Performance Based Earthquake Engineering (Atlayan and Charney 2013, Judd and Charney 2013b). The third system, Special Moment Frames, have been extensively evaluated in the past, but without explicit evaluation of the influence of the gravity framing on performance (Flores and Charney 2013). The modeling of Special Moment Frames with the gravity systems present is necessary for the collapse prevention systems, as these systems are dependent on the behavior of the gravity system. For each system, the P-58 analyses vary based on the crucial intensity levels for that system. An introduction to each system and their applicability is discussed next.

### *3.3.1. Hybrid Buckling Restrained Steel Braces*

The goal of the Hybrid Buckling Restrained Brace Frame (Hybrid BRBF) is to improve the behavior at multiple intensity levels with minimal adjustments to the traditional buckling restrained brace. A traditional buckling restrained brace consists of a steel core surrounded by a mortar-filled tube called a casing that prevents buckling of the steel core. The core and casing are uncoupled using a debonding material that prevents transfer of axial loads to the casing. Unlike traditional concentrically braced frames, the BRB has nearly identical compression and tension strength and deformation capacity. The Hybrid BRBF combines different steel materials within the core of the brace to adjust the behavior of the brace by controlling the sequence of yielding and the post-yield behavior. The steel materials that can make up the BRB core include traditional carbon steel, low yield point (LYP) steel, and high performance steel (HPS). The LYP

steel improves behavior at low intensity hazards by providing limited inelastic energy dissipation, and the HPS improves post-yield response under by limiting residual deformationhigh intensity hazards. These Hybrid BRBs are designed and built similarly to traditional BRBs, resulting in minor adjustments to the overall philosophy. However, reductions in the maximum drift and residual drift have been shown to be significant (Atlayan and Charney 2013).

The LYP steel used in this research is a low-carbon steel called LYP100, which has an average yield strength of 14.3 ksi (Saeki et al. 1998), or approximately 100 MPa. When comparing other properties to traditional A36 carbon steel (which has a yield strength of 36 ksi or 250 MPa), the modulus of elasticity is similar, but the LYP100 has a rupture strain equal to 1.5 to 2 times that of mild steel (Nakashima et al. 1994). When compared with A36 steel, the cost of LYP100 steel is approximately double and is currently available only in Japanese markets (Nippon Steel 2009).

Since the interaction of the different steel materials affects the behavior at different levels of ground motion intensity, this work investigates the behavior at multiple intensity levels. Four intensity levels are analyzed, including a serviceability level, the Design Based Earthquake (DBE), the Maximum Considered Earthquake (MCE), and a near-collapse level intensity. The structural systems used are discussed in more detail later, but it is important to note now that the systems are designed using the location neutral P-695 spectra. Since the structures do not have location specific hazard, generic intensity levels are used. The near-collapse intensity level is assumed at an intensity 1.33 times the MCE intensity. This may not equal the true collapse point of the structure, but it allows the behavior to be investigated well above the maximum considered level. The DBE level is two-thirds of the MCE level, similar to ASCE 7 provisions (ASCE 2010), and finally, the serviceability level is assumed to be 10 percent of the near-collapse level (or 0.133 times the MCE level). This serviceability level would also change with location specific hazards, but since the structural design is location neutral, this generic intensity level shows the behavior at low levels of ground motion intensity. Determining the P-58 behavior at these four intensity levels shows how the Hybrid BRBs compare to traditional BRBs at numerous intensities of interest. These were the intensity levels used by the developers of the system (Atlayan and Charney 2013), which is why they were chosen for this continuing work.

### *3.3.2. Collapse Prevention Systems*

The Collapse Prevention Systems are designed for life safety and intended for locations with infrequent seismicity (but where a strong earthquake is possible) such as the Central and Eastern United States (CEUS). Since the shaking under frequent earthquakes in these locations is negligible relative to those earthquakes with the same MRI in the Western United States (WUS), the structures designed for these locations must follow a unique design philosophy. The hazard of the CEUS is significantly different than the hazard of the WUS, so it is reasonable that the

seismic resisting systems would be different at each location. Both the WUS and CEUS are susceptible to large, rare earthquakes defined by the Maximum Considered Earthquake. However, in the Western United States, more frequent ground motions can cause significant damage, as was evident in the 1994 Northridge earthquake. This is not the case for the CEUS, where ground motions with moderate to low return periods tend to be significantly smaller than a ground motion of the same return period in the WUS (Judd and Charney 2013a).

Because the seismic hazard of the CEUS at short return periods is negligible, collapse prevention is the only crucial limit state, and the collapse prevention systems are designed on the basis of this principle. Collapse prevention design (CPD) assumes that a structure with little to no seismic detailing will have sufficient strength to withstand small, frequent earthquakes, and the additional reserve strength in the gravity framing system, combined with a collapse prevention mechanism (CPM), will satisfy the collapse prevention requirements. Two major requirements are critical to the CPM: (1) They are positioned in the gravity system, making them equally applicable to new construction and retrofits, and (2) they add no initial stiffness to the system. Additional stiffness increases the design base shear and requires a stronger seismic resisting system. Since CPD utilizes little to no seismic detailing, this additional stiffness goes against the design principles.

Numerous mechanisms can be used as a collapse prevention system. In this paper, the two mechanisms investigated are a slack cable and a loose linkage mechanism, as shown in Figure 3-1. Both of these systems remain inactive until the building has reached a specified level of drift, typically 2 percent of the total height, after which the CPM engages. The loose link mechanism is essentially a toggle brace without the added damper (Constantinou et al. 2001). Although it is out of the scope of this work, true toggle braces and other advanced systems that combine a CPM and a damper could be used to additionally improve the behavior under wind and low seismic loads (Judd and Charney 2013b).

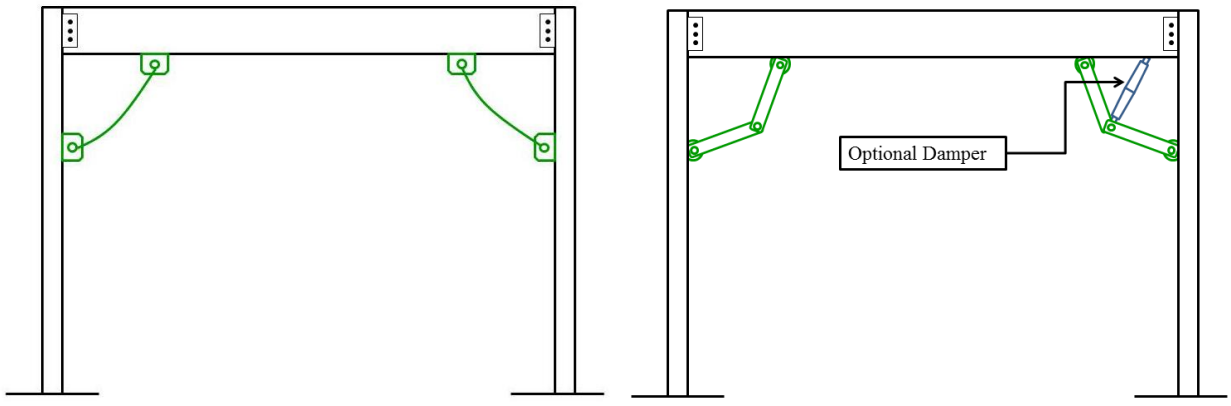


**Figure 3-1.** Slack cable CPM (left) and loose link CPM (right)

Since the only limit state of interest is collapse prevention, these systems are analyzed at a near-collapse level intensity. These intensities are taken as 90 percent of the median collapse intensity of the system without a collapse prevention mechanism. This was selected to show the potential behavior at large ground motions where collapse is possible, which changes with each structural configuration. The potential influence of the CPM on the consequences of the system is presented later.

### *3.3.3. Special Steel Moment Frames Modeled With and Without the Gravity System*

Typically in the analysis of structures, the gravity system is ignored, and only the lateral resisting system is modeled. Even if the gravity system is modeled to capture P-delta effects due to dead and live loads tributary to the gravity system only, the connections are generally modeled as pinned and are assigned no rotational strength or stiffness. However, evidence from past earthquakes has shown that gravity connections do have some rotational resistance, and thereby, the gravity framing contributes to the lateral stiffness and strength of the entire system. In some cases, the added resistance can be the difference between a collapsed or standing structure. This behavior was evident during the 1994 Northridge earthquake, where numerous steel moment frames experienced brittle failures of the connections in the lateral load resisting system, but the resistance in the gravity connections averted collapse (Leon 1998).

Other studies have investigated the effects of modeling the lateral strength and stiffness of the gravity system on the behavior of structures, although none have applied these results to the P-58 procedure. An initial study compared the behavior of steel moment frames with and without the modeled resistance of the gravity system under a variety of hazard levels (Gupta and Krawinkler 2000). The gravity system connections were modeled as simple rotational springs, and two different connection strengths were investigated. This study determined that the added strength and stiffness had a significant impact on the behavior, particularly at high intensity hazards. In another study, the gravity system connections were modeled using a more advanced model where the hysteretic behavior matched the results of partially restrained connection tests (NIST 2010a). Limited nonlinear static pushover analysis and nonlinear response history analyses were performed on the moment frame models with and without the partially restrained connections. Although the results varied with the structural configuration, the partially restrained connections typically reduced drifts and decreased the tendency of developing dynamic instabilities.

This collapse behavior of special moment frames with and without the lateral resistance of the gravity systems was further investigated using the FEMA P-695 methodology (Flores and Charney 2013). The addition of the gravity system resistance increased the median collapse intensity and decreased the probability of collapse, especially for taller structures. This increase in collapse capacity was less significant when column splices in the gravity system were

modeled as true hinges without moment resistance. The model with continuous columns (without splices) and the associated P-695 results are further investigated in this research, wherein overall performance is assessed using the P-58 methodology.

Similarly to the Hybrid BRB systems, the behavior at increasing levels of intensity of ground shaking is of interest for this system. This work determines when the explicit modeling of the gravity framing members and connections has a significant effect on the calculated consequences. These systems are analyzed at the same four hazard levels as the Hybrid BRBs: (1) serviceability, (2) DBE, (3) MCE, and (4) near- collapse.

## 3.4. Description of Models

### *3.4.1. Structures Used in Analyses*

All the structures used in this work are based on the structures used for the ATC 76 project (NIST 2010b), and all the structures are assumed to be used as commercial offices. The Hybrid Buckling Restrained Braces use the design of the BRB system in ATC 76 as a basis. The structures used for these analyses are the 4-story, 9-story and 18-story buildings from Performance Group 10, which are designed for the location neutral SDC $D_{max}$. The bay width of the BRB frames are 15 feet (4.57 meters), and all story heights are 13 feet (3.96 meters).

The Collapse Prevention Systems use the layout of the ATC 76 Special Moment Resisting Frames (SMRF), and based on these dimensions, an $R$ = 3 system is designed (Judd and Charney 2013b) using the requirements of ASCE 7 and AISC (ASCE 2010, AISC 2011). The gravity system is also designed, and the collapse prevention mechanisms are utilized within both the lateral and gravity systems.

The Special Moment Resisting Frames with and without gravity framing use the ATC 76 Special Moment Resisting Frames as the base system. The gravity system is designed (Flores and Charney 2013) using the requirements of ASCE 7 and AISC (ASCE 2010, AISC 2011) and is added to the ATC 76 design. The structures used are the 2-story, 4-story and 8-story structures designed for SDC $D_{max}$, using the Response Spectrum Analysis (RSA). The bay width of the SMRF frames are 20 feet (6.10 meters), and all story heights are 13 feet (3.96 meters), except the first story, which has a height of 15 feet (4.57 meters).

### *3.4.2. Mathematical Modeling Assumptions for Systems Analyzed*

*3.4.2.1. Modeling of the Hybrid Buckling Restrained Brace System*

All the Buckling Restrained Brace Frames are modeled as two-dimensional models in OpenSEES (McKenna 2011), with P-Delta effects being captured through a leaning column. The beams and columns in the frames are modeled using fiber elements to capture the nonlinearities, and gusset plates at the connections are modeled using rigid offsets. The column's bases are

fixed, and the columns resist bending loads along the strong axis. Corotational truss elements are used to model the BRBs, and the yielding core area is modeled with varying elastic modulus. The fatigue material in OpenSEES, which uses the Coffin-Manson fatigue relationship (Coffin 1954, Manson 1953), is also applied onto the BRBs to capture low cycle fatigue effects. Rayleigh damping is used to capture 2 percent damping in the first and third modes.

The 4-story, 9-story and 18-story structures are all modeled with four different levels of Hybridity: Regular, Hybrid-1, Hybrid-2, and Hybrid-3. The Regular BRBs are the traditional ATC 76 BRBs and have no hybridity. The Hybrid-1 model is a combination of carbon A36 steel, LYP100 steel, and HPS70W high performance steel (which has a yield strength of 73 ksi). The Hybrid-2 model uses LYP100 steel and HPS70W, and the Hybrid-3 model uses LYP100 steel and HPS100W high performance steels (which has a yield strength of 108 ksi). ). As the Hybrid number increases, the hybridity and expected performance improvement also increases. All the braces had the same total stiffness of 200,000 kip/inch and the same total strength of 290 kip. Additional details on the modeling and design on the BRB systems can be found elsewhere (Atlayan and Charney 2013).

*3.4.2.2. Modeling of the Collapse Prevention Systems*

The Collapse Prevention Systems are idealized using a phenomenological (concentrated plasticity) approach (Deierlein et al. 2010). Beams and columns are represented in OpenSEES using an assembly of rotational springs (zero-length elements) and elastic beam-column elements in series to simulate the potential for plastic behavior to be developed near the end.

The moment-rotation behavior of the non-ductile beam-to-column connections is represented using the Pinching4 and MinMax uniaxial materials in OpenSEES with load-deformation and hysteresis parameters based on FEMA P-440A (FEMA 2009b), ASCE 41 (ASCE 2006), and FEMA 355D (FEMA 2000). The non-ductile connections lose strength immediately after yielding for positive moments (simulating fracture of the bottom flange) and more gradually for negative moments. The connections exhibit cyclic degradation of both stiffness and strength, within a 15 percent residual strength boundary until approximately percent drift, after which the rotational stiffness and flexural strength of the connection is zero. The effect of composite action on moment-frame beam flexure strength is not included.

Column behavior is idealized similarly to beam behavior, except column plastic hinging moment-rotation behavior is represented using the Bilin uniaxial material in OpenSEES with parameters based on regression analysis of test data (Lignos and Krawinkler 2010), and with an approximate reduction to account for axial load. The reduction is based on the AISC P-M interaction equation (AISC 2011) using a constant axial load resulting from a nonlinear static (pushover) analysis that includes the gravity load plus half the lateral load (NIST 2010b).

Columns participating in the moment frame are idealized as fixed at the base; all other columns are idealized as pinned. Column panel zones are explicitly modeled using the Krawinkler joint model (Charney and Marshall 2006) represented using the Hysteretic uniaxial material option in OpenSEES.

The gravity framing system is included as described above for the primary moment frame, except that beam-to-column moment-rotation behavior is based on test data of shear tab connections (Lui and Astaneh-Asl 2000), corresponding analytical models (Lui and Astaneh-Asl 2004, Wen et al. 2013) and FEMA P-440A (FEMA 2009b). The shear tab connection behavior is asymmetric due to the effect of composite action with the concrete slab, and the maximum strength for positive moments is twice that for negative moments. The connections exhibit cyclic degradation of both stiffness and strength, until approximately 10 to 12 percent drift, after which the rotational stiffness and flexural strength of the connection is zero. Gravity framing connections to the column weak-axis are treated as un-restrained for moment transfer.

The Slack Cable CPM consists of 26-mm diameter structural steel cables with a 140 k breaking load. Slack cables are represented in the model using truss elements with multi-linear elastic uniaxial material behavior (to simulate initial slackness) until fracture at the breaking load. The Loose Link CPM consists of 1x2.5-inch A995-50 steel bars. Loose-linkages are represented in the model using corotational-truss elements that are elastic until fracture, approximated as the tensile yield limit state of the links. Additionally, it is important to note that the analysis of the CP systems used a minor adaptation to the FEMA P-695 method; instead of using the upper limit design period $C_u T_a$, the true computed fundamental period of the model is used because CP systems are used across multiple Seismic Design Categories.

*3.4.2.3. Modeling of the Special Moment Frames With and Without Gravity Framing*

The nonlinearities of the special moment resisting frame are modeled using phenomenological plastic hinges at the end of the members. The hinges are modeled in the reduced beam sections of the beams and in the columns at the bases and outside the moment frame connections. The reduced beam sections and column hinges use the Bilin material in OpenSEES (Lignos and Krawinkler 2010) to represent the hysteretic material. Additionally, a reduced bending strength is used in the columns to model the P-M interaction that is not included in the Bilin model. The nonlinearities in the panel zones are represented using the Krawinkler model (Charney and Marshall 2006).

The gravity system was also included in each model. The gravity columns are pinned at the base, oriented in the strong direction, and modeled using fiber elements to account for potential yielding. The partially restrained connections are modeled using a simple model from ASCE 41 (ASCE 2006), assuming a top and bottom clip angle connection is used and that the connection angles fail due to flexure. The strength of the connection is assumed to be a percentage of the

plastic moment strength of the attached beam, and for this research, all the 2-story, 4-story and 8-story structures are analyzed with 0 percent, 35 percent and 50 percent connection strength (referred herein as 0GS, 35GS and 50GS, respectively). Additional details on the modeling assumptions can be found elsewhere (Flores and Charney 2013).

### *3.4.3. Description of PACT Building Performance Models*

The building performance models used as the PACT input are described next. The estimations for replacement cost are based on data from the 2011 Engineering News-Record *Square Foot Costbook* (ENR 2011). The cost data in PACT are based on 2011 averages, so this is the appropriate *Costbook* to use for a date cost multiplier of 1.0. The *Costbook* contains examples of costs for real structures, and while there are no specific examples for commercial offices, a range of steel structures are presented. On the more expensive end, the examples include a 12-story steel convention center in Southern California with a total cost of $348 per square foot, and on the less expensive end, the examples include a 5-story steel history museum with a total cost of $231 per square foot. For a generic approximation based on the *Costbook* examples, the replacement cost is taken as a constant $300 per square foot. Since this research aims to compare the behavior of new structural systems to existing systems, it is more important to keep the cost estimation consistent between structures, as opposed to getting the estimation accurate to the dollar. In actuality, the cost per square foot for structures of varying location, use, size, and structural system would not be a constant value; however, for the comparative purposes of this research, a reasonably-chosen constant value should be sufficient. Additionally, since the structures are location neutral, the region cost multiplier is also assumed to be 1.0.

The total loss threshold, which is the percentage of the construction cost where the structure would be taken as irreparable, is assumed to be 1.0. While this value is closer to 0.4 in practice (FEMA 2012), a value of 1.0 insures that all the true consequence data is presented. If the value is less than 1.0, the consequences for realizations with higher costs would be replaced with the total repair costs and time, and the actual results would be lost. A value of 1.0 is the default in PACT and used in the examples provided with the P-58 documentation (Zareian 2013). Additionally, no irreparable residual drift ratio is included. Like the total loss threshold, the use of an irreparable residual drift causes the loss of some of the true data, which was avoided during this research.

For replacement time, the estimates were based on the number of stories and advice from practitioners. The replacement time is taken as 357 days for the 2-story models, 392 days for the 4-story models, 462 days for the 8-story models, 490 days for the 9-story model, and 672 days for the 18-story models. Figure 3-2 shows an example schedule for the 8-story model, and Table 3-1 shows the tasks included in the time estimation, as referenced in Figure 3-2.

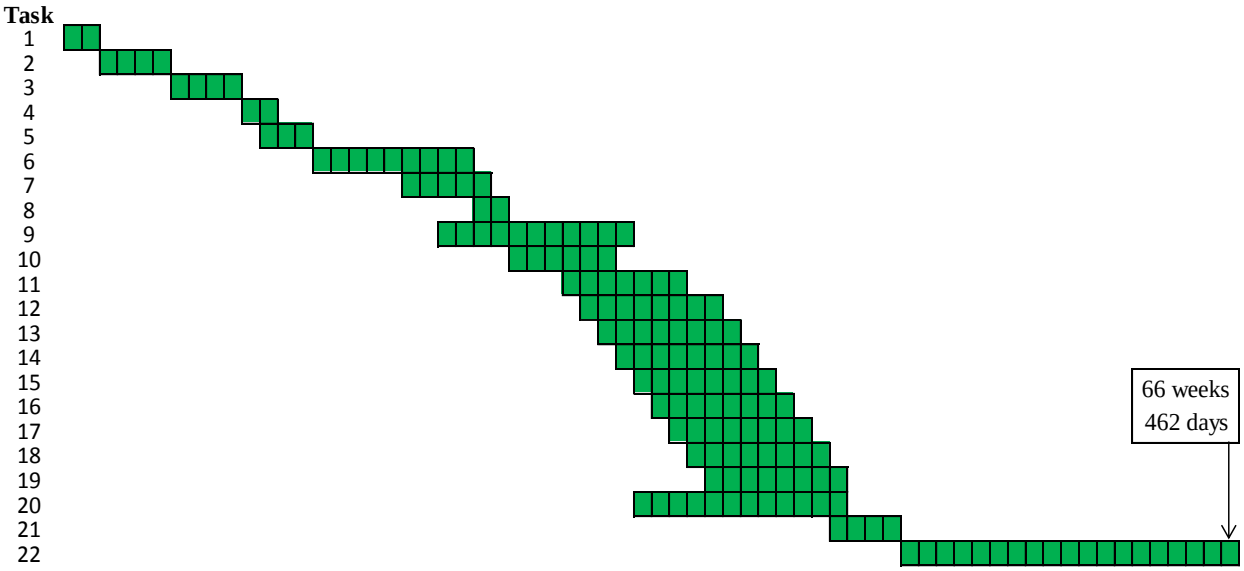


**Figure 3-2.** Example Schedule Estimation of the 8-story Models, where each block is one week

**Table 3-1.** Tasks Included in Replacement Time Estimations

| Number | Task | Time Estimate |
|---|---|---|
| 1 | Mobilize, Erosion Control | 2 weeks |
| 2 | Grading | 1 month |
| 3 | Caissons | 4 weeks |
| 4 | Foundations and Slab on Grade | 2 weeks |
| 5 | Elevator Mezzanines, Stair pop-ups, MEP preparation | 3 weeks |
| 6 | Erect Steel | 3000 sf/day ~ 1 floor/wk |
| 7 | Slab on metal deck | 2 weeks after steel erection |
| 8 | Fireproof | |
| 9 | Curtainwall | 4 weeks (1st floor), 1 week (other floors) |
| 10 | Roofing | 6 weeks |
| 11 | Elevators | 7 weeks |
| 12–19 | Interior Core and Shell, each floor | 8 weeks per floor (partially overlapping) |
| 20 | Lobby Build Out | 12 weeks |
| 21 | MEP, Life Safety | 4 weeks |
| 22 | Tenant Improvement | 12 weeks per floor (partially overlapping similarly to core and shell) |

For all the structures used in this work, the occupancy type is assumed to be for a commercial office, and the population model supplied with the PACT program is used. Non-structural component fragilities are chosen based on this occupancy type with the aid of the provided Normative Quantity Spreadsheet. This spreadsheet is a supplemental file provided with the P-58 products that estimates the type and number of non-structural components in a building based on

square footage and occupancy type. Since the designs from ATC 76 are academic models, as opposed to true structures, the spreadsheet provides a valuable resource to approximate the type and number of non-structural components in the building. Table 3-2 shows the structural fragilities used, based on the building type, and Table 3-3 shows the non-structural fragilities used, which stays constant for all the models.

It is important to note that fragility B1033.22a was added by the author for the Hybrid BRBs. Since the cost of the low strength and high performance steel is higher than traditional A36 steel, the Hybrid BRBs are given repair costs 20 percent higher than their traditional counterparts. This way, any comparison in repair costs considers this increase component cost. Shear tab connections are assumed for all the strong column connections, and column bases plates are assumed at fixed columns in the moment frames.

**Table 3-2.** Structural Fragilities Used in PACT Models

| **Buckling Restrained Brace Models** | | | |
|---|---|---|---|
| **Fragility** | **Name** | **Number Per Story** | **Models Used** |
| BRB | B1033.111a | 2 | All Regular Models |
| Hybrid BRB | B1033.222a | 2 | All Hybrid Models |
| Bolted Shear Tabs | B1031.001 | 4 | All Models |
| Column Base Plates | B1031.011a | 4 (at first story only) | All 4-Story Models |
| | B1031.011c | 4 (at first story only) | All 9- and 18-Story Models |
| **Moment Resisting Frame Models with and without Partially Restrained Connections** | | | |
| **Fragility** | **Name** | **Number Per Story** | **Models Used** |
| SMF Reduced Beam Section Connection | B1035.001<br>B1035.011 | 4<br>4 | All Models |
| Bolted Shear Tabs | B1031.001 | 24 | All Models |
| Column Base Plates | B1031.011a<br>B1031.011b | 4 (at first story only)<br>4 (at first story only) | All 8-Story Models |
| | B1031.011a | 8 (at first story only) | All 4-Story Models |
| **Collapse Prevention System Models** | | | |
| **Fragility** | **Name** | **Number Per Story** | **Models Used** |
| Non-ductile Moment Frame Connection | B1035.041<br>B1035.051 | 4<br>4 | All Models |
| Bolted Shear Tabs | B1031.001 | 24 | All Models |
| Column Base Plates | B1031.011a | 8 (at first story only) | All 4- and 8-Story Models |

For the nonstructural components, a story location of "ALL" means that the fragility is located at all levels, except the roof. In PACT, each component fragility assumes a specific quantity of that component, and therefore, the PACT Value is often different than the actual value. For example,

the wall partition fragility is developed assuming 100 linear feet (30.48 meters), and for the desired 106 linear feet (32.31 meters), based on the Normative Quantity Estimation Tool, a value of 1.06 (e.g. 106/100) is entered into PACT. The assumed quantities can be found in the PACT documentation. The fragilities used are compared with a PACT example (Zareian 2013), and similar fragilities were used in the example analyses.

**Table 3-3.** Non-Structural Fragilities Used in PACT Models

| Fragility | Name | PACT Value | Story Location |
|---|---|---|---|
| Curtain Walls | B2022.001 | 140 | ALL |
| Concrete tile roof | B3011.011 | 37.8 | ALL |
| Wall Partition | C1011.001a | 14 | ALL |
| Prefabricated Steel Stair | C2011.001b | 2 | ALL |
| Wall Partition | C3011.001a | 1.06 | ALL |
| Raised Access Floor | C3027.001 | 105 | ALL |
| Suspended Ceiling | C3032.001a | 50.4 | ALL |
| Independent Pendant Lighting | C3034.001 | 210 | ALL |
| Cold Water Piping | D2021.011a | 0.21 | ALL |
| HVAC Metal Ducting | D3041.011a | 1.05 | ALL |
| HVAC Metal Ducting | D3041.012a | 0.28 | ALL |
| HVAC Drops | D3041.031a | 12.6 | ALL |
| (VAV) box | D3041.041a | 9.8 | ALL |
| Fire Sprinkler Water Piping | D4011.021a | 2.8 | ALL |
| Fire Sprinkler Drop | D4011.031a | 1.26 | ALL |
| Low Voltage Switchgear | D5012.021a | 1 | ALL |
| Traction Elevator | D1014.011 | 4 | 1st only |
| Chiller | D3031.011a | 5 | Roof only |
| Cooling Tower | D3031.021a | 5 | Roof only |
| Air Handling Unit | D3052.011a | 23 | Roof only |
| Motor Control Center | D5012.013a | 6 | Roof only |

For this research, the ground motions are selected from the P-695 far field set and scaled per the requirements of FEMA P-695. Seven records are selected from this set, and both components are used in the analysis to simulate the three-dimensional behavior. It is important to note that the same mathematical model was used to represent the system in each direction. The modeling dispersion which is used during the Monte Carlo simulations to define the potential spread of response, is determined to be 0.354, assuming average building definition, average construction quality assurance and average quality and completeness of the analytical model. The analyses are performed at the intensity levels of interest, and story drift ratios and absolute acceleration are used as the demand parameters. Two hundred (200) Monte Carlo realizations are used to expand on these results. Since the buildings are designed using location neutral spectra, no hazard curve is available and therefore, no time-based assessment is performed.

## 3.5. Results

### *3.5.1. Hybrid Buckling Restrained Braces*

For the BRB systems, the results are presented in the order of the number of total stories, starting with the 4-story systems. Cost distributions are plotted for the intensity with the smallest reduction in average cost between systems and for the intensity with the largest reduction in average cost between systems. Figure 3-3 shows example cost distributions for the 4-story models at the serviceability level and the near-collapse levels. These plots display the range of consequence results, where each point is the cost from one realization. The cost values are plotted against the probability of non-exceedence. For this model, the largest improvement can be seen at the serviceability level, where the average costs are reduced by more than 12 percent when comparing the Regular system to the Hybrid 3 system.

For the higher intensity ground motions, the cost distributions tend to "flatten out." This is the distinction between partial repair cost and total repair cost, and these plots are representations of a mixed distribution. The cumulative probability distributions are developed including both the discrete distribution of the partial repairs and the continuous distribution of the total repairs. The points at $300 per square foot that stack on top of each other represent the total repair cost, assuming a collapse has occurred. The partial repair costs tend to be around $100 per square foot or less for this P-58 Building Information Model.

These cost distributions (as well as the results of other consequences) could be used by stakeholders and decision makers to determine if the building performance is satisfactory. Because the FEMA P-58 procedure does not provide any prescriptive acceptance criteria, these criteria must be developed on an individual basis. For some stakeholders, the average costs under a given intensity might be the basis of their acceptance criteria. For other stakeholders, it may be important to compare acceptance criteria to a higher probability of non-exceedence, like the $84^{th}$ percentile (the mean plus one standard deviation). One of the major benefits of the FEMA P-58 procedure and its consequence results is that it provides framework for decision makers to determine acceptable levels of response based on the individual applications of the structure, which is the inherent principle of Performance Based Earthquake Engineering.

Additionally, these distributions provide a method of evaluation between two systems, which is the primary focus of this work. For numerous values of probability of non-exceedence, the consequences between systems can be compared. As the distribution shifts to the left, the cost per square foot for a given probability is decreased. As an example, under the near-collapse intensity level, the repair cost for the regular system is $16.27 per square foot at a probability of non-exceedence of 0.5. At the same probability of non-exceedence, the repair cost per square foot is between $14.74 and $14.95 for the hybrid structures.

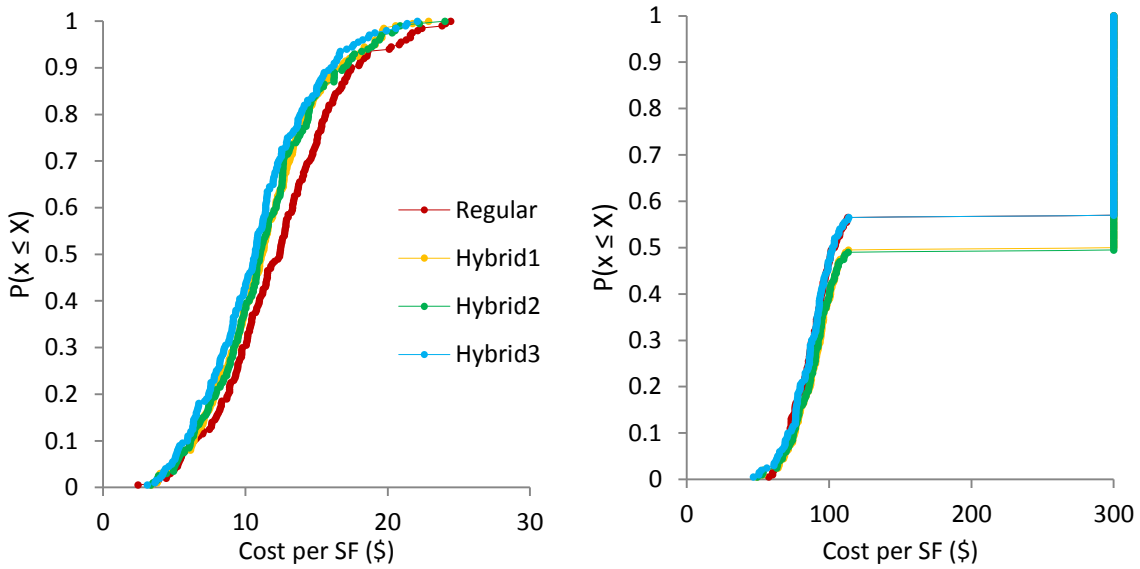


**Figure 3-3.** Probability distribution of the repair costs for the 4-story BRB models for the serviceability intensity level (left) and near-collapse intensity level (right)

To relate these distributions to the physical behavior of the model, the consequences can be broken down by the influence of the performance groups. This related the points on the distribution to the damaged components in the system. This breakdown will be different for every realization, but as an example, the influence to Realization 20 for the Regular BRB will be presented. For the serviceability level intensity, the total repair cost during Realization 20 was $707,155 (or $12.28 per square foot). Figure 3-4 shows the components whose damage contributed to the cost estimate. The values that are shown sum the damage over all stories, although the PACT program will break the costs down by floor and direction as well.

As expected, the contributions to cost come primarily from the non-structural components at the low ground motion intensity. If the same breakdown was investigated at higher intensities, more components would likely be damaged, including structural components. At the highest intensities, the contribution to cost can be dominated by collapse. These breakdowns of the consequence contribution are an additional benefit of the P-58 methodology, which allows the user to determine the components that are most susceptible to damage under various intensities. Additionally, engineers could use this information to determine where a design adjustment could be the most effective for reducing consequences. These breakdowns are also available for the other consequences, although they will not be presented in this work.

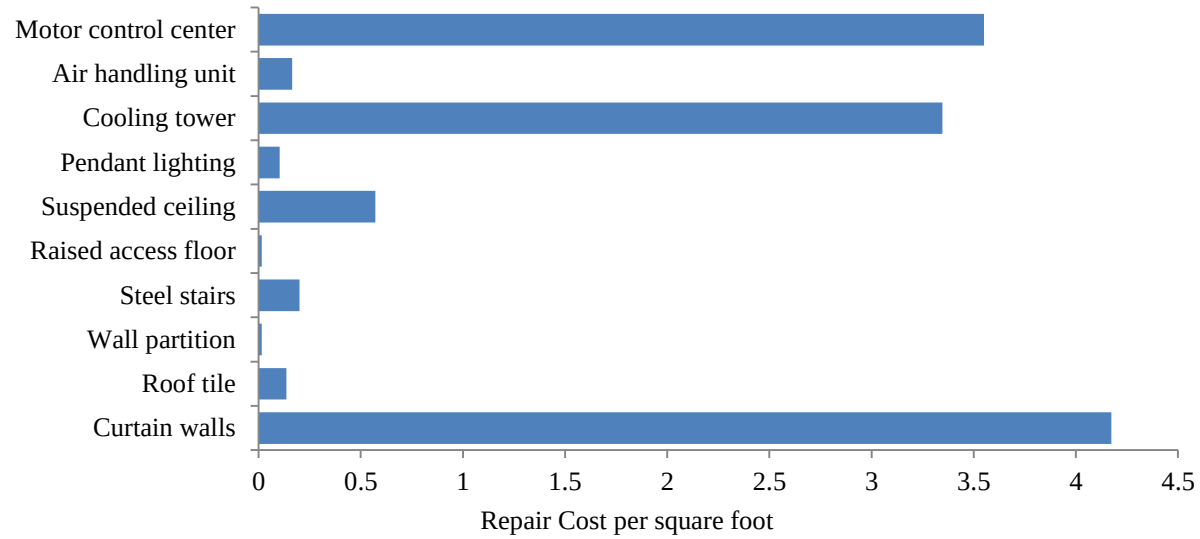


**Figure 3-4.** Component damages that contributed to the repair cost estimate

While only the cost distributions are presented in this research, the distributions of other consequences are also reported when using the FEMA P-58 procedure. In order to summarize the reductions in these other consequences, the noticeable reductions in the average consequences will be reported. For the 4-story model, at the serviceability level, the average repair time is reduced by up to 12 percent (from 105 days for the Regular system to 91 days for the Hybrid 3 system). At all other intensity levels, the change in repair time is negligible. Additionally, there was negligible change in the probability of receiving an unsafe placard between the systems. The average number of deaths under the serviceability intensity level is reduced by up to 14 percent; otherwise, the change in casualties is negligible. The median number of collapses is always zero, meaning there are more realizations that did not simulate casualties than realizations that did simulate casualties.

Figure 3-5 shows example cost distributions for the 9-story models at the serviceability level and the MCE level. For this model, the largest improvement can be seen at the MCE level, where the average costs are reduced by nearly 24 percent when comparing the Regular system to the Hybrid 3 system.

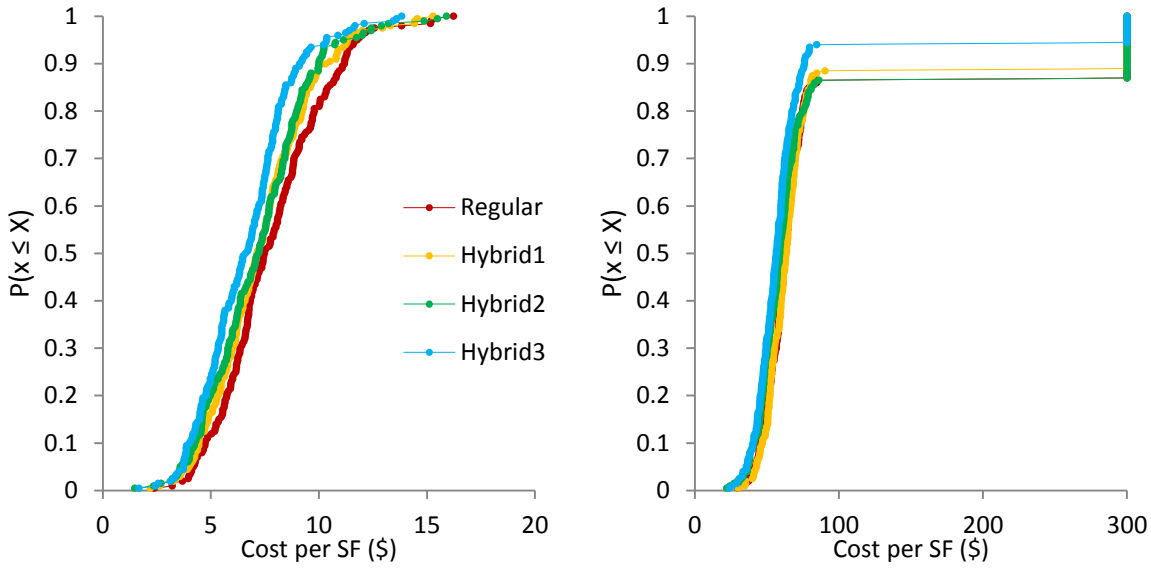


**Figure 3-5.** Probability distribution of the repair costs for the 9-story BRB models for the serviceability intensity level (left) and MCE intensity level (right)

At the serviceability level, the average repair time is reduced by up to 13 percent (from 166 days for the Regular system to 145 days for the Hybrid 3 system). At all other intensity levels, there is no change in repair time. The reduction in total probability of receiving an unsafe placard is 11 percent for the DBE level intensity (from 89 percent for the Regular system to 78 percent for the Hybrid 3 system) and negligible for all other intensity levels. The average number of deaths was reduced by up to 50 percent under the serviceability intensity level (from 6 deaths for the Regular system to 3 deaths for the Hybrid 3 system), up to 7 percent under the DBE level (from 39 deaths for the Regular system to 36 deaths for the Hybrid 3 system), up to 12 percent under the MCE level (from 56 deaths for the Regular system to 50 deaths for the Hybrid 3 system), and up to 9 percent under the near-collapse level (from 70 deaths for the Regular system to 64 deaths for the Hybrid 3 system). For the near-collapse level, the median number of casualties ranged between 8 and 9 deaths; all other median casualties are zero.

Figure 3-6 shows example cost distributions for the 18-story models at the serviceability level and the near-collapse levels. For this model, the largest improvement can be seen at the near-collapse level, where the average costs are reduced by more than 26 percent when comparing the Regular system to the Hybrid 3 system.

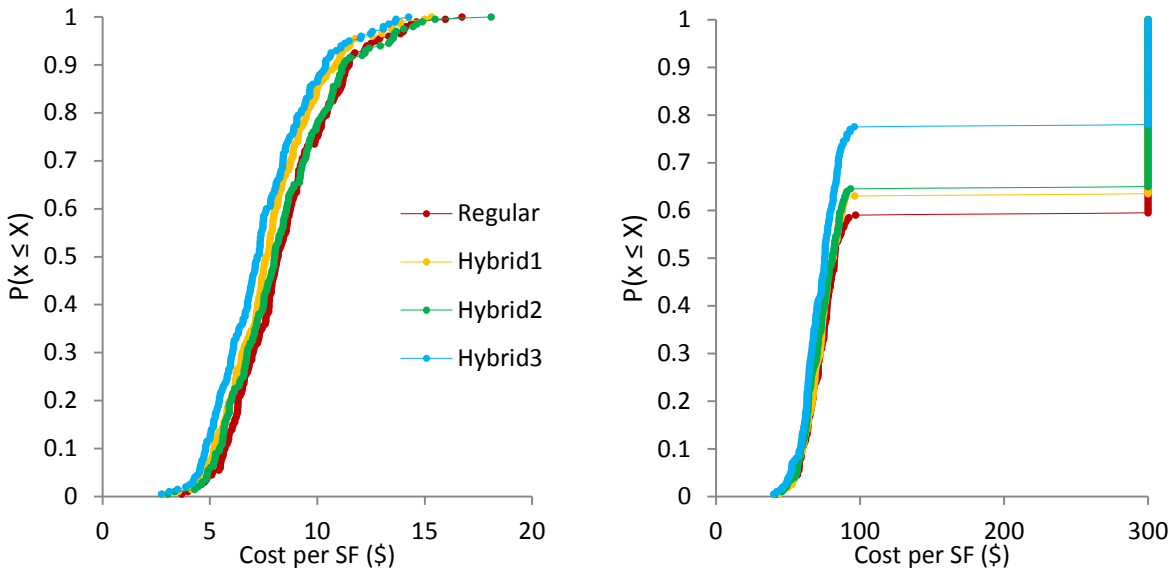


**Figure 3-6.** Probability distribution of the repair costs for the 18-story BRB models for the serviceability intensity level (left) and near-collapse intensity level (right)

At the serviceability level, the average repair time is reduced by up to 11 percent (from 402 days for the Regular system to 356 days for the Hybrid 3 system). At all other intensity levels, there is no change in repair time. The reduction in total probability of receiving an unsafe placard is more than 5 percent for the MCE level intensity (from 89 percent for the Regular system to 84 percent for the Hybrid 3 system) and negligible for all other intensity levels. The largest decrease of average number of deaths is seen under the near-collapse level (from 151 deaths for the Regular system to 124 deaths for the Hybrid 3 system). The median number of casualties is always zero.

### *3.5.2. Collapse Prevention Systems*

Figure 3-7 shows the cost distributions for the 2-story and 4-story models under the near-collapse level intensity. The collapse prevention systems decrease the average repair costs for all structures, particularly for the shorter structures. For the 2-story model, the slack cable and loose link mechanisms reduce the average repair cost by 35 percent and 18 percent, respectively. For the 4-story model, those reductions are 33 percent and 5 percent, respectively. In these figures, MF+GS refers to the moment frame plus gravity system, MF+GS+SC refers to the moment frame plus gravity system plus slack cable CPS, and MF+GS+LL refers to the moment frame plus gravity system plus loose-link CPS system.

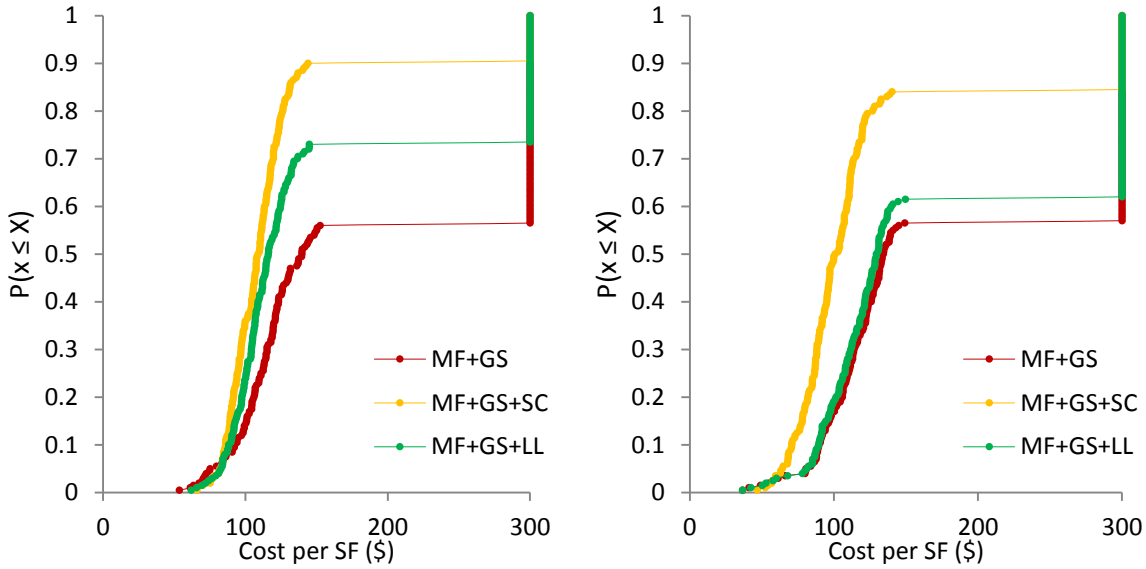


**Figure 3-7.** Probability distribution of the CPS repair costs for the near-collapse level intensity for the 2-story models (left) and 4-story models (right)

For all the models, the collapse prevention systems have negligible effect on the average repair time and total probability of receiving an unsafe placard. However, the average number of casualties is significantly decreased in many cases. The reduction from the slack cable mechanism is more than 32 percent for the 2-story model and nearly 15 percent for the 4-story model, and the reduction from the loose link mechanism is nearly 15 percent for the 2-story model and nearly 7 percent for the 4-story model. The median number of casualties is zero for all the models.

### 3.5.3. Special Moment Frames Modeled With and Without Gravity Systems

Like for the BRB systems, the results are presented in the order of the number of total stories, starting with the two story systems, and the cost distributions are plotted for the intensity with the least improvement between systems and for the intensity with the most improvement between systems. Figure 3-8 shows example cost distributions for the 2-story models at the serviceability level and the MCE levels. For this model, the largest improvement in average cost can be seen at the higher intensity levels. The average cost was decreased by more than 12 percent under the DBE level, by 21 percent under the MCE level, and by nearly 18 percent under the near-collapse level intensity. Under the serviceability levels, the average cost actually increased up to 10 percent when the partially restrained connections are modeled. This is due to the sensitivity of the nonstructural components to small changes in acceleration values. The accelerations experienced by the models with the gravity system at certain stories were occasionally higher than the models with no gravity system resistance. While these changes in acceleration were not excessive, they are reflected in the nonstructural costs during the realizations with higher total costs. Since the nonstructural components have a strong influence

in the consequences at the serviceability levels, this phenomenon is more prevalent at the lower intensities. The results between the two levels of gravity connection strengths are similar, and the higher strength does not necessarily cause a larger decrease in consequences.

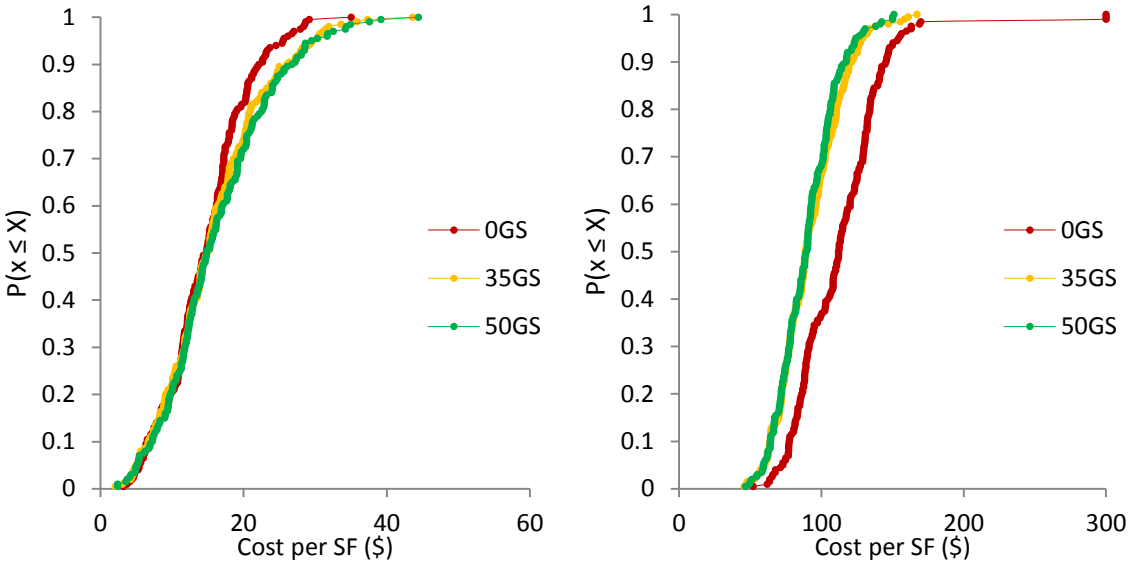


**Figure 3-8.** Probability distribution of the repair costs for the 2-story SMRF models for the serviceability intensity level (left) and MCE intensity level (right)

The repair time is decreased by more than 6 percent under the DBE level (from 355 days for the 0GS system to 345 days for the 35GS); the change is negligible for all other intensities. The probability of receiving an unsafe placard is decreased by 8 percent under the DBE level (from 98 percent for the 0GS system to 90 percent for the 50GS); the change is negligible for all other intensities. For all models, the average number of casualties is negligible. The median number of collapses is zero, except under the near-collapse level intensity. In this case, the median number of casualties is always around 1.0.

Figure 3-9 shows example cost distributions for the 4-story models at the serviceability level and the near-collapse levels. Like the 2-story model, the largest improvement can be seen at the higher intensity levels. The average cost was decreased by 17 percent under the DBE level, by 29 percent under the MCE level, and by nearly 32 percent under the near-collapse level intensity. Under the serviceability levels, the average cost actually increased up to 7 percent when the partially restrained connections are modeled. The results between the two levels of gravity connection strengths are similar, but the higher strength does cause a larger decrease in cost for this structure.

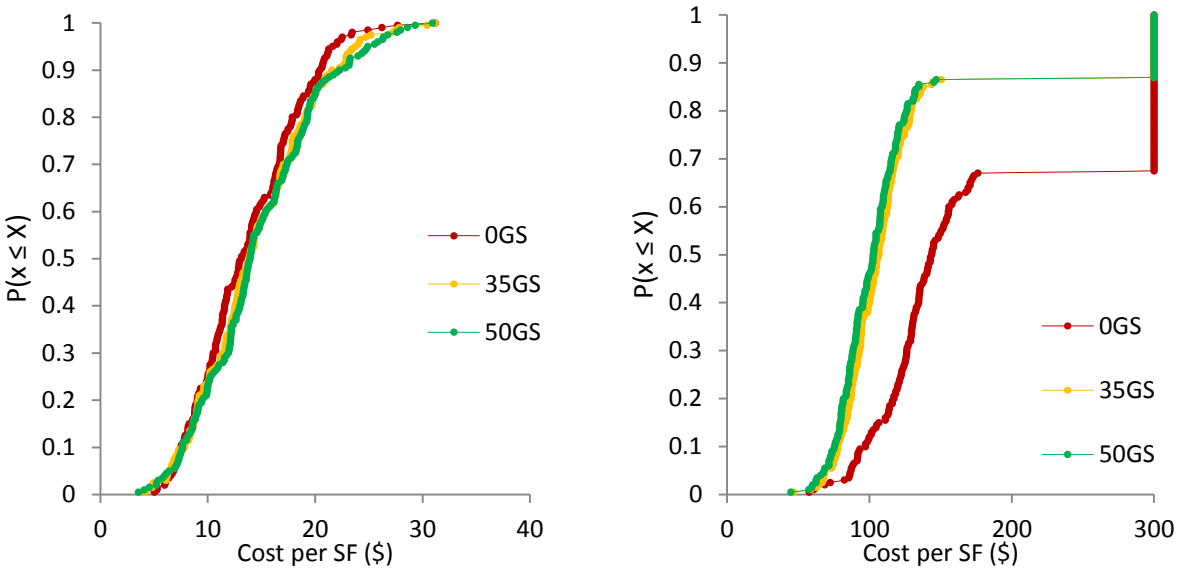


**Figure 3-9.** Probability distribution of the repair costs for the 4-story SMRF models for the serviceability intensity level (left) and near-collapse intensity level (right)

The changes in repair time and probability of receiving an unsafe placard for the 4-story model are negligible. The average number of casualties is reduced under the larger intensities. This reduction is up to 11 percent under the MCE and up to 23 percent under the near-collapse level intensity (from 33 deaths for the 0GS system to 26 deaths for the 50GS). The median number of collapses is always zero.

Figure 3-10 shows example cost distributions for the 8-story models at the serviceability level and the near-collapse levels. Like the previous models, the largest improvement can be seen at the higher intensity levels, but the average costs decrease at all intensity levels. The average cost was decreased by more than 3 percent under the serviceability level, by 10 percent under the DBE level, by nearly 10 percent under the MCE level, and by nearly 11 percent under the near-collapse level intensity. These reductions at the higher intensities are less than those for the shorter structures. The changes in repair time, probability of receiving an unsafe placard, and number of casualties for the 8-story mode are negligible. The median number of collapses is zero, except under the DBE level intensity. In this case, the median number of casualties is 7 deaths.

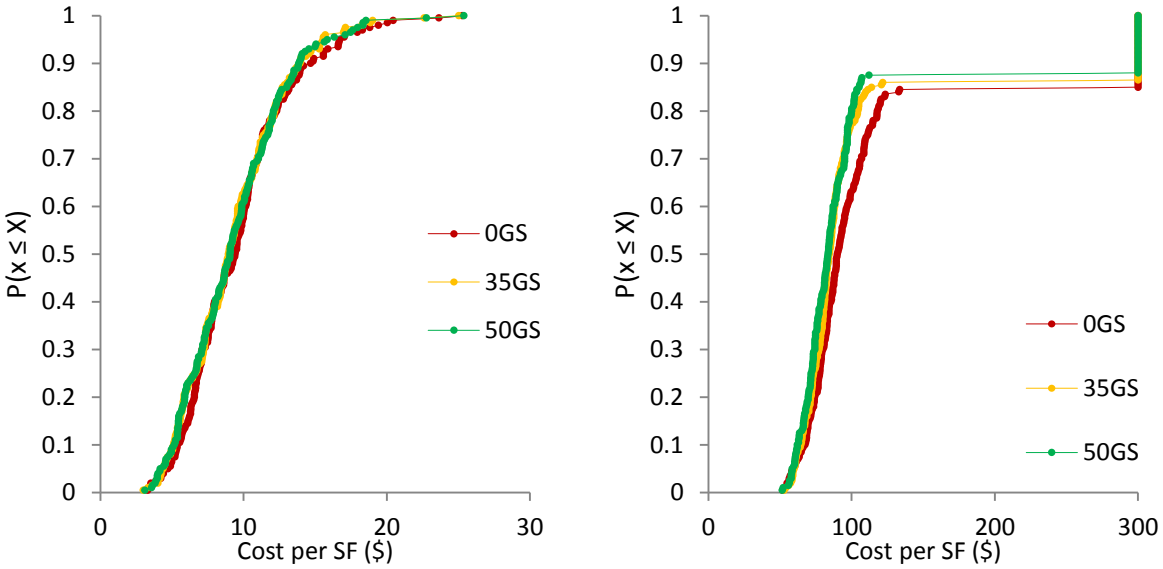


**Figure 3-10.** Probability distribution of the repair costs for the 8-story SMRF models for the serviceability intensity level (left) and near-collapse intensity level (right)

### 3.6. Summary and Conclusions

This research provides comparative analyses of new and traditional seismic resisting systems and modeling methodologies, shows the results of those analyses in terms of consequence, and gives numerous examples of the P-58 methodology. The results presented show how changes to the design or modeling of a system can have substantial influence in the behavior at multiple intensity levels. The results are presented in terms of repair costs, repair times, number of casualties, and probability of receiving an unsafe placard, which are more meaningful to owners and other decision makers. The innovative systems discussed here can provide significant benefit to the lateral resistance of a structure when analyzed using the principles of Performance Based Earthquake Engineering.

The first innovative system, the Hybrid BRBs, use a multi core system with steels of different strengths. These various strengths are used to control the sequence of yielding, and with a minimum change to the design of BRBs, the behavior can be significantly modified. When compared to traditional BRB systems, the repair costs are reduced by up to 12 percent at lower intensity levels for short structures and up to 26 percent at higher intensities for the taller structures. Additionally, the repair time at the serviceability level is always reduced by more than 10 percent. In general, there was negligible change in the probability of receiving an unsafe placards and the number of casualties. The more hybridity in the BRB, the more the consequences are reduced. This trend was similar to those found in the P-695 analyses (Atlayan and Charney 2013), where the Hybrid 3 system always had the smallest probability of collapse and residual drifts. While residual drifts were not included in the P-58 analyses (again, to prevent the loss of “true data”), one of the major benefits found in the P-695 analyses of the Hybrid

BRBs was the reduction in residual drifts. If these were included in the P-58 analyses, the consequences would likely be reduced even more with the hybrid systems.

The Collapse Prevention System is designed specifically for life safety in locations where that is the only crucial intensity level, like the Central and Eastern United States. In the CEUS, large rare ground motions must be designed for, but more frequently occurring ground motions are negligibly small. The collapse prevention mechanisms are added to the gravity system and remain inactive until the structure reaches a specified level of drift. At the near-collapse level, the average repair costs are always decreased by 5 to 36 percent when the collapse prevention mechanism is added. This reduction was greater for buildings with fewer stories and was greater for the slack cable device than the loose link device. For the 2-story model, the average number of casualties was significantly decreased (nearly 33 percent) by the slack cable mechanism. In general, there was negligible change in the repair time and the probability of receiving an unsafe placard. If a detailed cost analysis is done on the systems, it is likely that the Collapse Prevention Systems will have a lower initial cost than the comparable seismic resisting system, due to the lack of seismic detailing. Collapse Prevention systems that use non-ductile moment frames do not have demand-critical field welding, and they have fewer and less difficult special inspections when compared to welded ductile moment frames. With this in mind, the reduction in repair cost would likely be even more significant than shown in this work.

Including the lateral resistance from the gravity systems is a modeling assumption, instead of an innovative system like the previous two systems. By modeling this lateral resistance, the average costs can be reduced significantly (up to 32 percent), particularly at higher intensity levels. For the 4-story model, the number of casualties was noticeably reduced at higher intensities; otherwise, all other consequences had negligible change. It should be noted that these consequence reductions may be unconservative, due to the simplistic nature of the modeling of the partially restrained connections.

### 3.7. Recommendations and Future Work

The Hybrid Buckling Restrained Braces could be used where traditional Buckling Restrained Braces are acceptable. With a minimal change to the design of the BRB, the Hybrid BRBs can significantly reduce the consequences, particularly the repair costs, under multiple intensities. The collapse prevention systems, on the other hand, should be used in locations where the seismicity is controlled only by large, rare events. These systems provide a mechanism that only activates under large drifts to reduce the number of collapse and the consequences at these high intensities. The lateral strength and resistance of the gravity system could be included if the engineers wants a more accurate estimation of consequences from the mathematical model.

Additional analyses should be run with new structural configurations to determine how the trends expand to a wide variety of uses. The P-58 analyses for the Hybrid BRBs should be run with the residual drift inputs to determine the additional decrease in consequences, and the P-58 analyses of the Collapse Prevention Systems should be run with a more accurate cost estimate to determine the additional decrease in consequences. Additionally work should be done to improve the modeling of the gravity system connections. Simplistic models and limited test data result in a modeling methodology that may not be sufficient to capture the true behavior of the gravity connections.

While the PACT program includes a wide variety of fragilities, there are still numerous components in a typical building that do not have fragilities developed. For a more accurate estimation of consequences, these fragilities would need to be developed. Additionally, the cost estimates in PACT are based on 2011 estimates. These will need to be updated on a regular basis, or the P-58 procedure could become obsolete in a few years. These systems could also be analyzed for a specific location using a time-based assessment to see location specific benefits.

# Chapter 4: "Response-History Analysis for the Design of New Buildings: A Study of Assumptions"

Jordan A. Jarrett, Reid B. Zimmerman, Finley A. Charney, Afshar Jalalian

[To Be Submitted to Earthquake Spectra]

**Abstract**

Numerous assumptions are made when developing methodologies for nonlinear response history analyses. The accuracy of several assumptions is investigated using proposed changes to Chapter 16 of ASCE 7. The major findings of this work include: (1) Modeling the gravity system's lateral influence can have significant effect on the system behavior but is unnecessary unless a more accurate representation of the behavior is needed. (2) Exclusion of a residual drift check is acceptable when concerned with collapse prevention. (3) Spectrally matched ground motions should cautiously be used for near-field structures. (4) The effects of nonlinear accidental torsion can be influential, but there are insufficient studies to warrant modification of existing code language at this time. (5) Even if a structure is designed per ASCE 7, it may not have the assumed probability of collapse under the maximum considered earthquake when analyzed using FEMA P-695.

## 4.1. Introduction

### *4.1.1. Summary of Proposed ASCE 7 Chapter 16 Provisions*

The Building Seismic Safety Council Response History Analysis Issue Team has proposed changes for the next update of Chapter 16 for ASCE 7-16, which encompasses nonlinear response history analysis of building structures (Haselton et al. 2013). More than a minor update from ASCE 7-10, the proposed Chapter 16 for ASCE 7-16, hereinafter referred to simply as Chapter 16, makes significant changes to and replaces large portions of the existing provisions, which were identified as outdated and in some cases unclear. An introduction to these changes will be discussed here, but a more complete description of the development and application of the ASCE 7 Chapter 16 provisions can be found elsewhere (Haselton et al. 2013, Zimmerman et al. 2013).

The seismic hazard for Chapter 16 is set at the risk targeted maximum considered earthquake ($MCE_R$) level, instead of the design basis earthquake. Additionally, two methods are proposed for the $MCE_R$ design spectrum. The first is the traditional code-based spectrum developed for $MCE_R$ with or without site-specific procedures, as described in Chapter 21 of ASCE 7-10 (ASCE

2010). The second proposed method requires the development of two or more conditional spectra (Haselton et al. 2013).

A suite of eleven record sets for the traditional code-based spectrum, or one suite of eleven record sets for each conditional spectra, is defined as the minimum number of records. This new requirement replaces the old provisions of using a suite of three or more record sets. The chosen record sets should be consistent with the tectonic setting, magnitude and distance controlling the seismic hazard at the site and should have a spectrum that closely follows the target spectral shape. Simulated ground motions are considered acceptable, especially to fill any gaps where recorded motions are scarce. Chapter 16 additionally requires that ground motions used for near-fault sites include rupture directionality, velocity pulses, and fling step. Spectral matching is also permitted; however, the scaling requirements are different than those of amplitude-scaled and simulated ground motions.

Scaling of ground motions has been changed, motivated by the switch from a geometric mean to a maximum direction target spectrum. Instead of combining the two ground motion components using the square-root-of-the-sum-of-the-squares (SRSS) method, a maximum direction spectrum for each motion must be constructed, either by using the period-dependent scale factors, such as those listed in Table C21.2-1 of the 2009 NEHRP Recommended Seismic Provisions (FEMA 2009c), or by direct computation through rotation of the motion over all angles. The average over the suite of these maximum direction spectra must fit the target spectrum on average and cannot fall below 0.9 times the ordinate of the target spectrum within the period range of interest. If spectrally matched ground motions are used, the average of all the individual components must not fall below the target spectrum within the period range of interest. Due to the scaling of individual components rather than maximum direction spectra, this requirement adds an implicit penalty to spectral matching in these procedures. For near-fault sites, the as-recorded fault normal and fault parallel ground motion components must be applied in the fault normal and fault parallel directions at the site considering the controlling fault orientation. For non–near-fault sites, the ground motions are applied in arbitrary orientations.

Modeling requirements remain general, similar to previous provisions, with a few additions and modifications. These modifications include the designation of force and deformation controlled elements, a cap on inherent viscous damping, clearer provisions on soil-structure interaction, the required use of expected strengths, and removal of multiple gravity load conditions. Chapter 16 also gives the analyst the choice of directly modeling the stiffness and strength of the gravity system and does not require consideration of accidental torsion in the nonlinear analyses. Three-dimensional models are required, and thus, two-dimensional mathematical models will no longer be allowed.

The acceptance criteria, on the other hand, have been significantly modified. Chapter 16 still references testing and relies on other standards for specific values of acceptance criteria (PEER 2010, ASCE 2006), but provides a framework over which the available information can be translated into ASCE 7 checks. It does this by separating acceptance criteria into global and local designations, with the former including provisions for drift and the case of unacceptable response and the latter encompassing force- and deformation-controlled elements. Drift limits are taken from ASCE 7 Chapter 12 and modified for nonlinear response history analysis results at $MCE_R$ level ground motions. An unacceptable response is defined as any ground motion that causes dynamic instability, non-convergence, exceedance of the valid range of modeling for deformation controlled actions, or exceedance of capacity in critical force controlled actions. The provisions require that for Risk Category I and II structures, analyzed without spectral matched ground motions, no more than one in eleven motions can cause an unacceptable response. For Risk Category III and IV structures, no unacceptable responses are allowed. Deformation-controlled actions must additionally not exceed a given proportion of the point at which vertical load-carrying capacity is lost, while amplified force-controlled action demands may not exceed the corresponding strength capacity. The proportion for deformation-controlled and amplification for force-controlled actions depend on the severity of the failure with critical elements being those where failure should lead to local or global collapse. Examples of force- and deformation-controlled actions include axial force in columns and plastic rotation of beam-column connections, respectively.

The Chapter 16 methodology is assumed to implicitly satisfy a 10 percent probability of collapse under the $MCE_R$ level ground motion for Risk Category I and II, as described in Table C.1.3.1b in ASCE 7-10 (ASCE 2010). This level of probability was originally recommended in the FEMA P-695 methodology (FEMA 2009a) and then later adopted for ASCE 7. For a Risk Category III structure, this probability is reduced to 6 percent, and for a Risk Category IV structure, it is reduced further to 3 percent.

### *4.1.2. Description of Assumptions Investigated*

The proposed Chapter 16 provides a more comprehensive methodology for nonlinear response history analysis and related acceptance criteria of structures compared to the existing provisions (ASCE 2010). During its development, however, numerous assumptions have been made that require further investigation. This work highlights several aspects of the proposed update, including: (1) the influence of the inclusion of the lateral strength and stiffness of the gravity system, (2) the practicality of a residual drift check, (3) the applicability of spectrally matched ground motions, (4) the necessity of a nonlinear accidental torsion check, and (5) the accuracy of the assumed implicit satisfaction of a specified percent probability of collapse under the $MCE_R$ level ground motion. It is important to note that the conclusions made in this research could be

applicable to any methodology that uses nonlinear response history analysis, even though the basis is the proposed Chapter 16.

The first provision investigated is the effect that the stiffness and strength of the gravity framing system can have on satisfaction of the Chapter 16 provisions. Gravity systems are rarely included in analytical models for response history analysis, other than to capture P-Delta effects or identified interactions where gravity systems are thought to affect the demands on the lateral system. It is typically believed to provide conservative results when the gravity systems are omitted. In reality, this inclusion could provide more accurate results, since historical evidence has shown that the gravity system can provide significant resistance during earthquakes. For example, during the 1994 Northridge earthquake, many special moment frame connections developed brittle failures; however, these buildings did not collapse, in part because the gravity system provided additional seismic resistance (Lui and Astaneh-Asl 2000, Green et al. 2004). Including all the aspects of lateral strength and stiffness of the gravity system would provide a more realistic model and response. However, there is little agreement within differing provisions on how to handle the modeling of the gravity system. The FEMA P-58 methodology states that all elements that provide lateral resistance should be included, but it does not give a definite recommendation of the inclusion of the gravity system (FEMA 2012). The Tall Building Initiative recommends the inclusion of the gravity system resistance (PEER 2010), while the gravity system is never modeled when using the traditional P-695 methodology (FEMA 2009a). However, in the Appendix F methodology of FEMA P-695, which is discussed in more detail later, the modeling of the gravity system is recommended. Chapter 16 does not require explicit modeling of the gravity system unless it significantly affects the seismic response under the $MCE_R$ ground motions; however, the influence of the gravity system resistance is likely not known unless it is modeled. Due to this concern, the effects of this provision are investigated in this study.

In some performance-based design guidelines such as the Tall Building Initiative (PEER 2010) and the FEMA P-58 methodology (FEMA 2012), calculation of residual drifts is required. For the Tall Building Initiative, the mean residual drift ratio from a suite of ground motion records may not exceed 1 percent. Residual drifts are a key factor in procedures used to determine the post-earthquake capacity of a structure (Bazzurro et al. 2004), and high residual drifts often mean that it is more economically feasible to demolish the damaged structure than to repair it (McCormick et al. 2008, Ruiz-Garcia and Miranda 2010). However, studies have also shown that the magnitude of residual drifts rarely relates to collapse under typical aftershock events (Lee and Foutch 2004). Since Chapter 16 is mostly concerned with collapse prevention, it does not require a check on residual drifts. This study will determine if residual drift can be linked in any way to collapse, which would warrant the inclusion of a residual drift check.

The third assumption investigated is the acceptability of using tight spectral matching to modify ground motions, which is an option in the updated Chapter 16. In this paper, tight spectral matching is defined as frequency-modification of recorded ground motion acceleration time histories such that the resulting response spectrum fits a pre-determined target spectrum with little deviation over a selected period range. Tight spectral matching is the most common form of a broader class of spectral matching techniques and is often employed by practicing geotechnical engineers when providing ground motion time histories for the design of buildings. The appropriateness of tight spectral matching is heavily debated in the literature with well-founded arguments in support of and against using matched ground motions (NIST 2011, Hancock et al. 2008, Bazzuro and Luco 2006). Since this debate is extensive in the literature, it is not the intent of the authors to provide a final conclusion on this matter but rather to explore how tight spectral matching specifically affects the results of the updated Chapter 16 through several case studies. If spectrally matched ground motions generated by the Chapter 16 provisions produce comparable results to those of amplitude scaled motions, then it is likely that they are suitable if the design engineer choses to use them.

The effect of accidental torsion is investigated to determine the necessity for such a check within nonlinear response history analyses. Accidental torsion is typically ignored in performance-based earthquake engineering provisions, including the P-695 procedure (FEMA 2009a), the P-58 procedure (FEMA 2012) and the Tall Building Initiative (PEER 2010). However, this accidental torsion has been shown to have a significant effect on the inelastic behavior of structures (Mansuri 2009), which could warrant a check for accidental torsion within a nonlinear response history procedure. One method to assess accidental torsion is to extend linear procedures such as those that exist in ASCE 7 Chapter 12 (ASCE 2010) and ASCE 41 (ASCE 2006), where the center of mass is shifted 5 percent of the diaphragm dimension in each direction independently, to nonlinear procedures. Studies have shown that the uncertainty in the center of mass is typically the largest influence to accidental torsion (De la Llera and Chopra 1995), which is likely why the 5 percent offset procedure is typically used. The practical concern for response history analysis is that the shifts in mass quadruples the number of analyses performed, since the structure must be analyzed with the four shifted center of mass locations. The research presented herein will investigate whether accidental torsion should be included in the nonlinear analysis.

The final assumption investigated is the implicit satisfaction of the specified probability of collapse when subjected to $MCE_R$ motions. As discussed previously, the value of this maximum probability of collapse is dependent on the risk category of the structure, and structures with different risk categories are investigated in this work. Chapter 16 does not directly determine the probability of collapse but assumes that this limit will be satisfied if all other criteria are satisfied. The FEMA P-695 methodology, on the other hand, explicitly addresses the probability of collapse. This methodology is further discussed in the next section, but performing both

methodologies on the same structure will help investigate the accuracy of this implicit assumption of Chapter 16.

### *4.1.3. Summary of P-695 Methodologies*

FEMA P-695 provides a methodology for determining probabilities of collapse of structures, as well as their seismic performance factors ($R$, $C_d$, $\Omega_0$) used in design (FEMA 2009a). For this research, the application of this methodology will focus on the determination of the probability of collapse. There are two variations of the methodology, referred to herein as the Standard Methodology (which is typically performed on a set of archetypes) and the Appendix F Methodology (which is used for the evaluation of an individual structure).

The first step in either of the variations of the P-695 methodology is to determine a seismic design category. The P-695 process has included four "location neutral" spectra that can be used to design and analyze a structure. Once designed, a structure must be modeled, and in order to accurately determine the collapse parameters, a detailed nonlinear model of the structure needs to be constructed. To simulate collapse, the model should capture all significant nonlinear effects and must include strength and stiffness degradations under large deformations. Non-simulated collapses can be indirectly evaluated using alternative intensity level checks. A nonlinear static pushover analysis is performed, and then nonlinear dynamic analyses are performed using one of two scaled suites of record sets: 22 pairs of far-field ground motions or 28 pairs of near-field motions. If the structure is within 10 kilometers of an active fault, the near-field suite should be used; otherwise, the far-field suite is selected.

For the standard methodology, incremental dynamic analysis (IDA) is then performed by scaling each ground motion until the structure reaches a collapse point. This analysis is used to find the median collapse capacity, $\hat{S}_{CT}$, which is defined as the spectral intensity at which half of the ground motions have caused the structure to collapse or exceed the non-simulated collapse criteria. The collapse margin ratio (CMR) is calculated as the median collapse spectral acceleration, $\hat{S}_{CT}$, divided by the spectral acceleration at the maximum considered earthquake, $S_{MT}$. Once the CMR has been calculated, it can be converted to the adjusted collapse margin ratio (ACMR), which is equal to the CMR multiplied by the spectral shape factor, SSF, which is tabulated in the methodology. The ACMR will be used along with the total dispersion, $\beta_{TOT}$, to determine the probability of collapse of a structure, $P_c$, which can be calculated as shown in Equation 4-1. The probability of collapse is not a required calculation in the P-695 methodology, but it can provide insight into the behavior of the structure.

$$P_c = 1 - \int_0^{ACMR} \frac{1}{\beta_{TOT}\sqrt{2\pi}} e^{\left[-\frac{1}{2}\left(\frac{\ln(ACMR)}{\beta_{TOT}}\right)^2\right]} \tag{4-1}$$

For Appendix F of P-695, incremental dynamic analysis is not used. Instead, one scale factor is used for analysis that represents an acceptable collapse factor given a chosen maximum probability of collapse. The normalized ground motions will all be scaled by this singular scale factor, which is given in the methodology. Because Appendix F does not use IDA, an exact probability of collapse cannot be calculated. However, the results will show if the probability of collapse is above or below that limiting value.

## 4.2. Model Descriptions and Assumptions

### *4.2.1. Two-dimensional Structure Modeled with OpenSEES*

The first two systems used in this study are the 2-story and 8-story steel Special Moment Resisting Frames (SMRF) from the examples in ATC 76 (NIST 2010a), referred to hereafter as the MF2 and MF8 Models, respectively. These frames are modeled as two-dimensional (2D) structures in OpenSEES (McKenna 2011). In order to satisfy the modeling requirements of Chapter 16, all nonlinear behavior of the structural system is included. The locations of nonlinear components of the special moment resisting frames include reduced beam sections, panel zones, column bases, and columns at moment resisting joints.

The hysteretic behavior of the reduced beam sections (RBS) is modeled using a plastic hinge and the Modified Ibarra Krawinkler deterioration model (Lignos and Krawinkler 2010) in OpenSEES (the Bilin material). The model used to predict the hysteretic behavior of panel zones is the Krawinkler model (Charney and Marshall 2006). For the columns of the moment frame, a phenomenological model that includes hinges at the bases and story joints is used to predict deterioration. The hysteretic behavior of the columns is also modeled using the Modified Ibarra Krawinkler deterioration model in OpenSEES. This model has the ability to account for deterioration but not to account for P-M interaction. To include the P-M interaction, the columns are given a reduced bending strength based on the column axial load and the P-M interaction curve, per the guidelines in ATC 76 (NIST 2010a).

Both the MF2 and MF8 structures are modeled with and without the gravity system's lateral strength and stiffness. When the gravity system is included, the gravity columns are modeled using fiber sections to check for any nonlinearity. In order to capture the full nonlinear behavior of the gravity system, partially restrained (PR) connections are also modeled, assuming the strength of the partially restrained connection, $Q_{CE}$, is lower than the plastic capacity of the beam it is connecting. For this work, it is assumed that the strength of the partially restrained connections is 50 percent of the strength of the beam. While this percentage may be high when compared to true behavior, this value was taken to see the potential influence that a significant increase in lateral strength could have on the structural behavior. Because modeling of these PR connections can often be a complex endeavor (Rassati et al. 2004), a simple model given by

ASCE 41 (ASCE 2006) is used to represent the moment rotation relationship of these connections. This model depends on the type of connection, and the "top and bottom clip angle connection" is chosen. It is assumed that the connection angles fail due to flexure.

Since both the MF2 and MF8 Models are represented in 2D, floor constraints connect the frames acting in the same direction. P-Delta effects for models without the gravity system are modeled with a leaning column; for models that include the gravity system, P-Delta effects are satisfied by the explicit inclusion of the gravity columns.

### *4.2.2. Three-dimensional Structure Modeled with Perform-3D*

The three-dimensional model used in this paper, referred to hereafter as the 3D Model, is described completely elsewhere and is representative of an actual Risk Category III commercial building (Zimmerman et al. 2013). Its lateral force-resisting system consists of two lines of steel special moment-resisting frame (SMRF) in the longitudinal direction and four lines of buckling-restrained brace frame (BRBF) in the transverse direction over five stories. The lowest story relies on reinforced concrete walls around the building perimeter. Each floor has a rigid diaphragm constraint applied, except the first floor where the diaphragm flexibility is explicitly modeled. The SMRF and BRBF directions align with the fault normal and fault parallel components of ground motion, respectively. A leaning column is provided to capture the P-Delta effects arising from vertical loads acting on the excluded gravity system. Foundation flexibility and consideration of soil-structure interaction effects were not explicitly considered.

Extensive nonlinear modeling is employed in Perform 3D (CSI 2011), including localized axial-moment-moment (PMM) interacting hinges for SMRF and BRBF columns, moment-rotation hinges for SMRF beam-column connections and BRBF beams outside of gusset plates, buckling-restrained brace (BRB) elements and inelastic shear stress-shear strain material models for concrete walls. Values for plastic displacements at which vertical load-carrying capacity is lost for use in Chapter 16 deformation acceptance criteria checks are taken from ASCE 41 (ASCE 2006), testing (SSDA 2001), and a study conducted by Rutherford + Chekene (R+C 2011). The plan view of the Perform 3D model of the structure is found in Figure 4-1.

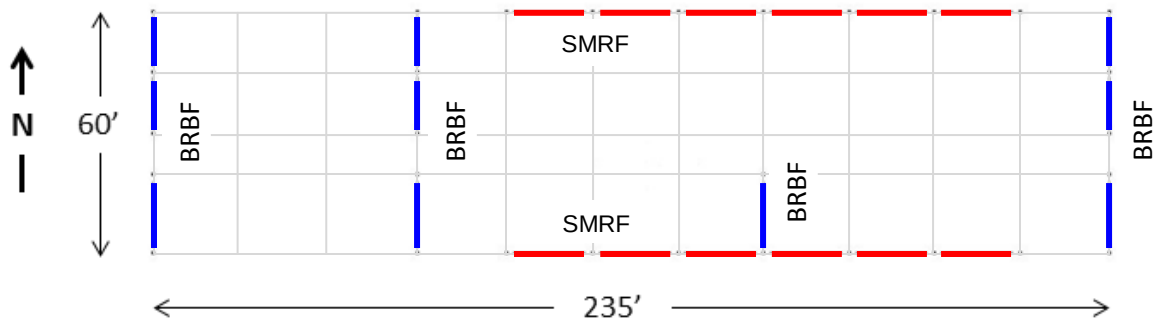


**Figure 4-1.** Schematic of the lateral force-resisting system of the 3D Model

## 4.3. Ground Motion Selection and Scaling

### *4.3.1. Design Spectra for 2D Models*

The code spectrum used for the design and analysis of the special moment resisting frames is the FEMA P-695 $D_{max}$ spectrum, which is defined in the methodology and is based on the ASCE 7-05 design spectra (ASCE 2005). Since the MF2 and MF8 Models are analyzed in 2D, only individual ground motion components are used, and the scaling procedures are similar to those laid out for spectrally matched ground motions. Each individual component is scaled such that the average never falls below the design spectrum. The same ground motions are used as seeds for the creation of a suite of tight spectrally matched ground motions, which are created with the program RSPMatch (Al Atik and Abrahamson 2010). As an example of the scaling procedure, Figure 4-2 shows the response spectra of those components after amplitude scaling (SCAL) and after spectrum matching (MTCH) for the MF2 Models. For the MF8 Model, the same spectrum is used, but the period range considered is changed to 0.46 seconds through 4.6 seconds.

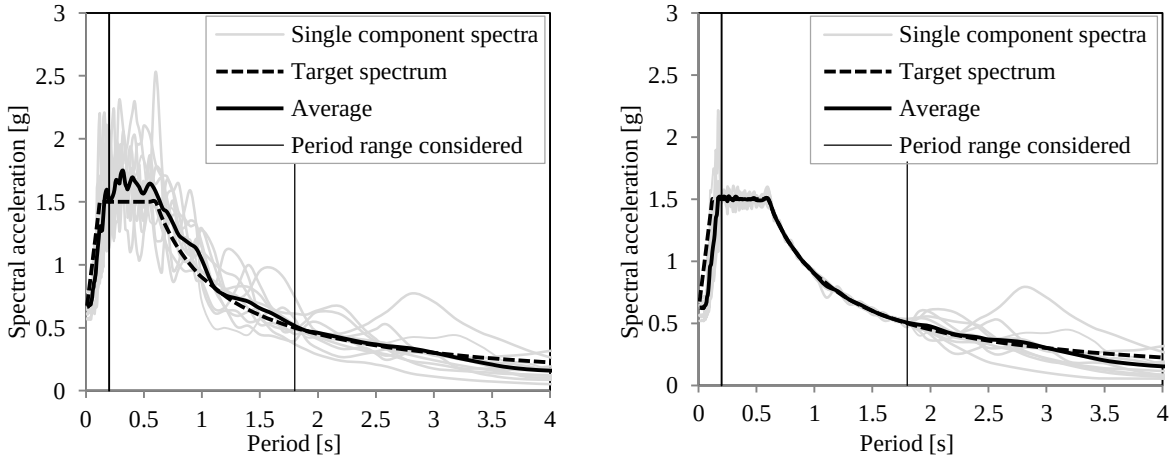


**Figure 4-2.** The response spectra of the amplitude scaled ground motions components (left) and the spectrum matched components (right) versus the target spectrum for the MF2 Model

### *4.3.2. Design Spectra for 3D Model*

A site-specific $MCE_R$ target spectrum was developed for the near-fault site of the 3D Model in Berkeley, California. Due to the proximity to the Hayward Fault, the target response spectrum is deterministically capped by the 80 percent lower limit of ASCE 7 Section 21.3 (ASCE 2010). Figure 4-3 presents the maximum direction spectra for the scaled suite (SCAL) and the single component spectra for the spectrally matched suite (MTCH).

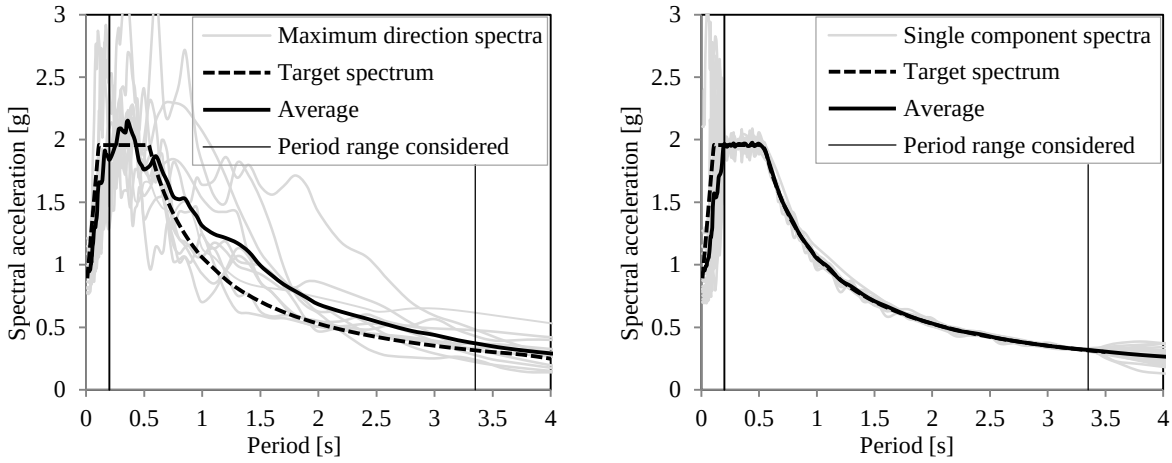


**Figure 4-3.** Maximum direction spectra versus the target spectrum for SCAL suite (left) and the component spectra versus the target spectrum for the MTCH suites (right) of the 3D Model

In addition to the code-based target spectrum, two scenario or conditional spectra were developed for the 3D Model. To capture the predominant periods of response and satisfy the Chapter 16 requirements, two conditional spectra were chosen, one conditioned at a period of 0.5 seconds and the other at 2.0 seconds. These spectra are developed such that the envelope of the scenario spectra is more than 75 percent of the site-specific $MCE_R$ spectrum within the period range of interest. Two suites of eleven motions, one for each spectrum, were then selected and scaled. In accordance with Chapter 16, results from both suites must satisfy all requirements for the structure to be deemed acceptable under the provisions. This is in contrast to using the amplitude scaled or spectrum matched suites, where only one suite of ground motions needs to provide acceptable results. Figure 4-4 presents the maximum direction spectra for the conditional spectra at 0.5 seconds (05CS) and for the conditional spectra at 2.0 seconds (20CS). A more detailed description of spectrum and ground motion development can be found elsewhere (Zimmerman et al. 2013).

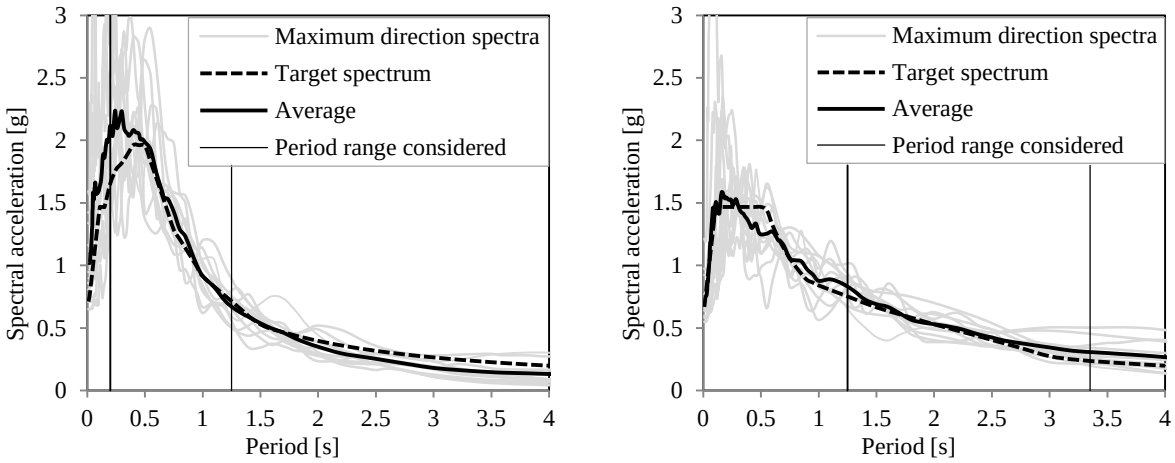


**Figure 4-4.** Maximum direction spectra for the 05CS (left) and 20CS (right) suites versus the target spectrum of 3D Model

### 4.4. Gravity System Modeling Study Results

To investigate the influence of the lateral resistance of the gravity system, both moment frame systems (MF2 and MF8 Models) are modeled with and without this influence. Since the 3D Model has excluded the gravity system, that structure is not addressed in this section. This section provides a discussion on the effects of modeling the gravity system as well as an overall example application of the proposed Chapter 16 methodology. The story drift ratios are presented to investigate the influence of including the lateral strength and stiffness of the gravity system. Using the drift limits in ASCE 7 Chapter 12 (ASCE 2010) and assuming Risk Category II, the allowable story drift ratios for moment frames are 2 percent of the story height. Chapter 16 drift acceptance criteria states that the suite mean story drift ratio should not exceed 2.0 times the drift ratio limits from Chapter 12, which for these moment frames equals 4 percent.

As mentioned previously, the 2D structures are modeled with and without the lateral resistance of the gravity system. Chapter 16 allows the user to determine whether or not to consider the gravity system influence. Figure 4-5 shows the mean drift ratios for the four analyses run on the 2D Models: with or without gravity system and under the SCAL or MTCH suites. Each line on the graph represents the suite mean drift ratio (the average of the maximum drift ratio over all eleven ground motions in each suite).

For the MF2 Model, it is important to note that one instability occurs under the SCAL suite when the strength and stiffness of the gravity system was excluded, which results in a change in the acceptance criteria per the proposed Chapter 16. In this case, the larger of 1.2 times the median of the eleven motions or the mean of the remaining ten motions is compared against the limit. For the MF2 Model under the SCAL suite, 1.2 times the median produces the largest drift ratios, which are 0.042 and 0.038 for the first and second stories, respectively. This first floor drift ratio

exceeds the limit of 0.04, making the analysis unacceptable. The other three analyses satisfy the global acceptance criteria of Chapter 16.

For the MF8 Model, multiple unacceptable responses occur in the lower levels when the gravity system's strength and stiffness are excluded. As mentioned previously, these unacceptable responses can be defined as any ground motion that causes dynamic instability or non-convergence. Under the SCAL suite, six records cause instabilities, while under the MTCH suite, four records cause instabilities. This number of unacceptable responses renders the analyses unacceptable under Chapter 16. Additionally, the system including the strength and stiffness of the gravity system analyzed using the SCAL suite exceeds the drift ratio limit at the first story, and therefore does not comply with the Chapter 16 provisions. The only analysis where the MF8 Model meets the drift requirements is under the MTCH suite when the gravity system is fully modeled.

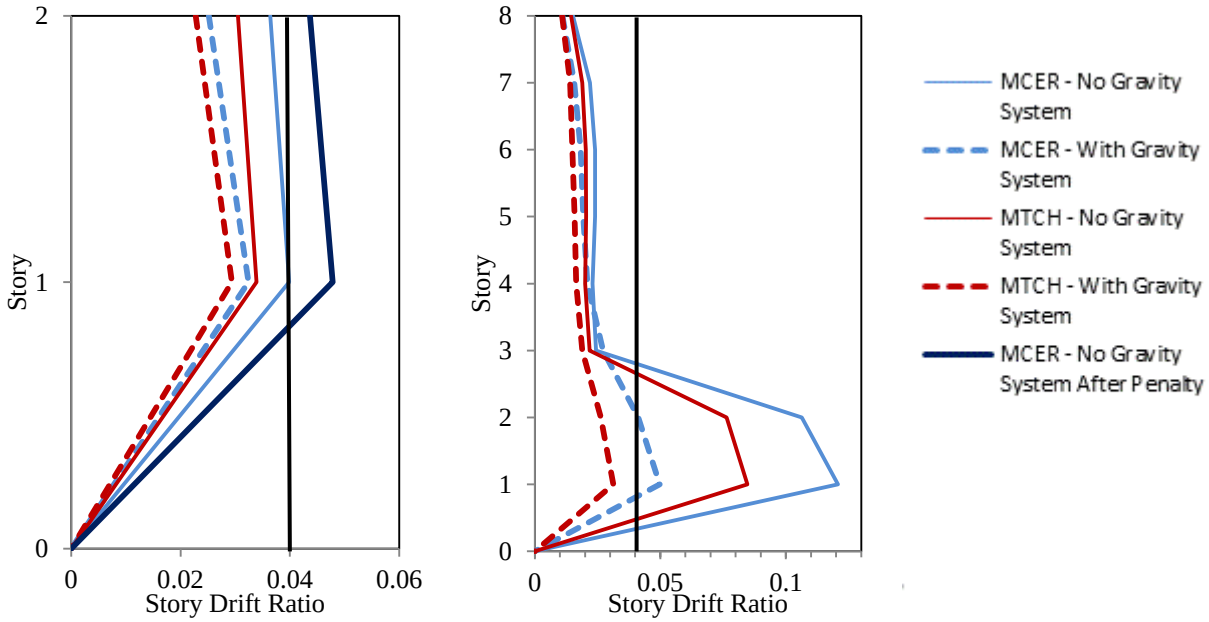


**Figure 4-5.** Suite mean maximum story drift ratio for the four analyses run on the MF2 Model (left) and the MF8 Model (right)

Both models show how the inclusion of gravity strength and stiffness can affect the conformance or non-conformance to the drift acceptance criteria of Chapter 16. As expected, the response and dispersion decrease when additional resistance is included in the form of gravity system modeling. Additionally, instabilities are eliminated when the gravity system influence is captured. The difference in results between the amplitude scaled and spectrally matched ground motions will be discussed in a later section.

## 4.5. Residual Drift Study Results

Chapter 16 remains does not require a check on residual drifts, and the following studies intend to analyze this parameter for structures that otherwise satisfy the provisions.

### *4.5.1. MF2 and MF8 Models Results*

Figure 4-6 shows the suite mean residual drifts for all four analyses of the MF2 and MF8 Models. The suite mean residual drift ratios follow similar trends to the suite mean drift ratios. For the MF2 Model, the ratio between the residual drift and mean drift ratios varies from 20 percent to more than 50 percent. For the MF2 Models that satisfied the Chapter 16 criteria (all except the system without gravity influence under the SCAL suite), the residual drift ratios approach 1 percent, and the standard deviation can also be significant. For the MF8 Model, the ratio between the suite mean residual drift ratios and the suite mean drift ratios varies from 5 percent to above 50 percent on the top six levels. In the bottom two levels, this ratio can exceed 90 percent, although that is a result of multiple instabilities at those levels.

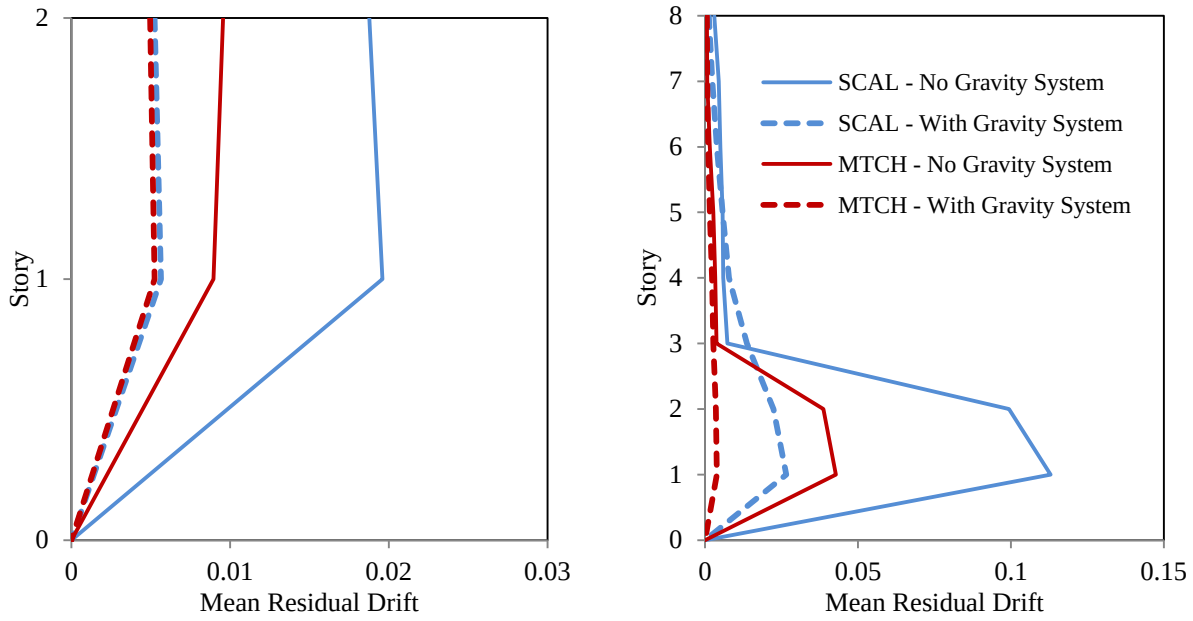


**Figure 4-6.** Suite mean residual drifts for the analyses of MF2 Model (left) and the MF8 Model (right)

Similar to the mean drift ratios, the mean residual drift ratios typically decrease when the gravity system strength and stiffness are modeled. Typically, the spectrally matched ground motions cause a significant decrease in both the residual drift ratios and the ratio between the residual and maximum drift ratios. The one exception is the MF2 Model when the gravity system resistance is included, when the SCAL and MTCH suites produce very similar results.

### *4.5.2. 3D Model Results*

Suite mean story drift ratios are shown in Figure 4-7 superimposed over the drift limit from Chapter 16. For a Risk Category III structure, the story drift ratio limit in ASCE 7 Chapter 12 is 1.5 percent. Chapter 16 thus allows a maximum drift ratio of twice that or 3 percent. Note that an unacceptable response occurred in the 05CS suite. Although an unacceptable response is not permitted per Chapter 16 for a Risk Category III structure, the Chapter 16 procedure for when one does occur has been applied here in order to report the global drifts for the 05CS suite. Therefore the 05CS suite "mean" is reported as the maximum of the mean of the remaining ten motions or 1.2 times the median of the full suite. All other suite means are calculated as the mean of the full suite. It is observed in Figure 4-7 that the SCAL suite mean in the SMRF direction exceeds the limit in two stories while all other suites pass this check. The conditional spectra suites tend to produce much smaller suite mean drifts than the SCAL and MTCH suites for both directions. As noted in the following section entitled "Spectral Matching of Ground Motions Study Results", the SCAL suite tends to exceed the MTCH suite results in the SMRF direction and vice versa in the BRBF direction.

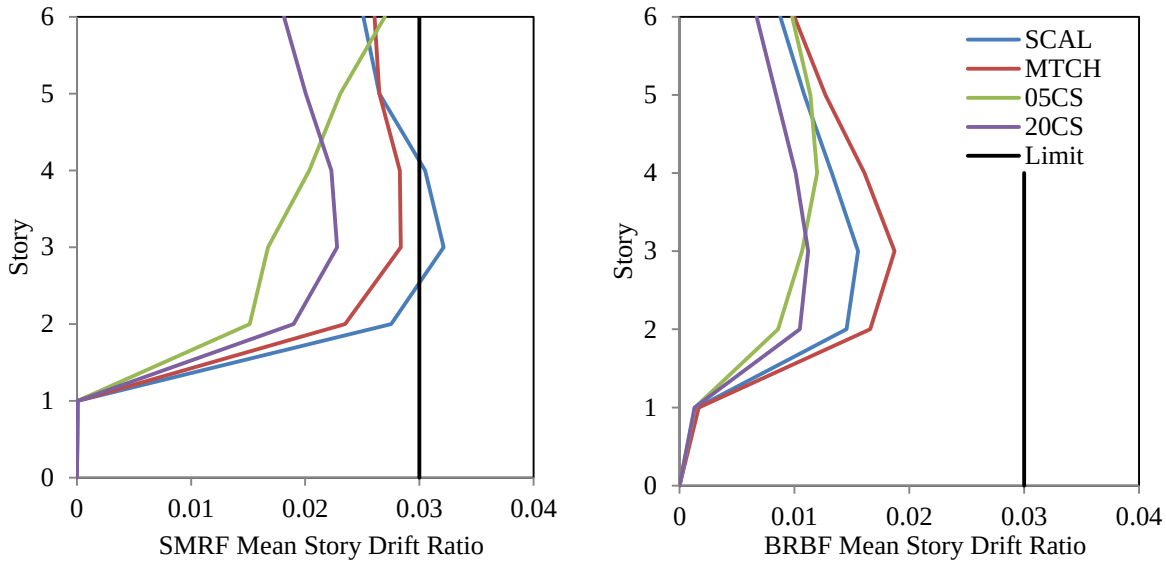


**Figure 4-7**. Suite mean maximum story drift ratio for the 3D Model in the SMRF (left) and BRBF (right) direction

The residual story drift ratios are shown in Figure 4-8. Due to the occurrence of dynamic instability in the 05CS suite, the suite mean is shown as the mean of the remaining ten motions. All other suite means are calculated as the mean of the full suite. The distribution of residual story drift ratios over the height closely matches that of story drift ratios. The residual drift ratios can get as high as 50 percent of the maximum drift ratios in some cases.

In general, the magnitude of the suite mean residual story drift ratios for the 05CS and 20CS suites are less than those of the SCAL and MTCH, consistent with the fact that magnitude of mean story drift ratios were less for the 05CS and 20CS suites. Story drifts in the BRBF direction also tend to be smaller in magnitude than the SMRF direction owing to the properties of each respective system. It is of special note that even for a structure complying with Chapter 16, the residual drift ratios can be significant as evidenced by more than 1 percent in the SMRF direction under the SCAL suite. Although not shown, the dispersion within a suite of residual drift ratio tends to be quite large. In many cases, the suite mean residual drift ratio is skewed due to one or two ground motions that produce larger than average residual drifts such as the SCAL suite in the SMRF direction of Figure 4-8.

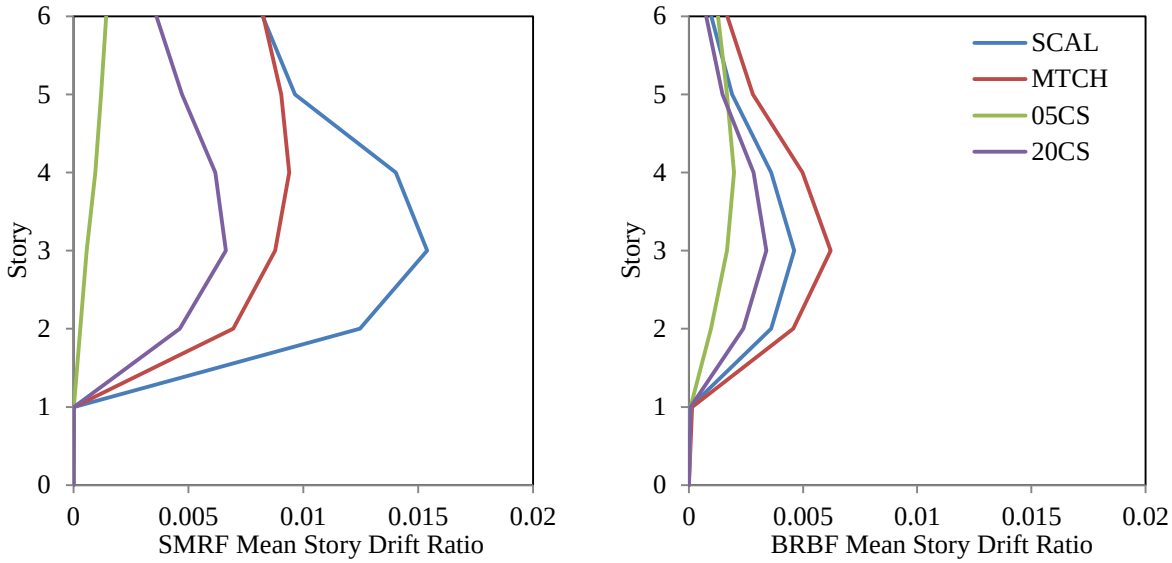


**Figure 4-8**. Suite mean residual story drift ratio for the 3D Model in the SMRF (left) and BRBF (right) direction

### *4.5.3. Residual Drift Incremental Dynamic Analyses*

To determine the potential consequences of residual drift, incremental dynamic analyses (IDA) are performed on selected ground motions that caused significant residual roof drift (greater than or equal to 1 percent) but no dynamic instability. The ground motion accelerations were increased in 10 percent increments up to 150 percent of their original scaling to determine how close the structures are to collapse. Figure 4-9 shows the IDA residual drift results, and the initial residual drift from each ground motion record is the x-intercept. Due to the higher initial residual drifts, this investigation was performed on the MF2 and MF8 Models that do not include modeling of the gravity system resistance and in the SMRF direction of the 3D Model.

Nine of the thirteen ground motions caused a collapse at or before a scale factor of 1.5; however, the ground motion needed to be scaled by a factor of at least 1.2 percent to cause collapse.

Typically, if the initial residual drift is greater than 2 percent, collapse will occur at or before a scale factor of 1.5. However, some structures with an initial residual drift less than 2 percent also collapsed as the ground motion was increased. There does appear to be some positive correlation between residual drift and the scale factor to cause collapse of the structure; however, the results are scattered, and there are multiple cases where a higher initial residual drift ratio motion requires a greater scale factor to cause collapse than a lower initial residual drift ratio motion. Therefore reliance on residual drift as a collapse indicator ]appears to be very approximate at best.

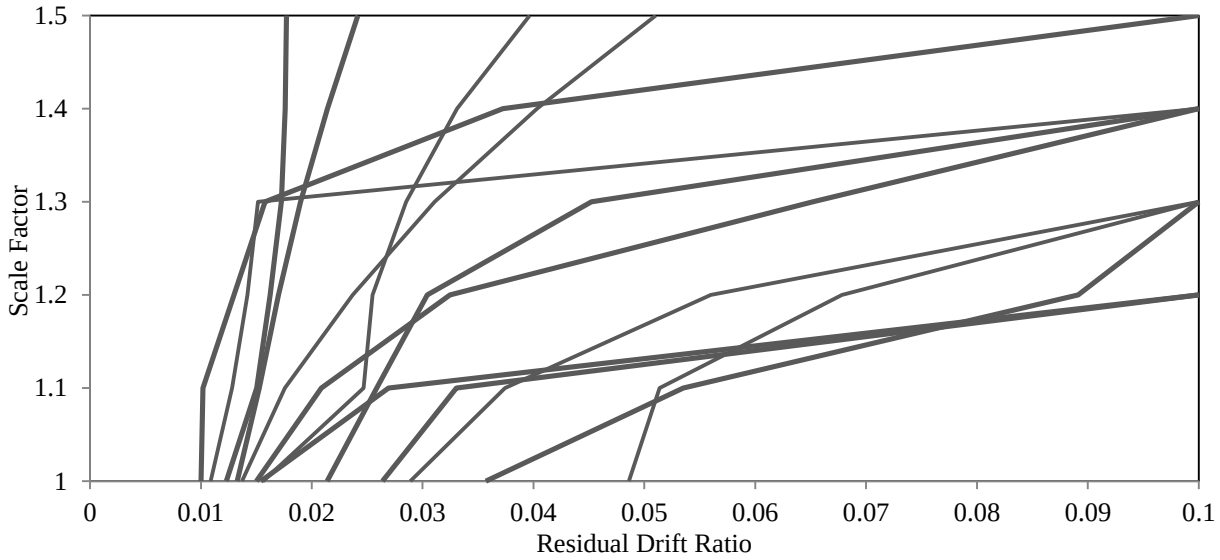


**Figure 4-9.** Incremental Dynamic Analysis residual drift results

## 4.6. Spectral Matching of Ground Motions Study Results

### *4.6.1. MF2 and MF8 Models Results*

All the results related to the spectrally matched ground motions of the MF2 and MF8 Models have been presented previously but will be discussed in this section. In general, spectrally matched ground motions tend to decrease the response, decrease the standard deviation of the response, and reduce or eliminate the number of instabilities. These trends can be seen in Figures 4-5 and 4-6, and they are evident in both the drift ratios and residual drift ratios. From the perspective of Chapter 16, these variations can be the difference between a conforming and non-conforming structure. If an engineer were to use spectrally matched motions, he or she may be able to show that a building passes Chapter 16 whereas it would not have passed using a scaled motion suite with the same set of motions. It must be noted, however, that the implicit penalty of spectral matching in Chapter 16 is negated when two-dimensional models are used, because a scaled suite would also require both components to meet the target individually, similar to a spectrally matched suite. These results cannot be assumed relevant to three-dimensional models,

since the implicit penalty will be included, as the scaling requirements differ between amplitude scaled and spectrally matched ground motions for three-dimensional models.

### *4.6.2. 3D Model Results*

In contrast with the MF2 and MF8 Models, the comparison between scaled and spectrally matched suites for the 3D Model indicated that the spectrally matched motions did not always reduce the suite mean drift ratio. It is postulated that this results from the directionality of ground motions in near-fault sites. Typically, the fault normal component of ground motion exceeds the fault parallel for near-fault sites. This is shown for the 3D Model in Figure 4-10, where the fault normal suite mean exceeds the fault parallel for nearly all periods of interest. When the Chapter 16 procedures for spectral matching are employed, namely matching each component rather than the maximum direction to the target, the scale factor in the fault parallel direction is increased more than the scale factor in the fault normal direction. Since neither the MF2 nor the MF8 Model is near-fault and since both are analyzed only in 2D, this issue does not appear in their results.

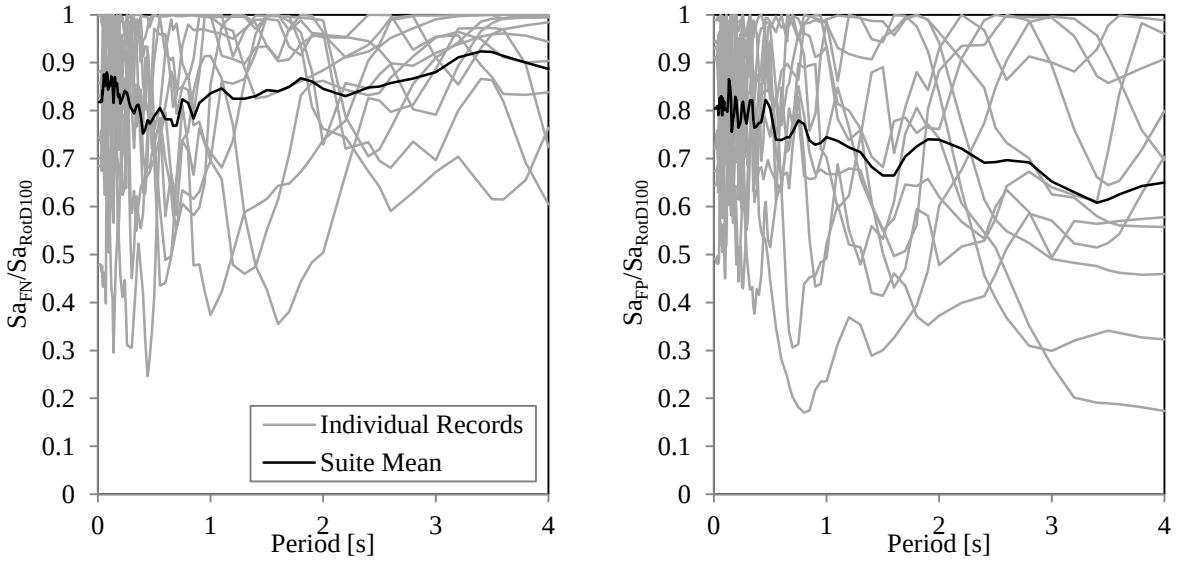


**Figure 4-10.** Ratio of fault normal (left) and fault parallel (right) versus maximum direction spectral acceleration for SCAL suite

Figure 4-7 shows that the SCAL suite mean drift ratio generally slightly exceeds the MTCH suite mean for the SMRF (fault-normal) direction. In the BRBF (fault-parallel) direction, the opposite is true. This is consistent with the previously described expected result given the Chapter 16 spectral matching provisions for near-fault sites. Although it was the intention that spectral matching would receive a de facto penalty under the Chapter 16 provisions, it is evident that in near-fault sites this may not occur when the suite mean maximum direction spectrum of the scaled motions exceeds the target in the period range of interest. Also of interest is that spectral

matching is often believed to reduce the dispersion in building response within a record suite as compared to one that is only scaled to a target. While this holds true for the SMRF direction, the MTCH suite in the BRBF direction exhibits a greater standard deviation than its corresponding SCAL suite. It is possible, however, that this is more a product of the structural system responding at higher drift ratios than a reflection on the ground motions.

### *4.7. Accidental Torsion Study Results*

Accidental torsion is typically only included in elastic procedures, such as those that exist in ASCE 7 Chapter 12 (ASCE 2010) and ASCE 41 (ASCE 2006 and 2013), which require that four different locations of the center of mass be considered. These four locations are computed by shifting the center of mass 5 percent of the diaphragm dimension in a specific direction at all floors simultaneously. In order to assess the applicability of a nonlinear accidental torsion requirement, these elastic procedures are expanded to inelastic analyses. The 3D Model was analyzed using the SCAL suite of ground motions with four shifts of the center of mass, corresponding to five total cases after including the expected center of mass location. The four cases are listed as 5% East, 5% West, 5% North, 5% South and None in Figure 11. It should be noted that the 3D Model was determined to meet the elastic requirements of ASCE 7 Chapter 12 (ASCE 2010) as a torsionally regular structure. The maximum ratio of $\delta_{max}$ to $\delta_{average}$ is very close to 1.0 in the SMRF direction and just less than 1.2 in the BRBF direction, which are both less than the limiting ratio of 1.2 for a torsionally irregular structure. To catch the full effect of the accidental torsion, the displacements are checked at the corners of the lateral system. All results previously reported in this work were at the expected center of mass location. The maximum corner drifts are averaged over the ground motion suite at each story.

The diaphragm geometry has a rather high aspect ratio with the dimension in the East-West far exceeding that in the North-South direction. Resulting from this, the 5 percent rule produces a greater shift in the East-West direction and therefore a larger change in the BRBF corner story drift ratios as seen in Figure 4-11. In this direction, the corner drifts increase as much as 25 percent when accidental torsion is added. As expected, the 5 percent East and 5 percent West locations of the center of mass produce the largest corner drifts in this direction. Note that results in the SMRF direction are nearly identical for all locations of the center of mass due to the small shift produced by the 5 percent rule. Note that to avoid biasing the mean, one ground motion that was shown to produce drifts well above the rest of the suite was eliminated for this accidental torsion study.

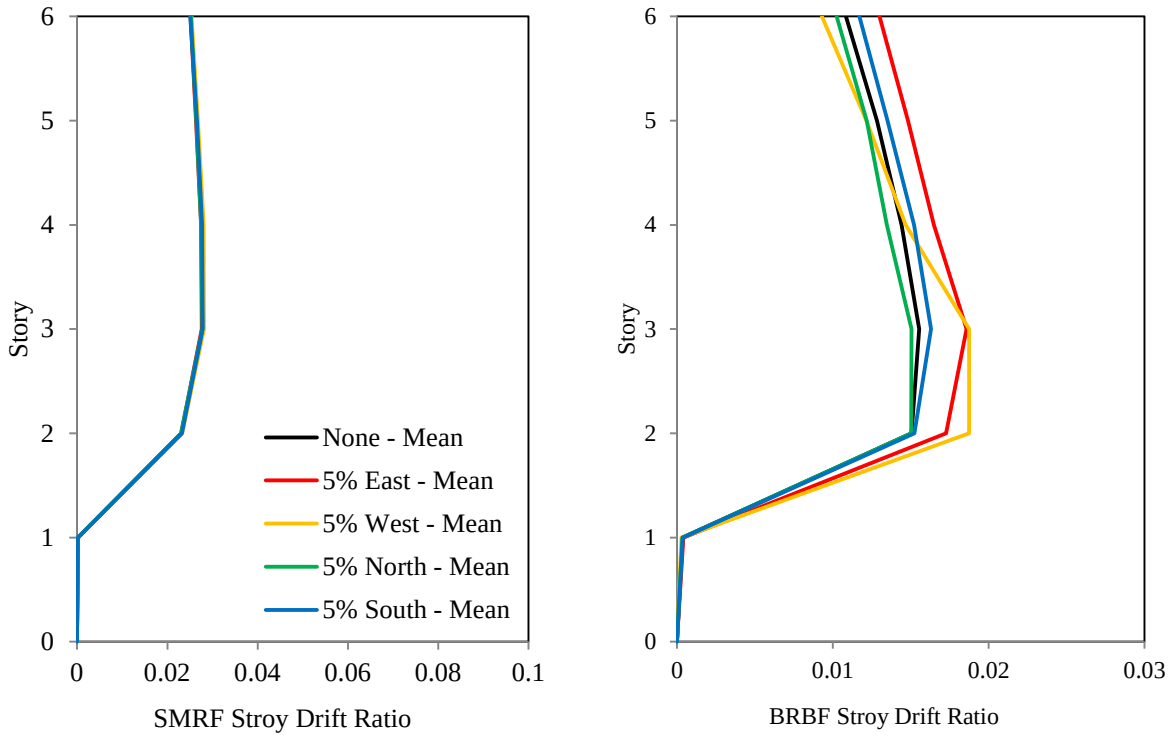


**Figure 4-11**. Mean corner story drift ratios for each mass eccentricity location of the 3D Model for SMRF (left) and BRBF (right) direction

## 4.8. Implicit Satisfaction of Collapse Probability Results

### *4.8.1. MF2 and MF8 Models Results*

The standard P-695 methodology to compute the probability of collapse is implemented for the MF2 and MF8 Models without the inclusion of the gravity system (as prescribed by the standard methodology). The MF2 and MF8 Models are analyzed as Risk Category II structures, and therefore, must have a probability of collapse less than or equal to 10 percent under the $MCE_R$ level ground motion. Using the 44 far-field ground motions scaled to the design spectrum, incremental dynamic analysis is performed until 22 ground motions cause collapse. For the MF2 Model, the probability of collapse is 1.08 percent, and for the MF8 Model, the probability of collapse is 4.68 percent. Both of these models have a probability of collapse below 10 percent.

Even though the MF8 Model did not satisfy the Chapter 16 drift requirements, it did satisfy the P-695 requirements. It is important to note that any analysis that creates an instability or non-convergence is deemed immediately unacceptable by Chapter 16 standards, which may not necessarily equal a total collapse. The P-695 procedure, on the other hand, only stops an analysis when a full collapse of the structure has occurred.

### *4.8.2. 3D Model Results*

Appendix F is used for the analysis of the 3D Model, as it is prescribed for individual structures. For this methodology, one single scale factor is determined for each direction, which is based on the acceptable probability of collapse (FEMA 2009a). The 3D Model is Risk Category III, and therefore, must have a probability of collapse less than or equal to 6 percent under the $MCE_R$ level ground motion. These scale factors are determined as 3.41 in the SMRF direction and 3.13 in the BRBF direction. The suite of 56 normalized near-fault ground motions is then scaled by these factors, and nonlinear response history analyses are run for each motion. If fewer than 28 of the ground motions cause collapse, the building performance is acceptable. A non-simulated collapse limit is chosen for the drift ratios as 10 percent, and if any drift ratios exceed this limit, the building will be considered to have collapsed. This value was chosen because it was previously used in ATC 76 for BRB Frames (NIST 2011), and the IDA curves for the moment frame systems of the MF2 and MF8 Models also tend to flatten near this limit during the incremental dynamic analyses discussed previously.

For the 3D Model, 33 ground motions caused collapse, which implies that the probability of collapse is greater than the maximum acceptable value of 6 percent. An exact probability of collapse cannot be calculated, because IDA is not performed. It is important to note that specific modeling choices (such as including the inclusion of the lateral resistance of the gravity system) could dramatically change the outcome for this structure. Additionally, there is subjectivity in the dispersion selections in the P-695 procedure, which will affect the results. Sensitivity to such variables was not undertaken for the 3D Model.

## 4.9. Summary and Conclusions

For both MF2 and MF8 Models, the systems are analyzed with and without the lateral strength and stiffness of the gravity system. In all cases, the mean response and the dispersion decrease, as expected when more resistance is captured. Additionally, the instabilities are always eliminated when the gravity system influence is included. For these examples, the inclusion of the gravity system was the difference between an acceptable and an unacceptable structure with respect to the Chapter 16 requirements. The addition always provides a relative improvement in performance, so it is the opinion of the authors that the absence of strict requirements by Chapter 16 to include the gravity system is acceptable. If the modeler chooses to develop a more accurate response and expects the lateral influence of the gravity system to be crucial to the overall response of the system, this option is still available. However, it is important for the modeler to acknowledge that the gravity system can provide a factor of safety against collapse during earthquake events, but this factor of safety is eliminated if the gravity system's lateral resistance is included in the design. If the structure is acceptable without modeling the lateral resistance of the gravity system, it would be unnecessary to include it. However, there is benefit in modeling the gravity system to model all P-Delta effects, whether the lateral resistance is included or not.

There are many factors for the engineer to consider regarding the modeling of the gravity system, which supports the lack of a stringent requirement.

In contrast to some performance-based design guidelines, Chapter 16 does not require a check of residual drifts, instead relying on other criteria. It is shown in the studies of the MF2, MF8 and 3D Models that residual drifts can be quite high for structures conforming to Chapter 16. However, no significant link is determined from the residual drift IDAs between the magnitude of residual drift and the proximity to collapse, which is the same conclusion found in the literature (Lee and Foutch 2003). Additionally, the $MCE_R$ level ground motion required scaling by at least 120 percent to reach collapse for every ground motion. This simple IDA process can provide valuable information on the post-earthquake condition of a structure and could be added in as commentary; however, the results of this investigation do not warrant a formal recommendation to require a residual drift check, since ASCE 7 is first tasked with preventing collapse.

All analyses were performed using a suite of recorded ground motions both amplitude scaled and spectrally matched to a target spectrum per Chapter 16. For the MF2 and MF8 Models, the spectrally matched ground motions tended to reduce the drift response and the dispersions when compared to the response of the amplitude scaled ground motions. These analyses show that spectral matching should not be applicable to two-dimensional models since the inherent penalty of spectral matching is negated. This problem is eliminated with the requirement that only three-dimensional models are acceptable. The 3D Model showed greater drifts and dispersion in the fault parallel direction for spectrally matched versus scaled suites and vice versa in the fault normal direction. Spectral matching in near-field sites tends to amplify fault parallel motions more than fault normal. It can, in fact, lead to decreased response in the fault normal direction as compared to a scaled record suite when the scaled suite's mean maximum direction spectrum does not perfectly match the target. Therefore, spectrally matched ground motions should be used cautiously, if at all, for near-field sites because of the inherent directionality of ground motions close to faults. These analyses also did not attempt to characterize the modification to the pulse characteristics of the near-fault records as is required in Chapter 16. Further work should be done to ensure that the spectral matching procedure is valid for three-dimensional far-field models. The inherent penalty could also deter their use in the Chapter 16 procedure.

Chapter 16 uses a simple approach to including accidental torsion. Rather than including it in the nonlinear response history analysis step, it simply requires that the Chapter 12 provisions (i.e. elastic accidental torsion checks) be satisfied. This research looks at the effects of nonlinear accidental torsion, which expands on the elastic procedure where the center of mass is shifted 5 percent of the diaphragm dimension in each direction. The analysis of the 3D Model provides preliminary verification that accidental torsion can have a significant effect on the nonlinear

behavior of a structure, even for a torsionally regular building. The elastic procedures are not comprehensive, and the issue of accidental torsion still needs more work for further versions of Chapter 16. However, due to the limited research currently completed on nonlinear accidental torsion, there is insufficient information to include provisions for it at this time. Additional work providing recommendations for methods of assessing accidental torsion in future nonlinear provisions are discussed elsewhere (Jarrett et al. 2014).

One of the major assumptions in Chapter 16 is that the methodology satisfies a specified probability of collapse given the $MCE_R$ through implicit criteria. To check this assumption, the MF2, MF8 and 3D Models were analyzed under both the Chapter 16 provisions and by the FEMA P-695 methodology. Even though the MF2 and MF8 Models without the gravity system failed the Chapter 16 criteria, the probability of collapse calculated by the P-695 methodology did not exceed the limit for Rick Category II structures of 10 percent. On the other hand, the Risk Category III 3D Model did not satisfy the acceptable probability of collapse of 6 percent but does satisfy the Chapter 16 requirements under some of the ground motion suites. It therefore does not appear that the satisfaction of Chapter 16 requirements positively implies satisfaction of the maximum probability of collapse or vice versa in all cases, especially considering the subjective choices in modeling and the P-695 procedure.

Although the assumptions investigated could easily be expanded to any other methodology that provides recommendations for the application of nonlinear response history, this work was developed using a limited number of examples. The assumptions should be analyzed for numerous different structures to determine the applicability of the results to any other structure types and configurations.

# Chapter 5: "Accidental Torsion in Nonlinear Response History Analysis"

Jordan A. Jarrett, Reid B. Zimmerman, Finley A. Charney

[Submitted to Tenth U.S. National Conference on Earthquake Engineering]

**Abstract**

Accidental torsion is not required in most of the recommended provisions for nonlinear response history analyses (NRHA), including those of FEMA P-695, FEMA P-58, and the PEER Tall Building Initiative. Linear procedures for assessing accidental torsion exist in ASCE 7 Chapter 12 and ASCE 41 Chapter 3 where the center of mass is shifted 5 percent of the diaphragm dimension in each direction independently. However, studies have shown that accidental torsion can have a significant effect on the inelastic behavior of structures, and the traditional elastic methods of assessing accidental torsion may not sufficiently capture the potential inelastic torsion behavior. These effects can be especially important for structures with minimal inherent elastic torsion. This research uses a torsionally-regular five-story steel structure to investigate the effects of accidental torsion in NRHA. Several methods to assess accidental torsion are considered in the research, one of which is to apply the linear procedures that shift the center of mass by 5 percent of each diaphragm dimension to NRHA. Accidental torsion from random modifications in strength and stiffness are also investigated. These analyses show that accidental torsion can have a significant effect on the inelastic behavior of this structure, particularly for shifts in mass; therefore, the inclusion of accidental torsion within provisions for NRHA is warranted. However, the four shifts in mass significantly increase the computational demand, so this work also investigates ways to minimize the required number of shifts by using either the calculated location of the center of rigidity or nonlinear pushover analyses. This paper provides suggested code language for a NRHA provision that includes an exception to reduce the number of mass shifts, as applicable.

## 5.1. Introduction

Under seismic loads, structures can be subjected to effects from two types of torsional influences: inherent torsion and accidental torsion. Inherent torsion includes the effects of the difference in location of the center of rigidity from the center of mass, while accidental torsion includes unaccounted effects from phenomena such as non-uniform ground motion input, variations in floor masses over the life of a structure, and strength and stiffness degradation during nonlinear response of lateral force-resisting elements. Accidental torsion is generally not included in performance-based earthquake engineering provisions, including the PEER Tall Building Initiative (PEER 2010), the FEMA P-695 procedure (FEMA 2009), and the FEMA P-

58 procedure (FEMA 2012). Typically, accidental torsion is only included in elastic procedures, such as ASCE 7 Chapter 12 (ASCE 2010) and ASCE 41 Chapter 3 (ASCE 2006), where the center of mass is shifted by 5 percent of the diaphragm dimension in each direction independently. The 2009 NEHRP provisions, in the resource paper on seismic response history analysis, recommend that if accidental torsion is included in the strength design of the nonlinear structural elements (i.e. ASCE 7 Chapter 12 requirements), it does not need to be included in the nonlinear response history analysis (FEMA 2009c). The effect of accidental torsion is investigated in this research to determine if there is a necessity for its inclusion within nonlinear response history analyses (NRHA) or if the current state of provisions for NRHA is correct in excluding it.

Studies have shown that the uncertainty in the location of the center of mass is normally the largest influence to accidental torsion (De la Llera and Chopra 1995). This explains why the 5 percent offset procedure is typically used, since it relates to the distribution of mass on each floor. The practical concern for response history analysis is that the four shifts in mass location quadruples the number of analyses performed, since the structure must be analyzed with four shifted center of mass locations, instead of the one computed center of mass location. Another concern with this method is that while the uncertainty in the center of mass tends to contribute the most to accidental torsion, it is not the only source of accidental torsion, particularly for elastically torsionally-regular structures. Damage during earthquakes such as experienced by the Clarendon Tower during the Canterbury Earthquake Sequence suggests that accidental torsion due to asymmetric changes in strength or stiffness can be significantly important even for structures with that are elastically torsionally-regular (Holmes and Zimmerman 2012). These effects can be especially substantial in (originally) perfectly symmetric structures, and the method of shifting the center of mass in the elastic analysis-based design (like those from ASCE 7 and ASCE 41) may not be sufficient to capture all the effects of accidental torsion (Dimova and Alashki 2003). It is important to distinguish buildings based on their sensitivity to torsional response. Some structures appear to be elastically torsionally sensitive, meaning that accidental torsion effects cause significant changes in the torsional rotation of the building when considered in the linear range of response. The classic case of this type of structure is one that is cruciform-shaped in plan. Inelastically torsionally sensitive buildings, like the previously mentioned Clarendon Tower, are those that may or may not exhibit elastic torsional sensitivity but for which accidental torsion effects significant changes in the torsional rotation of the building when responding in the inelastic range.

Recent research has shown that buildings designed with and without the traditional linear accidental torsion provisions often behave similarly when experiencing inelasticity, showing a flaw in the way accidental torsion is currently handled (Stathopoulos and Anagnostopoulos 2010). This was one of the first studies on accidental torsion that used a more realistic multi-

story structure to investigate torsional effects, as most of the previous studies on the topic use single story structures or simplified shear-beam models. Their recommendation was to remove the accidental torsion provision in its current state, except potentially for symmetric buildings. Several additional studies have come to a similar conclusion that current code-based accidental torsion provisions do not adequately deal with nonlinear behavior. A summary of these studies can be found in a research review by De Stefano and Pintucchi (DeStefano and Pintucchi 2008). While the general conclusion of these studies is that the inclusion of accidental torsion in design is unnecessary, the results could infer that linear design provisions cannot adequately capture inelastic torsional effects, especially for inelastically torsionally sensitive buildings, and that the inclusion of an accidental torsion provision should be moved to the nonlinear analysis of these structures.

This idea is reinforced in a study where the linear procedure of shifting the center of mass by 5 percent was applied to nonlinear analyses to compare the linear and inelastic responses (Mansuri 2009). That work found that the inelastic response to accidental torsion can be significantly greater than the elastic response. This method of shifting the center of mass during nonlinear analyses was also used to determine the effect of accidental torsion on the collapse capacity of structures (DeBock et al. 2013). The effects of shifting the mass in elastically torsionally regular structures had a small effect on the collapse capacity (less than 10 percent reduction), since the collapse was controlled by lateral movements. On the other hand, shifting the mass had significant effect on the collapse capacity of elastically torsionally irregular buildings. The work presented in this paper will also investigate the effects of accidental torsion during NRHA, but specifically for the maximum considered earthquake ground motion level.

### 5.2. Modeling Descriptions and Assumptions

To determine the accidental torsion effects in NRHA, a three-dimensional model representative of the lateral force-resisting system (LFRS) of an actual commercial building is used. Its LFRS consists of two lines of steel special moment-resisting frame (SMRF) in the longitudinal direction and four lines of buckling-restrained brace frame (BRBF) in the transverse direction over five stories. Reinforced concrete walls are located around the building perimeter at the lowest floor. Each floor is assumed to have a rigid diaphragm, except the first floor, where the diaphragm flexibility is explicitly modeled. The SMRFs align with the fault normal component of the ground motion, and the BRBFs align with the fault parallel component. The gravity system is not included in the model, and a leaning column is provided to capture the P-Delta effects. Foundation flexibility and soil-structure interaction were not included. It should be noted that the structure was determined to meet the elastic requirements of ASCE 7 Chapter 12 (ASCE 2010) as an elastically torsionally regular structure, as the maximum ratio of $\delta_{max}$ to $\delta_{average}$ is 1.02 in the SMRF direction and 1.18 in the BRBF direction, which are both less than the limiting ratio of 1.2.

The building is modeled in Perform 3D (CSI 2011), and all crucial nonlinear behavior is incorporated, including localized axial-moment-moment (PMM) interacting hinges for SMRF and BRBF columns, moment-rotation hinges for SMRF beam-column connections and BRBF beams outside of gusset plates, buckling-restrained brace (BRB) elements, and shear stress-shear strain material models for concrete walls. More detail on this structure and the modeling assumptions can be found elsewhere (Zimmerman et al. 2013). A plan view of the lateral force-resisting elements in the structure can be found in Figure 5-1, including the locations of the center of mass (COM) and center of rigidity (COR), each averaged over all the stories. It is important to note that the location of these points is based on the entire structure, not just the elements shown in Figure 5-1.

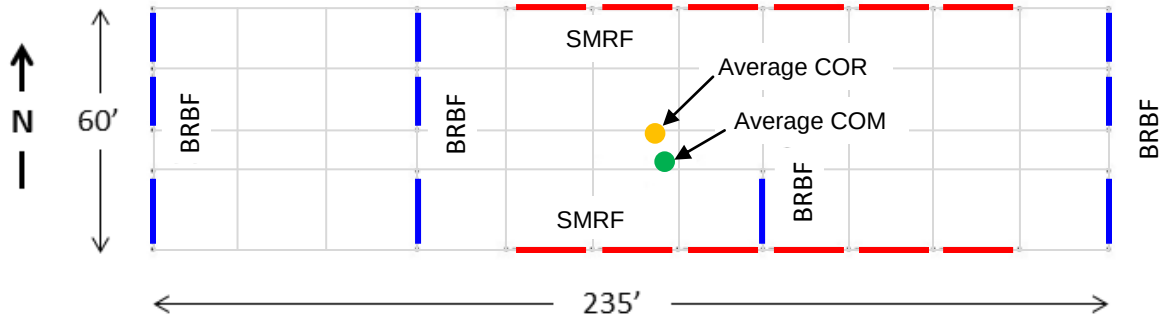


**Figure 5-1.** Schematic of the lateral force-resisting system of the example building

A target response spectrum for the maximum considered earthquake ($MCE_R$) is developed for the near-fault site of the structure in Berkeley, California. Due to the proximity to the Hayward Fault, the target spectrum is deterministically capped by the 80 percent lower limit of ASCE 7 Section 21.3 (ASCE 2010). A suite of eleven record sets are selected to match the tectonic setting, magnitude, distance and near-fault effects controlling the seismic hazard at the site. The horizontal ground motion components of a record set are used to construct a maximum direction spectrum. The maximum direction spectra are scaled such that the mean over the suite fits the target spectrum on average and does not fall below 0.9 times the ordinate of the target spectrum in the period range of interest. More detail about the design spectrum and the ground motion selection and scaling can be found elsewhere (Zimmerman et al. 2013). Note that the suite average maximum direction spectrum exceeds the target spectrum in the 1.0 to 2.5 sec period range due to near-fault effects which are included in the selected ground motions but are not reflected in the target spectrum. Figure 5-2 shows the maximum direction spectra of the scaled suite versus the target spectrum.

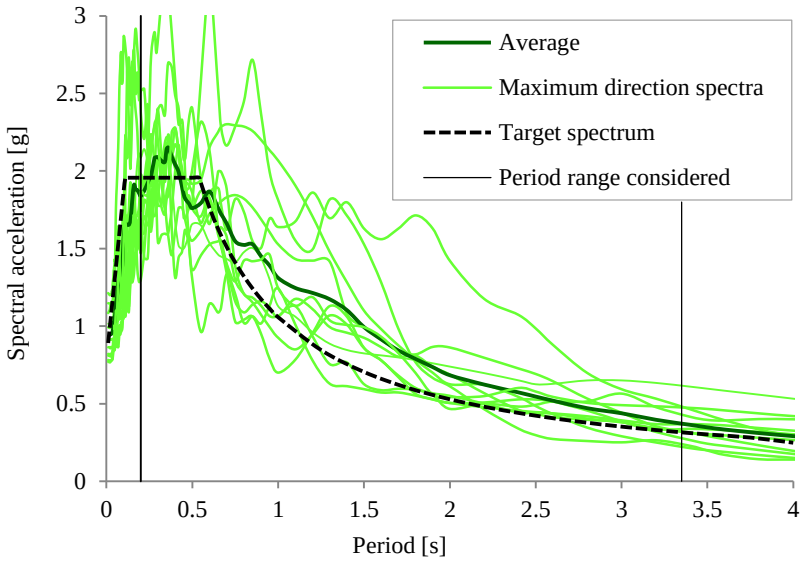


**Figure 5-2.** Maximum direction spectra versus the target spectrum for the suite of ground motions

In order to determine the effects of accidental torsion on the response during NRHA, accidental torsion is modeled in a variety of ways. Initially, the response from accidental torsion is modeled using the traditional method of shifting the center of mass. The effects of random strength and stiffness degradation are also investigated. The procedure and results of these various investigations are discussed next.

### 5.3. Accidental Torsion Modeled with Shifts in the Center of Mass

To investigate the effects of accidental torsion from shifts in the center of mass, eight shifts are investigated, corresponding to nine total cases including the expected center of mass location (the unaltered model). To see the most extreme effect that the torsion has on the structure, it is important to look at the displacements at the corners of the building, which are shown in Figure 5-3 for the nine cases. The eight shifts can be broken into two groups: the four traditional mass offset cases and four diagonal mass offsets. The traditional cases correspond to the following eccentricities (relative to the total building dimension in the same direction): 5% East, 5% West, 5% North, and 5% South. The diagonal mass offsets are defined as Northeast, Southeast, Southwest and Northwest, where there is a 5 percent eccentricity in each of the two orthogonal directions simultaneously. For example, the Northwest eccentricity has a 5 percent eccentricity in the north direction plus a 5 percent eccentricity in the west direction. Relative to the non-diagonal shifts, the 5 percent diagonal shifts may be too conservative, but these preliminary results will provide trends between different potential mass locations. The diaphragm geometry has a rather high aspect ratio, with the dimension in the East-West far exceeding that in the North-South direction. Resulting from this, the 5 percent mass offset produces a greater shift in the North-South (BRBF) direction, and the effects in the East-West (SMRF) direction are

negligible due to the small diaphragm dimension. Therefore, only the drifts in the BRBF direction are presented in Figure 5-3, which shows the maximum of the four average corner drift ratios along the height of the structure.

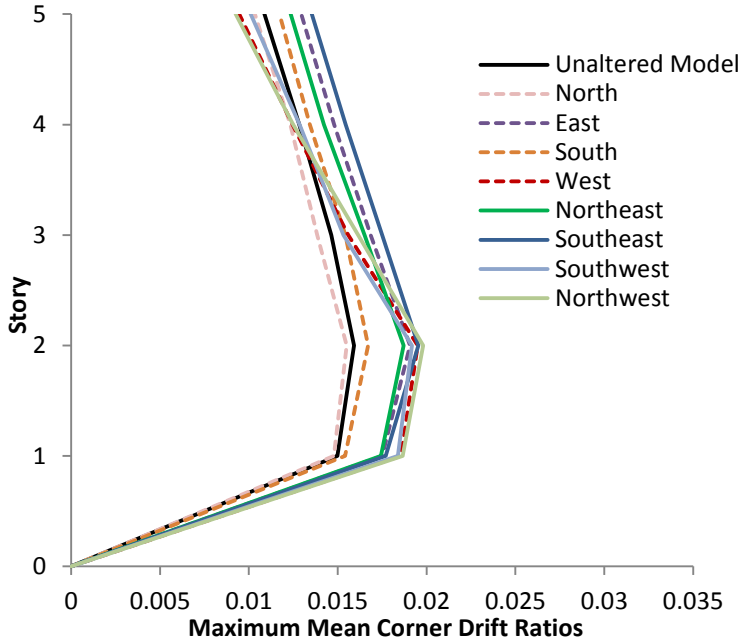


**Figure 5-3.** Corner story drift ratios computed by first averaging over all ground motions within a suite and then maximizing over each corner in the BRBF direction only

In the BRBF direction, these mean drift ratios can increase by up to 25 percent when the 5 percent eccentricities are included. Additionally, two of the diagonal mass offsets tend to envelope the four "traditional" mass offsets, which in this case are the southeast and northwest mass offsets. Since running multiple mass offsets is computationally demanding, two procedures to determine the most crucial mass offsets are discussed in the next two sections.

### *5.3.1. Determine Which Traditional Eccentricities to Evaluate Using Pushover Data*

Nonlinear pushover analysis is a method of analysis that is significantly less computationally demanding than nonlinear dynamic analyses, and it is often used to check a mathematical model for errors and to determine the distribution of inelasticity. In this procedure, nonlinear pushover analyses are additionally used to determine which traditional mass offset(s) should be analyzed using NRHA and which can be ignored. Nonlinear pushovers were performed in the North direction and the East direction at the true center of mass and at each traditional shift in the center of mass location, using the exact same mathematical model used in the dynamic analyses. Figure 5-4 shows the results from the pushover analyses in the North direction where there is a 5 percent eccentricity in the West or East direction. These figures plot the base shear against the

roof drift ratio in the North direction at three locations: the approximate center of the building (Roof Y), the northeast corner (Roof NE Y) and the northwest corner (Roof NW Y). Due to the small dimension of the structure in the North-South direction, the torsional influences from the pushovers in the East direction are negligible and not shown.

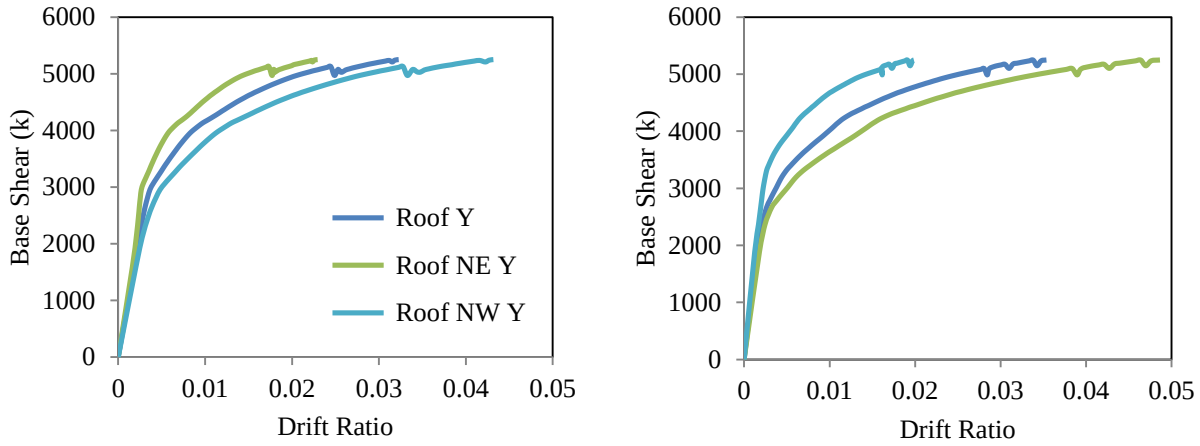


**Figure 5-4.** Pushover curves in the North direction where there is a 5% eccentricity to the West (left) and 5% eccentricity to the East (right)

When the pushover is performed at the West eccentricity, there is a 34 percent difference between the largest corner drift and the center drift at the end of the analysis. When the pushover is performed at the East eccentricity, there is a 44 percent difference between the largest corner drift and the center drift at the end of the analysis. These pushover results suggest that there could be a significant effect from accidental torsion on this structure in the nonlinear range of response, even though little is predicted for the linear range of response (recall that the structure was torsionally regular). Using the results of these pushover curves, a method to determine the necessary mass offsets could be developed. For example, the dynamic analysis associated with a given mass offset need not be performed if it is shown by nonlinear static pushover analysis using the same mass offset that the maximum corner displacement of every level is less than 1.2 times the average displacement at that same level. Figure 5-5 shows these ratios of maximum corner displacement to the displacement at the COM at the target drift for the pushovers in both the North and East direction.

For this example, the target displacement used in the pushover analysis is equal to 3 percent of the roof height, computed at the center of mass. The lateral load pattern for the pushover analysis is proportional to the first mode shape in the direction of interest. Based on these results, the only accidental torsion mass offsets that would be required for this structure under the above method would be the 5 percent eccentricity in the East and West directions. As was shown in Figure 5-3, the East and West eccentricity did in fact have the highest influence on the response history drift

results (with the East eccentricity controlling for the upper stories and the West one controlling for the lower stories). With this method, the computational demand is significantly reduced, since only two mass offsets are required, as opposed to the traditional four.

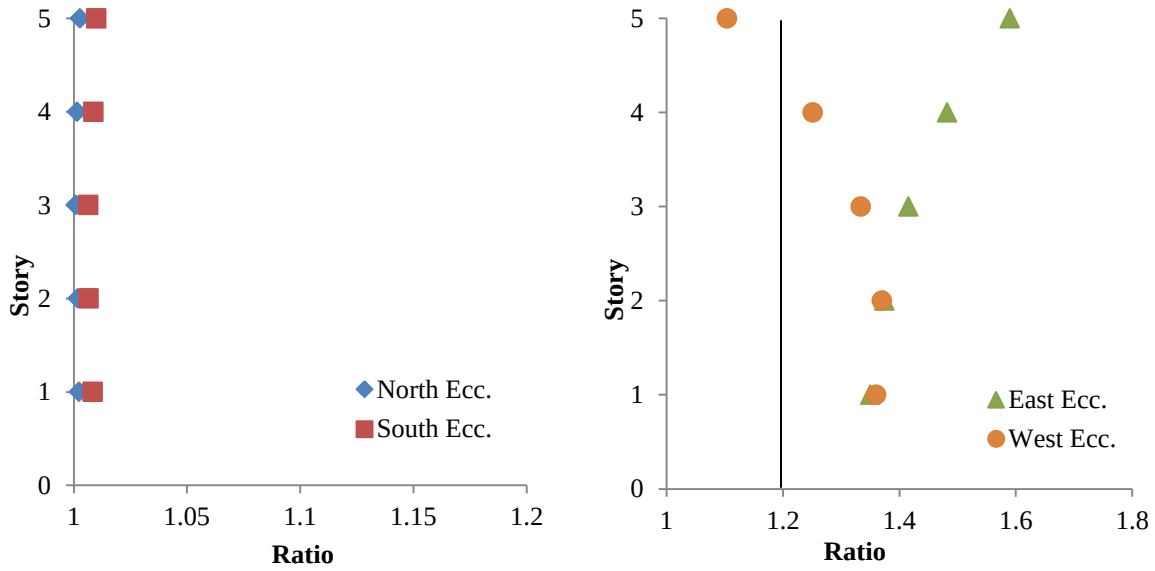


**Figure 5-5.** Ratio of maximum corner drift to center of mass drift at a COM drift ratio of 3% due to a pushover in the East direction (left) and North direction (right)

### *5.3.2. Alternative Method for Assessing Accidental Torsion*

As Figure 5-3 shows, there were two diagonal mass offsets that encompass all the traditional accidental torsion mass offsets. Assuming these diagonal mass offsets could be predicted, another method to assess accidental torsion influence would be just to run the two enveloping, diagonal mass offsets. The following procedure provides a method to determine these worst mass offsets. By calculating the true center of rigidity, the worst case scenario eccentricities could be determined as the diagonal in the quadrant near and opposite to the center of rigidity. The center of rigidity for this example is determined with the method used by ETABS (CSI 2012). For every story in this structure, the true center of rigidity is located in the northwest quadrant, and the average distance between the COM and the COR is (-20.3, 92) inches or (-0.7% X, 12.8% Y). This equates to an angle of 77.6 degrees clockwise from the West axis. This location of the center of rigidity would predict that the northwest and southeast diagonals would be worst case scenarios. This matches the results shown in Figure 5-3, where the two diagonal mass offsets that envelope the four "traditional" mass offsets are the southeast and northwest mass offsets.

Using the diagonal mass offsets with a 5 percent offset in each direction would still be an approximate solution, since the angle to the true location of the center of rigidity will differ from the angle to this approximate diagonal. To determine this effect, the NRHA is performed at mass locations with two different angles: at the "approximate angle" of 45 degrees and at the "true

angle" of 78 degrees clockwise from the West axes. The length of these offsets is held constant as the length determined from the approximate location. Figure 5-6 shows the maximum of the mean corner drift results of the response history analyses with no mass offset (Unaltered Model), at the enveloping "diagonal" mass offsets (Southeast and Northwest), and at the new mass offsets based on angle of the center of rigidity (Away from COR and Towards COR). The mass offset based on the center of rigidity provides similar results to those from the enveloping diagonal mass offset, particularly in the controlling quadrant, which is opposite to the center of rigidity. It appears, at least for this structure, that using just the approximate diagonal shift located in the quadrant opposite to the center of rigidity would sufficiently (and conservatively) predict the maximum response from the accidental torsion. Instead of four accidental torsion mass offsets, only one or two cases are needed.

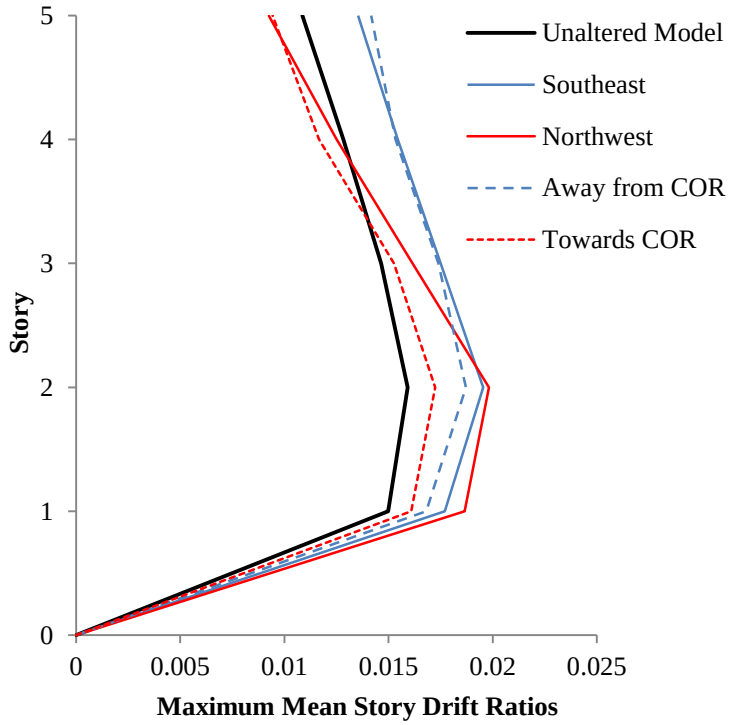


**Figure 5-6.** Corner story drift ratios computed by first averaging over all ground motions within a suite and then maximizing over each corner in the BRBF direction only

### 5.4. Accidental Torsion Modeled with Random Strength and Stiffness Degradation

One concern about the traditional methods of analyzing accidental torsion by shifting mass locations is that it can only indirectly capture the torsional response from changes in strength and stiffness. As discussed before, this source is often negligible but occasionally can produce significant effects. This section investigates another approach to assessing torsional sensitivity through explicit modification of individual component strength and stiffness. Twelve different

analyses were run with varying random reductions in stiffness and strength. Ten of these analyses reduce the strength or stiffness of five to ten randomly selected moment frame beams or buckling restrained braces by 10 percent. The other two analyses reduce the strength of an entire frame by 10 percent. Figure 5-7 compares the suite mean story drift ratio results without any strength or stiffness reduction (Unaltered Model) to the maximum of the randomly varying strength and stiffness analyses.

There is minimal effect on this structure under random decreases in strength and stiffness. The mean change in response under the scenarios where 5 to 10 members have strength or stiffness reduction is less than 1 percent. Even when the strength of an entire BRB frame is reduced by 10 percent and the reduction is limited to one side of the structure, the maximum increase in mean drift ratio is 6.5 percent, as the results in Figure 5-7 show. This procedure provides minimal insight into the behavior of this structure when compared to the method of moving the center of mass. However, this effect may have more influence on other structures, and the procedure could be useful to check if a particular structure is susceptible to this influence.

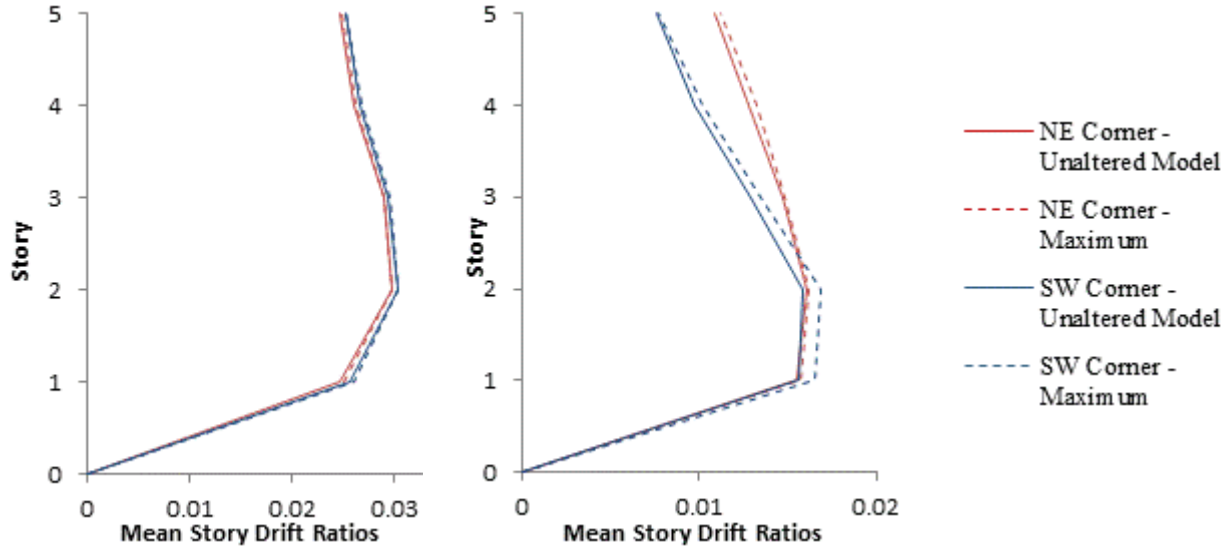


**Figure 5-7.** Comparison of the suite mean story drift ratio results without any strength or stiffness reduction (Unaltered Model) to the maximum of the randomly varying strength and stiffness analyses in the SMRF direction (left) and the BRBF direction (right)

### 5.5. Conclusions

This work demonstrates that accidental torsion can have a significant impact on the nonlinear behavior of a structure and that shifting the location of the center of mass has a greater influence than random variation in strength and stiffness for this example. This work also shows that it is possible to predict the worst cases for the location of the shifted center of mass using nonlinear pushover analysis. The authors believe that accidental torsion should be included in provisions

for nonlinear response history analyses, even for structures that are elastically torsionally regular, and example code language is shown next in italics. This example code language is based on an introductory set of analyses, and more examples and engineering expertise should be used to finalize the values underlined (e.g. *5 percent*) of this language.

*The analysis shall consider the effect of both inherent and accidental torsion. Accidental torsion shall be included by displacing the center of mass each way (i.e. plus or minus) from its expected location by a distance equal to 5 percent of the horizontal dimension of the structure at the given floor measured parallel to the direction of mass offset. The required 5 percent displacement of the center of mass need not be applied in both orthogonal directions at the same time.*

> *Exception: The dynamic analysis associated with a given center of mass offset shall not be required if the following is satisfied: It is shown by nonlinear static pushover analysis, using the same mass offset, that the maximum corner drift is less than 1.2 times the average drift at all levels of the structure. The roof target drift used in the nonlinear static analysis shall be equal to the maximum roof drift ratio permitted for the structure, and the lateral load pattern for the pushover analysis shall be proportional to the first mode shape in the direction of interest.*

Numerous previous works have highlighted the potential flaws of including the accidental torsion only in the design and linear analyses of the structure, and this work highlights the need for the inclusion of accidental torsion in nonlinear analyses. Assuming a structure barely satisfies the drift limits of a provision for NRHA without accidental torsion, the drifts including the nonlinear effects of accidental torsion could be dangerously large and unaccounted for. The addition of code language similar to the above would ensure the inclusion of accidental torsion in the NRHA of structures that are strongly influenced by its effect, while reducing the computational demand for structures where accidental torsion is not as critical.

# 6. Summary, Conclusions and Future Work

The performance assessment of seismic resistant structures is a broad research topic with many interesting facets. This work investigates a few topics related to this performance assessment, stemming from two different studies. The first study compared the performance of newly developed and traditional seismic resisting systems, and the second study investigated many of the assumptions made within provisions for nonlinear response history analyses.

This final chapter provides a summary of work contained in this dissertation. The first section provides an overview of the work and a summary of the results. The second section discusses the potential future work.

## 6.1. Summary and Conclusions

### *6.1.1. Comparison of Methodologies*

Preliminarily, this work focused on the comparison of various methods available for the performance assessment of seismic resistant structures. In the two studies presented in the manuscripts, three methodologies were used extensively: FEMA P-695, FEMA P-58, and the proposed updates to ASCE 7 Chapter 16. This section will summarize the comparison of these methodologies, particularly the advantages and disadvantages.

From a modeling standpoint, all these methodologies have very similar requirements. While some of the specific details vary, all the methodologies require a model that captures all the hysteretic behavior and nonlinearities of the elements. There are some differences (notably the inclusion of the gravity system resistance, force-controlled versus deformation-controlled elements, and the allowance of two-dimensional analysis), but the overall idea of creating a model that captures the true behavior of the structure as much as possible is the same throughout all the nonlinear analysis methodologies. The major differences between the methodologies are the evaluated limit states, the computational demand, the post processing of the results and the major outputs.

The ASCE 7 methodology is the most common methodology and the one referenced in coded design. Out of the three methodologies, it is the most simplistic method and requires the least amount of computational effort. However, from a performance based earthquake engineering standpoint, it is not an effective methodology. It only looks at one limit state, and once the demands (drifts and forces) are determined, no further post-processing is prescribed, and the output is left in terms that are not typically meaningful for stakeholders. It attempts to implicitly satisfy a probability of collapse limit, but this is not directly calculated as it is the P-695 process.

The P-695 methodology, on the other hand, is the most computational demanding methodology of the three. Hundreds, if not thousands, of nonlinear dynamic analyses must be run; a computational demand beyond the capabilities of most practicing engineers and likely even some academics. Just like ASCE 7, the methodology description only looks at one limit state, which in this case, is collapse. However, the incremental dynamic analyses provide valuable information that could be used to look at behavior at multiple levels of ground motion and fulfill the principles of PBEE.

The P-58 methodology shows the most promise, in this author's opinion. For intensity based assessments, the P-58 methodology takes about the same computational demand as the ASCE 7 method (assuming a simplified method is used for predicting collapse). If the time based assessment is used, the computational demand increases by around a factor of 8, which is still drastically less than the P-695 analysis. This methodology currently shows the most promise, because it takes the general ideas behind ASCE 7 and P-695, combines them, and expands on them. The methodology performs a limit state based analysis at one or more predetermined levels of intensity (similarly to ASCE 7), as well as a collapse analysis (which often could be the P-695 process). It then goes a few steps further by integrating hazard with fragility (assuming a time based assessment is used), running Monte Carlo simulation to expand the results and account for uncertainties (in modeling, ground motion selection and scaling, and overall building performance), and finally puts the results in terms of consequences that are more easily understood by decision makers and stakeholders.

However, this method does come with some anticipated disadvantages. While a large number of fragilities are included in the methodologies, including all the components of the building may be difficult. If all the components are not accurately included, the consequence estimation could be drastically wrong. The processes to add new fragilities are not simplistic and typically rely on significant amounts of test data. However, to provide accurate consequence distributions, a comprehensive set of fragilities must be developed for use within the PACT program. Additionally, from the perspective of cost changes over time, updating all the costs estimation with inflation and changes in supply and demands seems like a daunting task, and unless some other parties takes responsibility of the program (as the developing team hopes), the program could likely become abandoned and obsolete in a few years.

### *6.1.2. Summary and Conclusions from Comparative Study*

The work of the first study is presented in a manuscript entitled "Comparative Evaluation of Innovative and Traditional Steel Seismic Resisting Systems Using the FEMA P-58 Procedure," which is shown in Chapter 3. Three innovative systems and modeling assumptions are compared to their traditional counterparts using a combination of the FEMA P-695 and P-58 methodologies. The three systems analyzed are: hybrid buckling restrained braces, collapse

prevention systems, and moment frames evaluated with and without the lateral influence of the gravity system. The Hybrid BRBs and moment frames are analyzed at four intensity levels of interest: serviceability, DBE, MCE and near-collapse level. The Collapse Prevention Systems are only analyzed for a near-collapse level intensity, as they are designed specifically for life safety in locations where that is the only crucial intensity level, like the Central and Eastern United States. The results are presented in terms of repair costs, repair times, number of casualties, and probability of receiving an unsafe placard, which are more meaningful to owners and other decision makers.

The major results of this first study are as follows:

- When compared to traditional BRB systems, the repair costs of the Hybrid BRBs are reduced by up to 12 percent at lower intensity levels for short structures and up to 26 percent at higher intensities for the taller structures. Additionally, the repair time at the serviceability level is always reduced by more than 10 percent.
- In general for the Hybrid BRB, there was negligible change in the probability of receiving an unsafe placards and the number of casualties.
- The more hybridity in the BRB, the more the consequences are reduced. This trend was similar to those found in the P-695 analyses, where the Hybrid 3 system always had the smallest probability of collapse and residual drifts.
- For the Collapse Prevention System at the near-collapse level, the average repair costs are always decreased by 5 to 36 percent when the collapse prevention mechanism is added. This reduction was greater for the slack cable device than the loose link device.
- For the 2-story Collapse Prevention System model, the average number of casualties was significantly decreased (nearly 33 percent) by the slack cable mechanism.
- In general for the Collapse Prevention Systems, there was negligible change in the repair time and the probability of receiving an unsafe placard.
- By modeling this lateral resistance of the gravity system, the average costs can be reduced significantly (up to 32 percent), particularly at higher intensity levels. For the 4-story model, the number of casualties was noticeably reduced at higher intensities; otherwise, all other consequences had negligible change.

### *6.1.3. Summary and Conclusions from Assumptions Study*

The work of the second study on the assumptions in nonlinear response history analysis is presented in two manuscripts entitled “Response-History Analysis for the Design of New Buildings: A Study of Assumptions” and “Accidental Torsion in Nonlinear Response History Analysis,” which are shown in Chapters 4 and 5, respectively. The first manuscript discusses all the investigated assumptions with respect to the proposed updates to Chapter 16 of ASCE 7,

while the second manuscript focuses on one assumption, which is the use of accidental torsion in nonlinear response history analyses.

The major results of this second study are as follows:

- Modeling the gravity system's lateral influence can have significant effect on the system behavior, as the mean response and dispersion almost always decrease, and all instabilities are eliminated. Since the results are conservative when the gravity system resistance is included, its inclusion is unnecessary unless a more accurate representation of the behavior is needed or the structure will not satisfy the requirements without its inclusion.
- No significant link between the magnitude of residual drift and the proximity to collapse is determined from the residual drift IDAs in this work, and therefore, exclusion of a residual drift check is acceptable when concerned with collapse prevention.
- Spectrally matched ground motions tended to reduce the drift response and the dispersions when compared to the response of the amplitude scaled ground motions for the far field structures analyzed. However, for the near-field system, the spectral matching can amplify the fault parallel motions more than the fault normal motions if the pulse characteristics are altered. Spectrally matched ground motions should cautiously be used for near-field structures, and the pulse characteristics must be retained.
- Even though the Risk Category II models failed the Chapter 16 criteria, the probability of collapse calculated by the P-695 methodology did not exceed the limit of 10 percent. On the other hand, the Risk Category III model did not satisfy the acceptable probability of collapse of 6 percent but does satisfy the Chapter 16 requirements under some of the ground motion suites. Even if a structure is designed per ASCE 7, it may not have the assumed probability of collapse under the maximum considered earthquake when analyzed using FEMA P-695.
- The effects of nonlinear accidental torsion are investigated by expanding on the elastic procedure where the center of mass is shifted 5 percent of the diaphragm dimension in each direction. Accidental torsion can have a significant effect on the nonlinear behavior of a structure, even for a torsionally regular building. However, there are not sufficient studies on nonlinear accidental torsion provisions to include them in the next Chapter 16 update.
- Even though accidental torsion cannot be included in the proposed Chapter 16 updates, the elastic procedures are not comprehensive, and the issue of accidental torsion still needs more work for future NRHA provisions. The work in the third manuscript begins this process.
- Accidental torsion is assessed by applying the linear procedures that shift the center of mass by 5 percent of each diaphragm dimension to NRHA and by randomly modifying

the strength and stiffness of lateral resisting members. These analyses show that accidental torsion can have a significant effect on the inelastic behavior of this structure, particularly for shifts in mass.

- The four shifts in mass significantly increase the computational demand, so ways to minimize the required number of shifts by using either the calculated location of the center of rigidity or nonlinear pushover analyses are investigated. The pushover analyses was determined at the best way to determine which shifts should be run, and the third manuscripts provides suggested code language for a NRHA provision that includes an exception to reduce the number of mass shifts, as applicable.

## 6.2. Future Work

This section will be discussed in two sections: short-term future work and long-term future work. The short-term future work is directly related to expanding upon the research presented in this dissertation. The long-term future work relates to the general comparison and discussion of methodologies used for the performance assessment of seismic resistant structures.

### *6.2.1. Short-Term Future Work*

In the short term, additional analyses should be performed for the first study (that compares innovative and traditional systems), with new structural configurations to determine how the trends expand to a wide variety of uses. Initially, the results could be expanded to all the archetypes in the corresponding ATC 76 studies, as this research only presented a subset of the archetypes and performance groups. The inclusion of the gravity system resistance should then be expanded to a variety of other structural systems to see how the effect of this addition varies.

For the Hybrid BRBs, the P-58 analyses should be run with the residual drift inputs to determine the additional decrease in consequences. Since the residual drifts were greatly decreased in the P-695 analyses, this inclusion could decrease the consequences even further. For the Collapse Prevention Systems, a detailed cost estimate should be performed, since the lack of seismic detailing would likely decrease the overall costs. Using these accurate costs in the P-58 analyses would likely show an additional decrease in consequences. Additionally, augmented systems that combine the collapse prevention devices with dampers could improve behavior at numerous intensity levels. These additional systems should be modeled and analyzed at all intensity levels of interest, similarly for the other Hybrid BRBs and systems including the gravity system resistance. All these systems could also be analyzed for a specific location using a time-based assessment to see location specific benefits.

In the short term for the second study (about the assumptions within nonlinear response history provisions), the work needs to be expanded to a variety of additional systems with varying structural systems, configurations and materials. Particularly for the proposed accidental torsion

code language, these additional analyses should be used to finalize the recommended code language. This study was performed on a limited number of models, and while the results provide valuable insight into the assumptions, it is necessary to determine the applicability of the results to any generic structures.

### *6.2.2. Long-Term Future Work*

Numerous methodologies have been researched and discussed in this dissertation, particularly ASCE 7, FEMA P-695, and FEMA P-58. All the methodologies have benefits and disadvantages, which were summarized previously.

The largest conclusion that comes from this study of the various methodologies is that there is a wide variety of ways to assess the nonlinear performance of seismic resisting systems. While three methodologies are studied in detail in this work, numerous other provisions exist, including the Tall Building Initiative and ASCE 41. In the best interest of the profession, these methodologies should all be combined and standardized. However, this would require a significant amount of collaboration around the country and a significant number of studies to find the best, generic solution.

While this list should not be considered exhaustive, a single methodology for the performance assessment of seismic resisting structures should include:

- Assessment at numerous limits states, which can be adjusted based on the system and system location
- Minimal computational demand
- Integration of hazard with fragility
- Determination of consequences
- Standardized acceptance criteria
- Analysis of structural and non-structural components
- Inclusion of all potential nonlinear behaviors

The FEMA P-58 procedure is the methodology that satisfies more of these criteria than any other methodology. This procedure should provide the starting point for the development of a single, standard methodology. Primarily, the fragilities need to be expanded to be more inclusive and to ensure accurate cost estimations, and the best method for developing collapse fragility curves should be determined, based on the best balance between accuracy and simplicity. Additionally, the language should be adjusted to be prescriptive and include acceptance criteria. The modeling assumptions should satisfy the conclusions provided in the study on assumptions based on the proposed ASCE 7 updates, as they are applicable to all nonlinear response history analyses. In order to accomplish this daunting task, a significant amount of research would be required by

both academics and practitioners. However, this universalization would be a valuable change to the earthquake engineering profession and could potentially be the state of practice in a significant number of years.

# References


AISC (2011). *Steel Construction Manual*, American Institute of Steel Construction, Chicago, IL.

Akkar, S., Sucuo Lu, H., and Yakut, A. (2005). Displacement-Based Fragility Functions for Low-and Mid-Rise Ordinary Concrete Buildings. *Earthquake Spectra*, 21(4) 901–927.

Al Atik, L., and Abrahamson, N. (2010). An Improved Method for Nonstationary Spectral Matching. *Earthquake Spectra* 26, 601–617.

Ang, A., and Tang, W. (2007). *Probability Concepts in Engineering, 2nd edition*, John Wiley and Sons, Inc., Hoboken, NJ.

Antoniou, S., and Pinho, R. (2004). Advantages and Limitations of Adaptive and Non-Adaptive Force-Based Pushover Procedures. *Journal of Earthquake Engineering*, 8(4), 497–522.

ASCE (2005). *Minimum Design Loads for Buildings and Other Structures.* American Society of Civil Engineers, Reston, VA.

ASCE (2006). *Seismic Rehabilitation of Existing Buildings*, American Society of Civil Engineers, Reston, VA.

ASCE (2010). *Minimum Design Loads for Buildings and Other Structures.* American Society of Civil Engineers, Reston, VA.

ASCE (2013). *Seismic Rehabilitation of Existing Buildings*. American Society of Civil Engineers, Reston, VA.

Asgarian, B., Sadrinezhad, A., and Alanjari, P. (2010). Seismic Performance Evaluation of Steel Moment Resisting Frames through Incremental Dynamic Analysis. *Journal of Constructional Steel Research*, 66(2), 178–190.

Aslani, H., and Miranda, E. (2005). Fragility Assessment of Slab-Column Connections in Existing Non-Ductile Reinforced Concrete Buildings. *Journal of Earthquake Engineering*, 9 (6), 777–804.

Atlayan, O. (2008). *Effect of Viscous Fluid Dampers on Steel Moment Frame Designed for Strength and Hybrid Steel Moment Frame Design.* M.S. Thesis, Virginia Tech, Blacksburg, VA.

Atlayan, O., and Charney, F. (2012). Hybrid Steel Frames. *World Conference on Earthquake Engineering,* Lisbon, Portugal.

Atlayan, O., and Charney, F. (2013). Hybrid Buckling-Restrained Braced Frames. *Unpublished Manuscript.*

Ayoub, A., Mijo, C. and Chenouda, M. (2004). Seismic Fragility Analysis of Degrading Structural Systems. *13th World Conference on Earthquake Engineering*, Vancouver, B.C., Canada, Paper 2617.

Badillo-Almaraz, H., Whittaker, A., and Reinhorn, A. (2007). Seismic Fragility of Suspended Ceiling Systems. *Earthquake Spectra*, 23(1), 21–40.

Bazzurro, P., Cornell, C., Menun, C., and Motahari, M. (2004). Guidelines for Seismic Assessment of Damaged Buildings, in *Proceedings, 13th World Conference on Earthquake Engineering*, Paper 1708, Vancouver, Canada.

Bazzurro, P. and Luco, N. (2006). Do Scaled and Spectrum-matched Near-Source Records Produce Biased Nonlinear Structural Responses? in *Proceedings, 8th US National Conference on Earthquake Engineering*, San Francisco, CA.

Behnamfar, F., and Haghollahi, S. (2012). Collapse Performance Evaluation of Reinforced Concrete Special Moment Frame Systems Special Moment Frame Systems Considering Soil–Structure Interaction. *15th World Conference on Earthquake Engineering*, Lisbon, Portugal.

Bhuiyan, A., Alam, R., and Haque, N. (2012). Seismic Performance Assessment of a Continuous Highway Bridge Seismically Isolated by Lead Rubber Bearings. *Asian Transaction on Engineering*, 02(03), 62–71.

Bozorgnia, Y., and Bertero, V. (2004). *Earthquake Engineering: From Engineering Seismology to Performance-Based Engineering*, CRC Press.

Charney, F., and Marshall, J. (2006). A Comparison of the Krawinkler and Scissors Models for Including Beam-Column Joint Deformations in the Analysis of Moment-Resisting Steel Frames. *Engineering Journal – American Institute of Steel Construction* 43, 31–48.

Charney, F. A., Darling, S., and Eatherton, M. R. (2012). Seismic Performance of Very Short Period Buildings. *15th World Conference on Earthquake Engineering,* Lisbon, Portugal.

Chen, C. H., and Mahin, S. (2010). Seismic Collapse Performance of Concentrically Steel Braced Frames. *Structures Congress and 19th Analysis and Computation Specialty Conference,* Orlando, Florida.

Christovasilis, I., Filiatrault, A., Constantinou, M., and Wanitkorkul, A. (2009). Incremental Dynamic Analysis of Woodframe Buildings. *Earthquake Engineering and Structural Dynamics*, 38(4), 477–496.

Cimellaro, G., and Roh, H. (2010). Fragility Analysis of Structures with Controlled Rocking Beamcolumn Connections and Viscous Dampers. *9th U.S. National and 10th Canadian Conference on Earthquake Engineering*, Toronto, Ontario, Canada, Paper No 346.

Coffin L. F. (1954). A Study of the Effects of Cyclic Thermal Stresses on a Ductile Metal. *trans. ASME 76*, 931–950.

Comeau, G., Velchev, K., and Rogers, C. A. (2010). Development of Seismic Force Modification Factors for Cold-Formed Steel Strap Braced Walls. *Canadian Journal of Civil Engineering*, 37(2), 236–249.

Computers and Structures Inc. (CSI) (2011). *Nonlinear Analysis and Performance Assessment for 3D Structures, PERFORM 3D User Guide*, Berkeley, California.

Computers and Structures Inc. (CSI) (2012) *Knowledge Base: Modeling Techniques, Center of Rigidity*, Berkeley, CA.

Constantinou, M., Tsopelas, P., Hammel, W., and Sigaher, A. (2001). Toggle-brace-damper Seismic Energy Dissipation Systems. *Journal of Structural Engineering*, 127(2), 105–112.

Cundumi, O., and Laboy, S. (2010). Fragility Curves for Concrete Frame Buildings with Passive Controllers. *9th U.S. National and 10th Canadian Conference on Earthquake Engineering*, Toronto, Ontario, Canada, Paper No 1725.

DeBock, D. J., Liel, A. B., Haselton, C. B., Hooper, J. D., and Henige, R. A. (2013). Importance of Seismic Design Accidental Torsion Requirements for Building Collapse Capacity. *Earthquake Engineering & Structural Dynamics*.

Deierlein, G., Krawinkler, H., and Cornell, C. (2003). A Framework for Performance-Based Earthquake Engineering. *Pacific Conference on Earthquake Engineering*, 1–8.

Deierlein, G., Reinhorn, A., and Willford, M. (2010). Nonlinear Structural Analysis for Seismic Design. *NEHRP Seismic Design Technical Brief No. 4, NIST GCR 10-917-5*, National Institute of Standards and Technology, Gaithersburg, MD.

De la Llera, J. C., & Chopra, A. K. (1994a). Evaluation of Code Accidental-torsion Provisions from Building Records. *Journal of Structural Engineering*, 120(2), 597–616.

De la Llera, J. C., & Chopra, A. K. (1994b). Accidental Torsion in Buildings. *6th U.S. National Conference in Earthquake Engineering*, 401–410.

De la Llera, J. C., & Chopra, A. K. (1994c). Accidental Torsion in Buildings Due to Stiffness Uncertainty. *Earthquake Engineering and Structural Dynamics*, 23(2), 117–136.

De la Llera, J. C., & Chopra, A. K. (1994d). Accidental Torsion in Buildings Due to Base Rotational Excitation. *Earthquake Engineering and Structural Dynamics*, 23(9), 1003–1021.

De la Llera, J. C., and Chopra, A. K. (1995). Estimation of Accidental Torsion Effects for Seismic Design of Buildings. *Journal of Structural Engineering*, 121, 102–114.

De Stefano, M., and Pintucchi, B. (2008). A Review of Research on Seismic Behaviour of Irregular Building Structures Since 2002. *Bulletin of Earthquake Engineering*, 6(2), 285–308.

Dhakal, R., Mander, J., and Mashiko, N. (2006). Identification of Critical Ground Motions for Seismic Performance Assessment of Structures. *Earthquake Engineering & Structural Dynamics*, 35(8), 989–1008.

Dimova, S. L., and Alashki, I. (2003). Seismic Design of Symmetric Structures for Accidental Torsion. *Bulletin of Earthquake Engineering*, 1(2), 303–320.

Dimova, S., and Elenas, A. (2002). Seismic Intensity Parameters for Fragility Analysis of Structures with Energy Dissipating Devices. *Structural Safety*, 24 (1), 1–28.

Dolsek, M. (2009). Incremental Dynamic Analysis with Consideration of Modeling Uncertainties. *Earthquake Engineering and Structural Dynamics*, 38(6), 805–825.

Ellingwood, B., Rosowsky, D., Li, Y., and Kim, J. (2004). Fragility Assessment of Light-Frame Wood Construction Subjected to Wind and Earthquake Hazards. *Journal of Structural Engineering*, 130(12), 1921–1930.

Ellingwood, B. R., and Kinali, K. (2009). Quantifying and Communicating Uncertainty in Seismic Risk Assessment. *Structural Safety*, 31 (2), 179–187.

Elnashai, A. (2002). Do We Really Need Inelastic Dynamic Analysis? *Journal of Earthquake Engineering*, 6(spec01), 123–130.

Engineering News Record (ENR) (2011). *Square Foot Costbook*. Design and Construction Resources, Vista, CA.

Estekanchi, H., Vafai, A., and Sadeghazar, M. (2004). Endurance Time Method for Seismic Analysis and Design of Structures. *Scientia Iranica*, 11(4), 361–370.

Farahi, M., and Mofid, M. (2013). On the Quantification of Seismic Performance Factors of Chevron Knee Bracings, in Steel Structures. *Engineering Structures*, 46, 155–164.

FEMA (2000). *State of the Art Report on Connection Performance, FEMA-355D.* Prepared by the SAC Joint Venture for FEMA, Washington, D.C.

FEMA (2006). *Next-Generation Performance-Based Seismic Design Guidelines, FEMA 445*, Federal Emergency Management Agency, Washington, D.C.

FEMA (2009a). *Quantification of Building Seismic Performance Factors, FEMA P-695*, Applied Technology Council, Washington, D.C.

FEMA (2009b). *Effects of Strength and Stiffness Degradation on Seismic Response, FEMA P-440A.* Prepared by Applied Technology Council (ATC) for FEMA, Washington, D.C.

FEMA (2009c). *NEHRP Recommended Seismic Provisions for New Buildings and Other Structures, FEMA P-750*, Building Seismic Safety Council, Washington, DC.

FEMA (2012). *Seismic Performance Assessment of Buildings, FEMA P-58*, Applied Technology Council, Washington, D.C..

Flores, F., Jarrett, J., and Charney, F. (2012). The Influence of Gravity-Only Framing on the Performance of Steel Moment Frames. *15th World Conference on Earthquake Engineering*, Lisbon, Portugal.

Flores, F. and Charney, F. (2013). Influence of the Gravity Framing System on the Collapse Performance of Special Steel Moment Frames. *Unpublished Manuscript.*

Foschaar, J. C., Baker, J. W., and Deierlein, G. G. (2012). Preliminary Assessment of Ground Motion Duration Effects on Structural Collapse. *World Conference on Earthquake Engineering*, Lisbon, Portugal.

Green, T., Leon, R., and Rassati, G. (2004). Bidirectional Tests and Partially Restrained, Composite Beam Column Connections. *Journal of Structural Engineering* 130, 320–327.

Gupta, A., and Krawinkler, H. (2000). Behavior of Ductile SMRFs at Various Seismic Hazard Levels. *Journal of Structural Engineering*, 126(1), 98–107.

Han, S. W., and Chopra, A. K. (2006). Approximate Incremental Dynamic Analysis Using the Modal Pushover Analysis Procedure. *Earthquake Engineering and Structural Dynamics*, 35(15), 1853–1873.

Han, S. W., Moon, K.-H., and Chopra, A. K. (2010). Estimation of Collapse Capacity and Collapse Fragility Using Modal Pushover Analysis. *9th U.S. National and 10th Canadian Conference on Earthquake Engineering*, Toronto, Ontario, Canada, Paper No 909.

Hancock, J., Bommer, J. J., and Stafford, P. J. (2008). Numbers of Scaled and Matched

Accelerograms Required for Inelastic Dynamic Analyses, *Earthquake Engineering and Structural Dynamics* 37, 1585–1607.

Haselton, C. B., Fry, A., Baker, J. W., Hamburger, R. O., Whittaker, A. S., Stewart, J. P., Elwood, K. J., Luco, N., Hooper, J. D., and Charney, F. A. (2013). Response-History Analysis for the Design of New Buildings: Part I - Development of Recommendations for the NEHRP Provisions and the ASCE/SEI 7 Standard. *Unpublished manuscript*.

Holmes, W. and Zimmerman, R. (2012). *Seismic Performance Investigation, Clarendon Tower*, Report prepared for Canterbury Earthquakes Royal Commission by Rutherford + Chekene.

Huang, S. N., Lu, X. Z., and Ye, L. P. (2012). A Hysteretic Model of Conventional Steel Braces and an Analysis of the Collapse Prevention Effect of Brace Strengthening. *Applied Mechanics and Materials*, 174, 3–10.

Humar, J., Adams, J., Tremblay, R., Rogers, C. A., and Halchuk, S. (2010). Proposals for the Seismic Design Provisions of the 2010 National Building Code of Canada. *9th US National and 10th Canadian Conference on Earthquake Engineering, Toronto, Ont.*, Paper No. 1387.

Iervolino, I., Manfredi, G., and Cosenza, E. (2006). Ground Motion Duration Effects on Nonlinear Seismic Response. *Earthquake Engineering & Structural Dynamics*, 35 (1), 21–38.

Jarrett, J. A., Zimmerman R. B., and Charney, F. A. (2014). Accidental Torsion in Nonlinear Response History Analysis. *Unpublished manuscript*.

Judd, J. and Charney, F. (2013a). Performance-based Design in the Central and Eastern United States. *Unpublished Manuscript*.

Judd, J. and Charney, F. (2013b). Seismic Collapse Prevention System. *Unpublished Manuscript*.

Karim, K., and Yamazaki, F. (2003). A Simplified Method of Constructing Fragility Curves for Highway Bridges. *Earthquake Engineering and Structural Dynamics*, 32 (10), 1603–1626.

Kim, J., and Rosowsky, D. (2005). Fragility Analysis for Performance-Based Seismic Design of Engineered Wood Shearwalls. *Journal of Structural Engineering*, 131 1764.

Korkmaz, K. (2008). Evaluation of Seismic Fragility Analyses. *The 14th World Conference on Earthquake Engineering*, Beijing, China, Paper 09-01-0141.

Koutsourelakis, S., Prévost, J., and Deodatis, G. (2002). Risk Assessment of an Interacting Structure-Soil System Due to Liquefaction. *Earthquake Engineering & Structural Dynamics*, 31 (4), 851–879.

Lee, K., and Foutch, D. A. (2004). Performance Evaluation of Damaged Steel Frame Buildings Subjected to Seismic Loads. *Journal of Structural Engineering* 130, 588–599.

Leon, R. T. (1998). Composite Connections. *Progress in Structural Engineering and Materials*, 1(2), 159–169.

Liel, A., Haselton, C., and Deierlein, G. (2006). The Effectiveness of Seismic Building Code Provisions on Reducing the Collapse Risk of Reinforced Concrete Moment Frame Buildings. *4th International Conference on Earthquake Engineering*, Taipei, Taiwan.

Liel, A., and Tuwair, H. (2010). A Practical Approach for Assessing Structural Resistance to Earthquake-Induced Collapse. *19th Analysis & Computation Specialty Conference*, Orlando, FL.

Lignos, D., and Krawinkler, H. (2010). Deterioration Modeling of Steel Components in Support of Collapse Prediction of Steel Moment Frames Under Earthquake Loading. *Journal of Structural Engineering* 137, 1291–1302.

Liu, J., and Astaneh-Asl, A. (2000). Cyclic Testing of Simple Connections Including Effects of Slab. *Journal of Structural Engineering*, 126(1), 32–39.

Liu, J., and Astaneh-Asl, A. (2004). Moment-rotation Parameters for Composite Shear Tab Connections. *Journal of Structural Engineering*, 130(9), 1371–1380.

Lowes, L., and Li, J. (2010). Fragility Functions for Concrete Moment Frames. *9th U.S. National and 10th Canadian Conference on Earthquake Engineering*, Toronto, Ontario, Canada, Paper No 738.

Luco, N., Bazzurro, P., and Cornell, A. (2004). Dynamic Versus Static Computation of the Residual Capacity of a Mainshock-Damaged Building to Withstand an Aftershock. *13th World Conference on Earthquake Engineering*, Vancouver, B.C., Canada.

Luco, N., Gerstenberger, M., Uma, S., Ryu, H., Liel, A., and Raghunandan, M. (2011). A Methodology for Post-mainshock Probabilistic Assessment of Building Collapse Risk. *Ninth Pacific Conference on Earthquake Engineering Building an Earthquake-Resilient Society*, Auckland, New Zealand.

Mackie, K., and Stojadinovic, B. (2002). Relation between Probabilistic Seismic Demand Analysis and Incremental Dynamic Analysis. *7th US National Conference on Earthquake Engineering*, 21–25.

Mackie, K., and Stojadinovic, B. (2007). R-Factor Parameterized Bridge Damage Fragility Curves. *Journal of Bridge Engineering*, 12 (4), 500–510.

Malakoutian, M., Berman, J. W., Dusicka, P., and Lopes, A. (2012). Seismic Performance and Design of Linked Column Frame System (LCF). *World Conference on Earthquake Engineering*, Lisbon, Portugal.

Manson, S. S. (1953). *Behavior of Materials Under Conditions of Thermal Stress*. TN 2933: NACA.

Mansuri, M. (2009). *Torsional Effect on the Inelastic Seismic Response of Structures.* Dissertation, University of Southern California.

Mashal, M., and Filiatrault, A. (2012). Quantification of Seismic Performance Factors for Buildings Incorporating Three-dimensional Construction System. *World Conference on Earthquake Engineering*, Lisbon, Portugal.

MathWorks (2011). Matlab [computer software - version 2011b], Natick, Massachusetts, The MathWorks, Inc.

Marshall, J. D. (2008). *Development, Analysis and Testing of a Hybrid Passive Control Device for Seismic Protection of Framed Structures.* Ph.D. Dissertation, Virginia Tech, Blacksburg, VA.

McCormick, J., Aburano, H., Ikenaga, M., and Nakashima, M. (2008). Permissible Residual Deformation Levels for Building Structures Considering Both Safety and Human Elements, in *Proceedings, 14th World Conference on Earthquake Engineering*.

McGuire, R. (2004). *Seismic Hazard and Risk Analysis*, Earthquake Engineering Research Institute, Oakland, CA.

McKenna, F. (2011) *OpenSEES.* Version 2.3.1. Pacific Earthquake Engineering Research Center, Berkeley, CA.

Medina, R., and Krawinkler, H. (2005). Evaluation of Drift Demands for the Seismic Performance Assessment of Frames. *Journal of Structural Engineering*, 131(7), 1003.

Microsoft. (2010). Microsoft Excel [computer software]. Redmond, Washington.

Miyamoto, H., Gilani, A. S. J., Wada, A., and Ariyaratana, C. (2010). Collapse Risk of Tall Steel Moment Frame Buildings with Viscous Dampers Subjected to Large Earthquakes. *The Structural Design of Tall and Special Buildings*, 19(4), 421–438.

Moschonas, I., Kappos, A., Panetsos, P., Papadopoulos, V., Makarios, T., and Thanopoulos, P. (2009). Seismic Fragility Curves for Greek Bridges: Methodology and Case Studies. *Bulletin of Earthquake Engineering*, 7(2), 439–468.

Mwafy, A., and Elnashai, A. (2001). Static Pushover Versus Dynamic Collapse Analysis of Rc Buildings. *Engineering Structures*, 23(5), 407–424.

Nakashima, M., Iwai, S., Iwata, M., Takeuchi, T., Konomi, S., Akazawa, T., and Saburi, K. (1994). Energy Dissipation Behaviour of Shear Panels Made of Low Yield Steel. *Earthquake Engineering and Structural Dynamics*, 23(12), 1299–1313.

Nakazawa, T., Kishiki, S., Qu, Z., Miyoshi, A., and Wada, A. (2011). Fundamental Study on Probabilistic Evaluation of the Ultimate State of Base Isolated Structures. *Journal of Structural and Construction Engineering*, 76(662), 745–754.

Nippon Steel (2009). *Steel Plates*. Nippon Steel, N.S. Corporation.

NIST (2010a). *Evaluation of the FEMA P-695 Methodology for Quantification of Building Seismic Performance Factors, NIST GCR 10-917-8*, NEHRP Consultants Joint Venture, Redwood City, CA.

NIST (2010b). *Applicability of Nonlinear Multiple-Degree-of-Freedom Modeling for Design*, *NIST GCR 10-917-9*, Redwood City, CA.

NIST (2011). *Selecting and Scaling Earthquake Ground Motions for Performing Response-History Analyses. NIST GCR 11-917-15*, NEHRP, Gaithersburg, MD.

NIST (2012). *Tentative Framework for Development of Advanced Seismic Design Criteria for New Buildings. NIST GCR 12-917-20*, NEHRP Consultants Joint Venture, Redwood City, CA.

Oesterle, M. G. (2003). *Use of Incremental Dynamic Analysis to Assess the Performance of Steel Moment-Resisting Frames with Fluid Viscous Dampers.* M.S. Thesis, Virginia Tech, Blacksburg, VA.

PEER (2010). *Guidelines for Performance-Based Seismic Design of Tall Buildings, Report No. 2010/05*, Tall Building Initiative.

Peruš, I., and Fajfar, P. (2005). On the Inelastic Torsional Response of Single-Storey Structures Under Bi-axial Excitation. *Earthquake engineering & structural dynamics*, 34(8), 931–941.

Prowell, I., Elgamal, A., Uang, C., and Jonkman, J. (2010). Estimation of Seismic Load Demand for a Wind Turbine in the Time Domain. *Report No. NREL/CP 500*, 47536.

PTC (2012). Mathcad14 [computer software], Needham, MA.

Ott, R., and Longnecker, M. (2010). *An Introduction to Statistical Methods and Data Analysis, 6th Edition*, Brooks/Cole, Belmont, CA.

Porter, K., Kennedy, R., and Bachman, R. (2007). Creating Fragility Functions for Performance-Based Earthquake Engineering. *Earthquake Spectra*, 23(2), 471–489.

Rassati, G., Leon, R., and Noe, S. (2004). Component Modelling of Partially Restrained Composite Joints under Cyclic and Dynamic Loading. *Journal of Structural Engineering* 130, 342–351.

Richard, M., Albano, L., Kelly, D., and Liel, A. (2010). Case Study on the Seismic Performance of Reinforced Concrete Intermediate Moment Frames using ACI Design Provisions. *Structures Congress*, 3523–3534.

Ruiz-García, J., and Miranda, E. (2010). Probabilistic Estimation of Residual Drift Demands for Seismic Assessment of Multi-story Framed Buildings. *Engineering Structures* 32, 11–20.

Rutherford + Chekene (R+C) (2011). *Perform Nonlinear Component Modeling of StarSeismicTM Powercat BRBs*, Report to StarSeismic LLC.

Saeki, E., Sugisawa, M., Yamaguchi, T., and Wada, A. (1998). Mechanical Properties of Low Yield Point Steels. *Journal of Materials in Civil Engineering*, 10(3), 143–152.

Saunders, R. A. (2004). *Nonlinear Dynamic Analysis of Structures with Hyperelastic Devices.* M.S. Thesis, Virginia Tech, Blacksburg, VA.

Saxena, V., Deodatis, G., Shinozuka, M., and Feng, M. (2000). Development of Fragility Curves for Multi-Span Reinforced Concrete Bridges. *The International Conference on Monte Carlo Simulation*, 499–504.

Seismic Structural Design Associates Inc. (SSDA) (2001). *Description and Results of SSDA Tests No. 23, 24, 25 and 26*.

Shinozuka, M., Feng, M.Q., Lee, J., and Naganuma, T. (2000). Statistical Analysis of Fragility Curves. *Journal of Engineering Mechanics*, 126 (12), 1224–1231.

Shome, N., and Cornell, C. (1998). Normalization and Scaling Accelerograms for Nonlinear Structural Analysis. *Sixth U.S. National Conference on Earthquake Engineering*, EERI, Seattle, WA, 1–12.

Spears, P. (2004). *Parameters Influencing Seismic Structural Collapse with Emphasis on Vertical Accelerations and the Possible Related Risks for New and Existing Structures in the Central and Eastern United States.* M.S. Thesis, Virginia Tech, Blacksburg, VA.

Stathopoulos K. G. and Anagnostopoulos S. A. (2003) Inelastic Earthquake Response of Single-story Asymmetric Buildings: An Assessment of Simplified Shear-beam Models. *Earthquake Engineering and Structural Dynamics*, 32, 1813–1831.

Stathopoulos, K. G., and Anagnostopoulos, S. A. (2010). Accidental Design Eccentricity: Is it Important for the Inelastic Response of Buildings to Strong Earthquakes? *Soil Dynamics and Earthquake Engineering*, 30(9), 782–797.

Vamvatsikos, D. (2002). *Seismic Performance, Capacity and Reliability of Structures as Seen through Incremental Dynamic Analysis.* Ph.D. Dissertation, Stanford University, Palo Alto, CA.

Vamvatsikos, D., and Allin Cornell, C. (2002). Incremental Dynamic Analysis. *Earthquake Engineering and Structural Dynamics*, 31(3), 491–514.

Vamvatsikos, D., and Sigalas, I. (2005). Seismic Performance Evaluation of a Horizontally Curved Highway Bridge Using Incremental Dynamic Analysis in 3D. *4th European workshop on the seismic behavior of irregular and complex structures.*

Vamvatsikos, D., and Cornell, A. (2006). Incremental Dynamic Analysis with Two Components of Motion for a 3D Steel Structure. *8th US National Conference on Earthquake Engineering*.

van de Lindt, J. W., Rosowsky, D. V., Pang, W., and Pei, S. (2012). Performance-Based Seismic Design of Mid-Rise Woodframe Buildings. *Journal of Structural Engineering*.

Villaverde, R. (2007). Methods to Assess the Seismic Collapse Capacity of Building Structures: State of the Art. *Journal of Structural Engineering*, 133(1), 57.

Wen, R., Akbas, B., and Shen, J. (2013). Practical Moment–rotation Relations of Steel Shear Tab Connections. *Journal of Constructional Steel Research*, 88, 296–308.

Yun, S., Hamburger, R., Cornell, C., and Foutch, D. (2002). Seismic Performance Evaluation for Steel Moment Frames. *Journal of Structural Engineering*, 128(4), 534–545.

Zareian, F., and Krawinkler, H. (2007). Assessment of Probability of Collapse and Design for Collapse Safety. *Earthquake Engineering and Structural Dynamics*, 36 (13), 1901–1914.

Zareian, F., and Krawinkler, H. (2010). Structural System Parameter Selection Based on Collapse Potential of Buildings in Earthquakes. *Journal of Structural Engineering*, 136(8), 933–943.

Zareian, F. (2013). *PACT Beta Test Example: Building A Steel Special Moment Frame Building, Background Document FEMA P-58/BD-3.7.14.* Applied Technology Council, Washington, D.C.

Zimmerman, R. B., Baker, J., Haselton, C. B., Bono, S., Engel, A., Hooper, J., Hamburger, R., Celikbas, S., and Jalalian, A. (2013). Response History Analysis for the Design of New Buildings: Part II—Example Applications to Illustrate the Recommended Methodology. *Unpublished manuscript*.

Zsarnóczay, Á. (2012). Influence of Plastic Mechanism Development on the Seismic Performance of Buckling Restrained Braced Frames case study. *Conference of Junior Researchers in Civil Engineering*.

# Appendix A: Additional Information Regarding the Structures and Mathematical Models Used in the Manuscript "Comparative Evaluation of Innovative and Traditional Steel Seismic Resisting Systems Using the FEMA P-58 Procedure"

For each model used in this work, additional information regarding the design and modeling is provided in this appendix.

## A.1. Hybrid Buckling Restrained Steel Braces

The Hybrid Buckling Restrained Braces use the design of the BRB system in ATC 76 (NIST 2010a) as a basis. The structures used for these analyses are the 4-story, 9-story and 18-story buildings from Performance Group 10, which are designed for the location neutral SDC $D_{max}$. This Performance Group uses lightning bolt bracing, as shown in Figure A-1. The bay width of the BRB frames are 15 feet (4.57 meters), and all story heights are 13 feet (3.96 meters), as shown in Figure A-1.

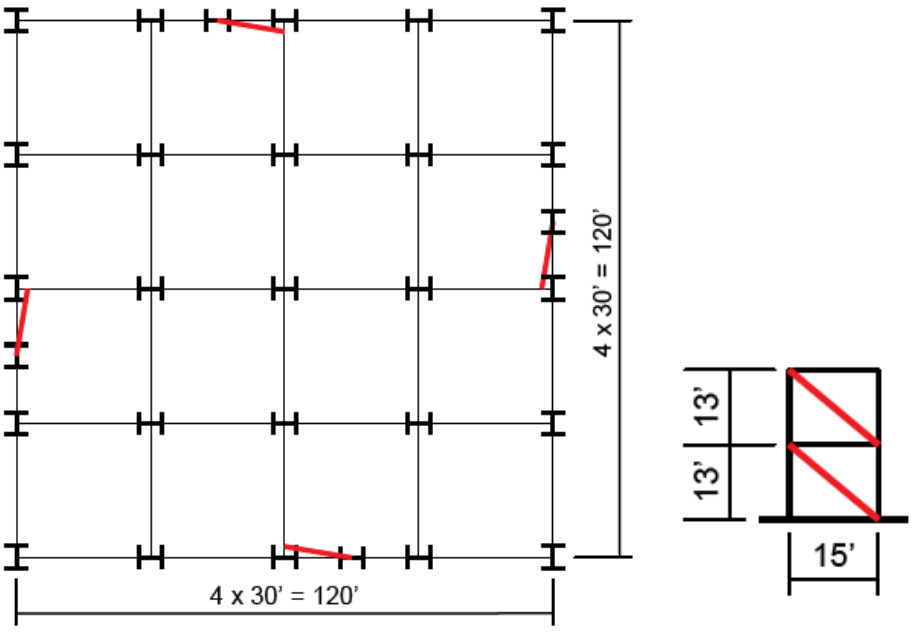


**Figure A-1.** Plan view of Performance Group 10 layout (left) and an example configuration of the lightning bolt bracing (right) (NIST 2010a)

The 4-story, 9-story and 18-story structures are all modeled with four different levels of Hybridity: Regular, Hybrid-1, Hybrid-2, and Hybrid-3 (Atlayan and Charney 2013). The Regular BRBs are the traditional ATC 76 BRBs and have no hybridity. The Hybrid-1 model is a combination of carbon A36 steel, LYP100 steel, and HPS70W high performance steel (which

has a yield strength of 73 ksi). The Hybrid-2 model uses LYP100 steel and HPS70W, and the Hybrid-3 model uses LYP100 steel and HPS100W high performance steels (which has a yield strength of 108 ksi). Table A-1 presents the amounts of hybridity for each model. As the hybrid "number" increases, the hybridity increases. All the braces had the same total stiffness of 200000 kip/inch and the same total strength of 290 kip.

**Table A-1.** Description of hybridity for each BRB model

| | **Steel Area Ratios** | | | |
|---|---|---|---|---|
| | **Regular** | **Hybrid 1** | **Hybrid 2** | **Hybrid 3** |
| A36 | 1.0 | 0.167 | 0 | 0 |
| LYP100 | 0 | 0.493 | 0.591 | 0.776 |
| HPS70W | 0 | 0.375 | 0.450 | 0 |
| HPS100W | 0 | 0 | 0 | 0.278 |

For each story height, the member sizes are also kept the same, regardless of which BRB was used. Table A-2 provides members sizes for the 4-story models, Table A-3 provides member sizes for the 9-story models, and Table A-5 provides member sizes for the 18-story models. Beam sizes are provided for the top of each story.

**Table A-2.** Members sizes for the 4-story BRB models

| **Story** | **Brace Area ($in^2$)** | **Beam size** | **Column Size** |
|---|---|---|---|
| 4 | 5 | W21x50 | W14x74 |
| 3 | 7 | W21x62 | W14x82 |
| 2 | 9 | W21x73 | W14x132 |
| 1 | 10 | W21x73 | W14x145 |

**Table A-3.** Members sizes for the 9-story BRB models

| **Story** | **Brace Area ($in^2$)** | **Beam size** | **Column Size** |
|---|---|---|---|
| 9 | 9 | W21x62 | W14x370 |
| 8 | 9 | W24x76 | W14x370 |
| 7 | 10 | W24x76 | W14x370 |
| 6 | 10 | W24x76 | W14x398 |
| 5 | 11 | W27x94 | W14x398 |
| 4 | 11 | W27x94 | W14x455 |
| 3 | 11 | W27x94 | W14x455 |
| 2 | 12 | W27x94 | W14x500 |
| 1 | 12 | W27x94 | W14x500 |

**Table A-4.** Members sizes for the 18-story BRB models

| Story | Brace Area ($in^2$) | Beam size | Column Size |
|---|---|---|---|
| 18 | 4 | W21x50 | W14x176 |
| 17 | 5 | W21x62 | W14x176 |
| 16 | 5 | W21x62 | W14x342 |
| 15 | 5 | W21x62 | W14x342 |
| 14 | 6 | W21x62 | W14x342 |
| 13 | 6 | W21x62 | W14x342 |
| 12 | 7 | W21x62 | W14x426 |
| 11 | 7 | W24x76 | W14x426 |
| 10 | 7 | W24x76 | W14x426 |
| 9 | 7 | W24x76 | W14x426 |
| 8 | 7 | W24x76 | W14x500 |
| 7 | 10 | W24x76 | W14x500 |
| 6 | 10 | W24x76 | W14x500 |
| 5 | 10 | W24x76 | W14x500 |
| 4 | 10 | W24x76 | W14x605 |
| 3 | 12 | W24x94 | W14x605 |
| 2 | 12 | W24x94 | W14x605 |
| 1 | 12 | W24x94 | W14x605 |

A summary of the analytical modeling of the Hybrid Buckling Restrained Systems is provided next. A detailed description of the modeling assumptions can be found in the manuscript contained in Chapter 3.

- Two-dimensional models
- Modeled in OpenSEES
- P-Delta effects captured through a leaning column.
- The beams and columns in the frames are modeled using fiber elements.
- Gusset plates at the connections are modeled using rigid offsets.
- The column's bases are fixed.
- The columns resist bending loads along the strong axis.
- Corotational truss elements are used to model the BRBs.
- The fatigue material in OpenSEES is also applied onto the BRBs to capture low cycle fatigue effects.
- Rayleigh damping is used to capture 2 percent damping in the first and third modes.

## A.2. Collapse Prevention Systems

The Collapse Prevention Systems use the layout of the ATC 76 (NIST 2010a) Special Moment Resisting Frames (SMRF), and based on these dimensions, an $R$ = 3 system is designed (Judd and Charney 2013b) using the requirements of ASCE 7 and AISC (ASCE 2010, AISC 2011). The building has a bay width of 20 feet and seismic resisting systems on the perimeter. The story height of the first story is 15 feet; the other story heights are 30 feet. For the 2-story model, all columns are pinned. For the 4-story system, the columns in the seismic resistant frame are fixed, and the columns in the gravity system are pinned and spliced above the third story. The gravity system is also designed, and the collapse prevention mechanisms are utilized within both the lateral and gravity systems. Figure A-2 shows the typical plan view of the Collapse Prevention Systems. Table A-5 provides the member sizes for the seismic resistant system for the 2-story model, Table A-6 provides the member sizes for the gravity system for the 2-story model, Table A-7 provides the member sizes for the seismic resistant system for the 4-story model, and Table A-8 provides the member sizes for the gravity system for the 4-story model. The building design is symmetric, so only half of the member sizes are reported.

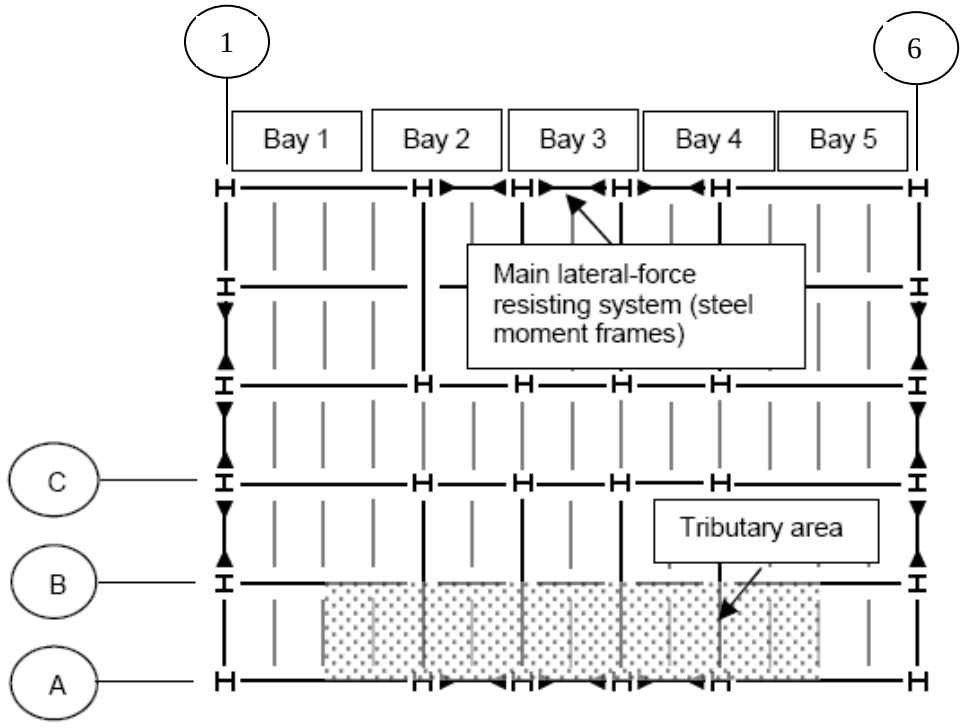


**Figure A-2.** Typical plan view of the Collapse Prevention Systems (Judd and Charney 2013b)

**Table A-5.** Member sizes for the seismic resistant system for the 2-story model of the Collapse Prevention System

| Story | Beam | Exterior Columns | Interior Columns |
|---|---|---|---|
| 2 | W16x31 | W18x71 | W18x76 |
| 1 | W21x44 | W18x71 | W18x76 |

**Table A-6.** Member sizes for the gravity system for the 2-story model of the Collapse Prevention System

| | Beams | | | Columns | | |
|---|---|---|---|---|---|---|
| Story | Line A Bay 1,5 | Line C Bay 1,5 | Line C Bay 2,3,4 | Line A Line 1,6 | Line C Line 2,5 | Line C Line 3,4 |
| 2 | W24x68 | W24x68 | W16x31 | W14x43 | W14x90 | W14x61 |
| 1 | W24x68 | W24x68 | W16x31 | W14x43 | W14x90 | W14x61 |

**Table A-7.** Member sizes for the seismic resistant system for the 4-story model of the Collapse Prevention System

| Story | Beam | Exterior Columns | Interior Columns |
|---|---|---|---|
| 4 | W16x31 | W18x40 | W18x46 |
| 3 | W18x35 | W18x40 | W18x46 |
| 2 | W21x44 | W18x76 | W18x86 |
| 1 | W16x40 | W18x76 | W18x86 |

**Table A-8.** Member sizes for the gravity system for the 4-story model of the Collapse Prevention System

| | Beams | | | Columns | | |
|---|---|---|---|---|---|---|
| Story | Line A Bay 1,5 | Line C Bay 1,5 | Line C Bay 2,3,4 | Line A Line 1,6 | Line C Line 2,5 | Line C Line 3,4 |
| 4 | W24x68 | W24x68 | W16x31 | W14x30 | W14x90 | W14x61 |
| 3 | W24x68 | W24x68 | W16x31 | W14x30 | W14x90 | W14x61 |
| 2 | W24x68 | W24x68 | W16x31 | W14x43 | W14x90 | W14x61 |
| 1 | W24x68 | W24x68 | W16x31 | W14x43 | W14x90 | W14x61 |

Numerous mechanisms can be used as a collapse prevention system. In this paper, the two mechanisms investigated are a slack cable and a loose linkage mechanism, as shown in Figure A-3. For this research, the Slack Cable CPM consists of 26-mm diameter structural steel cables with a 140 k breaking load, and the Loose Link CPM consists of 1x2.5-inch A995-50 steel bars. Both of these systems remain inactive until the building has reached a specified level of drift, typically 2 percent of the total height, after which the CPM engages. The loose link mechanism is essentially a toggle brace without the added damper (Constantinou et al. 2001). Although it is out of the scope of this work, true toggle braces and other advanced systems that combine a CPM

and a damper could be used to additionally improve the behavior under wind and low seismic loads (Judd and Charney 2013b).

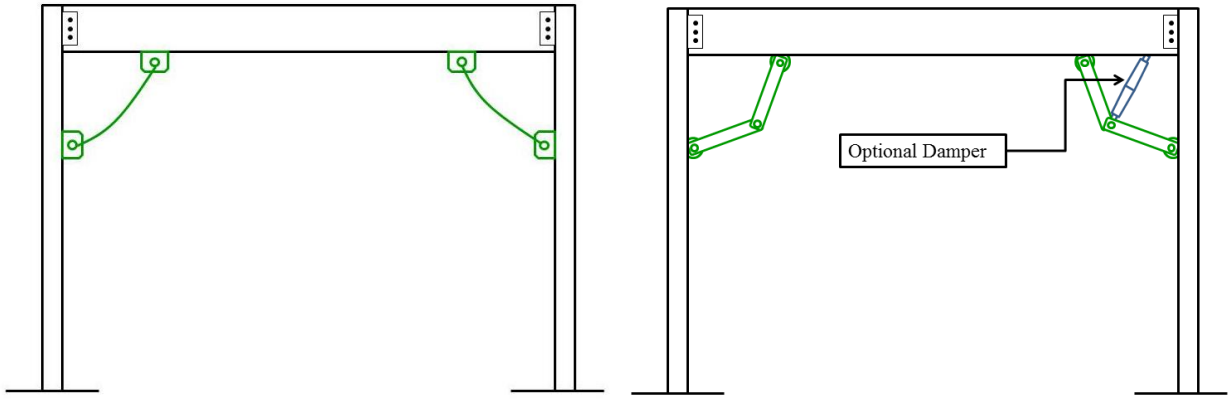


**Figure A-3.** Slack cable CPM (left) and loose link CPM (right)

Since the only limit state of interest is collapse prevention, these systems are analyzed at a near-collapse level intensity. These intensities are taken as 90 percent of the median collapse intensity of the system without a collapse prevention mechanism. This was selected to show the potential behavior at large ground motions where collapse is possible, which changes with each structural configuration.

A summary of the analytical modeling of the Collapse Prevention Systems is provided next. A detailed description of the modeling assumptions can be found in the manuscript contained in Chapter 3.

- Two-dimensional models
- Modeled in OpenSEES
- Nonlinearities are modeled using a phenomenological (concentrated plasticity) approach.
- The moment-rotation behavior of the non-ductile beam-to-column connections is represented using the Pinching4 and MinMax uniaxial materials in OpenSEES with load-deformation and hysteresis parameters based on FEMA P-440A (FEMA 2009b), ASCE 41 (ASCE 2006), and FEMA 355D (FEMA 2000).
- The effect of composite action on moment-frame beam flexure strength is not included.
- Column plastic hinging moment-rotation behavior is represented using the Bilin uniaxial material in OpenSEES
- Column behavior includes an approximate reduction to account for axial load
- Column panel zones are modeled using the Krawinkler joint model.

- The gravity framing system beam-to-column moment-rotation behavior is based on test data of shear tab connections (Lui and Astaneh-Asl 2000), corresponding analytical models (Lui and Astaneh-Asl 2004, Wen et al. 2013) and FEMA P-440A.
- Gravity framing connections to the column weak-axis are treated as un-restrained for moment transfer.
- Slack cables are represented in the model using truss elements with multi-linear elastic uniaxial material behavior (to simulate initial slackness) until fracture at the breaking load.
- Loose-linkages are represented in the model using corotational-truss elements that are elastic until fracture, approximated as the tensile yield limit state of the links.
- The analysis of the CP systems used the true computed fundamental period of the, instead of using the upper limit design period $C_u T_a$.

### A.3. Special Steel Moment Frames Modeled With and Without the Gravity System

The Special Moment Resisting Frames with and without gravity framing use the ATC 76 (NIST 2010a) Special Moment Resisting Frames as the base system. The gravity system is designed (Flores and Charney 2013) using the requirements of ASCE 7 and AISC (ASCE 2010, AISC 2011) and is added to the ATC 76 design. The structures used are the 2-story, 4-story and 8-story structures designed for SDC $D_{max}$, using the Response Spectrum Analysis (RSA). The bay width of the SMRF frames are 20 feet (6.10 meters), and all story heights are 13 feet (3.96 meters), except the first story, which has a height of 15 feet (4.57 meters). Figure A-4 shows the typical plan view of the SMRF systems. Table A-9 provides the member sizes for the seismic resistant system for the 2-story model, Table A-10 provides the member sizes for the gravity system for the 2-story model, Table A-11 provides the member sizes for the seismic resistant system for the 4-story model, Table A-12 provides the member sizes for the gravity system for the 4-story model, Table A-13 provides the member sizes for the seismic resistant system for the 8-story model, and Table A-14 provides the member sizes for the gravity system for the 8-story model. The building design is symmetric, so only half of the member sizes are reported. The location nomenclature is shown in Figure A-2.

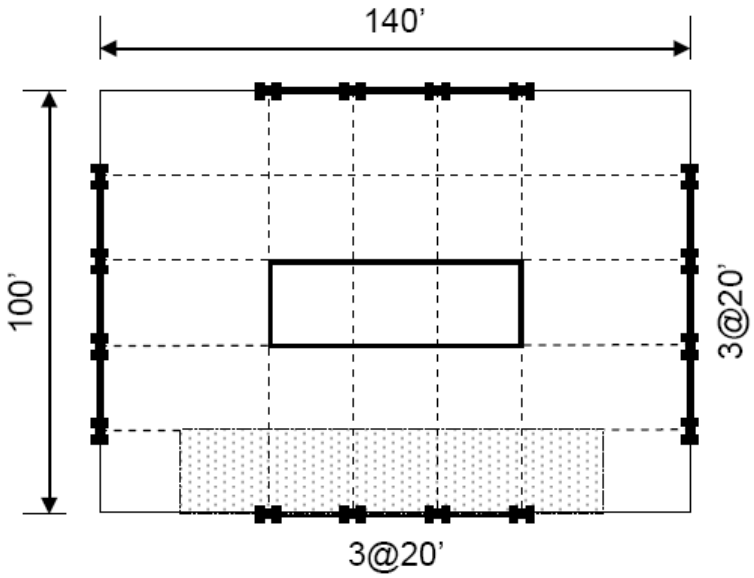


**Figure A-4.** Typical plan view of the SMRF systems (NIST 2010)

**Table A-9.** Member sizes for the seismic resistant system for the 2-story model of the Special Moment Resistant Frame System

| Story | Beam | Exterior Columns | Interior Columns |
|---|---|---|---|
| 2 | W16x31 | W24x131 | W24x162 |
| 1 | W30x132 | W24x131 | W24x162 |

**Table A-10.** Member sizes for the gravity system for the 2-story model of the Special Moment Resistant Frame System

| | Beams | | | Columns | | | |
|---|---|---|---|---|---|---|---|
| Story | Line A Bay 1,5 | Line C Bay 1,5 | Line C Bay 2,3,4 | Line A Line 1,6 | Line C Line 1,6 | Line C Line 2,5 | Line C Line 3,4 |
| 2 | W24x55 | W24x84 | W16x36 | W14x43 | W24x162 | W14x90 | W14x61 |
| 1 | W24x62 | W24x94 | W16x36 | W14x43 | W24x162 | W14x90 | W14x61 |

**Table A-11.** Member sizes for the seismic resistant system for the 4-story model of the Special Moment Resistant Frame System

| Story | Beam | Exterior Columns | Interior Columns |
|---|---|---|---|
| 4 | W21x57 | W24x62 | W24x62 |
| 3 | W21x57 | W24x62 | W24x62 |
| 2 | W21x73 | W24x103 | W24x103 |
| 1 | W21x73 | W24x103 | W24x103 |

**Table A-12.** Member sizes for the gravity system for the 4-story model of the Special Moment Resistant Frame System

| | Beams | | | Columns | | | |
|---|---|---|---|---|---|---|---|
| **Story** | **Line A Bay 1,5** | **Line C Bay 1,5** | **Line C Bay 2,3,4** | **Line A Line 1,6** | **Line C Line 1,6** | **Line C Line 2,5** | **Line C Line 3,4** |
| 4 | W24x55 | W24x84 | W16x36 | W14x30 | W24x62 | W14x90 | W14x61 |
| 3 | W24x62 | W24x94 | W16x36 | W14x30 | W24x62 | W14x90 | W14x61 |
| 2 | W24x62 | W24x94 | W16x36 | W14x43 | W24x103 | W14x90 | W14x61 |
| 1 | W24x62 | W24x94 | W16x36 | W14x43 | W24x103 | W14x90 | W14x61 |

**Table A-13.** Member sizes for the seismic resistant system for the 8-story model of the Special Moment Resistant Frame System

| **Story** | **Beam** | **Exterior Columns** | **Interior Columns** |
|---|---|---|---|
| 8 | W21x68 | W24x94 | W24x94 |
| 7 | W24x84 | W24x94 | W24x94 |
| 6 | W24x84 | W24x131 | W24x131 |
| 5 | W27x94 | W24x131 | W24x131 |
| 4 | W27x94 | W24x131 | W24x162 |
| 3 | W30x116 | W24x131 | W24x162 |
| 2 | W30x116 | W24x131 | W24x162 |
| 1 | W30x108 | W24x131 | W24x162 |

**Table A-14.** Member sizes for the gravity system for the 8-story model of the Special Moment Resistant Frame System

| | Beams | | | Columns | | | |
|---|---|---|---|---|---|---|---|
| **Story** | **Line A Bay 1,5** | **Line C Bay 1,5** | **Line C Bay 2,3,4** | **Line A Line 1,6** | **Line C Line 1,6** | **Line C Line 2,5** | **Line C Line 3,4** |
| 8 | W24x55 | W24x94 | W16x36 | W18x40 | W24x94 | W18x50 | W18x40 |
| 7 | W24x62 | W24x94 | W16x36 | W18x40 | W24x94 | W18x50 | W18x40 |
| 6 | W24x62 | W24x94 | W16x36 | W18x50 | W24x131 | W18x76 | W18x50 |
| 5 | W24x62 | W24x94 | W16x36 | W18x50 | W24x131 | W18x76 | W18x50 |
| 4 | W24x62 | W24x94 | W16x36 | W18x50 | W24x162 | W18x76 | W18x50 |
| 3 | W24x62 | W24x94 | W16x36 | W18x76 | W24x162 | W18x143 | W18x76 |
| 2 | W24x62 | W24x94 | W16x36 | W18x76 | W24x162 | W18x143 | W18x76 |
| 1 | W24x62 | W24x94 | W16x36 | W18x76 | W24x162 | W18x143 | W18x76 |

A summary of the analytical modeling of the Special Moment Resisting Frame Systems is provided next. A detailed description of the modeling assumptions can be found in the manuscript contained in Chapter 3.

- Two-dimensional models
- Modeled in OpenSEES
- The nonlinearities of the special moment resisting frame are modeled using phenomenological plastic hinges at the end of the members.
- The hinges are modeled in the reduced beam sections of the beams and in the columns at the bases and outside the moment frame connections.
- The reduced beam sections and column hinges use the Bilin material in OpenSEES (Lignos and Krawinkler 2010) to represent the hysteretic material.
- Additionally, a reduced bending strength is used in the columns to model the P-M interaction that is not included in the Bilin model. The nonlinearities in the panel zones are represented using the Krawinkler model (Charney and Marshall 2006).
- The gravity columns are pinned at the base, oriented in the strong direction, and modeled using fiber elements to account for potential yielding.
- The partially restrained connections are modeled using a simple model from ASCE 41 (ASCE 2006).
- The strength of the connection is assumed to be a percentage of the plastic moment strength of the attached beam, and for this research, all the 2-story, 4-story and 8-story structures are analyzed with 0 percent, 35 percent and 50 percent connection strength.

# Appendix B: Additional Results from "Comparative Evaluation of Innovative and Traditional Steel Seismic Resisting Systems Using the FEMA P-58 Procedure"

Numerous results were found in the P-58 studies of the innovative systems and modeling assumptions that were not included in the manuscript. This appendix is used to show all the P-58 results.

## B.1. Hybrid Buckling Restrained Braces

For the BRB systems, the results are presented on a story-by-story basis. The cost distribution is shown for each system to show the dispersion of results from the realizations. Additionally, the average repair time, total probability of unsafe placard, and average number of casualties are tabulated.

### *B.1.1. Four-Story Models*

Figure B-1 shows the cost distributions for the 4-story models. For this model, the largest improvement can be seen at the serviceability level, where the average costs are reduced by more than 12 percent when comparing the Regular system to the Hybrid 3 system. For the higher intensities, the cost distributions tend to "flatten out." This is the distinction between partial repair cost and total repair cost. The points at $300 per square foot that stack on top of each other represent the total repair cost, assuming a collapse has occurred. The partial repair costs tend to be around $100 per square foot or less for this structure.

Tables B-1, B-2 and B-3 show the average repair time, total probability of unsafe placard, and average number of casualties, respectively. At the serviceability level, the average repair time is reduced by up to 12 percent. At all other intensity levels, the change in repair time is negligible. Additionally, the change in total probability of receiving an unsafe placard is negligible. The average number of deaths under the serviceability intensity level is reduced by up to 14 percent; otherwise, the change in casualties is negligible. The median number of collapses is always zero, meaning there are more realizations that did not simulate casualties than realizations that did simulate casualties.

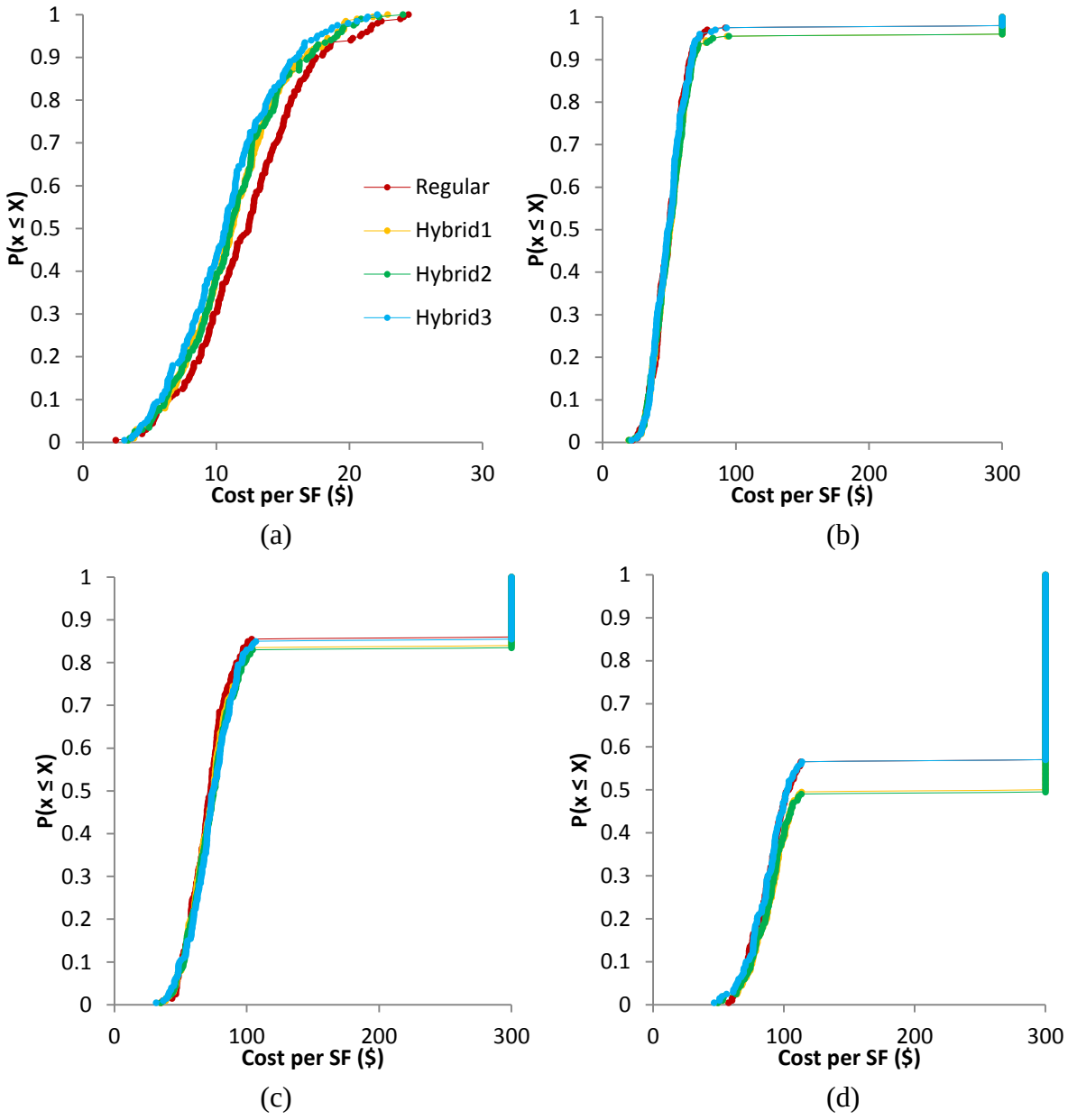


**Figure B-1.** Probability distribution of the repair costs for the 4-story BRB models for the (a) serviceability intensity level, (b) DBE intensity level, (c) MCE intensity level, and (d) near-collapse intensity level

**Table B-1.** Average parallel repair time (in days) for the 4-story BRB models with varying levels of hybridity

| | Regular | Hybrid 1 | Hybrid 2 | Hybrid 3 |
|---|---|---|---|---|
| **Serviceability** | 105 | 95 | 96 | 91 |
| **DBE** | 379 | 378 | 378 | 379 |
| **MCE** | 392 | 392 | 391 | 391 |
| **Near-collapse level** | 392 | 392 | 392 | 392 |

**Table B-2.** Total probability of receiving an unsafe placard for the 4-story BRB models with varying levels of hybridity

| | Regular | Hybrid 1 | Hybrid 2 | Hybrid 3 |
|---|---|---|---|---|
| **Serviceability** | 0.04 | 0.03 | 0.03 | 0.02 |
| **DBE** | 0.92 | 0.91 | 0.91 | 0.91 |
| **MCE** | 0.99 | 0.99 | 0.99 | 0.98 |
| **Near-collapse level** | 1.0 | 1.0 | 1.0 | 1.0 |

**Table B-3.** Average number of casualties for the 4-story BRB models with varying levels of hybridity

| | Regular | Hybrid 1 | Hybrid 2 | Hybrid 3 |
|---|---|---|---|---|
| **Serviceability** | 2 | 2 | 2 | 2 |
| **DBE** | 17 | 18 | 18 | 17 |
| **MCE** | 26 | 27 | 27 | 27 |
| **Near-collapse level** | 35 | 37 | 37 | 35 |

### *B.1.2. Nine-Story Models*

Figure B-2 shows the cost distributions for the 9-story models. For this model, the largest improvement can be seen at the MCE level, where the average costs are reduced by nearly 24 percent when comparing the Regular system to the Hybrid 3 system.

Tables B-4, B-5 and B-6 show the average repair time, total probability of unsafe placard, and average number of casualties, respectively. At the serviceability level, the average repair time is reduced by up to 13 percent. At all other intensity levels, there is no change in repair time. The reduction in total probability of receiving an unsafe placard is 12 percent for the MCE level intensity and negligible for all other intensity levels. The average number of deaths was reduced by up to 50 percent under the serviceability intensity level, up to 7 percent under the DBE level, up to 12 percent under the MCE level, and up to 9 percent under the near-collapse level. For the near-collapse level, the median number of casualties ranged between 8 and 9 deaths; all other median casualties are zero.

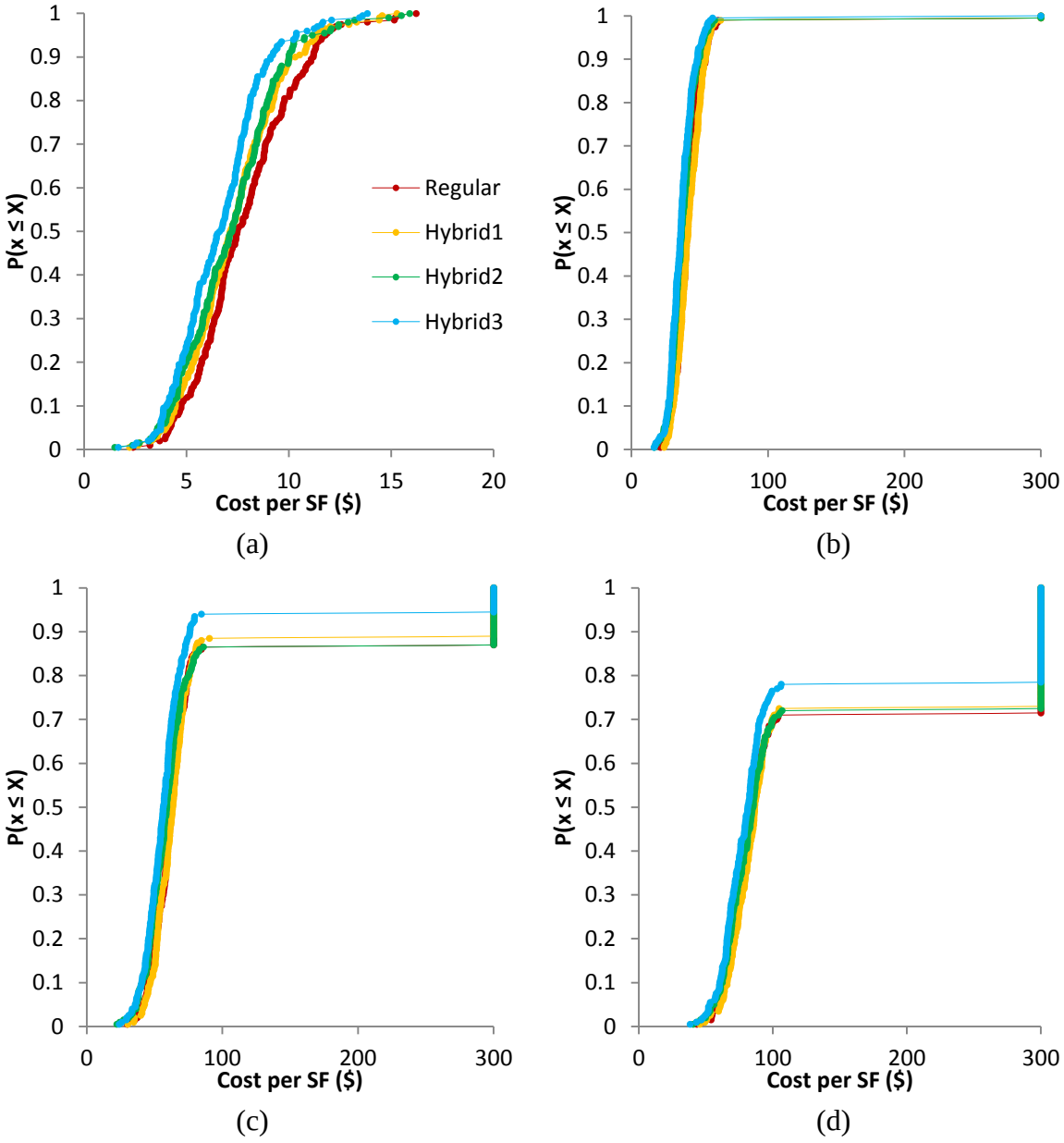


**Figure B-2.** Probability distribution of the repair costs for the 9-story BRB models for the (a) serviceability intensity level, (b) DBE intensity level, (c) MCE intensity level, and (d) near-collapse intensity level

**Table B-4.** Average series repair time (in days) for the 9-story BRB models with varying levels of hybridity

| | Regular | Hybrid 1 | Hybrid 2 | Hybrid 3 |
|---|---|---|---|---|
| **Serviceability** | 166 | 154 | 158 | 145 |
| **DBE** | 490 | 490 | 489 | 488 |
| **MCE** | 490 | 490 | 490 | 490 |
| **Near-collapse level** | 490 | 490 | 490 | 490 |

**Table B-5.** Total probability of receiving an unsafe placard for the 9-story BRB models with varying levels of hybridity

| | Regular | Hybrid 1 | Hybrid 2 | Hybrid 3 |
|---|---|---|---|---|
| **Serviceability** | 0 | 0 | 0 | 0 |
| **DBE** | 0.89 | 0.86 | 0.82 | 0.78 |
| **MCE** | 0.99 | 1.0 | 0.96 | 0.96 |
| **Near-collapse level** | 1.0 | 1.0 | 0.99 | 0.99 |

**Table B-6.** Average number of casualties for the 9-story BRB models with varying levels of hybridity

| | Regular | Hybrid 1 | Hybrid 2 | Hybrid 3 |
|---|---|---|---|---|
| **Serviceability** | 6 | 6 | 4 | 3 |
| **DBE** | 39 | 39 | 36 | 36 |
| **MCE** | 56 | 54 | 56 | 50 |
| **Near-collapse level** | 70 | 69 | 70 | 64 |

### *B.1.3. Eighteen-Story Models*

Figure B-3 shows the cost distributions for the 18-story models. For this model, the largest improvement can be seen at the near-collapse level, where the average costs are reduced by more than 26 percent when comparing the Regular system to the Hybrid 3 system.

Tables B-7, B-8 and B-9 show the average repair time, total probability of unsafe placard, and average number of casualties, respectively. At the serviceability level, the average repair time is reduced by up to 11 percent. At all other intensity levels, there is no change in repair time. The reduction in total probability of receiving an unsafe placard is more than 5 percent for the MCE level intensity and negligible for all other intensity levels. The average number of deaths was reduced by up to 9 percent under the serviceability intensity level, up to 2 percent under the DBE level, up to 7 percent under the MCE level, and up to 18 percent under the near-collapse level. The median number of casualties is always zero.

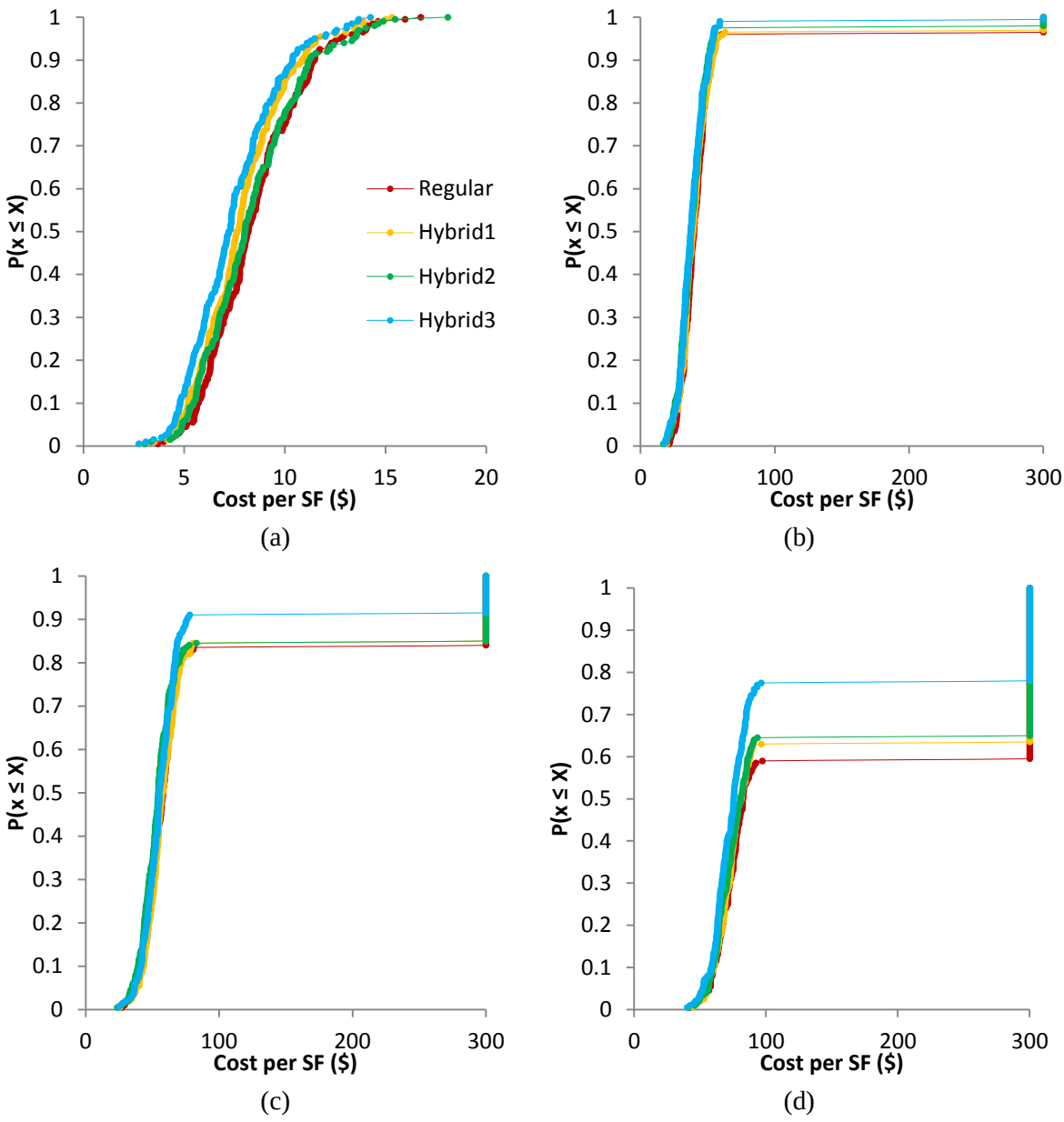


**Figure B-3.** Probability distribution of the repair costs for the 18-story BRB models for the (a) serviceability intensity level, (b) DBE intensity level, (c) MCE intensity level, and (d) near-collapse intensity level

**Table B-7.** Average series repair time (in days) for the 18-story BRB models with varying levels of hybridity

| | Regular | Hybrid 1 | Hybrid 2 | Hybrid 3 |
|---|---|---|---|---|
| **Serviceability** | 402 | 374 | 396 | 356 |
| **DBE** | 672 | 672 | 672 | 672 |
| **MCE** | 672 | 672 | 672 | 672 |
| **Near-collapse level** | 672 | 672 | 672 | 672 |

**Table B-8.** Total probability of receiving an unsafe placard for the 18-story BRB models with varying levels of hybridity

| | Regular | Hybrid 1 | Hybrid 2 | Hybrid 3 |
|---|---|---|---|---|
| **Serviceability** | 0.01 | 0.01 | 0.03 | 0 |
| **DBE** | 0.89 | 0.87 | 0.83 | 0.84 |
| **MCE** | 0.99 | 0.98 | 0.98 | 0.98 |
| **Near-collapse level** | 1.0 | 1.0 | 1.0 | 1.0 |

**Table B-9.** Average number of casualties for the 18-story BRB models with varying levels of hybridity

| | Regular | Hybrid 1 | Hybrid 2 | Hybrid 3 |
|---|---|---|---|---|
| **Serviceability** | 10 | 9 | 9 | 9 |
| **DBE** | 94 | 92 | 94 | 92 |
| **MCE** | 122 | 121 | 121 | 113 |
| **Near-collapse level** | 151 | 139 | 137 | 124 |

### B.2. Collapse Prevention Systems

Figure B-4 shows the cost distributions for all the models. The collapse prevention systems decrease the average repair costs for all structures, particularly for the shorter structures. For the 2-story model, the slack cable and loose link mechanisms reduce the average repair cost by more than 35 percent and nearly 18 percent, respectively. For the 4-story model, those reductions are 33 percent and 5 percent, respectively.

Tables B-10, B-11 and B-12 show the average repair time, total probability of unsafe placard, and average number of casualties, respectively. For all the models, the collapse prevention systems have negligible effect on the average repair time and total probability of receiving an unsafe placard. However, the average number of casualties is significantly decreased for the 2-story model. That reduction is nearly 33 percent for the slack cable and more than 13 percent for the loose link. The reduction in the average number of casualties is nearly 15 percent for the slack cable and nearly 7 percent for the loose link. The median number of casualties is zero for all the models.

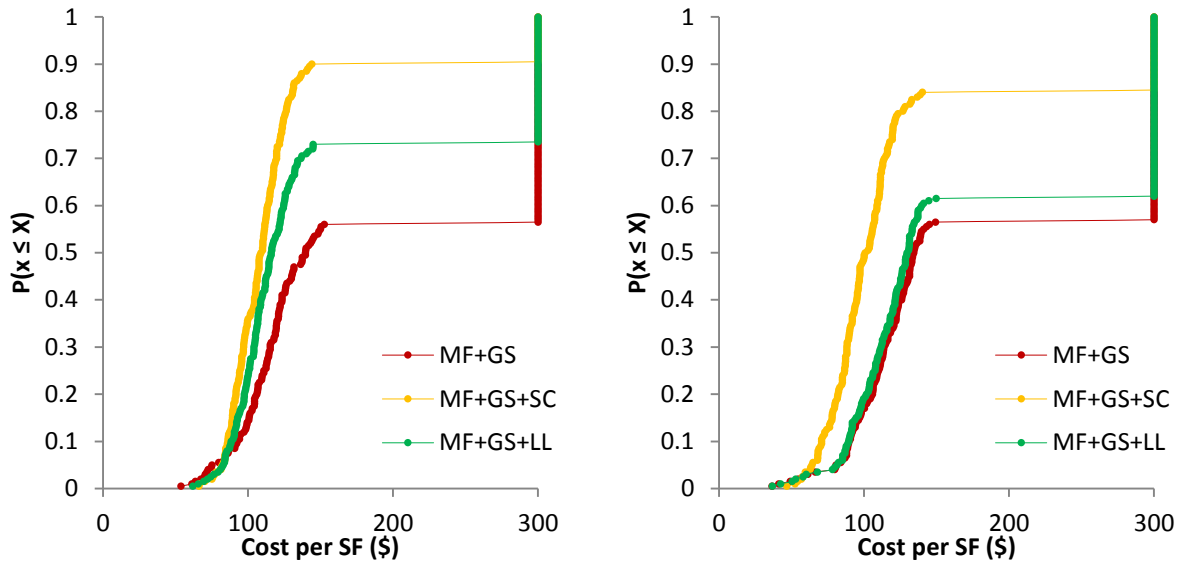


**Figure B-4.** Probability distribution of the repair costs for the near-collapse level intensity for the (a) 2-story CPS models and (b) 4-story CPS models

**Table B-10.** Average parallel repair time (in days) for the models with and without collapse prevention mechanisms

| | **2-Story** | **4-Story** |
|---|---|---|
| **MF + GS** | 355 | 392 |
| **MF + GS + SC** | 356 | 392 |
| **MF + GS + LL** | 356 | 392 |

**Table B-11.** Total probability of receiving an unsafe placard for the models with and without collapse prevention mechanisms

| | **2-Story** | **4-Story** |
|---|---|---|
| **MF + GS** | 1 | 0.99 |
| **MF + GS + SC** | 1 | 1 |
| **MF + GS + LL** | 1 | 0.99 |

**Table B-12.** Average number of casualties for the models with and without collapse prevention mechanisms

| | **2-Story** | **4-Story** |
|---|---|---|
| **MF + GS** | 16 | 30 |
| **MF + GS + SC** | 11 | 25 |
| **MF + GS + LL** | 14 | 28 |

## B.3. Special Moment Frames Modeled With and Without Gravity Systems

For the Special Moment Frame Systems modeled with and without the gravity systems, the results are presented on a story-by-story basis. The cost distribution is shown for each system to show the dispersion of results from the realizations. Additionally, the average repair time, total probability of unsafe placard, and average number of casualties are tabulated.

### *B.3.1. Two-Story Models*

Figure B-5 shows the cost distributions for the 2-story models. For this model, the largest improvement in average cost can be seen at the higher intensity levels. The average cost was decreased by nearly 18 percent under the near-collapse level intensity, by 21 percent under the MCE level, and by more than 12 percent under the DBE level. Under the serviceability levels, the average cost actually increased up to 10 percent when the partially restrained connections are modeled. This is due to the sensitivity of the nonstructural components to small changes in acceleration values. The accelerations experienced by the models with the gravity system at certain stories were occasionally higher than the models with no gravity system resistance. While these changes in acceleration were not excessive, they are reflected in the nonstructural costs during the realizations with higher total costs. Since the nonstructural components have a strong influence in the consequences at the serviceability levels, this phenomenon is more prevalent at the lower intensities. The results between the two levels of gravity connection strengths are similar, and the higher strength does not necessarily cause a larger decrease in consequences. There was negligible difference between the system with 35 percent strength and 50 percent strength.

Tables B-13, B-14 and B-15 show the average repair time, total probability of unsafe placard, and average number of casualties, respectively. The repair time is decreased by more than 6 percent under the DBE level; the change is negligible for all other intensities. The probability of receiving an unsafe placard is decreased by more than 8 percent under the DBE level; the change is negligible for all other intensities. For all models, the average number of casualties is negligible. The median number of collapses is zero, except under the near-collapse level intensity. In this case, the median number of casualties is always around 1.0.

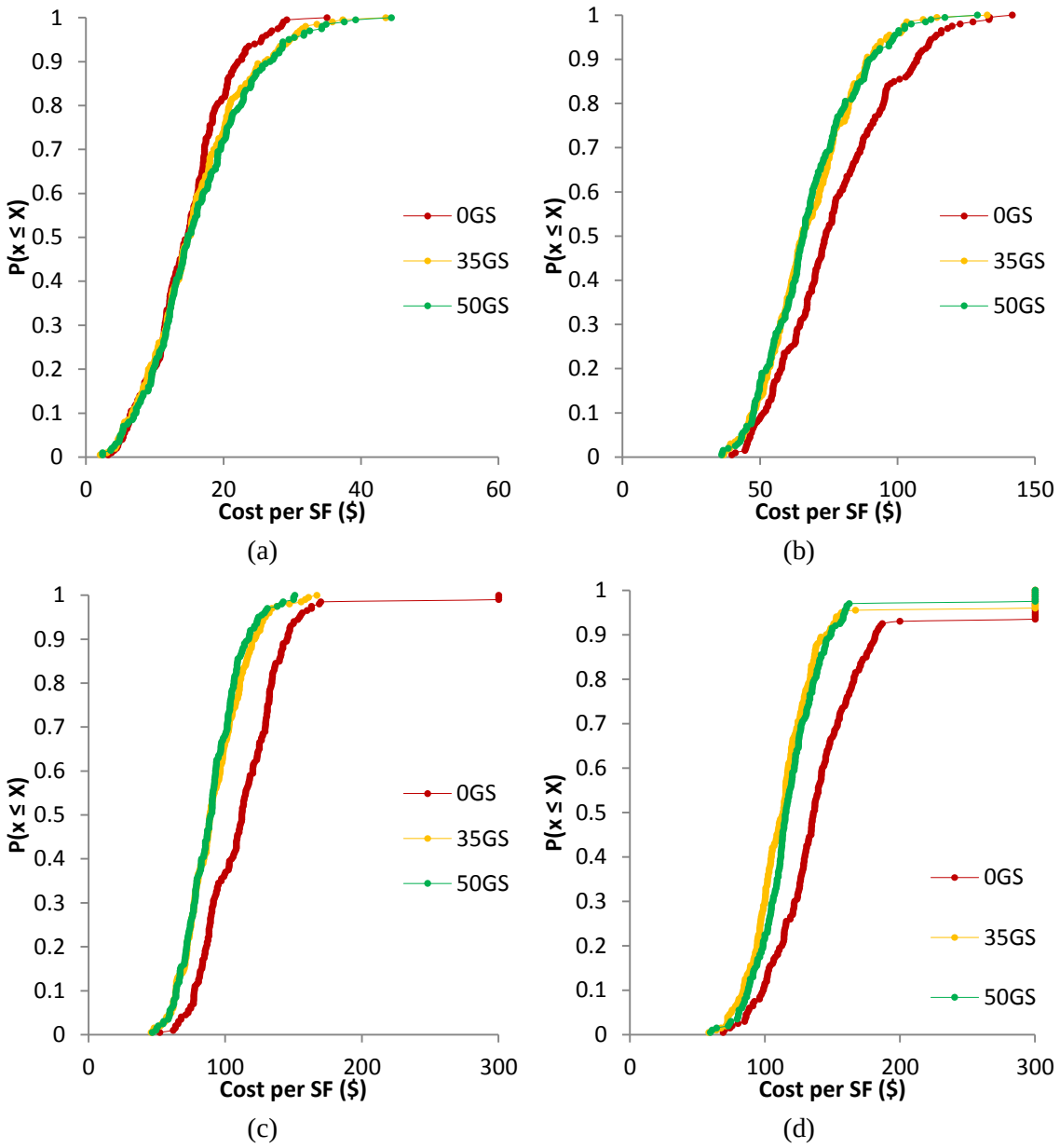


**Figure B-5.** Probability distribution of the repair costs for the 2-story SMRF models for the (a) serviceability intensity level, (b) DBE intensity level, (c) MCE intensity level, and (d) near-collapse intensity level

**Table B-13.** Average series repair time (in days) for the 2-story SMRF models with varying levels of gravity connection strength

| | 0GS | 35GS | 50GS |
|---|---|---|---|
| **Serviceability** | 59 | 60 | 62 |
| **DBE** | 319 | 298 | 297 |
| **MCE** | 355 | 345 | 346 |
| **Near-collapse level** | 357 | 356 | 356 |

**Table B-14.** Total probability of receiving an unsafe placard for the 2-story SMRF models with varying levels of gravity connection strength

| | 0GS | 35GS | 50GS |
|---|---|---|---|
| **Serviceability** | 0.04 | 0.05 | 0.03 |
| **DBE** | 0.98 | 0.92 | 0.90 |
| **MCE** | 0.99 | 0.98 | 0.98 |
| **Near-collapse level** | 1.0 | 1.0 | 1.0 |

**Table B-15.** Average number of casualties for the 2-story SMRF models with varying levels of gravity connection strength

| | 0GS | 35GS | 50GS |
|---|---|---|---|
| **Serviceability** | 0 | 1 | 1 |
| **DBE** | 10 | 10 | 10 |
| **MCE** | 10 | 10 | 10 |
| **Near-collapse level** | 14 | 14 | 13 |

### *B.3.2. Four-Story Models*

Figure B-6 shows the cost distributions for the 4-story models. Like the 2-story model, the largest improvement can be seen at the higher intensity levels. The average cost was decreased by nearly 32 percent under the near-collapse level intensity, by 29 percent under the MCE level, and by 17 percent under the DBE level. Under the serviceability levels, the average cost actually increased up to 7 percent when the partially restrained connections are modeled. The results between the two levels of gravity connection strengths are similar, but the higher strength does cause a larger decrease in cost for this structure. There was negligible difference between the system with 35 percent strength and 50 percent strength.

Tables B-16, B-17 and B-18 show the average repair time, total probability of unsafe placard, and average number of casualties, respectively. The changes in repair time and probability of receiving an unsafe placard are negligible. The average number of casualties is reduced under the larger intensities. This reduction is up to 11 percent under the MCE and up to 23 percent under the near-collapse level intensity. The median number of collapses is always zero.

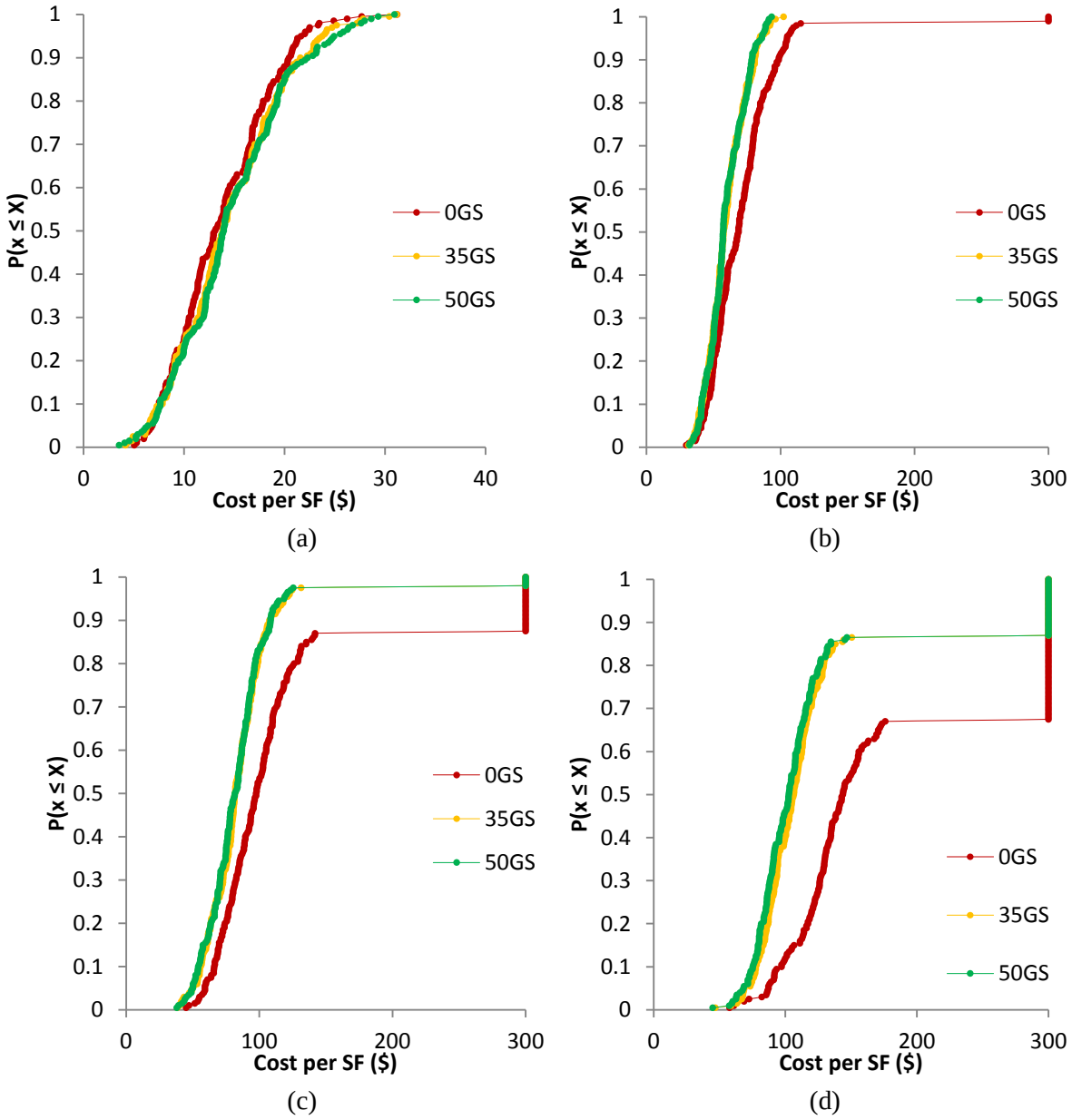


**Figure B-6.** Probability distribution of the repair costs for the 4-story SMRF models for the (a) serviceability intensity level, (b) DBE intensity level, (c) MCE intensity level, and (d) near-collapse intensity level

**Table B-16.** Average series repair time (in days) for the 4-story SMRF models with varying levels of gravity connection strength

| | 0GS | 35GS | 50GS |
|---|---|---|---|
| **Serviceability** | 128 | 134 | 136 |
| **DBE** | 391 | 390 | 391 |
| **MCE** | 392 | 392 | 392 |
| **Near-collapse level** | 392 | 392 | 392 |

**Table B-17.** Total probability of receiving an unsafe placard for the 4-story SMRF models with varying levels of gravity connection strength

| | 0GS | 35GS | 50GS |
|---|---|---|---|
| **Serviceability** | 0.08 | 0.08 | 0.07 |
| **DBE** | 0.98 | 0.97 | 0.97 |
| **MCE** | 1.0 | 0.99 | 0.99 |
| **Near-collapse level** | 1.0 | 1.0 | 1.0 |

**Table B-18.** Average number of casualties for the 4-story SMRF models with varying levels of gravity connection strength

| | 0GS | 35GS | 50GS |
|---|---|---|---|
| **Serviceability** | 4 | 4 | 5 |
| **DBE** | 17 | 17 | 17 |
| **MCE** | 21 | 19 | 19 |
| **Near-collapse level** | 33 | 26 | 26 |

### *B.3.3. Eight-Story Models*

Figure B-7 shows the cost distributions for the 8-story models. Like the previous models, the largest improvement can be seen at the higher intensity levels, but the average costs decrease at all intensity levels. The average cost was decreased by nearly 11 percent under the near-collapse level intensity, by nearly 10 percent under the MCE level, by 10 percent under the DBE level, and by more than 3 percent under the serviceability level. These reductions at the higher intensities are less than those for the shorter structures.

Tables B-19, B-20 and B-21 show the average repair time, total probability of unsafe placard, and average number of casualties, respectively. The changes in repair time, probability of receiving an unsafe placard, and number of casualties are negligible. The median number of collapses is zero, except under the DBE level intensity. In this case, the median number of casualties is 7 deaths.

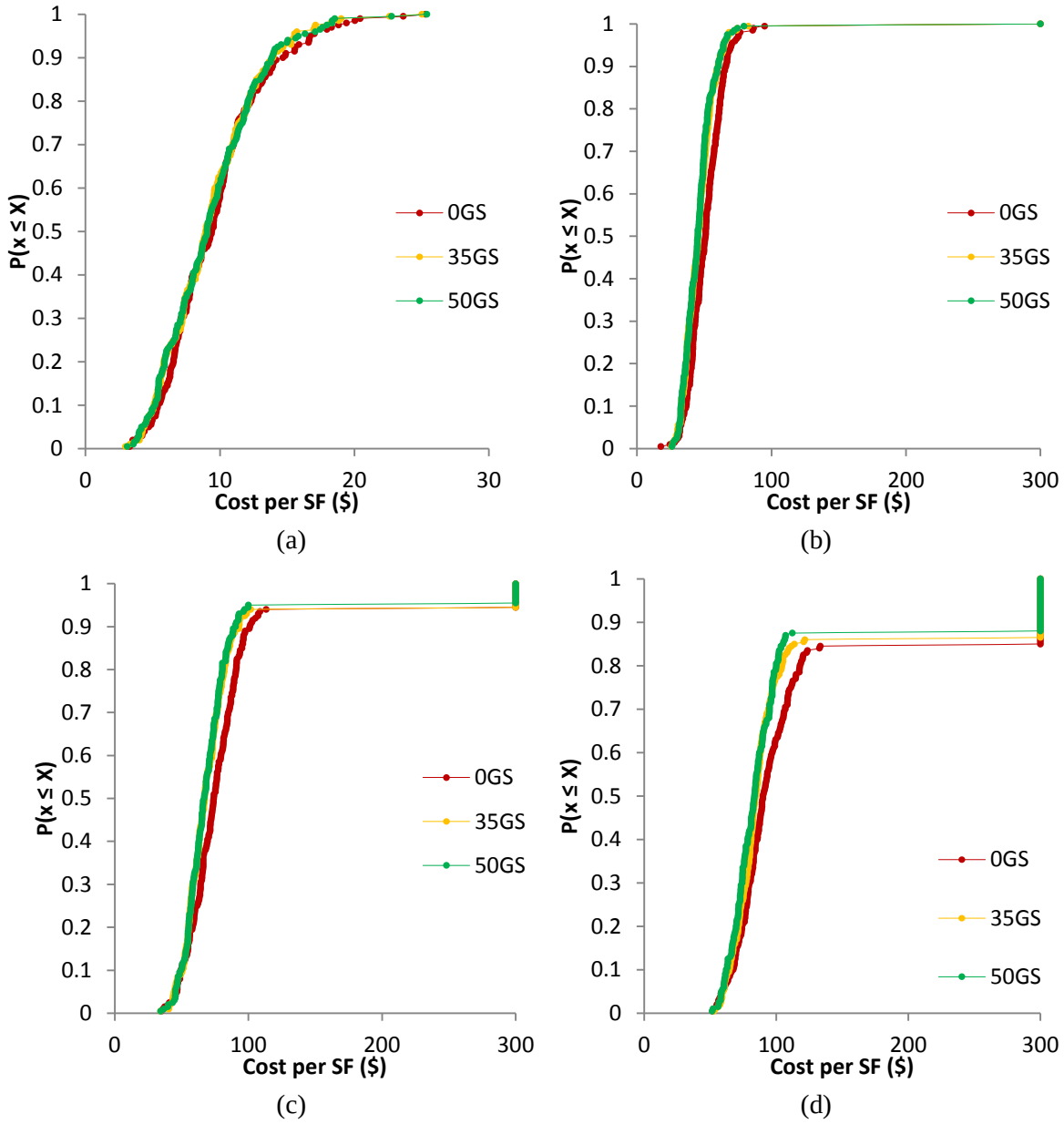


**Figure B-7.** Probability distribution of the repair costs for the 8-story SMRF models for the (a) serviceability intensity level, (b) DBE intensity level, (c) MCE intensity level, and (d) near-collapse intensity level

**Table B-19.** Average parallel repair time (in days) for the 8-story SMRF models with varying levels of gravity connection strength

| | 0GS | 35GS | 50GS |
|---|---|---|---|
| **Serviceability** | 201 | 194 | 196 |
| **DBE** | 462 | 462 | 462 |
| **MCE** | 462 | 462 | 462 |
| **Near-collapse level** | 462 | 462 | 462 |

**Table B-20.** Total probability of receiving an unsafe placard for the 8-story SMRF models with varying levels of gravity connection strength

| | 0GS | 35GS | 50GS |
|---|---|---|---|
| **Serviceability** | 0.03 | 0.02 | 0.02 |
| **DBE** | 0.94 | 0.94 | 0.93 |
| **MCE** | 0.99 | 0.99 | 0.98 |
| **Near-collapse level** | 1.0 | 1.0 | 1.0 |

**Table B-21.** Average number of casualties for the 8-story SMRF models with varying levels of gravity connection strength

| | 0GS | 35GS | 50GS |
|---|---|---|---|
| **Serviceability** | 7 | 8 | 8 |
| **DBE** | 37 | 38 | 38 |
| **MCE** | 51 | 51 | 48 |
| **Near-collapse level** | 61 | 61 | 59 |

# Appendix C: Ground Motions Used in "Response-History Analysis for the Design of New Buildings: A Study of Assumptions" and "Accidental Torsion in Nonlinear Response History Analysis."

Numerous ground motion sets are used in the analyses for the research presented in the manuscripts "Response-History Analysis for the Design of New Buildings: A Study of Assumptions" and "Accidental Torsion in Nonlinear Response History Analysis." While the manuscripts provide the spectra of the ground motions sets, no further data is included, due to space limitations. Primarily, tables are provided to summarize the ground motions used within each record set. Table C-1 summarizes the ground motions used for the analysis of the MF2 Model, Table C-2 summarizes the ground motions used for the analysis of the MF8 Model, Table C-3 summarizes the ground motions used for the SCAL and MTCH suites of the 3D Model, Table C-4 summarizes the ground motions used for the 05CS suite of the 3D Model, and Table C-5 summarizes the ground motions used for the 20CS suite of the 3D Model.

Additionally, acceleration time histories are provided for the spectrum matched ground motion sets. The other time histories are provided in the NGA files previously tabulated; however, these spectrum-matched time histories are developed using RSPMatch specifically for this work. Figure C-1, C-2 and C-3 show the acceleration time histories for the spectrum matched ground motions developed for the MF2 Model, the MF8 Model and the 3D Model, respectively.

**Table C-1.** Ground motions used for the analysis of the MF2 Model

| NGA # | Earthquake Name | Moment Magnitude | Distance (km) | Vs30 - m/s (Site Class) | Source Type | Scale Factor |
|---|---|---|---|---|---|---|
| 169 | Imperial Valley 06 | 6.5 | 22.0 | 275 (D) | Strike Slip | 2.7 |
| 313 | Corinth, Greece | 6.6 | 10.3 | 339 (D) | Normal | 3.2 |
| 829 | Cape Mendocino | 7.0 | 14.3 | 312 (D) | Reverse | 2.1 |
| 1236 | Chi-Chi, Taiwan | 7.6 | 37.5 | 273 (D) | Reverse Oblique | 4.0 |
| 161 | Imperial Valley 06 | 6.5 | 10.4 | 209 (D) | Strike Slip | 3.2 |
| 573 | Taiwan SMART1(45) | 7.3 | 76.4 | 275 (D) | Reverse | 4.0 |
| 959 | Northridge-01 | 6.7 | 14.7 | 267 (D) | Reverse | 1.7 |
| 1048 | Northridge-01 | 6.7 | 12.1 | 281 (D) | Reverse | 1.3 |
| 1208 | Chi-Chi, Taiwan | 7.6 | 24.1 | 442 (C) | Reverse Oblique | 3.6 |
| 1762 | Hector Mine | 7.1 | 43.1 | 271 (D) | Strike Slip | 4.0 |
| 3268 | Chi-Chi, Taiwan 06 | 6.3 | 33.6 | 543 (C) | Reverse Oblique | 4.0 |

**Table C-2.** Ground motions used for the analysis of the MF8 Model

| NGA # | Earthquake Name | Moment Magnitude | Distance (km) | Vs30 - m/s (Site Class) | Source Type | Scale Factor |
|---|---|---|---|---|---|---|
| 169 | Imperial Valley-06 | 6.5 | 22.0 | 275 (D) | Strike Slip | 2.9 |
| 549 | Chalfant Valley-02 | 6.2 | 17.2 | 271 (D) | Strike Slip | 4.0 |
| 573 | Taiwan SMART1(45) | 7.3 | 76.4 | 275 (D) | Reverse | 4.0 |
| 577 | Taiwan SMART1(45) | 7.3 | 78.2 | 275 (D) | Reverse | 4.0 |
| 728 | Superstition Hills-02 | 6.5 | 13.0 | 194 (D) | Strike Slip | 3.8 |
| 1198 | Chi-Chi, Taiwan | 7.6 | 11.0 | 545 (C) | Reverse Oblique | 3.1 |
| 1484 | Chi-Chi, Taiwan | 7.6 | 26.3 | 273 (D) | Reverse Oblique | 3.4 |
| 161 | Imperial Valley-06 | 6.5 | 10.4 | 209 (D) | Strike Slip | 3.5 |
| 776 | Loma Prieta | 6.9 | 27.9 | 371 (D) | Reverse Oblique | 3.8 |
| 1208 | Chi-Chi, Taiwan | 7.6 | 24.1 | 442 (C) | Reverse Oblique | 3.9 |
| 1762 | Hector Mine | 7.1 | 43.1 | 271 (D) | Strike Slip | 4.0 |

**Table C-3**. Ground motions used for the analysis of the 3D Model – SCAL and MTCH suites

| NGA # | Earthquake Name | Moment Magnitude | Distance (km) | Vs30 - m/s | Source Type | Scale Factor |
|---|---|---|---|---|---|---|
| 126 | Gazli, USSR | 6.80 | 5.5 | 660 | Unknown | 1.2 |
| 160 | Imperial Valley-06 | 6.53 | 2.7 | 223 | Strike-Slip | 1.2 |
| 165 | Imperial Valley-06 | 6.53 | 7.3 | 275 | Strike-Slip | 2.4 |
| 189 | Imperial Valley-06 | 6.53 | 9.6 | 339 | Strike-Slip | 2.3 |
| 367 | Coalinga-01 | 6.36 | 8.4 | 257 | Reverse | 2.2 |
| 496 | Nahanni, Canada | 6.76 | 4.9 | 660 | Reverse | 2.9 |
| 1004 | Northridge-01 | 6.69 | 8.4 | 380 | Reverse | 0.9 |
| 1197 | Chi-Chi, Taiwan | 7.62 | 3.1 | 543 | Reverse-Oblique | 0.9 |
| 1549 | Chi-Chi, Taiwan | 7.62 | 1.8 | 664 | Reverse-Oblique | 1.3 |
| 1596 | Chi-Chi, Taiwan | 7.62 | 1.8 | 664 | Reverse-Oblique | 1.4 |
| 1605 | Duzce, Turkey | 7.14 | 6.6 | 276 | Strike-Slip | 1.2 |

**Table C-4**. Ground motions used for the analysis of the 3D Model – 05CS suite

| NGA # | Earthquake Name | Moment Magnitude | Distance (km) | Vs30 - m/s | Source Type | Scale Factor |
|---|---|---|---|---|---|---|
| 179 | Imperial Valley-06 | 6.53 | 7.0 | 209 | Strike-Slip | 1.9 |
| 183 | Imperial Valley-06 | 6.53 | 3.9 | 206 | Strike-Slip | 1.9 |
| 184 | Imperial Valley-06 | 6.53 | 5.1 | 202 | Strike-Slip | 1.7 |
| 723 | Superstition Hills-02 | 6.54 | 1.0 | 349 | Strike-Slip | 1.7 |
| 802 | Loma Prieta | 6.93 | 8.5 | 371 | Reverse-Oblique | 2.2 |
| 983 | Northridge-01 | 6.69 | 5.4 | 526 | Reverse | 0.9 |
| 1013 | Northridge-01 | 6.69 | 5.9 | 629 | Reverse | 1.9 |
| 1063 | Northridge-01 | 6.69 | 6.5 | 282 | Reverse | 1 |
| 1202 | Chi-Chi, Taiwan | 7.62 | 12.7 | 474 | Reverse-Oblique | 2.6 |
| 1493 | Chi-Chi, Taiwan | 7.62 | 6.0 | 455 | Reverse-Oblique | 3.6 |
| 1528 | Chi-Chi, Taiwan | 7.62 | 2.1 | 273 | Reverse-Oblique | 2.9 |

**Table C-5**. Ground motions used for the analysis of the 3D Model – 20CS suite

| NGA # | Earthquake Name | Moment Magnitude | Distance (km) | Vs30 - m/s | Source Type | Scale Factor |
|---|---|---|---|---|---|---|
| 6 | Imperial Valley-02 | 6.95 | 6.1 | 213 | Strike-Slip | 2.1 |
| 179 | Imperial Valley-06 | 6.53 | 7.0 | 209 | Strike-Slip | 1.4 |
| 183 | Imperial Valley-06 | 6.53 | 3.9 | 206 | Strike-Slip | 1.5 |
| 184 | Imperial Valley-06 | 6.53 | 5.1 | 202 | Strike-Slip | 1.3 |
| 802 | Loma Prieta | 6.93 | 8.5 | 371 | Reverse-Oblique | 1.8 |
| 821 | Erzican, Turkey | 6.69 | 4.4 | 275 | Strike-Slip | 1.1 |
| 879 | Landers | 7.28 | 2.2 | 685 | Strike-Slip | 1.5 |
| 1013 | Northridge-01 | 6.69 | 5.9 | 629 | Reverse | 1.3 |
| 1504 | Chi-Chi, Taiwan | 7.62 | 0.6 | 434 | Reverse-Oblique | 1.1 |
| 1528 | Chi-Chi, Taiwan | 7.62 | 2.1 | 273 | Reverse-Oblique | 2.1 |
| 1546 | Chi-Chi, Taiwan | 7.62 | 9.3 | 476 | Reverse-Oblique | 2.3 |

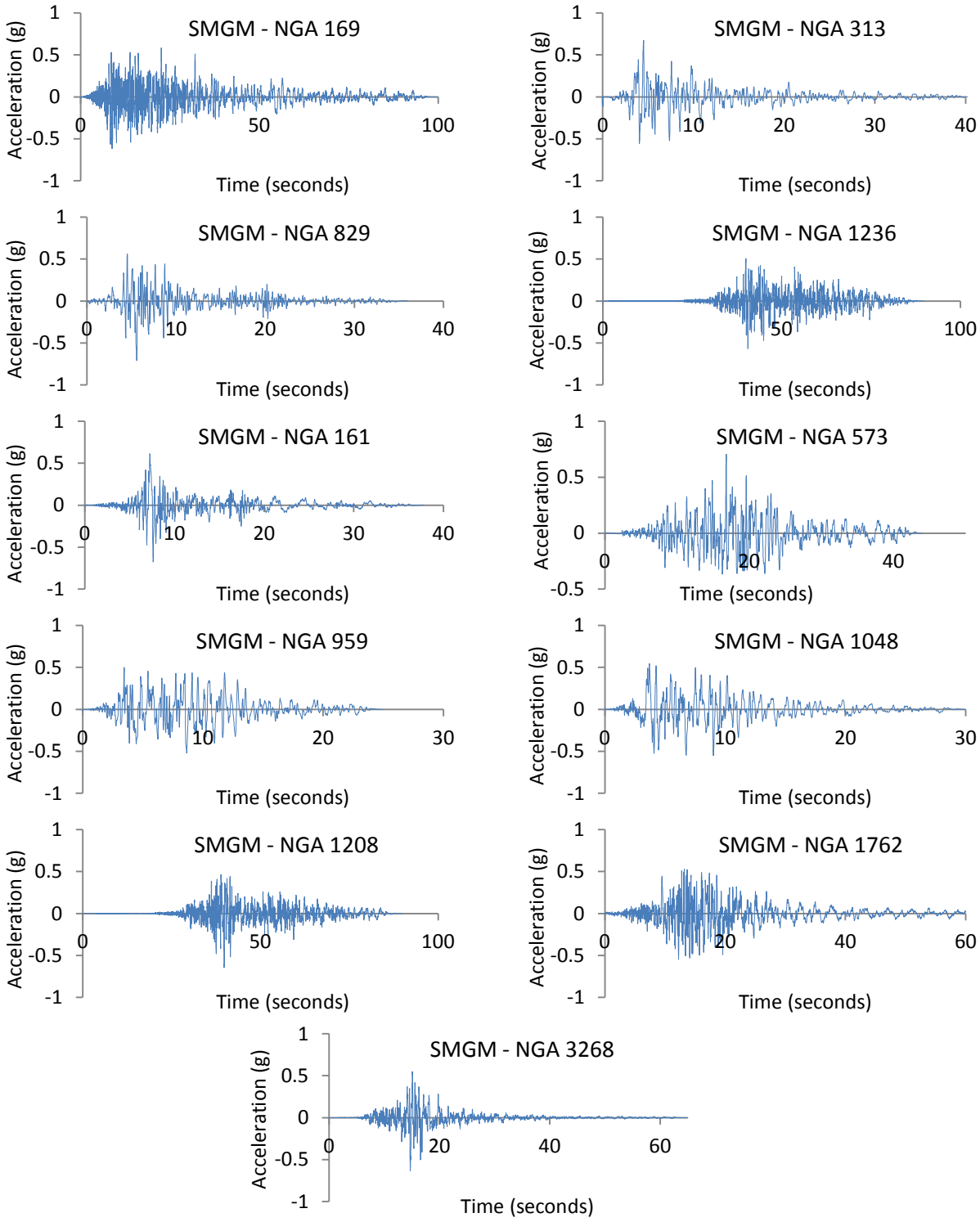


**Figure C-1.** Acceleration time histories of spectrum matched ground motions used to analyze the MF2 Model, defined by NGA record used as the seed ground motion

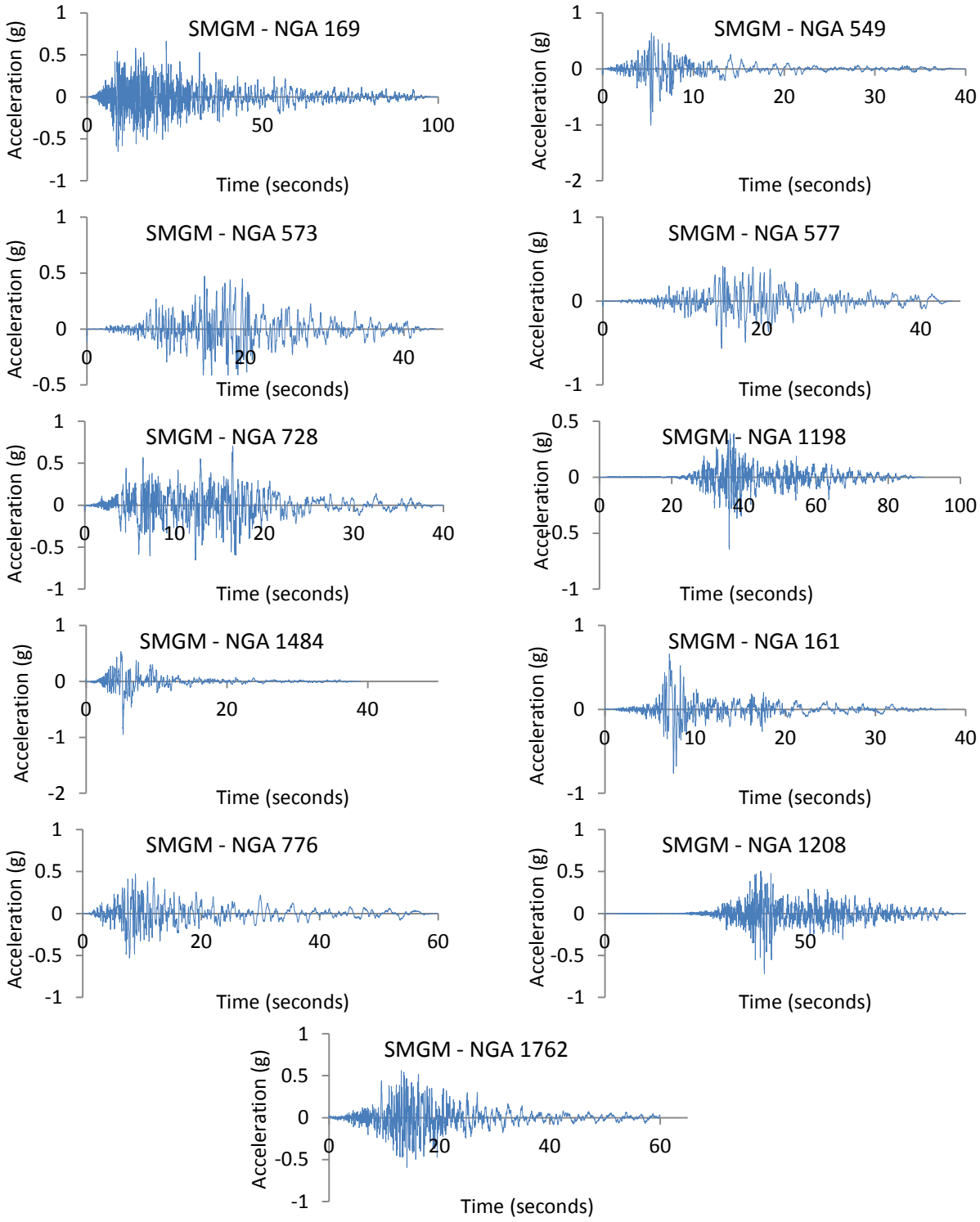


**Figure C-2.** Acceleration time histories of spectrum matched ground motions used to analyze the MF8 Model, defined by NGA record used as the seed ground motion

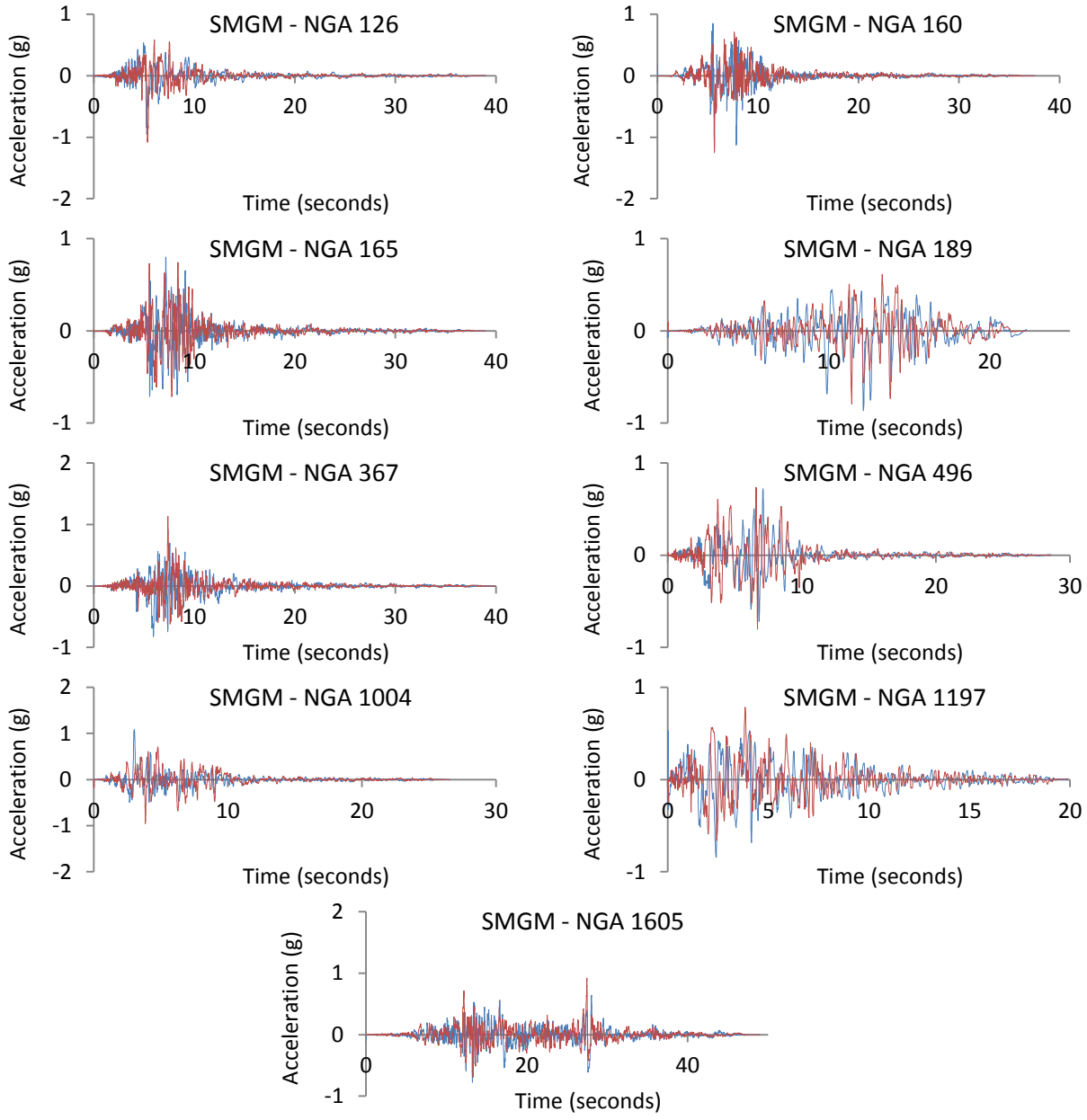


**Figure C-3.** Acceleration time histories of both components of spectrum matched ground motions used to analyze the 3D Model, defined by NGA record used as the seed ground motion

# Appendix D: Fair Use Analysis Results

The next four pages contain Virginia Tech ETD Fair Use Analysis Results for Figures 2-8, A1, A2 and A4.

**Draft 09/01/2009**

(Questions? Concerns? Contact Gail McMillan, Director of the Digital Library and Archives at Virginia Tech's University Libraries: gailmac@vt.edu)

(Please ensure that Javascript is enabled on your browser before using this tool.)

# Virginia Tech ETD Fair Use Analysis Results

***This is not a replacement for professional legal advice but an effort to assist you in making a sound decision.***

Name: Jordan Jarrett

Description of item under review for fair use: Figure 2-8. Process of a Monte Carlo simulation Source: FEMA (2012). Seismic Performance Assessment of Buildings, FEMA P-58, Applied Technology Council, Washington, D.C..

Report generated on: 12-12-2013 at : 20:51:57

## Based on the information you provided:

### Factor 1

Your consideration of the purpose and character of your use of the copyright work weighs: ***in favor of fair use***

### Factor 2

Your consideration of the nature of the copyrighted work you used weighs: ***in favor of fair use***

### Factor 3

Your consideration of the amount and substantiality of your use of the copyrighted work weighs: ***in favor of fair use***

### Factor 4

Your consideration of the effect or potential effect on the market after your use of the copyrighted work weighs: ***in favor of fair use***

## Based on the information you provided, your use of the copyrighted work weighs: *in favor of fair use*

**Draft 09/01/2009**

(Questions? Concerns? Contact Gail McMillan, Director of the Digital Library and Archives at Virginia Tech's University Libraries: gailmac@vt.edu)

(Please ensure that Javascript is enabled on your browser before using this tool.)

# Virginia Tech ETD Fair Use Analysis Results

***This is not a replacement for professional legal advice but an effort to assist you in making a sound decision.***

Name: Jordan Jarrett

Description of item under review for fair use: Figure A-1. Plan view of Performance Group 10 layout and an example configuration of the lightning bolt bracing. Source: NIST (2010). Evaluation of the FEMA P-695 Methodology for Quantification of Building Seismic Performance Factors, NIST GCR 10-917-8, NEHRP Consultants Joint Venture, Redwood City, CA

Report generated on: 12-12-2013 at : 20:44:01

## Based on the information you provided:

### Factor 1

Your consideration of the purpose and character of your use of the copyright work weighs: ***in favor of fair use***

### Factor 2

Your consideration of the nature of the copyrighted work you used weighs: ***in favor of fair use***

### Factor 3

Your consideration of the amount and substantiality of your use of the copyrighted work weighs: ***in favor of fair use***

### Factor 4

Your consideration of the effect or potential effect on the market after your use of the copyrighted work weighs: ***in favor of fair use***

## Based on the information you provided, your use of the copyrighted work weighs: ***in favor of fair use***

**Draft 09/01/2009**

(Questions? Concerns? Contact Gail McMillan, Director of the Digital Library and Archives at Virginia Tech's University Libraries: gailmac@vt.edu)

(Please ensure that Javascript is enabled on your browser before using this tool.)

# Virginia Tech ETD Fair Use Analysis Results

***This is not a replacement for professional legal advice but an effort to assist you in making a sound decision.***

Name: Jordan Jarrett

Description of item under review for fair use: Figure A-2. Typical plan view of the Collapse Prevention Systems Source:Judd, J. and Charney, F. (2013). Seismic Collapse Prevention System. Unpublished Manuscript.

Report generated on: 12-12-2013 at : 20:46:10

## Based on the information you provided:

### Factor 1

Your consideration of the purpose and character of your use of the copyright work weighs: ***in favor of fair use***

### Factor 2

Your consideration of the nature of the copyrighted work you used weighs: ***against fair use***

### Factor 3

Your consideration of the amount and substantiality of your use of the copyrighted work weighs: ***in favor of fair use***

### Factor 4

Your consideration of the effect or potential effect on the market after your use of the copyrighted work weighs: ***in favor of fair use***

## Based on the information you provided, your use of the copyrighted work weighs: *in favor of fair use*

**Draft 09/01/2009**

(Questions? Concerns? Contact Gail McMillan, Director of the Digital Library and Archives at Virginia Tech's University Libraries: gailmac@vt.edu)

(Please ensure that Javascript is enabled on your browser before using this tool.)

# Virginia Tech ETD Fair Use Analysis Results

***This is not a replacement for professional legal advice but an effort to assist you in making a sound decision.***

Name: Jordan Jarrett

Description of item under review for fair use: Figure A-4. Typical plan view of the SMRF systems Source: NIST (2010). Evaluation of the FEMA P-695 Methodology for Quantification of Building Seismic Performance Factors, NIST GCR 10-917-8, NEHRP Consultants Joint Venture, Redwood City, CA.

Report generated on: 12-12-2013 at : 20:49:32

## Based on the information you provided:

### Factor 1

Your consideration of the purpose and character of your use of the copyright work weighs: ***in favor of fair use***

### Factor 2

Your consideration of the nature of the copyrighted work you used weighs: ***in favor of fair use***

### Factor 3

Your consideration of the amount and substantiality of your use of the copyrighted work weighs: ***in favor of fair use***

### Factor 4

Your consideration of the effect or potential effect on the market after your use of the copyrighted work weighs: ***in favor of fair use***

## Based on the information you provided, your use of the copyrighted work weighs: ***in favor of fair use***